ISSN 1881-7831 Online ISSN 1881-784X

DD&T

Drug Discoveries & Therapeutics

Volume 20, Number 1
February 2026

IRCA BSSA

IACMHR

www.ddtjournal.com

DD&T
Drug Discoveries & Therapeutics

ISSN: 1881-7831
Online ISSN: 1881-784X
CODEN: DDTRBX
Issues/Year: 6
Language: English
Publisher: IACMHR Co., Ltd.

Drug Discoveries & Therapeutics is one of a series of peer-reviewed journals of the International Research and Cooperation Association for Bio & Socio-Sciences Advancement (IRCA-BSSA) Group. It is published bimonthly by the International Advancement Center for Medicine & Health Research Co., Ltd. (IACMHR Co., Ltd.) and supported by the IRCA-BSSA.

Drug Discoveries & Therapeutics publishes contributions in all fields of pharmaceutical and therapeutic research such as medicinal chemistry, pharmacology, pharmaceutical analysis, pharmaceutics, pharmaceutical administration, and experimental and clinical studies of effects, mechanisms, or uses of various treatments. Studies in drug-related fields such as biology, biochemistry, physiology, microbiology, and immunology are also within the scope of this journal.

Drug Discoveries & Therapeutics publishes Original Articles, Brief Reports, Reviews, Policy Forum articles, Case Reports, Communications, Editorials, News, and Letters on all aspects of the field of pharmaceutical research. All contributions should seek to promote international collaboration in pharmaceutical science.

Editorial Board

Editorial and Head Office:

Pearl City Koishikawa 603,
2-4-5 Kasuga, Bunkyo-ku,
Tokyo 112-0003, Japan
E-mail: office@ddtjournal.com

Drug Discoveries & Therapeutics

Editorial and Head Office

Pearl City Koishikawa 603, 2-4-5 Kasuga, Bunkyo-ku,
Tokyo 112-0003, Japan

E-mail: office@ddtjournal.com
URL: www.ddtjournal.com

CONTENTS

Volume 20, Number 1, 2026

Editorial

Review

Original Article

Brief Report

Editorial

DOI: 10.5582/ddt.2026.01004

Protein persulfidation: The missing link in Alzheimer's disease defense mechanisms

Ya-nan Ma[1], Xiaoxi Huang[2], Ying Xia[3], Peipei Song[4,5], Xiqi Hu[3,*]

[1] Department of Neurosurgery, Haikou Affiliated Hospital of Central South University Xiangya School of Medicine, Haikou, China;
[2] Department of Gastroenterology, Haikou Affiliated Hospital of Central South University Xiangya School of Medicine, Haikou, China;
[3] Department of Neurosurgery, Integrated Neuroscience Center, Geriatric Hospital of Hainan, Haikou, China;
[4] Center for Clinical Sciences, Japan Institute for Health Security, Tokyo, Japan;
[5] National College of Nursing, Japan Institute for Health Security, Tokyo, Japan.

SUMMARY: Despite decades of research dominated by the amyloid-beta hypothesis, clinical treatment of Alzheimer's disease (AD) has yet to achieve a decisive breakthrough. This editorial advances an alternative pathological paradigm: the collapse of endogenous hydrogen sulfide (H_2S) signaling represents a central failure point in the brain's intrinsic defense mechanisms against AD. We dissect the molecular cascade triggered by cystathionine γ-lyase (CSE) deficiency, focusing on how reduced persulfidation of glycogen synthase kinase 3β (GSK3β) directly promotes Tau hyperphosphorylation and subsequent neuronal injury. A critical message of this commentary is the need to dispel the oversimplified notion that sulfide supplementation alone can confer neuroprotection. Because H_2S works within a narrow therapeutic window and has complex hormetic effects, untargeted dietary or environmental exposure cannot match the spatiotemporal precision of endogenous signaling. Instead, it may increase the risk of toxicity. By integrating analyses of transsulfuration metabolism, mitochondrial function, and nutritional status, we propose a precision medicine framework centered on brain-targeted delivery technologies and metabolic correction strategies to selectively restore compromised H_2S signaling networks. This conceptual shift marks a new direction in AD research, shifting the focus from clearing toxic protein aggregates to restoring endogenous neuronal resilience.

Keywords: gasotransmitter, thiol modification, neurofibrillary tangles, homocysteine metabolism, S-sulfhydration, blood-brain barrier

1. Introduction

Alzheimer's disease (AD), the most prevalent neurodegenerative disorder worldwide, has proven far more mechanistically complex than early investigators anticipated (*1*). Although the amyloid-beta (Aβ) hypothesis has dominated the research agenda for the past three decades, recent immunotherapies targeting Aβ have achieved some notable advances. However, their clinical outcomes have remained underwhelming (*2*). This reality compels us to re-examine the pathological underpinnings of AD and to identify novel intervention targets (*3,4*). Against this backdrop, research into endogenous hydrogen sulfide (H_2S) signaling is uncovering a previously overlooked neuroprotective mechanism, offering fresh perspectives on both the fundamental nature of AD and potential therapeutic strategies.

2. A paradigm shift in our understanding of H_2S

For much of its history, H_2S was regarded simply as a foul-smelling toxic gas, and its neurotoxic properties were well documented (*5*). However, a series of landmark studies beginning in the early 2000s fundamentally transformed our view of this molecule. H_2S is now recognized as the third endogenous gasotransmitter, following nitric oxide (NO) and carbon monoxide (CO), and plays indispensable regulatory roles in the cardiovascular, nervous, and immune systems (*6*).

As a researcher with longstanding experience in neurodegenerative diseases, I believe the pivotal breakthrough in H_2S signaling has been the elucidation of its unique signal transduction mechanism: protein persulfidation. Unlike conventional post-translational modifications such as phosphorylation or acetylation (*7*), persulfidation reversibly converts the thiol group (-SH) of cysteine residues to a persulfide group (-SSH), thereby fine-tuning the activity and function of target proteins (*8*). The reversibility of this modification enables cells to

respond rapidly to environmental changes. Persulfides exhibit greater nucleophilicity and reducing capacity than thiols, which makes them a critical line of defense against oxidative stress.

3. The CSE-H_2S-GSK3β-Tau axis

As early as 2002, researchers reported that H_2S levels were significantly reduced in brain tissue of AD patients (*9*). However, the functional significance of this finding remained unclear for many years. In 2021, the research team led by Solomon H. Snyder at Johns Hopkins University published a landmark study in *Proceedings of the National Academy of Sciences*, which systematically elucidated the critical protective mechanisms of H_2S in AD from the perspective of enzyme activity regulation (*10*). This study delineated the molecular cascade linking protein persulfidation to the core pathological processes of AD, providing important theoretical insights into disease pathogenesis.

The key findings of this study can be summarized at three levels. At the level of enzyme activity regulation, wild-type Tau protein directly binds to cystathionine γ-lyase (CSE) and enhances its catalytic activity. In contrast, the AD-associated Tau P301L mutant lacks this binding capacity, leading to a marked reduction in local H_2S production. At the level of signal transduction, H_2S effectively inhibits glycogen synthase kinase 3β (GSK3β) activity by persulfidating critical cysteine residues. In cortical tissue from patients with AD, GSK3β persulfidation is markedly reduced, which in turn promotes Tau hyperphosphorylation, a central molecular event in neurofibrillary tangle formation. At the level of therapeutic intervention, long-term treatment with the slow-releasing H_2S donor Na-GYY4137 led to approximately 50% improvement in both cognitive and motor functions in 3xTg-AD transgenic mice. This treatment was accompanied by a restoration of overall brain persulfidation levels (*10*).

These findings clarify the fundamental nature of H_2S signaling abnormalities in AD. The abnormality does not reflect a simple deficiency of a signaling molecule, but instead indicates a systemic failure of endogenous protective mechanisms. Under normal physiological conditions, neurons continuously generate H_2S *via* CSE to maintain GSK3β in a persulfidated state, thereby suppressing Tau hyperphosphorylation. During the pathological progression of AD, multiple factors act in a coordinated manner, including CSE downregulation, dysfunction of the transsulfuration pathway, and oxidative stress-induced reversal of persulfidation. Together, these changes compromise the protective regulatory circuit and ultimately establish a vicious cycle (Figure 1).

4. Endogenous versus exogenous H_2S

Some have suggested that inhaling H_2S-containing gases or supplementing the diet with sulfur-containing compounds could prevent AD. As a neuroscience researcher, I must state unequivocally that this notion not

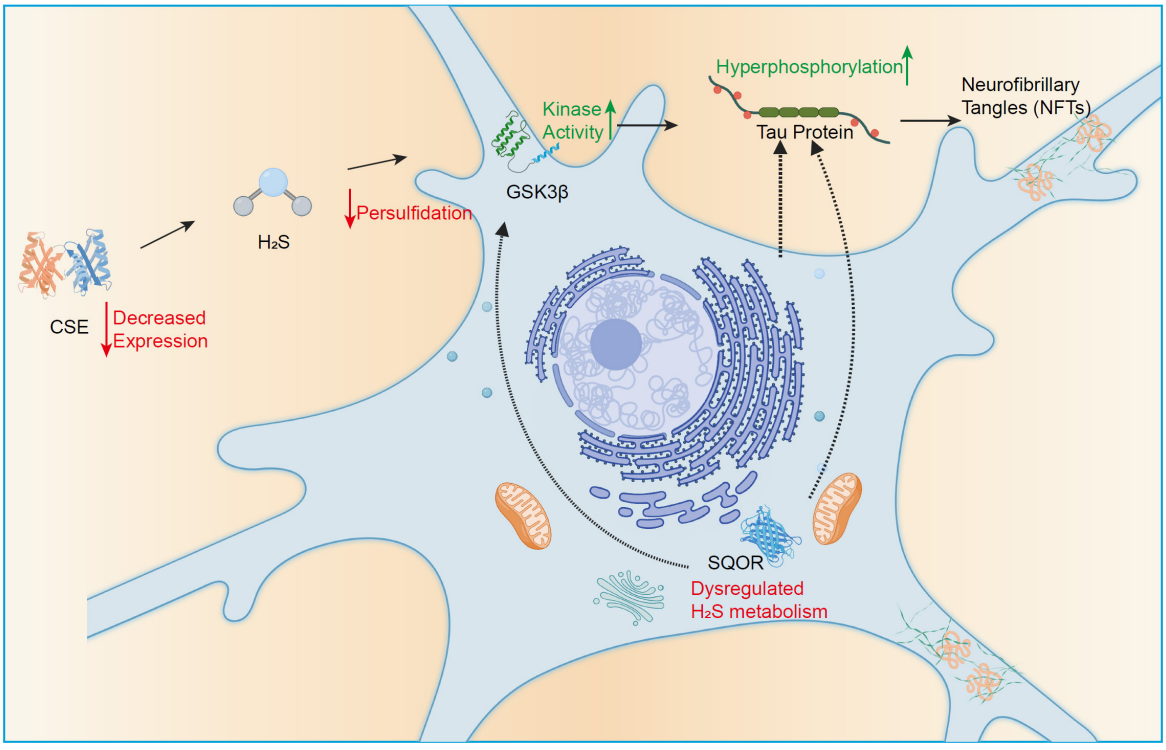

Figure 1. Molecular mechanisms underlying H_2S-mediated neuroprotection and its dysregulation in Alzheimer's disease. CSE: cystathionine γ-lyase; GSK3β, glycogen synthase kinase 3β; SQOR: Sulfide:quinone oxidoreductase.

only lacks scientific support but also risks endangering public safety through misinformation. A strict distinction must be drawn between uncontrolled environmental or dietary exposure and precisely engineered pharmacological donors. The former readily induces toxicity because of its unpredictable concentrations and lack of targeting. The latter, exemplified by GYY4137 and brain-targeted nanomedicines currently under development, is designed to restore endogenous signaling levels and represents an entirely different therapeutic strategy.

Endogenous and exogenous H_2S differ in fundamental ways. First, endogenous H_2S is produced by specific cell types at defined subcellular locations and acts directly on neighboring target proteins (*11,12*). The spatial proximity of CSE to GSK3β is a prerequisite for persulfidation to occur (*10*). Inhaled exogenous H_2S cannot be directionally delivered to specific intraneuronal sites, let alone replicate such precise molecular interactions. Second, H_2S exhibits classic hormesis. At physiological concentrations in the nanomolar to low micromolar range, it exerts robust cytoprotective effects, whereas at higher concentrations it exhibits neurotoxic effects (*13*). According to the U.S. Centers for Disease Control and Prevention (CDC) and the Agency for Toxic Substances and Disease Registry (ATSDR), exposure to 100–150 ppm H_2S causes olfactory fatigue, while concentrations above 500 ppm can induce unconsciousness or death within minutes (*14,15*). Inhalation exposure cannot finely control brain H_2S levels and readily exceeds the narrow physiological window. Third, endogenous H_2S production is dynamically coupled to neural activity and metabolic state, following precise temporal patterns that participate in synaptic plasticity and long-term potentiation (LTP) (*16*). Exogenous exposure cannot replicate this dynamic regulation matched to physiological demand.

Furthermore, it must be stressed that H_2S produced by intestinal sulfate-reducing bacteria is metabolically compartmentalized from brain H_2S signaling. The vast majority of gut-derived H_2S is cleared by sulfide oxidation pathways in the intestinal mucosa and liver; circulating free H_2S concentrations remain exceedingly low and are unlikely to cross the blood-brain barrier (BBB) effectively (*17*). While direct evidence that gut-derived gaseous molecules traverse the BBB into the parenchyma is lacking, whether they indirectly modulate brain function *via* the neuroimmune axis remains an open question. For now, intestinal H_2S should not be regarded as a direct source of cerebral H_2S signaling.

5. A metabolic bridge linking nutritional status to neuroprotection

The homeostasis of H_2S depends not only on local enzyme activity but also on the systemic supply of metabolic substrates. Endogenous H_2S synthesis relies on the transsulfuration pathway. This pathway converts homocysteine (Hcy) to cysteine, which serves as the direct substrate for H_2S production (*18*). Within the cerebrovascular system, multiple cell types utilize cysteine to generate H_2S. Cystathionine β-synthase (CBS) primarily catalyzes H_2S production in the brain parenchyma. CSE serves a similar role in the cerebral microvasculature. In addition, 3-mercaptopyruvate sulfurtransferase (MST) contributes to H_2S biosynthesis in neurons and mitochondria (*19*). Epidemiological evidence has established hyperhomocysteinemia as an independent risk factor for AD. The early Framingham Study reported that each 5 μmol/L increase in plasma Hcy was associated with an approximately 40% higher risk of AD (*20,21*). More recent meta-analyses, however, suggest a more modest risk increase of about 12%–15% (*22,23*).

From a metabolic integration perspective, the significance of this association extends well beyond statistical correlation. Efficient operation of the transsulfuration pathway requires the coordinated participation of several B vitamins. Folate and vitamin B(12) serve as essential cofactors for Hcy remethylation (*24*). Vitamin B6, in its active form pyridoxal 5'-phosphate, functions as a coenzyme for both CBS and CSE (*25*). It therefore directly participates in the enzymatic synthesis of H_2S (*26,27*). Consequently, reduced enzyme activity caused by nutritional deficiency leads to the accumulation of Hcy. It also impairs transsulfuration efficiency and thereby limits the capacity for H_2S production. Clinical intervention studies support this mechanism. In individuals with elevated Hcy levels, B vitamins supplementation effectively slows brain atrophy and cognitive decline (*28*). By contrast, such interventions show limited efficacy in those with normal Hcy levels. This seemingly paradoxical observation in fact reinforces a fundamental principle of precision medicine. Metabolic interventions should be tailored to individuals with demonstrable metabolic abnormalities rather than applied indiscriminately across populations.

6. Mitochondrial function and H_2S homeostasis

Mitochondria serve not only as the central hub of cellular energy metabolism but also as a critical node in H_2S metabolic regulation (*29,30*). Sulfide:quinone oxidoreductase (SQOR), located on the inner mitochondrial membrane, is the key enzyme catalyzing H_2S oxidation (*31*). Its reaction product, persulfide, possesses important endogenous antioxidant properties (*32*). Under physiological conditions, H_2S helps maintain mitochondrial membrane potential and suppresses excessive accumulation of reactive oxygen species (ROS). In doing so, it attenuates oxidative stress and bioenergetic impairment and preserves mitochondrial functional homeostasis (*33*).

Studies targeting mitochondrial H_2S delivery further support its protective role. Mitochondria-targeted H_2S

donors such as AP39 have been shown to enhance cellular energy production, improve cell viability, and exert protective effects on mitochondrial DNA (*34*). From a clinical genetics standpoint, mutations in the SQOR gene cause Leigh syndrome, a severe mitochondrial encephalopathy characterized by abnormal H_2S accumulation and pronounced mitochondrial dysfunction (*35*). This observation underscores that dysregulated H_2S oxidation per se can inflict serious damage on the nervous system.

The mitochondrial dysfunction prevalent in AD may affect SQOR activity and alter H_2S metabolic flux. These changes may disrupt H_2S clearance and utilization and thereby contribute to early pathological processes in the disease (*36*). This bidirectional interaction between mitochondrial function and H_2S metabolism likely represents an incompletely characterized metabolic node in neurodegeneration and warrants further systematic investigation.

7. Future research directions

At present, we lack reliable indicators capable of assessing individual "H_2S signaling status" at the clinical level. Developing biomarker panels in blood or cerebrospinal fluid that reflect cerebral H_2S metabolic status is a prerequisite for early diagnosis and precision intervention (*37*). Recent advances in persulfidome technologies have laid the methodological groundwork for achieving this goal (*38*). The precise transcriptional and translational regulators underlying CSE downregulation in AD remain unclear. Elucidating these mechanisms will not only deepen our understanding of pathological progression but may also reveal actionable nodes. For example, enabling the development of small-molecule CSE activators or expression inducers. Given the challenges associated with systemic administration of exogenous H_2S, including concentration control and targeted delivery, delivery systems targeted to the brain that enable slow release and can cross the BBB represent a promising translational strategy.. Existing donors such as GYY4137 have shown encouraging results in animal models, yet substantial work remains for translation from animals to humans (*39*). The preventive efficacy of metabolic interventions, including B vitamins and *N*-acetylcysteine (NAC), in high-risk populations urgently requires validation in large-scale clinical trials. Such interventions are low-cost and safe; if proven effective, they would carry major public health significance. Although this editorial focuses on Tau pathology, H_2S's potential interference with Aβ aggregation and its regulation of neuroinflammation mediated by microglia are equally worthy of attention (*40*). How does H_2S metabolism in neurons, astrocytes, and microglia change respectively in AD? How do their H_2S signaling networks interact? Answering these questions will require the application of emerging technologies such as single-cell omics and spatial omics (*41*).

8. Conclusion

Research on endogenous H_2S signaling pathways is revealing a previously neglected dimension of neuroprotective mechanisms. The essence of H_2S signaling dysregulation in AD is not a simple deficiency of a signaling molecule that can be corrected by exogenous supplementation; rather, it represents the systemic collapse of an endogenous protective apparatus. A scientifically accurate understanding of this fundamental distinction is critical for avoiding public misconceptions, safeguarding public health, and guiding research priorities. We propose adopting an integrative perspective that encompasses transsulfuration metabolism, mitochondrial function, and cell-type specificity. By combining this approach with novel methodologies such as persulfidome profiling and single-cell technologies, we anticipate breakthrough progress in the early intervention and prevention of AD. The establishment of this new paradigm not only expands the boundaries of our understanding of AD pathogenesis but also provides fresh strategic avenues for the prevention and treatment of neurodegenerative diseases in the era of precision medicine.

Funding: This work was supported by a grant from the Hainan Province Postdoctoral Research Project, the Grants-in-Aid from the Ministry of Education, Culture, Sports, Science and Technology of Japan (24K14216) and the National Natural Science Foundation of China (No. 82460268).

Conflict of Interest: The authors have no conflicts of interest to disclose.

References

1. Ma YN, Wang Z, Tang W. Deep cervical lymphaticovenous anastomosis in Alzheimer's disease: A promising frontier or premature enthusiasm? Biosci Trends. 2025; 19:144-149.
2. Gu X, Qi L, Qi Q, Zhou J, Chen S, Wang L. Monoclonal antibody therapy for Alzheimer's disease focusing on intracerebral targets. Biosci Trends. 2024; 18:49-65.
3. Masters CL, Bateman R, Blennow K, Rowe CC, Sperling RA, Cummings JL. Alzheimer's disease. Nat Rev Dis Primers. 2015; 1:15056.
4. Ma YN, Hu X, Karako K, Song P, Tang W, Xia Y. Exploring the multiple therapeutic mechanisms and challenges of mesenchymal stem cell-derived exosomes in Alzheimer's disease. Biosci Trends. 2024; 18:413-430.
5. Jin YQ, Yuan H, Liu YF, Zhu YW, Wang Y, Liang XY, Gao W, Ren ZG, Ji XY, Wu DD. Role of hydrogen sulfide in health and disease. MedComm (2020). 2024; 5:e661.
6. Wang R. Physiological implications of hydrogen sulfide: A whiff exploration that blossomed. Physiol Rev. 2012; 92:791-896.

7. Kim JS, Cho Y, Lee J, *et al.* N(5)-((perfluorophenyl) amino)glutamine regulates BACE1, tau phosphorylation, synaptic function, and neuroinflammation in Alzheimer's disease models. Biosci Trends. 2025; 19:102-115.
8. Paul BD, Snyder SH. H_2S signalling through protein sulfhydration and beyond. Nat Rev Mol Cell Biol. 2012; 13:499-507.
9. Eto K, Asada T, Arima K, Makifuchi T, Kimura H. Brain hydrogen sulfide is severely decreased in Alzheimer's disease. Biochem Biophys Res Commun. 2002; 293:1485-1488.
10. Giovinazzo D, Bursac B, Sbodio JI, Nalluru S, Vignane T, Snowman AM, Albacarys LM, Sedlak TW, Torregrossa R, Whiteman M, Filipovic MR, Snyder SH, Paul BD. Hydrogen sulfide is neuroprotective in Alzheimer's disease by sulfhydrating GSK3beta and inhibiting Tau hyperphosphorylation. Proc Natl Acad Sci U S A. 2021; 118:e2017225118.
11. Filipovic MR, Zivanovic J, Alvarez B, Banerjee R. Chemical biology of H_2S signaling through persulfidation. Chem Rev. 2018; 118:1253-1337.
12. Rimnacova H, Moravec J, Stiavnicka M, Havrankova J, Monsef L, Hosek P, Prokesova S, Zalmanova T, Fenclova T, Petr J, Kralickova M, Nevoral J. Evidence of endogenously produced hydrogen sulfide (H_2S) and persulfidation in male reproduction. Sci Rep. 2022; 12:11426.
13. Yang G, Wang R. H_2S and blood vessels: An overview. Handb Exp Pharmacol. 2015; 230:85-110.
14. Agency for Toxic Substances and Disease Registry (ATSDR). Toxicological profile for hydrogen sulfide and carbonyl sulfide. Atlanta, GA: U.S. Department of Health and Human Services; 2016.
15. Centers for Disease Control and Prevention, National Institute for Occupational Safety and Health. NIOSH pocket guide to chemical hazards: Hydrogen sulfide. 2023. *https://www.cdc.gov/niosh/npg/npgd0337.html* (accessed December 16, 2025).
16. Munteanu C, Galaction AI, Onose G, Turnea M, Rotariu M. Hydrogen sulfide (H_2S- or H_2S_n-polysulfides) in synaptic plasticity: Modulation of NMDA receptors and neurotransmitter release in learning and memory. Int J Mol Sci. 2025; 26:3131.
17. Singh SB, Lin HC. Hydrogen sulfide in physiology and diseases of the digestive tract. Microorganisms. 2015; 3:866-889.
18. Kamat PK, Kyles P, Kalani A, Tyagi N. Hydrogen sulfide ameliorates homocysteine-induced Alzheimer's disease-like pathology, blood-brain barrier disruption, and synaptic disorder. Mol Neurobiol. 2016; 53:2451-2467.
19. Sharif AH, Iqbal M, Manhoosh B, Gholampoor N, Ma D, Marwah M, Sanchez-Aranguren L. Hydrogen sulphide-based therapeutics for neurological conditions: Perspectives and challenges. Neurochem Res. 2023; 48:1981-1996.
20. Smith AD, Refsum H. Homocysteine, B vitamins, and cognitive impairment. Annu Rev Nutr. 2016; 36:211-239.
21. Seshadri S, Beiser A, Selhub J, Jacques PF, Rosenberg IH, D'Agostino RB, Wilson PW, Wolf PA. Plasma homocysteine as a risk factor for dementia and Alzheimer's disease. N Engl J Med. 2002; 346:476-483.
22. Zhou F, Chen S. Hyperhomocysteinemia and risk of incident cognitive outcomes: An updated dose-response meta-analysis of prospective cohort studies. Ageing Res Rev. 2019; 51:55-66.
23. Wang Q, Zhao J, Chang H, Liu X, Zhu R. Homocysteine and folic acid: Risk factors for Alzheimer's disease-An updated meta-analysis. Front Aging Neurosci. 2021; 13:665114.
24. Froese DS, Fowler B, Baumgartner MR. Vitamin B(12) , folate, and the methionine remethylation cycle-biochemistry, pathways, and regulation. J Inherit Metab Dis. 2019; 42:673-685.
25. Gregory JF, DeRatt BN, Rios-Avila L, Ralat M, Stacpoole PW. Vitamin B6 nutritional status and cellular availability of pyridoxal 5'-phosphate govern the function of the transsulfuration pathway's canonical reactions and hydrogen sulfide production *via* side reactions. Biochimie. 2016; 126:21-26.
26. Martinez M, Cuskelly GJ, Williamson J, Toth JP, Gregory JF, 3rd. Vitamin B-6 deficiency in rats reduces hepatic serine hydroxymethyltransferase and cystathionine beta-synthase activities and rates of *in vivo* protein turnover, homocysteine remethylation and transsulfuration. J Nutr. 2000; 130:1115-1123.
27. DeRatt BN, Ralat MA, Kabil O, Chi YY, Banerjee R, Gregory JF, 3rd. Vitamin B-6 restriction reduces the production of hydrogen sulfide and its biomarkers by the transsulfuration pathway in cultured human hepatoma cells. J Nutr. 2014; 144:1501-1508.
28. Douaud G, Refsum H, de Jager CA, Jacoby R, Nichols TE, Smith SM, Smith AD. Preventing Alzheimer's disease-related gray matter atrophy by B-vitamin treatment. Proc Natl Acad Sci U S A. 2013; 110:9523-9528.
29. Star BS, van der Slikke EC, Ransy C, Schmitt A, Henning RH, Bouillaud F, Bouma HR. GYY4137-derived hydrogen sulfide donates electrons to the mitochondrial electron transport chain *via* sulfide: Quinone oxidoreductase in endothelial cells. Antioxidants (Basel). 2023; 12:587.
30. Murphy B, Bhattacharya R, Mukherjee P. Hydrogen sulfide signaling in mitochondria and disease. FASEB J. 2019; 33:13098-13125.
31. Peng MH, Zhang KL, Ma ZW, Zhang HW, Guan SW, Yu HB. SQOR as a metabolic rheostat of H_2S: Structure, redox homeostasis, and disease therapy. Front Cell Dev Biol. 2025; 13:1685252.
32. Yang CT, Devarie-Baez NO, Hamsath A, Fu XD, Xian M. S-Persulfidation: Chemistry, chemical biology, and significance in health and disease. Antioxid Redox Signal. 2020; 33:1092-1114.
33. Zhou L, Wang Q. Advances of H_2S in regulating neurodegenerative diseases by preserving mitochondria function. Antioxidants (Basel). 2023; 12:652.
34. Zhao FL, Fang F, Qiao PF, Yan N, Gao D, Yan Y. AP39, a mitochondria-targeted hydrogen sulfide donor, supports cellular bioenergetics and protects against Alzheimer's disease by preserving mitochondrial function in APP/PS1 mice and neurons. Oxid Med Cell Longev. 2016; 2016:8360738.
35. Friederich MW, Elias AF, Kuster A, *et al.* Pathogenic variants in SQOR encoding sulfide:quinone oxidoreductase are a potentially treatable cause of Leigh disease. J Inherit Metab Dis. 2020; 43:1024-1036.
36. Paul BD, Pieper AA. Protective roles of hydrogen sulfide in Alzheimer's disease and traumatic brain injury. Antioxidants (Basel). 2023; 12:1095.
37. Hu S, Yu H, Gao J. The pTau217/$A\beta_{1-42}$ plasma ratio: The first FDA-cleared blood biomarker test for diagnosis of Alzheimer's disease. Drug Discov Ther. 2025; 19:208-209.

38. Zivanovic J, Kouroussis E, Kohl JB, *et al.* Selective persulfide detection reveals evolutionarily conserved antiaging effects of s-sulfhydration. Cell Metab. 2019; 30:1152-1170 e1113.
39. Li L, Whiteman M, Guan YY, Neo KL, Cheng Y, Lee SW, Zhao Y, Baskar R, Tan CH, Moore PK. Characterization of a novel, water-soluble hydrogen sulfide-releasing molecule (GYY4137): New insights into the biology of hydrogen sulfide. Circulation. 2008; 117:2351-2360.
40. Munteanu C, Turnea MA, Rotariu M. Hydrogen sulfide: An emerging regulator of oxidative stress and cellular homeostasis-A comprehensive one-year review. Antioxidants (Basel). 2023; 12:1737.
41. Ma YN, Xia Y, Karako K, Song P, Tang W, Hu X. Decoding Alzheimer's disease: Single-cell sequencing uncovers brain cell heterogeneity and pathogenesis. Mol Neurobiol. 2025; 62:14459-14473.

Received January 20, 2026; Revised February 5, 2026; Accepted February 5, 2026.

**Address correspondence to:*
Xiqi Hu, Department of Neurosurgery, Integrated Neuroscience Center, Geriatric Hospital of Hainan, Haikou 570300, China.
E-mail: 218302048@csu.edu.cn

Released online in J-STAGE as advance publication February 8, 2026.

Mini-Review

DOI: 10.5582/ddt.2025.01129

Potworm (*Enchytraeus japonensis*) as a potential platform for drug screening in regenerative medicine

Toshiyuki Fujita, Shinji Yamaguchi*

Department of Biological Sciences, Faculty of Pharmaceutical Sciences, Teikyo University, Tokyo, Japan.

SUMMARY: Regenerative medicine holds substantial promise for restoring the function of damaged or lost organs and tissues. However, the development of effective small-molecule drugs in this field has been limited, partially owing to the lack of suitable regenerative animal models for drug discovery. *Enchytraeus japonensis*, a small annelid with exceptional regenerative capacity, is emerging as a valuable model for regeneration research. *E. japonensis* regenerates in a shorter period, in only 4 days, than other major regenerative animal models. Moreover, novel experimental systems have recently been developed to enhance the utility of *E. japonensis*, including a soaking RNA interference system for easy, non-invasive gene knockdown, an imaging system for quantifying cell distribution in the blastema, and soaking-based pharmacological inhibition using small-molecule compounds. This review highlights *E. japonensis* as a potential platform for chemical screening in regenerative medicine.

Keywords: regeneration, blastema, annelid, chemical screening, RNA interference

1. Introduction

"Regenerative medicine replaces or regenerates human cells, tissues, or organs to restore or establish normal function" (*1*). This approach is often based on the principles of stem cell technology and tissue engineering (*2*). For instance, recombinant human growth factors have been used as biopharmaceuticals to promote fibroblast proliferation during wound healing (*3*). However, only a limited number of effective small-molecule compounds have been developed, and one reason for this is the lack of suitable regenerative animal models for drug discovery. Therefore, model systems that are easy to use and effective for chemical screening, such as nematodes (*4*) and silkworms (*5*), are required in the field of regenerative medicine.

Annelids, including earthworms, ragworms, and leeches, exhibit remarkable regenerative capacity (*6*). The potworm (*Enchytraeus*) is a small annelid species measuring approximately 1 cm in size that is typically found in garden plant pots. The genus *Enchytraeus* derives from the Greek words *en* ("in") and *chytra* ("pot") (*7*). When some potworms are cut transversely, undifferentiated proliferative cell masses named "blastemas" form at the cut ends, which serve as the material for regenerating lost organs, mirroring the regenerative phenomena observed in many living organisms (*6*). This review discusses the utility of potworms in regeneration research and explores their potential applications as chemical screening platforms for regenerative medicine.

2. *Enchytraeus japonensis* as a regenerative animal model

Annelid species such as *Pristina leidyi* (freshwater annelid), *Capitella teleta* (marine annelid), and *Platynereis dumerilii* (marine annelid) have been extensively used as model annelids for studying regeneration (*6*). In some annelids, pharmacological inhibition using small-molecule inhibitors has been used to investigate various biological processes, such as key signaling pathways. For example, Wnt/β-catenin signaling has been studied during regeneration in *Capitella teleta* (*8*), *Aeolosoma viride* (*9-11*), and *Lumbriculus variegatus* (*12*) and during development in *Platynereis dumerilii* (*13-16*). Because these pharmacological studies employed the soaking method, annelids offer the advantage of a technically simple model that can be used to study regeneration in living organisms.

Enchytraeus japonensis (a Japanese potworm) was first reported in Japan in 1993 (*17*) and has since been developed as an experimental model for regeneration research (*18-31*). In laboratory settings, *E. japonensis* can be easily maintained on agar plates at 24°C with

powdered oatmeal used as a food source. Its body length is approximately 1 cm (Figure 1A), facilitating easy handling. Once matured, it asexually reproduces by fragmenting its body; however, sexual reproduction can be induced under specific culture conditions (*18*). Its body surface is whitish and semi-transparent, enabling the direct visualization of internal structures, including the brain, pharynx, testes, ovaries, intestine, and ventral nerve cord. Upon transverse amputation, *E. japonensis* completes blastema formation within 24 h and achieves full regeneration within four days (*18*). Compared to other regeneration model organisms, *E. japonensis* exhibits faster blastema formation (~1 day versus ~2 weeks in axolotl (*32*) and ~2 days in zebrafish (*33*)) and has a smaller body size (~1 cm in length versus 30 cm for axolotl (*34*) and ~4 cm for zebrafish (*33*)). Collectively, these features make *E. japonensis* a powerful model system for investigating the cellular and molecular basis underlying blastema formation.

Invertebrate blastema models, including the potworm blastema, may appear relatively simple compared with the cellular behaviors underlying organ regeneration in vertebrates such as zebrafish. However, recent advances in single-cell analysis now make it possible to directly compare cellular homology and similarity even between evolutionarily distant organisms (*35*). Consequently,

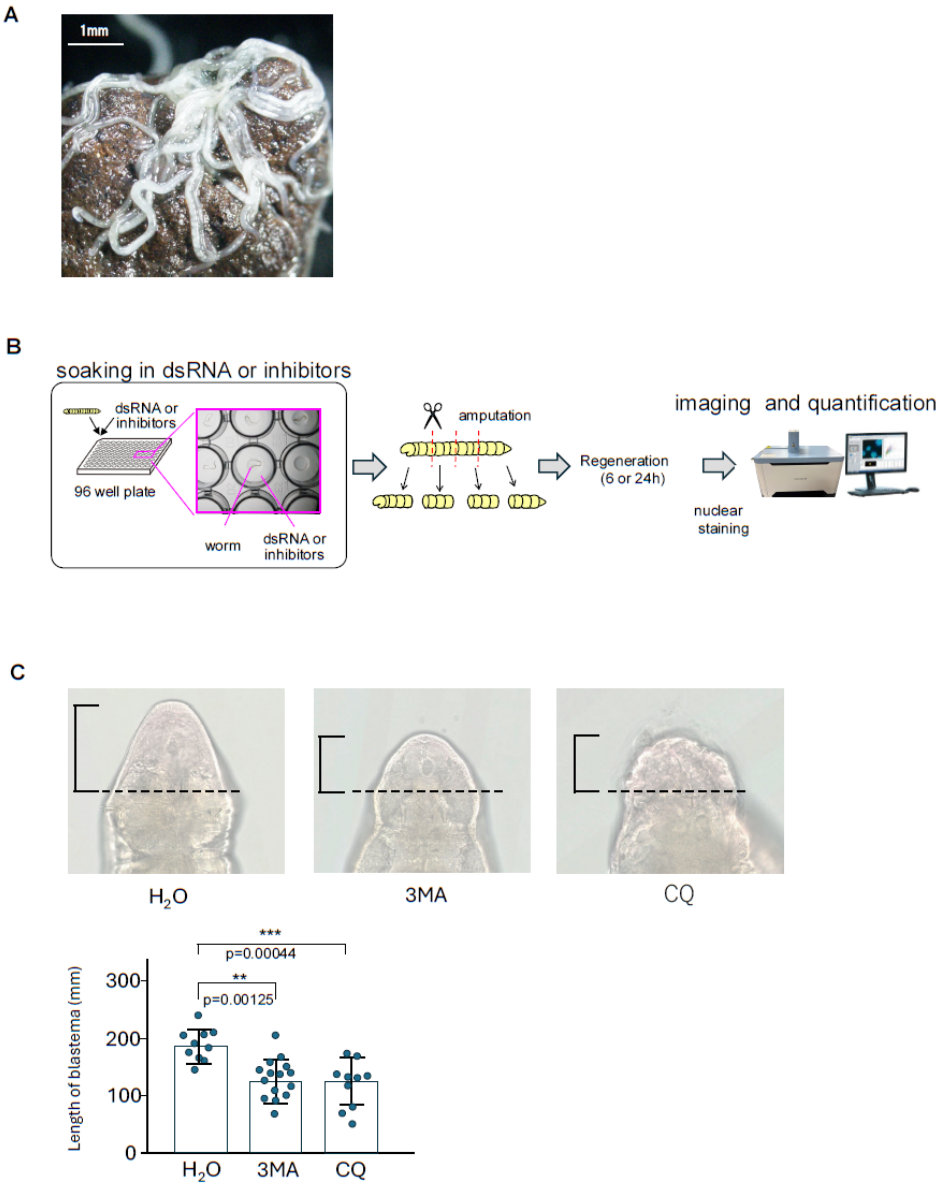

Figure 1. (**A**) Photograph showing multiple *E. japonensis* potworms. (**B**) Schematic illustration of recent experimental systems developed for regeneration research using *E. japonensis*: (1) A soaking RNAi system, (2) an imaging system for quantitative analysis of cell distribution, and (3) a soaking chemical inhibition system. These systems have enhanced the utility of *E. japonensis* as an animal model for regenerative research. (**C**) Example of a soaking chemical inhibition system. The autophagy inhibitors 3-methyladenine (3MA; 100 μM) and chloroquine diphosphate (CQ; 100 μM) were used. Both treatments reduced blastema length, indicating that pharmacological inhibition with both 3MA and CQ using this system was effective in *E. japonensis*. Brackets indicate blastema length. Dotted lines indicate the amputation sites. The bars and the error bars in the graph indicate the mean and standard deviation (SD), respectively. *$p < 0.05$, **$p < 0.01$, ***$p < 0.001$ (Dunnett's test). dsRNA: double-stranded RNA.

future studies could clarify which vertebrate regenerative or developmental processes the potworm blastema model most closely resembles, and which cell types can serve as useful models. In this context, the simplicity of the potworm system and its amenability to quantitative analysis are expected to offer substantial advantages, thereby advancing our understanding of these processes. A comparison of key features among regeneration model organisms is summarized in Table 1.

3. Recent advances in experimental systems for regeneration research using *E. japonensis*

Recently, *SoxC*-expressing cells were demonstrated to play an important role as the cellular basis, and *mmpReg* is a key molecular basis for blastema formation in *E. japonensis.* Three experimental systems were developed in this study: (1) a soaking RNA interference (RNAi) system, (2) an imaging system for the quantitative analysis of cell distribution, and (3) a soaking chemical inhibition system. These advances have enhanced the utility of *E. japonensis* as a regenerative animal model.

3.1. Soaking RNAi system

The first RNAi study in *E. japonensis* employed microinjection of double-stranded RNA (dsRNA) (*27*). Although this system was effective, it was also complex and invasive. A recently developed soaking RNAi system overcomes these issues (*31*). In this system, worms were immersed in dsRNA solution in a 96-well plate for 24 h, followed by amputation and quantitative polymerase chain reaction (qPCR) analysis. For instance, treating worms with *soxC* dsRNA reduced *soxC* expression levels by approximately 40% compared to that in worms treated with *GFP* dsRNA as a negative control. Similarly, qPCR analysis revealed that treatment with *mmpReg* dsRNA reduced *mmpReg* expression levels by 50%. Notably, this soaking RNAi system is particularly advantageous because it provides a straightforward, easily reproducible, and minimally invasive method for inducing gene knockdown in *E. japonensis*.

3.2. Imaging system for quantitative analysis of cell distribution within the blastema

A simple cell quantification system is useful for measuring cell proliferation and accumulation. Fujita *et al*. (2024) developed such a system for *E. japonensis* (*31*). In this system, intact worms were first treated with dsRNA using a soaking method, followed by amputation to initiate regeneration. Regenerated blastemas were sampled over time, and their nuclei were stained with 4',6-diamidino-2-phenylindole (DAPI) and subsequently analyzed using an image cytometer CQ-1 (Yokogawa). The number of nuclei in the blastemas was quantified using the CellPathwayFinder software (Yokogawa). This system has enabled the evaluation of the effects of RNAi on blastema formation. For instance, under *soxC* RNAi conditions, analysis of blastema size and cell number at 6 and 24 h post-amputation revealed a reduction in blastema size, accompanied by a marked decrease in cell number (~30% at 6 h; ~45% at 24 h) (*31*) (Figure 1B). Similarly, soaking RNAi was used to knock down *mmpReg* during blastema formation, resulting in reduced blastema size and decreased cell numbers at 6 and 24 h post-amputation (~ 40% at 6 h; ~ 40% at 24 h) (*31*) (Figure 1B). Therefore, these results indicate that *soxC* and *mmpReg* are essential for blastema formation (*31*). Overall, this imaging system enables robust and reproducible quantification of blastema cell distribution.

3.3. Pharmaceutical inhibition in *E. japonensis*

Similar to other annelids, pharmacological inhibition using the soaking method is also effective in *E. japonensis*. For example, treatment with a metalloproteinase inhibitor (MMP2/MMP9 inhibitor

Table 1. Comparison of features among regeneration model organisms

	Potworm	Nematode	Zebrafish	Salamander
Regenerative organs	whole-body	axons	heart, fins, spinal cord, retina, *etc.*	tail, limbs, spinal cord, heart, *etc.*
Compatibility with 96-well plate	Yes	Yes	No	No
Manual/automated operation	possible	possible	possible	possible
Cost (money and space)	small	small	moderate	moderate
Genetic homogeneity	high (clone)	high (clone)	high (inbred strain available)	not high (inbred strain not available)
Functional genetics	RNAi only	Many approaches established	Many approaches established	Many approaches established
phylogenetic proximity to humans	distant	distant	intermediate	intermediate

RNAi: RNA interference.

I; *N*-([1,1′-biphenyl]-4-ylsulfonyl)-D-phenylalanine) *via* the soaking method reduced blastema size (*31*). The resulting phenotype was identical to that obtained by RNAi-mediated gene silencing, highlighting the effectiveness of this approach (*31*). Another example is the use of the small-molecule autophagy inhibitors 3-methyladenine (3MA) and chloroquine diphosphate (CQ). Worms were immersed in water containing 3MA or CQ, and blastema length was measured two days post-amputation (Figure 1C). In both treatments, blastema length was reduced, indicating that pharmacological inhibition using both 3MA and CQ was effective in *E. japonensi*s. Thus, this demonstrates that the effects of chemical inhibitors can be easily assessed in *E. japonensis*.

4. Future perspectives

This review highlights the utility and recent advances in experimental systems using *E. japonensis* in regeneration research. First, a soaking RNAi system was developed that provides a simple, reproducible, and minimally invasive method for inducing gene knockdown in *E. japonensis*. Second, an imaging system was established to quantitatively analyze cell distribution within the blastema following dsRNA exposure, enabling efficient measurement of changes in cell number in the blastema (*31*). Third, pharmacological inhibition using the soaking method was effective in *E. japonensis*, offering a technically simple approach. Collectively, these systems enhanced the utility of *E. japonensis* as a regenerative animal model. Specifically, combining the imaging system with soaking-based pharmacology can be used to screen for chemical compounds that modulate cell numbers during blastema formation (Figure 1B). Importantly, by combining the soaking RNAi system with pharmacological inhibition may enable preliminary genetic-level investigations into the relevant signaling pathways and the mechanisms of action of the identified compounds. Similarly, although genomic annotation remains incomplete, transcriptomic approaches integrated with pharmacological inhibition may facilitate informative preliminary studies of compound mechanisms of action. Overall, *E. japonensis* could serve as a regenerative animal model for screening chemical compounds in regenerative medicine.

Acknowledgements

We thank the anonymous reviewer(s) for their constructive comments and suggestions, which have greatly helped us improve our manuscript. We also thank Editage (*www.editage.com*) for English language editing.

Funding: This study was supported by a Teikyo University Research Encouragement Grant (T.F.), ACRO Team Research Grants of Teikyo University (T.F., S.Y.), ACRO incubation Grant of Teikyo University (T.F., S.Y), The research foundation for Pharmaceutical Sciences (RFPS) (T.F.), a Fund for the Promotion of Joint International Research (Fostering Joint International Research [B]) (T. F.), Grants-in-Aid for Scientific Research from the Japan Society for the Promotion of Science (S.Y., 15K07945, 18K06667, 21K06535, 25K09943).

Conflict of Interest: The authors have no conflicts of interest to disclose.

References

1. Mason C, Dunnill P. A brief definition of regenerative medicine. Regen Med. 2008; 3:1-5.
2. Mao AS, Mooney DJ. Regenerative medicine: Current therapies and future directions. Proc Natl Acad Sci U S A. 2015; 112:14452-14459.
3. Tanaka E, Ase K, Okuda T, Okumura M, Nogimori K. Mechanism of acceleration of wound healing by basic fibroblast growth factor in genetically diabetic mice. Biol Pharm Bull. 1996; 19:1141-1148.
4. Jones AK, Buckingham SD, Sattelle DB. Chemistry-to-gene screens in Caenorhabditis elegans. Nat Rev Drug Discov. 2005; 4:321-330.
5. Ishii M, Matsumoto Y, Nakamura I, Sekimizu K. Silkworm fungal infection model for identification of virulence genes in pathogenic fungus and screening of novel antifungal drugs. Drug Discov Ther. 2017; 11:1-5.
6. Ozpolat BD, Bely AE. Developmental and molecular biology of annelid regeneration: a comparative review of recent studies. Curr Opin Genet Dev. 2016; 40:144-153.
7. Henle FGJ. Ueber Enchytraeus, eine neue Anneliden-Gattung. Müllers Archiv für Anatomie, Physiologie und Wissenschaftliche Medizin, Berlin. 1837; 74-90.
8. Kunselman LF, Seaver EC. Wnt/beta-catenin signaling promotes posterior axial regeneration in non-regenerative tissue of the annelid Capitella teleta. Dev Biol. 2025; 525:26-43.
9. Chen CP, Fok SK, Chen CY, Hsu FM, Hsieh YW, Chen JH. Studying Annelida Regeneration in a Novel Model Organism: The Freshwater Aeolosoma viride. Methods Mol Biol. 2022; 2450:179-194.
10. Fok SK, Chen CP, Tseng TL, Chiang YH, Chen JH. Caspase dependent apoptosis is required for anterior regeneration in Aeolosoma viride and its related gene expressions are regulated by the Wnt signaling pathway. Sci Rep. 2020; 10:10692.
11. Chen CY, Yueh WT, Chen JH. Canonical Wnt Signaling is Involved in Anterior Regeneration of the Annelid Aeolosoma viride. bioRxiv. 2020.
12. Tellez-Garcia AA, Arellano-Carbajal F. Wnt/beta-catenin signaling pathway regulates the regeneration of the annelid Lumbriculus variegatus. Gene Expr Patterns. 2025; 56:119403.
13. Steinmetz PR, Zelada-Gonzales F, Burgtorf C, Wittbrodt J, Arendt D. Polychaete trunk neuroectoderm converges and extends by mediolateral cell intercalation. Proc Natl Acad Sci U S A. 2007; 104:2727-2732.
14. Schneider SQ, Bowerman B. beta-Catenin asymmetries after all animal/vegetal- oriented cell divisions in Platynereis dumerilii embryos mediate binary cell-fate

specification. Dev Cell. 2007; 13:73-86.
15. Demilly A, Steinmetz P, Gazave E, Marchand L, Vervoort M. Involvement of the Wnt/beta-catenin pathway in neurectoderm architecture in Platynereis dumerilii. Nat Commun. 2013; 4:1915.
16. Zidek R, Machon O, Kozmik Z. Wnt/beta-catenin signalling is necessary for gut differentiation in a marine annelid, Platynereis dumerilii. Evodevo. 2018; 9:14.
17. Nakamura Y. A new fragmenting enchytraeid species, Enchytraeus japonensis from a cropped Kuroboku soil in Fukushima, Northern Japan (enchytraeids in Japan 5). Edaphologia 1993; 50:37-39.
18. Myohara M, Yoshida-Noro C, Kobari F, Tochinai S. Fragmenting oligochaete Enchytraeus japonensis: a new material for regeneration study. Dev Growth Differ. 1999; 41:549-555.
19. Yoshida-Noro C, Myohara M, Kobari F, Tochinai S. Nervous system dynamics during fragmentation and regeneration in Enchytraeus japonensis (Oligochaeta, Annelida). Dev Genes Evol. 2000; 210:311-319.
20. Kawamoto S, Yoshida-Noro C, Tochinai S. Bipolar head regeneration induced by artificial amputation in Enchytraeus japonensis (Annelida, Oligochaeta). J Exp Zool A Comp Exp Biol. 2005; 303:615-627.
21. Miyachi Y, Kanao T, Okamoto T. Low dose beta-emitter source induces sexual reproduction instead of fragmentation in an earthworm, Enchytraeus japonensis. J Environ Radioact. 2005; 79:1-5.
22. Myohara M, Niva CC, Lee JM. Molecular approach to annelid regeneration: cDNA subtraction cloning reveals various novel genes that are upregulated during the large-scale regeneration of the oligochaete, Enchytraeus japonensis. Dev Dyn. 2006; 235:2051-2070.
23. Tadokoro R, Sugio M, Kutsuna J, Tochinai S, Takahashi Y. Early segregation of germ and somatic lineages during gonadal regeneration in the annelid Enchytraeus japonensis. Curr Biol. 2006; 16:1012-1017.
24. Niva CC, Lee JM, Myohara M. Glutamine synthetase gene expression during the regeneration of the annelid Enchytraeus japonensis. Dev Genes Evol. 2008; 218:39-46.
25. Sugio M, Takeuchi K, Kutsuna J, Tadokoro R, Takahashi Y, Yoshida-Noro C, Tochinai S. Exploration of embryonic origins of germline stem cells and neoblasts in Enchytraeus japonensis (Oligochaeta, Annelida). Gene Expr Patterns. 2008; 8:227-236.
26. Takeo M, Yoshida-Noro C, Tochinai S. Morphallactic regeneration as revealed by region-specific gene expression in the digestive tract of Enchytraeus japonensis (Oligochaeta, Annelida). Dev Dyn. 2008; 237:1284-1294.
27. Takeo M, Yoshida-Noro C, Tochinai S. Functional analysis of grimp, a novel gene required for mesodermal cell proliferation at an initial stage of regeneration in Enchytraeus japonensis (Enchytraeidae, Oligochaete). Int J Dev Biol. 2010; 54:151-160.
28. Yoshida-Noro C, Tochinai S. Stem cell system in asexual and sexual reproduction of Enchytraeus japonensis (Oligochaeta, Annelida). Dev Growth Differ. 2010; 52:43-55.
29. Sugio M, Yoshida-Noro C, Ozawa K, Tochinai S. Stem cells in asexual reproduction of Enchytraeus japonensis (Oligochaeta, Annelid): proliferation and migration of neoblasts. Dev Growth Differ. 2012; 54:439-450.
30. Ogawa S, Mizuno M, Suzuki M, Goto K, Hirose Y, Matsuda A, Saito T, Oguri S, Furukawa K. Isolation of a methylated mannose-binding protein from terrestrial worm Enchytraeus japonensis. Glycoconj J. 2017; 34:591-601.
31. Fujita T, Aoki N, Mori C, Homma KJ, Yamaguchi S. SoxC and MmpReg promote blastema formation in whole-body regeneration of fragmenting potworms Enchytraeus japonensis. Nat Commun. 2024; 15:6659.
32. Joven A, Elewa A, Simon A. Model systems for regeneration: salamanders. Development. 2019; 146.
33. Gemberling M, Bailey TJ, Hyde DR, Poss KD. The zebrafish as a model for complex tissue regeneration. Trends Genet. 2013; 29:611-620.
34. Masselink W, Tanaka EM. Toward whole tissue imaging of axolotl regeneration. Dev Dyn. 2021; 250:800-806.
35. Maynard A, Soretic M, Treutlein B. Single-cell genomic profiling to study regeneration. Curr Opin Genet Dev. 2024; 87:102231.

Received December 11, 2025; Revised February 9, 2026; Accepted February 11, 2026.

*Address correspondence to:
Shinji Yamaguchi, Department of Biological Sciences, Faculty of Pharmaceutical Sciences, Teikyo University, 2-11-1 Kaga, Itabashi-ku, Tokyo 173-8605, Japan.
E-mail: shinji-y@pharm.teikyo-u.ac.jp

Released online in J-STAGE as advance publication February 13, 2026.

Review

DOI: 10.5582/ddt.2025.01134

Equivalence in the modernization of Chinese medicine: A multi-dimensional analysis of active components, processing methods, and clinical outcomes in formula granules

Bo Xie[1], Xi Qu[1], Huijing Shi[1], Yi Zhou[1], Dan Deng[1], Yuanru Liu[1], Rong Jiang[2], Ling Wang[1,3,*]

[1] Department of Obstetrics, The First Affiliated Hospital of Guizhou University of Traditional Chinese Medicine, Guiyang, Guizhou, China;
[2] Tongren Hospital of Traditional Chinese Medicine, Guizhou, China;
[3] Guizhou University of Traditional Chinese Medicine, Guiyang, Guizhou, China.

SUMMARY: The feasibility of substituting traditional decoction pieces with Chinese herbal formula granules fundamentally hinges on the equivalence of their active components. Formula granules face complex compositional changes during manufacturing: volatile oils suffer substantial losses (retention rates below 30% in aromatic herbs), thermolabile glycosides undergo degradation during high-temperature processing, and Maillard reactions generate novel compounds whose pharmacological contributions remain unclear. Although advanced analytical technologies such as ultra-performance liquid chromatography quadrupole time-of-flight mass spectrometry (UPLC-Q-TOF-MS) can identify thousands of components, existing quality control standards still rely on 1-3 pharmacopeial markers, and fingerprint similarity criteria lack uniformity (0.80-0.95), inadequately reflecting the true quality of multi-component systems. Bioequivalence studies demonstrate that formula granules generally exhibit 60-90% performance of traditional decoctions *in vitro*, with comparable area under the curve (AUC) and Cmax values for certain components but significant discrepancies for others. Critically, high chemical similarity cannot guarantee clinical therapeutic equivalence—the logical chain from"component equivalence" to "therapeutic equivalence" remains unestablished. Clinical research is sparse, with high-quality randomized controlled trials (RCTs) representing less than 5% of studies and head-to-head comparisons particularly scarce. Future research must develop volatile component preservation technologies, establish comprehensive synergistic effect evaluation methodologies, and most importantly, conduct large-scale clinical trials. Without these efforts, the scientific credibility and international acceptance of formula granules will remain questionable.

Keywords: formula granules, traditional decoction pieces, active components, manufacturing process, component synergy

1. Introduction

As a modernized dosage form of Traditional Chinese Medicine (TCM) decoction pieces, Chinese herbal formula granules achieve clinical advantages of convenient dispensing and immediate preparation through standardized processes of aqueous extraction, concentration, drying, and granulation of individual herbs. The production of formula granules employs highly controlled processing workflows that ensure stability of active components and inter-batch consistency through precise regulation of parameters such as extraction temperature, solvent concentration, and drying time (*1*). In 2023, the market revenue for Chinese herbal formula granules reached 56.71 billion yuan, with a compound annual growth rate of 27.34% from 2012 to 2023 (*2*), and the market scale of China's formula granule industry reached 63.84 billion yuan in 2024 (*3*). However, the fundamental prerequisite for formula granules to truly substitute traditional decoction pieces lies in their equivalence, particularly quality equivalence at the level of active components. Current quality standards predominantly rely on content control of single or limited marker compounds listed in the Chinese Pharmacopoeia, but whether this simplified evaluation model can guarantee overall pharmacological equivalence of complex multi-component systems has become a critical scientific issue constraining the scientific development and international recognition of formula granules. The formula granule field still faces practical challenges including contradictions between fixed equivalence ratios and raw material variability,

relatively limited production processes, insufficient national standards with fragmented provincial standards (*3*)—all of these issues fundamentally point to one core proposition: can chemical similarity truly ensure clinical therapeutic equivalence?

From the perspective of chemical material basis, systematic differences exist in the component profiles between formula granules and traditional decoction pieces. Following aqueous extraction, the chemical composition of formula granules inevitably differs substantially from that of crude herbs and decoction pieces (*4*). Breakthroughs in modern analytical technologies have enabled precise characterization of these differences: high-resolution mass spectrometry techniques such as ultra-high-performance liquid chromatography coupled with Q-Exactive Orbitrap mass spectrometry (UHPLC-Q-Exactive Orbitrap-MS) can identify hundreds to thousands of chemical components, while metabolomics approaches can capture degradation of thermolabile components, loss of volatile oils, and newly generated constituents arising from chemical transformation processes such as Maillard reactions during formula granule preparation. Studies have demonstrated that formula granules differ from equivalent-dose traditional decoctions in antihypertensive effects, with granule preparations exhibiting efficacy similar to high-dose decoctions but superior to equivalent-dose decoctions (*5*). This phenomenon reveals the complexity of relationships between component transformation and pharmacological effects: certain components preserved during traditional decoction may be lost during granulation, while newly formed transformation products may possess unknown pharmacological contributions or synergistic effects. The Special Regulations on TCM Standards Management explicitly emphasizes (*6*) that research and formulation of formula granule standards should focus on consistency of fundamental quality attributes between formula granules and traditional decoctions, yet how to scientifically define and quantify this "consistency" currently lacks a unified methodological framework and assessment criteria.

The complexity of equivalence evaluation stems not only from the diversity of chemical components but also from the incomplete evidence chain between "component equivalence" and "therapeutic equivalence". In recent years, integrated application of multi-omics technologies has provided new insights for addressing this challenge: metabolomics enables panoramic scanning of component changes *in vitro* and *in vivo*, network pharmacology can construct "component-target-pathway" association networks, and pharmacokinetic studies reveal differences in systemic behavior between absorbed components and parent compounds. Advanced analytical technologies such as UHPLC-Q-Exactive Orbitrap-MS, with unparalleled resolution and mass accuracy, can precisely identify and quantify complex TCM components and their metabolites (*7*). However, current research still faces critical knowledge gaps: the pharmacological contributions of formula granule-specific transformation products remain unclear, mechanisms of multi-component synergistic actions lack systematic elucidation, and *in vitro-in vivo* correlations (IVIVC) are difficult to establish. Furthermore, the heterogeneity of raw material quality in traditional decoction pieces, variations in processing parameters across different manufacturers, and individualized differences in decoction methods all make it challenging to standardize benchmarks for equivalence comparative studies (*8*). Therefore, this review focuses on the core scientific question of active component equivalence between formula granules and traditional decoction pieces, systematically summarizing recent research data on chemical equivalence and bioequivalence evaluation methods, analyzing methodological limitations and cognitive bottlenecks in current research, and prospecting future directions for establishing multi-dimensional equivalence evaluation systems, with the aim of providing theoretical support for the scientization and internationalization of quality standards for formula granules (Figure 1).

2. Evaluation methods and research status of chemical component equivalence

2.1. Application of analytical technologies

2.1.1. Quantitative comparison of marker components

As of January 2024, national standards for Chinese herbal formula granules in China have been established for over 300 species (*1*), with quality standards for each species relying on content control of specific marker components. In recent years, extensive quantitative comparative studies on marker components between formula granules and traditional decoction pieces have been conducted, primarily focusing on content determination of characteristic constituents such as flavonoids, saponins, and alkaloids listed in the Chinese Pharmacopoeia. These studies typically employ high-performance liquid chromatography (HPLC) or ultra-high-performance liquid chromatography (UPLC) to measure absolute contents of single or multiple marker components through establishment of standard curves, and calculate transfer rates of formula granules relative to decoction piece decoctions (*9*). The quantitative analysis of multi-components by single marker (QAMS) method has been widely applied in TCM quality control, which not only addresses challenges of obtaining reference standards or their high costs but also substantially reduces detection costs and time. However, this evaluation approach based on single or limited marker components possesses inherent deficiencies: inadequate representativeness constitutes its core problem. As complex multi-component systems, the pharmacological effects of Chinese herbal formula granules often result from synergistic actions of dozens or

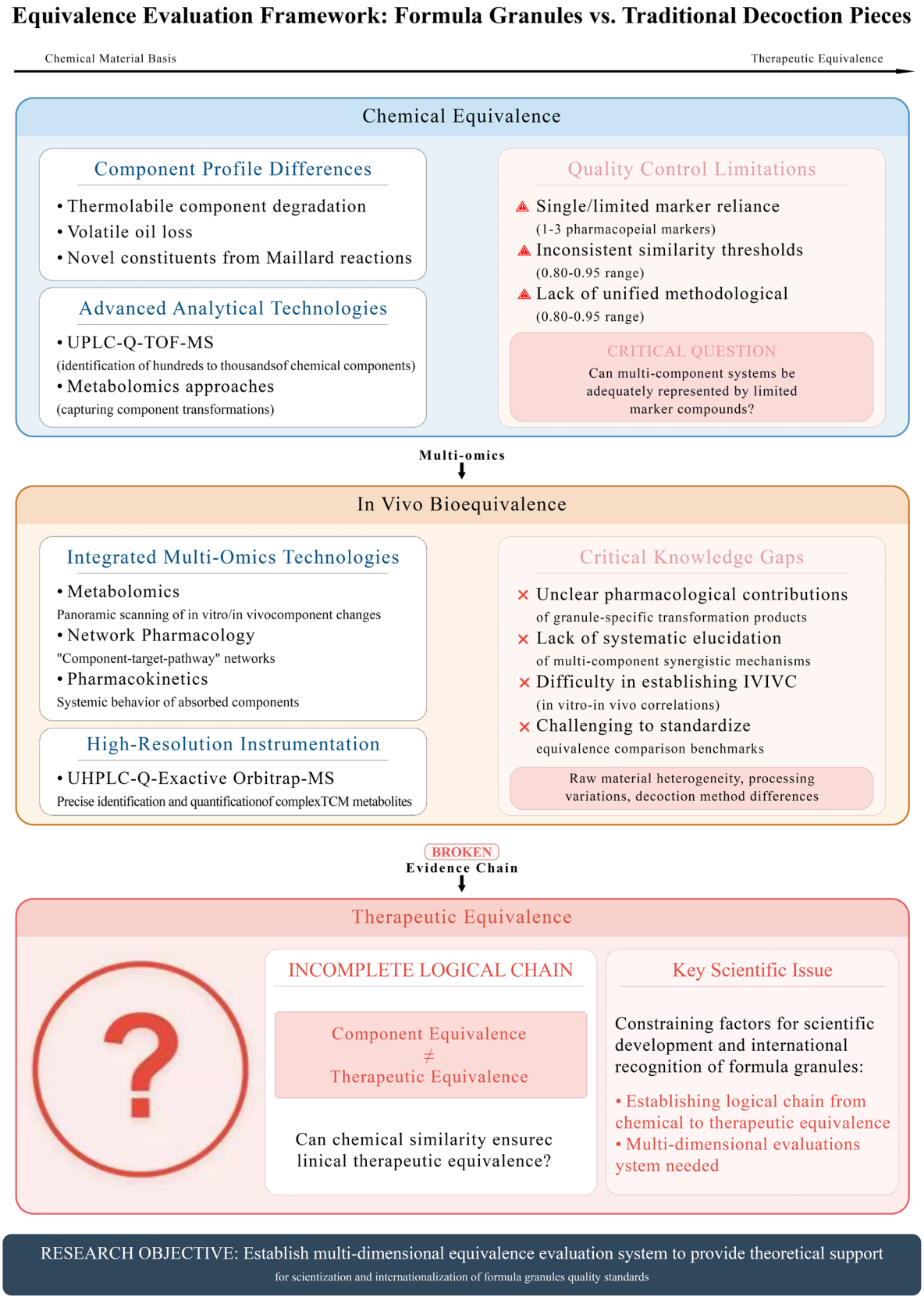

Figure 1. Multi-dimensional research framework and critical knowledge gaps in establishing equivalence between Chinese herbal formula granules and traditional decoctions. The framework illustrates three progressive levels of equivalence assessment: chemical component profile differences addressed by advanced analytical technologies, *in vivo* bioequivalence evaluated through multi-omics approaches, and therapeutic equivalence validated by clinical outcomes. Red boxes highlight current quality control limitations and critical knowledge gaps at each level, emphasizing the incomplete logical chain from component equivalence to therapeutic equivalence.

herbs, decoction pieces, and formula granule production processes, which, while ensuring consistency of industry quality standards, substantially increase production costs of formula granules (*10*). Although such stringent marker component control enhances product stability, it neglects potential pharmacological contributions of non-marker components, potentially leading to risks of "compliant components but inequivalent efficacy".

2.1.2. Holistic chemical fingerprinting

To overcome limitations of single marker component evaluation, chemical fingerprinting technology has become an important tool for equivalence assessment of formula granules. With advances in TCM quality control technologies, combined application of chemical fingerprints and physical fingerprints has become a trend, enabling comprehensive evaluation of formula granule quality from both chemical composition and physical property dimensions (*11*). This technology records the holistic chromatographic profile of samples through multi-wavelength detection (diode array detector (DAD), evaporative light scattering detector (ELSD), *etc*.), generating a "chemical identity card" containing dozens of characteristic peaks, and then employs similarity evaluation algorithms (such as cosine angle method and correlation coefficient method) to calculate the degree of similarity between fingerprints of formula granules and traditional decoction pieces. HPLC-DAD technology, through diode array detectors, can simultaneously acquire multi-wavelength chromatographic data, significantly improving detection sensitivity and accuracy for trace components compared to single-wavelength detection (*12*). Similarity and hierarchical cluster analysis have been applied to identify Xiao Chai Hu granules produced by different manufacturers, with peak pattern matching used to evaluate preparation processes (*13*). Fingerprint similarity evaluation is widely applied in formula granule quality control.

For instance, Chen Shengjun *et al*. demonstrated that similarities of different processed products of Dahuang (Rhubarb) formula granules were 0.85, 0.90, and 0.90 respectively (*14*); Wang Yingjun *et al*. showed fingerprint similarities ranging from 0.824 to 0.989 in studies of 35 batches of Danggui (Angelica sinensis) samples (*15*). However, similarity threshold settings lack unified standards: different species in national standards adopt 0.85 or 0.90 as acceptance criteria (*14*), while academic research also employs various thresholds such as 0.80 and 0.95 (*16*), and this inconsistency in standards undermines comparability of evaluation results. Although the fingerprinting method has been approved by WHO, US FDA, European Medicines Agency, and Chin's National Medical Products Administration, it has limitations in evaluating TCM quality, as characteristic common peaks may not reflect representative information of TCM quality (*17*).

2.1.3. Untargeted metabolomics for comprehensive component profiling

The introduction of untargeted metabolomics technology has brought revolutionary breakthroughs to chemical equivalence evaluation of formula granules. Metabolomics analytical methods based on UPLC-Q-TOF-MS/MS have been established to evaluate chemical consistency before and after compatibility of Zhenwu Decoction (*5*). This technology, without presetting target compounds, can identify hundreds to thousands of chemical components in a single analysis, precisely determine molecular formulas through high-resolution mass spectrometry (resolution exceeding 50,000), and infer compound structures by combining secondary mass spectral fragmentation information. UHPLC-Q-TOF-MS has been established as a powerful and reliable analytical technology due to its exceptional sensitivity, superior resolution, and accurate mass measurement, holding significant importance in analyzing complex compounds in TCM formulae (*18*).

At the data processing level, principal component analysis (PCA) can intuitively display clustering relationships among samples, orthogonal partial least squares- discriminant analysis (OPLS-DA) can screen chemical markers with significant differences, and S-plots are used to locate key components causing differences. Chemical differences have been identified between traditional decoctions and formula granule decoctions of Taohong Siwu Decoction, with paeoniflorin, albiflorin, gallic acid, amygdalin, and safflor yellow A identified as components undergoing significant changes during decoction (*19*). The formula granule preparation process involves high-temperature concentration and drying procedures, which theoretically may induce Maillard reactions (non-enzymatic browning between sugars and amino acids), generating new components such as pyrazines and furans (*13*), while certain volatile components and thermolabile glycosides may degrade or dissipate. However, systematic identification of formula granule-specific components and quantitative comparative studies with traditional decoction pieces remain insufficient, requiring further in-depth investigation using modern analytical technologies such as UPLC-Q-TOF-MS (*20*). These findings provide molecular-level evidence for understanding chemical differences between formula granules and decoction pieces, but simultaneously raise new scientific questions: what are the contributions of these differential components to overall pharmacological effects?

2.2. Component changes induced by processing

2.2.1. Loss of thermolabile components

High-temperature treatment during formula granule preparation (extraction temperatures typically 60-100°C,

concentration and drying temperatures up to 80-120°C) inevitably leads to degradation or dissipation of certain thermolabile components. Volatile oil constituents represent the most severely affected category. Thermal degradation of certain phytochemicals in specific aromatic crops may result in reduced levels of key aroma substances or formation of new volatile compounds, potentially negatively impacting sensory characteristics of final products (*21*).

During traditional decoction piece decoction, volatile oils partially dissipate with water vapor but a considerable proportion remains in the decoction, whereas during concentration and drying stages of formula granules, volatile oils are almost completely lost. Taking aromatic herbs such as Bohe (Mentha) and Huoxiang (Pogostemon) as examples, retention rates of volatile components like menthol and patchouli alcohol in formula granules are generally below 30%. Although steam distillation technology is faster and suitable for large-scale production, higher temperatures may lead to degradation of thermosensitive compounds (*22*). Thermal stability of alkaloid components varies significantly: tropane alkaloids (such as atropine and scopolamine) undergo significant degradation above 270°C, as tropane alkaloids atropine and scopolamine possess thermal instability and may be overlooked due to degradation at high temperatures (*23*); whereas berberine-type alkaloids are relatively stable. Heat treatment leads to increased levels of pyrrolizidine alkaloids while simultaneously decreasing their N-oxide forms, indicating concurrent transformation (*24*). Glycoside components such as ginsenosides and flavonoid glycosides may undergo hydrolysis reactions under prolonged heating conditions, generating corresponding aglycones. Studies have demonstrated that rare ginsenosides and aglycones generated from hydrolysis of orally administered ginsenosides in the intestine represent the primary forms absorbed into blood and exerting pharmacological effects (*25*), with intestinal microbiota-mediated stepwise deglycosylation reactions playing important roles in their *in vivo* metabolism and pharmacokinetic behavior. During formula granule preparation, retention of different component types exhibits significant differences: volatile oil components are lost substantially due to high-temperature treatment, alkaloid components are relatively stable but certain thermosensitive structures may degrade, and glycoside components may be accompanied by generation of hydrolysis products — all these changes may influence final pharmacological performance (*13*).

2.2.2. Generation of new components

Formula granule preparation is not only a process of component loss but also one of new component generation. The Maillard reaction represents one of the most important chemical transformation pathways, occurring between reducing sugars and amino acids, proteins, or other nitrogen-containing compounds, generating a series of brown pigments and flavor substances under heating conditions (*26*). During the concentration and drying stage of formula granules (80-120°C), Maillard reactions occur significantly, with generated products including pyrazines (such as 2,5-dimethylpyrazine and 2,3,5-trimethylpyrazine), furans (such as 5-hydroxymethylfu rfural, 5-HMF), pyrroles, and other heterocyclic compounds (*26,27*).

Studies have shown that 11 volatile Maillard reaction products were identified during steaming of Heshouwu (Polygonum multiflorum), including 4 furanones, 2 furans, 2 nitrogen-containing compounds, 1 pyran, 1 alcohol, and 1 sulfur compound. These newly generated components significantly enhanced DPPH free radical scavenging activity of the processed product (processed Heshouwu) compared to the raw material, with IC_{50} values decreasing from 2.9 mg/mL to 0.43 mg/mL (*27*). During the steaming process, DDMP (2,3-dihydro-3,5-dihydroxy-6-methyl-4H-pyran- 4-one) and 5-HMF gradually form, while 16 amino acids (especially lysine and arginine) undergo significant consumption (*28*). These newly generated components possess characteristic roasted and nutty aromas, and some compounds have been demonstrated to possess biological activities including antioxidant, anti-inflammatory, hepatoprote ctive, and immunomodulatory effects, though they may also contain trace amounts of potentially harmful components such as acrylamide and advanced glycation end products (*26,29*).

Glycation products and oxidation products constitute two other important categories of newly generated components. Under high-sugar environments and heating conditions, certain polyphenolic and flavonoid compounds can undergo non-enzymatic glycation reactions with sugars, forming new glycation derivatives. These melanoidins possess high molecular weights and complex structures, potentially improving solubility and stability of active components (*29,30*). Unsaturated fatty acids and terpenoid compounds readily undergo autoxidation under heating and air exposure conditions, generating degradation products such as peroxides, aldehydes (*e.g.*, hexanal, heptanal), and ketones. These lipid oxidation products (LOPs) increase significantly after heating at 200°C, potentially leading to quality loss and reduced pharmacological properties (*31*).

The critical question lies in: the pharmacological effects of newly generated components remain unclear. Existing research mostly remains at the component identification level, lacking systematic pharmacodynamic evaluation of these transformation products. Do newly generated components compensate for pharmacological effects of partially lost components, or do they introduce potential safety risks? For example, 5-HMF, as a common Maillard reaction product, although possessing antioxidant activity in steamed Heshouwu products (*27*),

may also produce cytotoxicity and neurotoxicity at high doses (*26*). Answers to these questions are crucial for scientifically evaluating equivalence between formula granules and traditional decoction pieces (Figure 2).

2.3. Controversies in chemical equivalence assessment criteria

Formulation of chemical equivalence assessment criteria for formula granules represents a controversial scientific issue, with core disagreements concentrated in three dimensions. First, single marker *vs.* multi-marker control. Traditional quality standards tend to select 1-3 pharmacopoeia-listed marker components for content control; this simplified approach is convenient to implement but scientifically insufficient. According to Academician Zhang Boli's 2024 Two Sessions proposal, inconsistent provincial review standards result in different standards for the same species across provinces, including variations in content and specifications, and recommended abolishing provincial-level standard formulation for formula granules to avoid duplicate research and waste of social resources (*32,33*). Multi-marker control can more comprehensively reflect chemical composition, but marker number selection (5, 10, or 20?), weight allocation, and acceptable range settings all lack recognized scientific foundations. The Special Regulations on TCM Standards Management explicitly emphasizes that research and formulation of formula granule standards should focus on consistency of fundamental quality attributes between formula granules and traditional decoctions (*32*), but how to scientifically define and quantify this "consistency" currently lacks a unified methodological framework. Second, content equivalence *vs.* ratio equivalence. Content equivalence requires that absolute contents of marker components in formula granules approximate those in decoction piece decoctions (typically allowing 80-120% deviation), but this ignores quality fluctuations in raw decoction piece materials across different batches. Ratio equivalence emphasizes that relative proportional relationships among components within formula granules should be consistent with decoction pieces; this approach better aligns with TCM's "holistic" philosophy but presents greater technical implementation challenges. National standards adopt a clinical application-oriented approach examining formula granules as an integrated whole, emphasizing water-soluble properties consistent with decoctions (*34,35*), which is relatively comprehensive and rational. However, current research predominantly employs content equivalence standards, while evaluation methodologies for ratio equivalence remain immature, and differences in enterprise production processes and equipment, along with lack of reasonable evaluation standards, pose challenges for product consistency evaluation (*34*). Third, significant domestic and international standard differences impact the internationalization process of formula granules. Chinese standards emphasize marker component content control combined with fingerprint similarity evaluation, establishing quantity transmission data tables and characteristic spectrum control indicators based on "standard decoctions" as benchmarks (*35*). Japanese Kampo preparation standards focus on overall quality consistency: the 17th edition of the Japanese Pharmacopoeia includes 176 crude drugs and 35 Kampo extracts, with official definitions of sources, descriptions, limits, and detection methods (*36*), achieving quality control through standardized extraction processes (over 95% being extract preparations) (*37*). The European Pharmacopoeia requires detailed phytochemical data and biological activity data, with all limits formulated by referencing multiple national pharmacopoeias (Chinese Pharmacopoeia, British Pharmacopoeia, European Pharmacopoeia, Japanese Pharmacopoeia, and United States Pharmacopeia) (*36*). This lack of standardization uniformity results in the same formula granule species facing different entry thresholds in different countries/regions, constraining international circulation of products and academic exchange. Establishing scientific, unified, and internationally recognized chemical equivalence assessment criteria requires integration of multidimensional evidence from chemical analysis, pharmacodynamic validation, and clinical evaluation—a direction urgently requiring breakthroughs in current research.

3. Methods and research progress in bioequivalence evaluation

3.1. *In vitro* biological activity comparison

3.1.1. Antioxidant activity testing

Antioxidant activity serves as one of the fundamental indicators for evaluating the bioequivalence between formula granules and traditional decoction pieces. Commonly employed methods include the DPPH (2,2-diphenyl-1-picrylhydrazyl) free radical scavenging assay and the ABTS [2,2'-azino-bis-(3-ethylbenzothiazoline-6-sulfonic acid)] free radical scavenging assay. The DPPH method, owing to its rapidity, simplicity, and cost-effectiveness, has been widely applied to assess the potential of substances as hydrogen donors or free radical scavengers (*38*). This method is based on the principle that DPPH free radicals exhibit purple absorption at 517 nm wavelength, which undergoes decolorization upon reaction with antioxidant substances. The free radical scavenging rate is calculated by measuring changes in absorbance (*39*).

Antioxidant activity values determined by different methods exhibit variations: DPPH and RP methods yield higher antioxidant activity values compared to ABTS and FRAP methods. Consequently, methodological

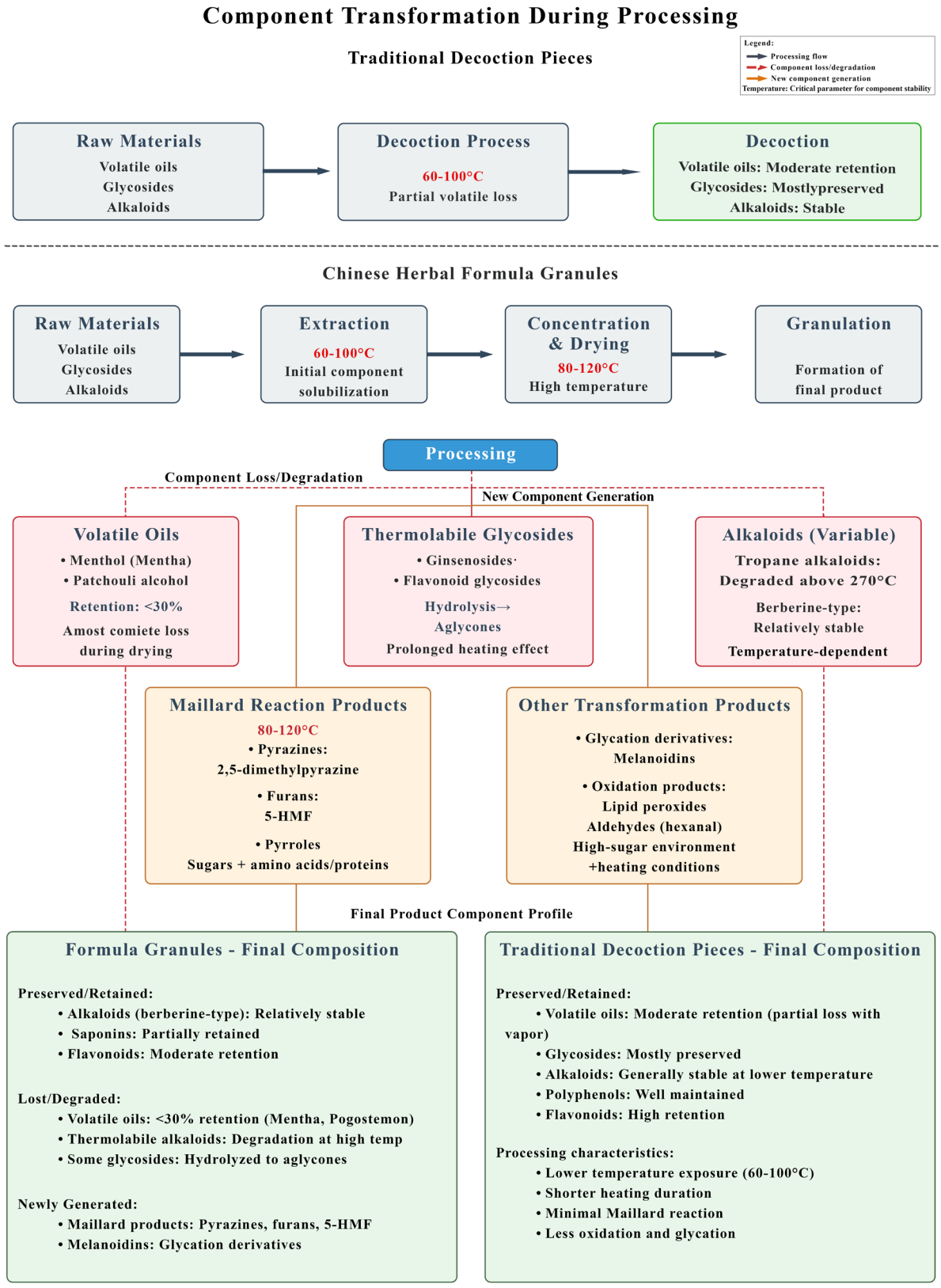

Figure 2. Component transformation pathways during the processing of traditional decoction pieces and formula granules, and their impact on final product composition. The diagram illustrates how thermal processing conditions (60-100°C for extraction, 80-120°C for concentration and drying) induce differential component changes in both preparation methods. Key transformation mechanisms include: (1) volatile oil partial loss and component degradation, (2) thermolabile glycoside hydrolysis and aglycone formation, (3) alkaloid temperature-dependent degradation, (4) Maillard reaction products generation from reducing sugars and amino acids/proteins (80-120°C), and (5) oxidation-induced derivative formation. The comparison reveals that formula granules experience higher temperature exposure during concentration and spray drying, leading to more pronounced component losses and transformation compared to traditional decoctions, ultimately resulting in compositional differences between the two preparation forms.

consistency must be maintained when comparing formula granules with decoction pieces (*40*). DPPH measurements correlate only with other methods, suggesting that due to different reaction mechanisms, it reflects distinct antioxidant properties. Total antioxidant capacity (T-AOC) determination evaluates the comprehensive antioxidant potential of samples through methods such as FRAP (ferric reducing antioxidant power) (*41*). Recent comparative data on antioxidant activity between formula granules and decoction pieces demonstrate that the DPPH scavenging capacity of most formula granules ranges from 70-95% of traditional decoction pieces, though significant variations exist among different varieties. For instance, formula granules of species rich in polyphenolic components, such as Salvia miltiorrhiza and Scutellaria baicalensis, retain high antioxidant activity (> 85%), whereas those containing volatile oil components, such as Mentha haplocalyx and Pogostemon cablin, show significant reduction (< 60%) (*41*). This variability suggests that antioxidant activity cannot serve as the sole criterion for equivalence evaluation and must be comprehensively assessed in conjunction with the chemical characteristics of specific varieties.

3.1.2. Cell model validation

Cell model-based biological activity validation provides more direct functional evidence for equivalence evaluation of formula granules. Anti-inflammatory activity evaluation commonly employs lipopolysaccharide (LPS)-induced RAW264.7 macrophage inflammation models, assessing anti-inflammatory effects by detecting the release of inflammatory factors such as tumor necrosis factor-α (TNF-α), interleukin-6 (IL-6), and interleukin-1β (IL-1β), as well as the phosphorylation levels of key proteins in the nuclear factor-κB (NF-κB) signaling pathway (*42*). Polyphyllin can block the NF-κB signaling pathway in bone marrow-derived macrophages, inhibiting the phosphorylation of IKKα/β and p65, and significantly reducing the production of key pro-inflammatory cytokines IL-1β, TNF-α, and IL-6. Oral administration of Yangqing Chenfei Formula can alleviate pathological changes, reduce inflammatory cell infiltration, inhibit collagen deposition, and decrease inflammatory factor levels. This combined *in vitro* and *in vivo* research model provides a paradigm for equivalence evaluation of formula granules (*43*). Protective effect evaluation involves multiple target cell models: HepG2 hepatocytes for assessing hepatoprotective activity (by detecting ALT and AST release and cell viability), PC12 neuronal cells for evaluating neuroprotective effects (by detecting apoptosis rate and axonal growth), and H9c2 cardiomyocytes for assessing cardioprotective effects (*44*). Recent research cases indicate that the protective effects of formula granules in cell models are generally slightly lower than equivalent doses of traditional decoction liquids (activity retention 60-90%), but the regulatory trends of key signaling pathways remain consistent. For example, both Salvia miltiorrhiza formula granules and decoction pieces exert their effects by activating the Nrf2/HO-1 pathway when inhibiting oxidative damage in H9c2 cardiomyocytes. Although the EC50 value of formula granules is slightly higher (1.2-1.5 times), the shape of the dose-response curve is similar, suggesting equivalence in the mechanism of action between the two (*45*).

3.1.3. *In vitro* dissolution/release studies

In vitro dissolution/release studies draw upon classic methods from chemical drug bioequivalence evaluation, though their application in the field of Chinese medicine formula granules remains in the exploratory stage. Dissolution curve comparison methods typically employ the paddle method (Chinese Pharmacopoeia general rule 0931) or basket method, measuring the cumulative dissolution percentage of indicator components in various media such as simulated gastric fluid (pH 1.2) and simulated intestinal fluid (pH 6.8), and plotting time-dissolution curves. The similarity factor (f2) calculation is an FDA-recommended method for comparing dissolution curves, with the formula: $f2 = 50\times\log\{[1+(1/n)\Sigma(Rt-Tt)^2]^{(-0.5)}\times100\}$, where Rt and Tt represent the average dissolution at time t for the reference and test formulations respectively, and n is the number of sampling points. When the f2 value falls between 50-100, the two dissolution curves are considered similar (*46*). However, dissolution studies of formula granules face particular challenges: traditional decoction liquids are in liquid form and can be directly absorbed without dissolution, whereas formula granules require steps such as dissolution upon administration and gastrointestinal disintegration. Therefore, the f2 similarity factor is more suitable for evaluating quality consistency among different batches of formula granules rather than determining equivalence between formula granules and decoction pieces. The lack of established *in vitro-in vivo* correlation (IVIVC) represents a major limitation of current research (*47*). Mature IVIVC models (A/B/C level correlations) in the chemical drug field require clear quantitative relationships between pharmacokinetic parameters (such as AUC, Cmax) and *in vitro* dissolution parameters. However, the multi-component nature of Chinese medicine formula granules makes it difficult for IVIVC of a single component to represent overall efficacy, while establishing multi-component combined IVIVC models faces tremendous technical challenges and data requirements.

3.2. *In vivo* pharmacokinetic equivalence

3.2.1. Blood-entering component analysis

Blood-entering component analysis serves as a critical bridge connecting chemical equivalence and bioequivalence. Liquid chromatography-tandem mass

spectrometry (LC-MS/MS) detection technology for plasma samples has become the mainstream method. Through ultra-high performance liquid chromatography-triple quadrupole mass spectrometry (UPLC-QqQ-MS/MS) in multiple reaction monitoring (MRM) mode, highly sensitive quantification of trace prototype components and metabolites in plasma can be achieved (detection limits reaching pg/mL level) (*48,49*). UPLC-Q-TOF-MS can be combined with exogenous metabolomics for qualitative analysis of prototype components and metabolites, making the data analysis process more accurate. Identification of prototype components and metabolites requires integration of *in vitro* metabolic stability experiments and *in vivo* metabolite identification (*50,51*). After oral administration, significant differences exist in the blood-entering component profiles between formula granules and decoction pieces: some macromolecular polysaccharides and tannins with high content in decoction liquids are difficult to enter the bloodstream due to poor absorption. Components that truly enter blood circulation and exert pharmacological effects are often small-molecule glycosides, alkaloids, flavonoids, and their metabolites. Comparison of pharmacokinetic parameters for typical components focuses on key indicators such as maximum plasma concentration (Cmax), time to peak (Tmax), and area under the concentration-time curve (AUC). Recent summarized research data show: ginsenoside Rg1 after administration of ginseng formula granules has a Cmax of 85-110% of the decoction group, AUC of 90-115%, with no significant difference in Tmax (*52*); salvianolic acid B in *Salvia miltiorrhiza* formula granules has a Cmax of 70-95% of the decoction group, but the AUC ratio can reach 85-105%, suggesting slightly slower absorption rate but similar total absorption (*53*); baicalin bioavailability in *Scutellaria baicalensis* formula granules is generally higher than decoction pieces (F = 110-130%), possibly related to glycoside hydrolysis to aglycone during formula granule preparation, with the latter showing better absorption. These data reveal that pharmacokinetic equivalence of a single component does not equate to overall pharmacological equivalence, requiring comprehensive consideration of multi-component synergistic pharmacokinetic characteristics.

3.2.2. Tissue distribution studies

Tissue distribution studies reveal the targeting and accumulation characteristics of active components *in vivo*. By collecting major organ tissues such as heart, liver, spleen, lung, kidney, and brain at different time points after administration, and measuring indicator component content using LC-MS/MS, tissue concentration-time curves are plotted to calculate differences in target organ accumulation (*54*). Representative studies show: ginsenoside components (such as Rg1, Rb1, Re) distribute at higher concentrations in the heart and spleen, suggesting their cardiovascular protective and immunomodulatory effects may be related to target organ accumulation; the tissue distribution pattern of formula granule groups is essentially consistent with decoction piece groups, but peak concentrations (Cmax, tissue) are generally reduced by 10-25% (*55*). Salvianolic acid components (salvianolic acid A, salvianolic acid B) are highly enriched in the liver, with liver AUC of formula granules at 80-95% of the decoction group, supporting the equivalence of hepatoprotective activity (*56*). Flavonoid components (such as quercetin, kaempferol) have relatively limited tissue distribution due to high plasma protein binding rates, but selective accumulation in inflammatory tissues can be observed. Notably, differences in brain tissue distribution between formula granules and decoction pieces warrant attention: some components with neuroprotective effects (such as ginsenoside Rg1) need to penetrate the blood-brain barrier, and transformation products generated during formula granule preparation may affect their brain delivery efficiency (*55*). Additionally, biotransformation of Chinese medicine components by gut microbiota (such as ginsenoside → rare ginsenoside, flavonoid glycoside → flavonoid aglycone) also affects tissue distribution patterns. Differences in intestinal residence time and degree of contact with microbiota between formula granules and decoction pieces may lead to changes in transformation product profiles, thereby affecting target organ exposure.

3.2.3. Pharmacokinetic equivalence determination

Bioequivalence (BE) evaluation standards are well-established in the chemical drug field. Bioavailability is typically assessed by measuring the area under the plasma concentration-time curve (AUC), which is the most reliable measurement of drug bioavailability. Bioavailability refers to the extent to which the active form of a drug reaches systemic circulation unchanged, with this definition assuming that 100% of the active drug entering systemic circulation can successfully reach the target site (*57,58*). Both Food and Drug Administration (FDA) and National Medical Products Administration (NMPA) guidelines require that the 90% confidence interval (CI) of AUC and Cmax for two formulations must fall within the equivalence boundary range of 80.00-125.00% to be determined as bioequivalent. However, application in formula granule research faces numerous difficulties. First, Chinese medicine formula granules are complex multi-component systems—which component pharmacokinetic parameters should serve as the basis for equivalence determination? Current research predominantly selects indicator components included in the pharmacopoeia, but whether these components represent the true pharmacodynamic material basis remains controversial. Second, even with selected indicator components, pharmacokinetic characteristics vary tremendously among different components: some components (such as alkaloids, saponins) can be

directly absorbed into blood (*59*), while others (such as polysaccharides, tannins) can only exert effects after gut microbiota metabolism—how should these be comprehensively evaluated? Third, reference standards between formula granules and traditional decoction pieces are not uniform: pharmacokinetic parameters of decoction pieces from different origins and under different decoction conditions exhibit considerable variation themselves — which decoction pieces should serve as the reference? Challenge: the complexity of equivalence determination in multi-component systems is the fundamental reason restricting the in-depth development of pharmacokinetic equivalence research. The ideal solution is to establish a comprehensive evaluation system based on "pharmacodynamic material basis groups": first screening 5-10 core components highly correlated with efficacy through spectrum-effect relationship studies, then measuring the pharmacokinetic parameters of these components separately, and calculating a comprehensive bioequivalence index using a weighted scoring method (assigning weights according to each component's contribution to efficacy). However, implementation of this method requires substantial preliminary research accumulation and has only been preliminarily explored in a few bulk formula granule varieties (such as ginseng, *Salvia miltiorrhiza*, and *Astragalus*).

3.3. Spectrum-effect relationship studies

3.3.1. Correlation analysis between chemical components and pharmacological effects

Spectrum-effect relationship studies aim to establish quantitative relationships between the chemical component spectrum of formula granules and pharmacological effects, identifying key components for equivalence. Grey relational analysis (GRA) is a commonly used mathematical tool that identifies components with the greatest contribution by calculating grey relational coefficients between chromatographic peak areas of chemical components and pharmacological indicators (such as antioxidant activity, cell protection rate) (*60,61*). The advantage of this method lies in its lack of requirement for large sample sizes, making it suitable for scenarios in Chinese medicine research with limited samples. Partial least squares regression (PLSR) is a more powerful multivariate statistical method that can simultaneously process multiple independent variables (chemical component concentrations) and dependent variables (pharmacological indicators) to establish predictive models (*62,63*). Network pharmacology analysis shows that 210 potential action targets of Qingjin Yiqi Granules for anti-fatigue are mainly enriched in signaling pathways such as PI3K-AKT, MAPK, HIF-1, and FoxO. In formula granule spectrum-effect relationship studies, the typical workflow includes: (1) preparing formula granule samples of different batches or different extraction processes ($n \geq 15$); (2) obtaining chemical fingerprints using HPLC or UPLC-MS, calibrating and quantifying major chromatographic peaks; (3) conducting *in vitro* or *in vivo* pharmacological evaluations to obtain quantitative pharmacological data; (4) establishing correlation models between chemical components and pharmacological effects using GRA or PLSR, calculating correlation coefficients or regression coefficients for each component, and identifying key pharmacodynamic components (*64,65*). Recent research cases show: the immune-enhancing effect of *Astragalus* formula granules has the highest correlation with astragaloside IV and calycosin glycoside ($r > 0.85$), while the contribution of polysaccharide components is relatively small; the antiplatelet aggregation effect of *Salvia miltiorrhiza* formula granules is mainly contributed by salvianolic acid B (PLSR coefficient 0.72), while the contribution of tanshinones is limited (coefficient 0.15) (*66*). These findings provide data support for identifying key components of equivalence: in equivalence evaluation, priority should be given to ensuring content consistency of highly correlated components rather than simply requiring proportional retention of all components.

3.3.2. Network pharmacology-assisted prediction

Network pharmacology provides a holistic "component-target-pathway" perspective for equivalence evaluation of formula granules by integrating cheminformatics, bioinformatics, and systems biology. The standard procedure for "component-target-pathway" network construction includes: (1) retrieving chemical components of formula granules through databases such as TCMSP, HERB, and PubChem, setting oral bioavailability (OB $\geq$ 30%) and drug-likeness (DL $\geq$ 0.18) to screen active components (*67*); (2) predicting action targets of active components using tools such as SwissTargetPrediction, SEA, and STITCH (*68*); (3) obtaining relevant disease targets from disease databases such as GeneCards, OMIM, and DisGeNet (*68*); (4) taking the intersection of drug targets and disease targets to construct a protein-protein interaction (PPI) network (*69*); (5) visualizing the network using Cytoscape software, calculating topological parameters such as node degree and betweenness centrality to identify core targets (*70*); (6) performing Gene Ontology (GO) functional annotation and Kyoto Encyclopedia of Genes and Genomes (KEGG) pathway enrichment analysis through platforms such as DAVID and Metascape (*71*). Network pharmacology combined with spectrum-effect relationship analysis shows that the main anti-inflammatory substances of Wuwei Ganlu are flavonoids, which exert anti-inflammatory effects by inhibiting NLRP3 inflammasome activation (*72,73*). Virtual screening of key active components employs molecular docking technology to assess the binding affinity between chemical components and core target proteins. Binding energy < -5.0 kcal/mol is generally considered to have good binding activity, while <

-7.0 kcal/mol suggests strong binding (*74*). Validation experimental design is an indispensable component of network pharmacology research: it is necessary to confirm the authenticity of the predicted "component-target-pathway" relationships through *in vitro* enzyme inhibition experiments, cellular signaling pathway detection (Western blot detection of key protein phosphorylation), and animal model pharmacological validation (*75*). In formula granule equivalence research, the value of network pharmacology lies in: even if differences exist in the chemical component spectra between formula granules and decoction pieces, pharmacological equivalence may still be achieved as long as both regulate the same core targets and key pathways (*76*). This provides theoretical basis for establishing more scientific and systematic equivalence evaluation standards.

4. Future development directions and prospects

The future development of formula granules should focus on the synergistic advancement of technological innovation, standard refinement, and clinical translation. In terms of technology, novel extraction and stabilization approaches — such as ultrasound-microwave synergistic extraction, supercritical CO_2 extraction, nano-lipid carriers, and cyclodextrin inclusion complexes— can significantly improve the retention of volatile and thermolabile components. Moreover, the integration of AI-driven quality control models offers a transformative opportunity. Machine learning algorithms can analyze high-dimensional chemical fingerprint, metabolomic, and pharmacodynamic data to establish predictive correlations between process parameters and key quality attributes, enabling real-time monitoring and adaptive optimization of manufacturing processes. Intelligent systems based on the Internet of Things and AI can achieve precise control of critical parameters (error < 1%), fundamentally enhancing inter-batch consistency and product stability.

From a regulatory and industrial perspective, the internationalization of formula granules requires accelerated participation in international standard development and technical alignment with major pharmacopoeias. Blockchain technology could be leveraged to establish transparent, tamper-proof traceability systems for the entire supply chain — from raw material sourcing to finished product distribution — ensuring data integrity and building international trust. Clinical translation must prioritize large-sample, head-to-head randomized controlled trials (RCTs) comparing formula granules with traditional decoctions, supported by real-world evidence. Furthermore, personalized medication strategies based on genetic polymorphisms and the development of patient-centric dosage forms (*e.g.*, instant-dissolving granules) should be explored to improve therapeutic outcomes and adherence. Ultimately, through coordinated progress in science, standards, clinical validation, and industrial upgrading, formula granules can evolve from an "alternative" to a "preferred" modern TCM dosage form, offering globally accessible, quality-assured therapeutic options.

Funding: None.

Conflict of Interest: The authors have no conflicts of interest to disclose.

References

1. Gu ZX, Wang ZH, Zhang XQ, Zhou GH, Liang GH, Zeng LF, Liu J. Research advances in the study of traditional Chinese medicine formula granules on signaling pathway-mediated disease mechanisms. Front Pharmacol. 2025; 16:16 09211.
2. Zhang XQ, Wei XD, Gu ZX, Zhou GH, Huang CJ, Luo MH, Zeng LF, Yang WY. Application of artificial intelligence-assisted traditional Chinese medicine formula granules in bone and joint degenerative diseases in the field of holistic health. Front Med (Lausanne). 2025; 12:1630824.
3. Zhu PP, Li G, Yang HJ. Trend analysis and regulatory strategies for Traditional. Chinese Medicine formula granules. Zhongguo Zhong Yao Za Zhi. 2024; 49:4249-4260. (in Chinese)
4. Liu CJ, Liu YK, Zhang JH, Yao YC, Li JD, Zhang FC, Liu XC, Zhang YW, Cao GY, Meng ZQ. Analysis of anti-inflammatory, anti-tumor active components of *Menispermum rhizoma* formula granules: Based on UPLC-Q-TOF-MS and network pharmacology. Xinan Da Xue Xue Bao. 2024; 46:227-240. (in Chinese)
5. Li H, Wang L, Zhang H, Yu W, Li Y, Jiang H, Wang D, Wang Y. Study on material basis and anti-hypertensive metabolomics of Zhengan-Xifeng-Tang (ZXT): A comparison between ZXT decoction and granules. J Chromatogr B Analyt Technol Biomed Life Sci. 2024; 1236:124063.
6. Publication of Special Regulations on the Management of Chinese Medicine Standards. Zhongguo Yao Xue Za Zhi. 2024; 65:1686. (in Chinese)
7. Wang Y, Yang R, Shi Y, Liu S. Elucidating the pharmacological basis of Xianling Cifang granules against breast cancer. A Metabolomic Profiling Study. Drug Des Devel Ther. 2025; 19:8213-8236.
8. Shen J, Tong Z, Han B, Zhang Z, Xian Z, Yuan Y, Duan X, Han S, Liu P, Wang Z. Synergistic wound healing: Unraveling the multi-target effects of traditional Chinese medicine and its biomaterials on chronic wound pathways. Int J Nanomed. 2025; 20:12889-12912.
9. Shi LY, Fang YG, Chen LM, Li ZY, Wang R, Wang ZM, Gao HM. Application of QAMS for quality evaluation and control of Chinese patent medicines: taking *Bufonis Venenum*-contained preparations as examples. Zhongguo Zhong Yao Za Zhi. 2021; 46:2931-2941. (in Chinese)
10. Li C, Yang J, Chu L, Tian J, Xiao J, Huang Y, Wang Q, Guo B, Huang L, Hu Y, Luo Y. The function of Bazhen decoction in rescuing progeroid cell senescence *via* facilitating G-quadruplex resolving and telomere elongation. J Ethnopharmacol. 2024; 323:117694.
11. Zhang YH, Wang YW, Su JHm, Dai SY, Qiao YJ, Luo G, Xu B. Physical Fingerprint of Traditional Chinese Medicine Powders: A Review. Fen Xi Ce Shi Xue Bao.

2021; 40:139-148. (in Chinese)
12. Zheng Y, Zhou S, Zhang H, Lu Z, Deng R, Feng Y, Liu P. Comparative study of the flavonoid content in radix scutellaria from different cultivation areas in China. Int J Anal Chem. 2023; 2023:3754549.
13. Yang HN, Zhang JC, Wu SH, Li JB. Research on preparation process and quality evaluation of traditional Chinese medicine dispensing granules and its consistency with traditional decoction: A review. Zhongguo Shi Yan Fang Ji Xue Za Zhi. 2023; 29:266-274. (in Chinese)
14. Chen SJ, Jiang HM, Xu X, *et al*. Discussion on technical characteristics of National Drug Standards for Traditional Chinese Medicine dispensing granule. Zhongguo Shi Yan Fang Ji Xue Za Zhi. 2025; 31:1-13. (in Chinese)
15. Li CC, Zhu D, Fu HZ, Ren Q. Quality evaluation of *Jingli* based on HPLC fingerprint combined with chemometrics and multi-Indicator content determination. Zhongguo Yao Xue Za Zhi. 2025; 60:1809-1818. (in Chinese)
16. Zhao JF, Zhang X, Qi J, Song ZH. Retrospective analysis on the application of fingerprint and characteristic chromatography technology in the National Standards of Traditional Chinese Medicine Dispensing Granules. Zhongguo Xian Dai Ying Yong Xue Za Zhi. 2023; 40:1278-1281. (in Chinese)
17. Wang G,Xu G, Xie XY, *et al*. China Parkinson's disease report 2025. Shen Jing Bing Xue Yu Shen Jing Kang Fu Xue Za Zhi. 2025; 21:63-98. (in Chinese)
18. Zhou B, Xiao JF, Tuli L, Ressom HW. LC-MS-based metabolomics. Mol Biosyst. 2012; 8:470-481.
19. Yang L, Zhang X, Wang Z, Lin X, Zhang Y, Lu J, Wu L, Yao S, Jing W, Huang X, Wang P. Decoction regulating phytochemicals' micromorphology changes and anti-inflammation activity enhancements originated from herb medicine supermolecules. Chin Med. 2024; 19:19.
20. Wei J, Liu Z, Li M, Du L, Zhu X, Leng Y, Han C, Xu Q, Zhang C. Based on UPLC-Q-TOF/MS and network pharmacology to explore the mechanism of Qingre Lishi decoction in the treatment of psoriasis. Drug Des Devel Ther. 2024; 18:3871-3889.
21. Wu YQ, Gou YQ, Han J, Bi YY, Feng SL, Hu FD, Wang CM. Evaluation preparation technology of Xiaochaihu granules using fingerprint-peak pattern matching. J Pharm Anal. 2011; 1:119-124.
22. Zhao J, Tian G, Qu H. Research on comprehensive quality consistency evaluation strategy for TCM Granules: A case study with sugar-free Yangwei Granules produced by fluid-bed granulation. Chin Herb Med. 2024; 17:575-583.
23. Li Y, Yu B, Zhao W, Pu X, Zhong X, Tao X, Wang Y, Cao W, Zhang D. UPLC fingerprinting combined with quantitative analysis of multicomponents by a single marker for quality evaluation of YiQing granules. Front Chem. 2025; 13:1632033.
24. Kucukoglu AS, Hiz G, Karaca H. Effects of thermal and nonthermal treatments on microorganisms, pyrrolizidine alkaloids and volatile compounds in oregano (*Origanum vulgare* L.). Food Chem. 2024; 440:138235.
25. Song W, Zheng W, Zhang J, Zhang T, Liu SC, Yu LY, Ma BP. Metabolism of saponins from Traditional Chinese Medicines: A review. Yao Xue Xue Bao. 2018; 53:1609-1619. (in Chinese)
26. Shengbu M, Ai L, Shi Q, Zhao Q, Liu XN, Lai XR. Research progress of Maillard reaction and its application in processing of Traditional Chinese Medicine. Nat Prod Commun. 2024; 19:1934578X241290620.
27. Liu Z, Liu Y, Chao Z, Song Z, Wang C, Lu A. *In vitro* antioxidant activities of Maillard reaction products produced in the steaming process of *Polygonum multiflorum* Root. Nat Prod Commun. 2011; 6:55-58.
28. Liu Z, Chao Z, Liu Y, Song Z, Lu A. Maillard reaction involved in the steaming process of the root of *Polygonum multiflorum*. Planta Medica. 2009; 75:84-88.
29. Wang HY, Qian H, Yao WR. Melanoidins produced by the Maillard reaction: Structure and biological activity. Food Chem. 2011; 128:573-584.
30. Nooshkam M, Varidi M, Bashash M. The Maillard reaction products as food-born antioxidant and antibrowning agents in model and real food systems. Food Chem. 2019; 275:644-660.
31. Zhuang Y, Dong J, He X, Wang J, Li C, Dong L, Zhang Y, Zhou X, Wang H, Yi Y, Wang S. Impact of heating temperature and fatty acid type on the formation of lipid oxidation products during thermal processing. Front Nutr. 2022; 9:913297.
32. Zhang JH, Wu NN, Lyn YN, Cao GY, Dong XD, Lin YQ, Lin JX, Meng ZQ. Quality evaluation of *Siphonostegiae* Herba formula granules based on specific chromatograms combined with chemometrics and quantitative analysis of multi-components with a single-marker. Zhong Cao Yao Za Zhi. 2024; 55:4722-4734. (in Chinese)
33. Gao J, Li J, Wang J, Wang Y, Yang D, Zhang Z, Fu Z, Wang F, Wang L, Chai S, Han L. Comprehensive chemical profiling and quality marker discovery in Shenxiao granules *via* orthogonal HILIC×RP 2D-LC/MS and mass defect filtering algorithm. Anal Bioanal Chem. 2025; 417:6915-6931.
34. Chen SJ, Li S, Guo KJ, Zhang YT, Zhou HQ, Pu XL. Discussion on technical characteristics of National Drug Standards for Traditional Chinese Medicine dispensing granule. Zhongguo Shi Yan Fang Ji Xue Za Zhi. 2025; 31:1-13. (in Chinese)
35. Hao YD, Ma K, Wen RQ, Li DH. Discussion on Current National Standards for Traditional Chinese Medicine Dispensing Granules. Zhongguo Shi Yan Fang Ji Xue Za Zhi. 2023; 29:158-164. (in Chinese)
36. Chan K, Leung KS, Zhao SS. Harmonization of monographic standards is needed to ensure the quality of Chinese medicinal materials. Chin Med. 2009; 4:18.
37. Hakamatsuka T. Standardization of Crude Drugs for the Japanese Pharmacopoeia. Yakugaku Zasshi. 2020; 140:783-788.
38. Wong SP, Leong LP, Koh JHW. Polyphenols contents and antioxidant capacity of 68 Chinese herbals suitable for medical or food uses. Food Chem. 2008; 113:23-31.
39. Liu A, Xu T, Yang W, Zhou D, Sha Y. Quantitative Determination of 7 Saikosaponins in Xiaochaihu Granules Using High-Performance Liquid Chromatography with Charged Aerosol Detection. J Anal Methods Chem. 2021; 2021:6616854.
40. Yang Y, Yang T, Yang BZ, Sun BH, Sun GX. A quality control method for the quality consistency evaluation of XiaoChaiHu granules based on the quantitative combination of four bioactive components and chromatographic fingerprint combined with differential scanning calorimetry and antioxidant activity analysis. Microchem J. 2025; 218:115539-115539.
41. Xian Z, Valentina R, Raynold M, John T, Kelvin C. A comparative study of *Salvia miltiorrhiza* Radix & Rhizoma raw material and granule products using chromatographic analysis and antioxidant activity. J Tradit Chin Med Sci. 2022; 9:311-320.

42. Li RJ, Gao CY, Guo C, Zhou MM, Luo J, Kong LY. The anti-inflammatory activities of two major withanolides from physalis minima *via* acting on NF-κB, STAT3, and HO-1 in LPS-stimulated RAW264.7 cells. Inflammation. 2017; 40:401-413.
43. Zhou Y, Tao H, Wang A, Zhong Z, Wu X, Wang M, Bian Z, Wang S, Wang Y. Chinese herb pair Paeoniae Radix Alba and Atractylodis Macrocephalae Rhizoma suppresses LPS-induced inflammatory response through inhibiting MAPK and NF-κB pathway. Chin Med. 2019; 14:2.
44. Yin Y, Guan Y, Duan J, Wei G, Zhu Y, Quan W, Guo C, Zhou D, Wang Y, Xi M,Wen A. Cardioprotective effect of Danshensu against myocardial ischemia/re perfusion injury and inhibits apoptosis of H9c2 cardiomyocytes *via* Akt and ERK1/2 phosphorylation. Eur J Pharmacol. 2013; 699:219-226.
45. Wang L, Ma R, Liu C, Liu H, Zhu R, Guo S, Tang M, Li Y, Niu J, Fu M, Gao S, Zhang D. *Salvia miltiorrhiza*: A potential red light to the development of cardiovascular diseases. Curr Pharm Des. 2017; 23:1077-1097.
46. Shah VP, Tsong Y, Sathe P, Liu JP. *In vitro* dissolution profile comparison-- statistics and analysis of the similarity factor, f2. Pharm Res. 1998; 15:889-896.
47. Guo P, Wang Q, Xiang X, Zhang Y, Pan Y, Zuo Z, Wang J. Establishment of dissolution test method for multi-components in Traditional Chinese Medicine preparations based on *In Vitro-In Vivo* correlation. Pharmaceuticals (Basel). 2024; 17:1065.
48. Wu Y, Wang P, Yang H, Sui F. UPLC-Q-TOF-MS and UPLC-MS/MS methods for metabolism profiles and pharmacokinetics of major compounds in Xuanmai Ganjie Granules. Biomed Chromatogr. 2019; 33:e4449.
49. Chen Y, Jiang E, Yan J, Tao Y. Validation of an analytical method using UPLC-MS/MS to quantify four bioactive components in rat plasma and its application to pharmacokinetic study of traditional and dispensing granules decoction of *Ziziphi spinosae semen*. Biomed Chromatogr. 2020; 34:e4797.
50. Zhou K, Zhang A, Miao JH, H Sun H, Yan GL, Wu FF, Wang XJ. Serum pharmacochemistry in herbal medicine and its active ingredients: Current evidence and future development. Open J Proteom Genom. 2018; 3:001-010.
51. Pei L, Bao Y, Liu S, Zheng J, Chen X. Material basis of Chinese herbal formulas explored by combining pharmacokinetics with network pharmacology. PLoS ONE. 2013; 8:e57414.
52. Feng L, Wang L, Hu C, Jiang X. Pharmacokinetics, tissue distribution, metabolism, and excretion of ginsenoside Rg1 in rats. Arch Pharm Res. 2010; 33:1975-1984.
53. Kim HJ, Oh TK, Kim YH, Lee J, Moon JM, Park YS, Sung CM. Pharmacokinetics of ginsenoside Rb1, Rg3, Rk1, Rg5, F2, and compound K from Red ginseng extract in Healthy Korean Volunteers. Evid Based Complement Alternat Med. 2022; 2022:8427519.
54. Cheng J, Long J, Zhang J, Han L, Hu Y, Liu J, Qiu R, Zhu Z, Fan H. Safety, tolerance, and pharmacokinetics of salvianolic acid B in healthy Chinese volunteers: A randomized, double-blind, placebo-controlled phase 1 clinical trial. Front Pharmacol. 2023; 14: 1146309.
55. Du G, Fu L, Jia J, Pang X, Yu H, Zhang Y, Fan G, Gao X, Han L. Validated UPLC-MS/MS method for quantification of seven compounds in rat plasma and tissues: Application to pharmacokinetic and tissue distribution studies in rats after oral administration of extract of *Eclipta prostrata* L. Biomed Chromatogr. 2018; 32:e4191.
56. Han D, Zhao Z, Mao T, Gao M, Yang X, Gao Y. Ginsenoside Rg1: A neuroprotective natural dammarane-type triterpenoid saponin with anti-depressive properties. CNS Neurosci Ther. 2024; 30:e70150.
57. He G, Chen G, Liu W, Ye D, Liu X, Liang X, Song J. Salvianolic acid B: A review of pharmacological effects, safety, combination therapy, new dosage forms, and novel drug delivery routes. Pharmaceutics. 2023; 15:2235.
58. Lyons E, Line C, Lee JJ. Developing drugs for prevention of chemotherapy-induced nausea and vomiting: Draft guidance from the FDA. Clin Cancer Res. 2021; 27:6072-6074.
59. Hauck WW, Parekh A, Lesko LJ, Chen ML, Williams RL. Limits of 80%-125% for AUC and 70%-143% for Cmax. What is the impact on bioequivalence studies? Int J Clin Pharmacol Ther. 2001; 39:350-355.
60. Zhu CS, Lin ZJ, Xiao ML, Niu HJ, Zhang B. The spectrum-effect relationship-a rational approach to screening effective compounds, reflecting the internal quality of Chinese herbal medicine. Chin J Nat Med. 2016; 14:177-184.
61. Xu GL, Xie M, Yang XY, Song Y, Yan C, Yang Y, Zhang X, Liu ZZ, Tian YX, Wang Y, Jiang R, Liu WR, Wang XH, She GM. Spectrum-effect relationships as a systematic approach to traditional chinese medicine research: Current status and future perspectives. Molecules. 2014; 19:17897-17925.
62. Qiu Q, Jiang L, Huang C, Yu L, Zhen D, Ye M, Liu Y, Shi J, Liu X, Gu B, Zhen H. Study on the spectrum-effect correlation of anti-Inflammatory active extract of *Sauropus spatulifolius* Beille. J Anal Methods Chem. 2022; 2022:5646546.
63. Xu Y, Li C, Chen T, Li X, Wu X, Zhang Q, Zhao L. Quantitative analysis of the multicomponent and spectrum-effect correlation of the antispasmodic activity of Shaoyao-Gancao decoction. J Anal Methods Chem. 2022; 2022:2279404.
64. Deng X, Lei HY, Ren YS, Ai J, Li YQ, Liang S, Chen LL, Liao MC. A novel strategy for active compound efficacy status identification in multi-tropism Chinese herbal medicine (*Scutellaria baicalensis* Georgi) based on multi-indexes spectrum-effect gray correlation analysis. J Ethnopharmacol. 2023; 300:115677.
65. Rao SW, Duan YY, Pang HQ, Xu SH, Hu SQ, Cheng KG, Liang D, Shi W. Spectrum-effect relationship analysis of bioactive compounds in *Zanthoxylum nitidum* (Roxb.) DC. by ultra-high performance liquid chromatography mass spectrometry coupled with comprehensive filtering approaches. Front Pharmacol. 2022; 13:794277.
66. He P, Zhang C, Yang Y, Tang S, Liu X, Yong J, Peng T. Spectrum-effect relationships as an effective approach for quality control of natural products: A review. Molecules. 2023; 28:7011.
67. Chen Q, Zhao Y, Li M, Zheng P, Zhang S, Li H, Chen J. HPLC-MS and network pharmacology analysis to reveal quality markers of Huo-Xue-Jiang-Tang Yin, a Chinese herbal medicine for type 2 diabetes mellitus. Evid Based Complement Alternat Med. 2021; 2021:1072975.
68. Wu Y, Zhu Y, Xie N, Wang H, Wang F, Zhou J, Qu F. A network pharmacology approach to explore active compounds and pharmacological mechanisms of a patented Chinese herbal medicine in the treatment of endometriosis. PLoS One. 2022; 17:e0263614.
69. Zhang C, Ji Z, Xu N, Yuan J, Zeng W, Wang Y, He Q, Dong J, Zhang X, Yang D, Jiang W, Yan Y, Shang W,

Chu J, Chu Q. Integrating network pharmacology and experimental validation to decipher the pharmacological mechanism of DXXK in treating diabetic kidney injury. Sci Rep. 2024; 14:22319.
70. Zheng W, Wu J, Gu J, Weng H, Wang J, Wang T, Liang X, Cao L. Modular characteristics and mechanism of action of herbs for endometriosis treatment in Chinese medicine: A data mining and network pharmacology-based identification. Front Pharmacol. 2020; 11:147.
71. Wang L, Xu X, Wang Z, Chen Q, Wei X, Xue J, Zhang Z, Wang M, Li Y, Zhang J, Wei D. Network pharmacology and molecular docking-based strategy to investigate the multitarget mechanisms of Shenqi Yizhi granule on Alzheimer"s disease. Evid Based Complement Alternat Med. 2022; 2022:8032036.
72. Gao LQ, Xu J, Chen SD. *In silico* screening of potential Chinese herbal medicine against COVID-19 by targeting SARS-CoV-2 3CLpro and angiotensin converting Enzyme II using molecular docking. Chin J Integr Med. 2020; 26:527-532.
73. Yuan J, Yan F, Li W, Yuan G. Network pharmacological analysis of Xuefu Zhuyu decoction in the treatment of atherosclerosis. Front Pharmacol. 2022; 13:1069704.
74. Forli S, Huey R, Pique ME, Sanner MF, Goodsell DS, Olson AJ. Computational protein-ligand docking and virtual drug screening with the AutoDock suite. Nat Protoc. 2016; 11:905-919.
75. Wang M, He L, Yan P. Integrated network pharmacology, molecular docking and experimental validation to investigate the mechanism of tannic acid in nasopharyngeal cancer. Sci Rep. 2025; 15:5645.
76. Wang Y, Xu TF, Chen XY, Ye Y, Liu LQ,Wang YF, Zhang P. Network pharmacology and molecular docking approach to investigate the mechanism of a Chinese herbal formulation Yougui pills against steroid-related osteonecrosis of the femoral head. Arab J Chem. 2024; 17:105597.

Received December 22, 2025; Revised February 23, 2026; Accepted February 24, 2026.

**Address correspondence to:*
Ling Wang, Guizhou University of Traditional Chinese Medicine, No. 4 Dongqing Road, Huaxi University Town, Huaxi District, Guiyang City, Guizhou Province 550025, China.
E-mail: dr.wangling@vip.163.com

Released online in J-STAGE as advance publication February 27, 2026.

Original Article

DOI: 10.5582/ddt.2025.01121

Development of ginger extract-loaded self-nanoemulsifying drug delivery system for enhanced solubility of ginger extract

Maung Maung Than[1], Chuda Chittasupho[2], Songwut Yotsawimonwat[2], Kantaporn Kheawfu[2,*]

[1] Ph.D. Degree Program in Pharmacy, Faculty of Pharmacy, Chiang Mai University, Chiang Mai, Thailand;
[2] Department of Pharmaceutical Sciences, Faculty of Pharmacy, Chiang Mai University, Chiang Mai, Thailand.

SUMMARY: The well-known medicinal plant ginger (*Zingiber officinale* Roscoe) has numerous health benefits, but its key bioactive compound, 6-gingerol, suffers from poor water solubility and stability. This study aimed to enhance the oral delivery of ginger extract by formulating a self-nanoemulsifying drug delivery system (SNEDDS) using a design of experiments (DoE) approach. Ginger rhizomes were extracted by ultrasound-assisted extraction, with a 10-min extraction time yielding the highest 6-gingerol content. An I-optimal mixture design was then applied to develop SNEDDS formulations using castor oil, Cremophor RH40, various co-surfactants (Span 20 or Span 80), and co-solvents (polyethyleneglycol 400 (PEG 400) or ethanol). The optimized SNEDDS readily self-emulsified in gastric medium, producing nano-sized droplets (42.5-78.1 nm) with low polydispersity (0.12-0.58) within 10 min. The ginger extract-loaded SNEDDS (G-SNEDDS) achieved high encapsulation efficiencies, exceeding 90% for both 6-gingerol and 6-shogaol, and significantly enhanced the *in vitro* release of 6-gingerol, reaching cumulative release levels of approximately 90-100% over 48 h, compared to only 67% from the unformulated extract. Transmission electron microscopy (TEM) confirmed the formation of uniform, spherical nanoemulsion droplets. Short-term stability testing indicated that the optimized formulation remained physically stable, as evidenced by minimal changes in droplet size, and preserved most of the 6-gingerol content under ambient storage conditions; however, exposure to elevated temperatures accelerated the conversion of 6-gingerol to 6-shogaol. Overall, the optimized SNEDDS significantly enhanced the solubility, dissolution, and storage stability of ginger extract, offering a promising strategy to improve the oral bioavailability of the therapeutically active constituents present in ginger.

Keywords: ginger extract, self-nanoemulsifying drug delivery systems (SNEDDS), lipid-based formulation, 6-gingerol, 6-shogaol

1. Introduction

The well-known medicinal plant ginger (*Zingiber officinale* Roscoe) has been traditionally used for centuries to treat a variety of ailments. It possesses a wide range of pharmacological properties, including anti-inflammatory, antioxidant, anti-nausea, antimicrobial, anticancer, anti-ulcer, antidiabetic, and immunomodulatory effects, mainly attributed to its bioactive constituents such as gingerols and shogaols (*1-3*). Despite these promising biological activities, the use of ginger extract as an antioxidant is often limited due to the chemical instability of its active constituents. These compounds are volatile and sensitive to environmental factors such as light, air, and heat, which negatively affect their solubility, stability, and ultimately, their bioavailability (*4*).

Among the major active components, 6-gingerol is the most abundant and extensively studied. However, it exhibits poor aqueous solubility, contributing to its low oral bioavailability. It dissolves more readily in organic solvents such as ethanol (30 mg/mL), dimethylformamide (DMF, 30 mg/mL), and dimethyl sulfoxide (DMSO, 25 mg/mL), whereas its solubility in phosphate-buffered saline (PBS, pH 7.2) is significantly lower, approximately 1 mg/mL (*5,6*). This limited aqueous solubility presents a major challenge for formulating effective oral dosage forms. Despite these limitations, plant-derived medications, including ginger-based preparations, are generally more accessible and cost-effective and are associated with fewer adverse effects than synthetic drugs (*7*).

To overcome the challenges associated with the poor solubility and instability of ginger extract, various advanced drug delivery systems have been investigated. Nanostructured lipid carriers have been reported to enhance the aqueous solubility of 6-gingerol and improve its antioxidant and anti-inflammatory activities

(*8*). Chitosan-based nanoparticles containing gingerol demonstrated improved anticancer efficacy by markedly increasing cancer cell inhibition within 48 h (*9*). In addition, microemulsion-based delivery systems have been shown to improve the solubility, stability, and anti-inflammatory effects of ginger extract (*10*).

One promising strategy is the self-nanoemulsifying drug delivery system (SNEDDS), which consists of an isotropic mixture of oil, surfactant, and co-surfactant. SNEDDS can spontaneously form fine oil-in-water nanoemulsions (< 200 nm) upon contact with aqueous media in the gastrointestinal tract, thereby improving solubilization, absorption, and stability of lipophilic drugs. A self-microemulsifying drug delivery system (SMEDDS) containing 6-gingerol reported enhanced release in various pH media and prolonged systemic exposure (6.58-fold) compared to the unformulated extract (*11*). Similarly, SNEDDS containing ginger extract using snakehead fish oil have demonstrated improved *in vivo* antioxidant activity, as evidenced by increased superoxide dismutase levels, despite slightly lower *in vitro* radical-scavenging activity (*12*). These findings collectively highlight the potential of SNEDDS in addressing the challenges associated with ginger extract delivery. Nonetheless, further optimization and evaluation of the formulation are necessary to ensure efficacy and safety.

Design of experiment (DoE) is a powerful statistical tool used in pharmaceutical development to optimize formulation parameters and identify critical variables affecting product performance (*13*). In the context of SNEDDS development, formulation factors such as the type and concentration of oil, surfactant, and co-surfactant can be systematically varied to study their impact on droplet size, polydispersity index (PDI), and other critical quality attributes (*14*). This approach is more efficient than traditional trial-and-error methods, reducing time and resources required for formulation development.

Therefore, the objective of this study was to develop a ginger extract-loaded SNEDDS (G-SNEDDS) using a DoE-based approach and to evaluate the physicochemical properties of the resulting formulation.

2. Materials and Methods

2.1. Materials

Standard 6-gingerol (6G) was purchased from Sigma-Aldrich (Burlington, MA, USA) Acetonitrile and methanol (high-performance liquid chromatography (HPLC) grade) as well as ethanol (AR grade), were purchased from RCI Labscan (Bangkok, Thailand). Ultrapure water used throughout this study was obtained from a Milli-Q reverse osmosis (RO) system, Maxima (Merck Millipore, Burlington, MA, USA). Castor oil, Cremophor RH 40 (polyethylene glycol-40 hydrogenated castor oil), Tween 80 (polyoxyethylene sorbitan mono oleate), Span 80 (sorbitan mono oleate), and Span 20 (sorbitan mono laurate) were purchased from Namsiang Company Limited (Bangkok, Thailand). Polyethyleneglycol 400 (PEG 400) was purchased from Srichand United Dispensary (Bangkok, Thailand).

2.2. Extraction method for ginger rhizomes

The 1-year-old ginger rhizomes were sourced from Samoeng District in Chiang Mai Province, and obtained from a local market in Chiang Mai, Thailand. The extraction method was adapted from a previously published method (*15*). The rhizomes were preliminary cleaned to remove impurities and excess moisture, then peeled and sliced into thin pieces (approximately 3 mm thick). The sliced rhizomes were dried in a controlled oven at 50ºC for 24 h. The dried slices were subsequently ground into a fine powder (< 200 mesh) using an electric blade mill. The powdered ginger was stored at room temperature prior to extraction.

Ultrasound-assisted extraction (UAE) was performed using an ultrasonic bath. For each experiment, 0.3 g of ginger powder was mixed with 20 mL of 95% ethanol in centrifuge tubes. Extraction times of 10, 20, and 30 min were evaluated while maintaining the extraction temperature below 60ºC. After extraction, the mixtures were filtered through Whatman No. 1 filter paper. The filtrates were then concentrated to dryness using a rotary evaporator to determine the crude extract yield. The obtained extracts were stored in light-resistant containers at 4 ± 2ºC until further analysis. The percentage yield (% yield) was calculate using the following equation (1):

$$\% \text{ Yield} = \frac{\text{Crude Extract Weight}}{\text{Dried Sample Weight}} \times 100 \text{ -------- (1)}$$

2.3. Quantification of active compounds in ginger extract

The quantification of active constituents in ginger extract was performed using HPLC, with 6-gingerol and 6-shogaol as the reference standard. The analytical procedure was adapted from the Thai Herbal Pharmacopoeia 2021 (*16*). A stock solution of 6-gingerol and 6-shogaol was prepared with a concentration of 1 mg/mL. The stock solution was diluted to prepare a five-point calibration curve within the range of 0.0025-0.1 μg/mL. A quantity of 10 mg of dried ginger extract, or an appropriate amount, was accurately weighed and dissolved in methanol with gentle mixing.

The HPLC analysis was performed on an Agilent Technologies 1260 Series liquid chromatograph (Agilent Technologies, Pittsburgh, PA, USA) equipped with a quaternary pump, autosampler, thermostatic column chamber, and diode array detector (DAD). Detection was performed at 282 nm. Chromatographic separation was achieved on a C18 reverse-phase column (Knauer,

Berlin, Germany; Eurospher II 100-5, 250 × 4.6 mm, 5 µm). The mobile phase consisted of buffer solution (A) and acetonitrile (B), delivered at a flow rate of 1.0 mL/min. Mobile phase A was prepared by mixing 550 mL of acetonitrile, 440 mL of 0.1% phosphoric acid in water, and 10 mL of methanol. Gradient elution was applied as follows: 100% B at 0 min, decreasing to 0% B by 2 min and held until 12 min, then linearly increased to 100% B by 14 min and maintained until 35 min. Chromatographic analysis was performed in triplicate. The data were recorded and processed using Agilent Chemstation software (Agilent Technologies, Pittsburgh, PA, USA).

2.4. Development of the SNEDDS

2.4.1. Selection of oil, surfactant, co-surfactant, and co-solvent

A preliminary selection of excipients for the SNEDDS formulation was carried out based on a literature review. The chosen components included castor oil as the oil phase; Cremophor RH40 as the surfactants; Span 80 and Span 20 as co-surfactant; and PEG 400 and ethanol as co-solvents, owing to their emulsifying capacity, compatibility, and oral safety profiles. The maximum permissible oral dosage ranges of these components were also reviewed and considered in the experimental design.

2.4.2. Experimental design

The formulation optimization was performed using the Design-Expert® software (Version 13, Stat-Ease Inc., Minneapolis, MN, USA), employing an I-optimal mixture design. The design aimed to determine the optimal ratio of oil, surfactant, co-surfactant, and co-solvent for efficient self-nanoemulsification. Four formulation systems (Systems 1 to 4), each consisting of varying proportions of oil, surfactant, co-surfactant, and co-solvent, as detailed in Table 1, were studied. The independent variable ranges were set as follows: oil (5-40% w/w), surfactant combined with co-surfactant (50-85% w/w), and co-solvent (0-10% w/w). The composition of the 18 experimental formulations is shown in Table 2. Droplet size, size distribution, and self-emulsification time required to obtain uniform nanosized droplets of the dispersed SNEDDS were considered as response variables. The relationship between the response and the formulation variables was determined using a quadratic mixture model, as shown in Equation (2):

$$Y = m_1A + m_2B + m_3C + m_4D + m_5AB + m_6AC + m_7AD + m_8BC + m_9BD + m_{10}CD \quad (2)$$

where Y is the response variable, and m_1–m_{10} are the regression coefficients corresponding to the components A–D, which denote the proportions of oil, surfactant, co-surfactant, and co-solvent, respectively. The intercept term was omitted, as the model was fitted using mixture design coding, where the sum of all component proportions equals 100%. Model performance was evaluated using the coefficient of determination (R^2), adjusted R^2, and predicted R^2 values. R^2 and adjusted R^2 values close to 1 indicate a strong model fit, whereas a predicted R^2 value greater than 0.5 suggests good predictive ability.

2.4.3. Formulation preparation

Each formulation was prepared according to the composition specified in the design matrix. The respective quantities of oil, surfactant, co-surfactant, and co-solvent were accurately weighed and mixed thoroughly to obtain a homogenous preconcentrate suitable for self-nanoemulsification.

2.4.4. Evaluation of physical characteristics

The physical properties of the SNEDDS formulations were evaluated based on self-emulsification time, droplet size, and PDI. To assess emulsification performance, 1 mL of each formulation was added to 250 mL of 0.1 N hydrochloric acid maintained at 37 ± 0.5°C under gentle stirring. The time required for the formation of a clear or slightly bluish nanoemulsion was recorded. Droplet size and PDI were determined using dynamic light scattering (DLS) with a Zetasizer

Table 1. Type and composition ranges (% w/w) of components used in each SNEDDS system for experimental design

Component	System 1	System 2	System 3	System 4
Oil:				
Castor oil	5-40	5-40	5-40	5-40
Surfactant:				
Cremophor RH 40	0-85	0-85	0-85	0-85
Co-surfactant:				
Span 20	0-85	-	0-85	-
Span 80	-	0-85	-	0-85
Co-solvent:				
PEG 400	0-10	0-10	-	-
Ethanol	-	-	0-10	0-10

Table 2. Experimental compositions (% w/w) of SNEDDS formulations obtained from the I-optimal mixture design

Exp No. (System 1-4)	Composition (% w/w)			
	Oil (A)	Surfactant (B)	Co-surfactant (C)	Co-solvent (D)
1	40.0	60.0	0.0	0.0
2	40.0	26.7	24.9	8.4
3	40.0	9.7	40.3	10.0
4	37.3	0.0	61.2	1.5
5	32.8	44.9	12.2	10.0
6	23.8	39.2	31.9	5.2
7	23.8	39.2	31.9	5.2
8	23.8	39.2	31.9	5.2
9	22.6	0.0	67.4	10.0
10	22.1	17.3	50.6	10.0
11	20.8	69.2	0.0	10.0
12	15.0	35.6	49.4	0.0
13	15.0	35.6	49.4	0.0
14	11.7	85.0	0.0	3.3
15	10.2	0.0	85.0	4.8
16	5.6	63.0	21.4	10.0
17	5.0	16.2	68.8	10.0
18	5.0	44.0	41.0	10.0

Nano ZS (Malvern Instruments Ltd., Malvern, UK) after appropriate dilution (1:100, v/v) with distilled water to minimize multiple scattering effects.

2.4.5. Selection of the optimal SNEDDS formulation

The selection criteria included a self-emulsification time of ≤ 10 min, a mean droplet size ≤ 200 nm, and a PDI ≤ 0.3, indicating a narrow and uniform particle size distribution. Formulations that met all these parameters were considered suitable for oral delivery, as they demonstrated efficient spontaneous emulsification, nanoscale droplet formation, and consistent physical stability. These optimal formulations were subsequently selected for further investigation.

2.5. Preparation of G-SNEDDS

The ginger extract was initially dissolved in the selected co-solvent and subsequently combined with the surfactant and co-surfactant under continuous stirring. The oil phase was then gradually added to the mixture. The resulting system was vortexed overnight to ensure uniform dispersion and formation of a stable preconcentrate. The optimized G-SNEDDS formulation was stored in sealed amber glass vials at 4 ± 2°C until further analysis.

2.6. Determination of drug entrapment efficiency (EE)

The EE of 6-gingerol and 6-shogaol within the G-SNEDDS formulation was determined based on a method adapted from a previously published method (*17*). Briefly, ultrafiltration using a 3,500 Da molecular weight cut-off membrane was employed to separate free (unentrapped) 6-gingerol and 6-shogaol from the nanoemulsion. The samples were centrifuged at 10,000× *g* for 10 min, and the resulting filtrate was collected. The concentrations of 6-gingerol and 6-shogaol in the filtrate (free drug) and the SNEDDS (total drug) were quantified using HPLC. The entrapment efficiency was calculated using the following equation (3):

$$EE\ (\%) = (W_t - W_f)/W_t \times 100 \text{ ------- (3)}$$

where W_t is the total amount of 6-gingerol or 6-shogaol in the formulation and W_f is the amount of free (unentrapped) 6-gingerol or 6-shogaol in the filtrate.

2.7. Morphological characterization of G-SNEDDS

The morphology of the dispersed droplets was investigated using transmission electron microscopy (TEM), according to a previous report (*18*), with some modifications. In brief, the samples were prepared by diluting 1 g of G-SNEDDS with 100 mL of 0.1 N hydrochloric acid and gently mixing them using a magnetic stirrer at 100 rpm. Subsequently, the sample was placed on copper grids (200 mesh), then the dried sample was stained with 1% phosphotungstic acid and dried at 25°C overnight. After that, the grid was loaded into a TEM sample holder. The droplet morphology was observed and recorded using a JEM 2100 Plus TEM (JEOL Ltd., Tokyo, Japan) with an energy filter installed (Omega filter, JEOL Co., Tokyo, Japan) and was operated at 100 kV.

2.8. *In vitro* drug release study

The *in vitro* drug release profile of the G-SNEDDS was evaluated using the dialysis bag diffusion method. The release medium was 0.1 N hydrochloric acid. In each

experiment, 1 g of G-SNEDDS was diluted with an equal volume of the respective medium (1:1, w/v) and placed in a dialysis bag, which was then immersed in 100 mL of fresh release medium contained in a 150 mL beaker. The system was maintained at 37 ± 0.5°C in a thermostatic shaking water bath set at 100 rpm. Samples were collected at predetermined time intervals over a 48 h period. At each time point, a 10 mL aliquot of the release medium was withdrawn and immediately replaced with an equal volume of fresh medium to maintain sink conditions. Each formulation was tested in triplicate. The collected samples were analyzed using HPLC at a detection wavelength of 282 nm to quantify the amount of 6-gingerol released as the major component. The cumulative percentage of drug release was calculated and plotted as a function of time.

2.9. Stability study of G-SNEDDS

The stability of the G-SNEDDS formulations was assessed using both heating-cooling cycle testing and a short-term storage stability study under different temperature conditions. For the heating-cooling test, each cycle involved storing the formulations at 4°C for 48 h, followed by 45°C for an additional 48 h. This cycle was repeated five times to simulate thermal stress. For the short-term stability study, the formulations were stored at 4°C, 30°C, and 45°C for a period of 90 days. Samples were withdrawn and analyzed at day 0, 30, 60, and 90. After each time point, physical stability was evaluated by measuring particle size and PDI using a Zetasizer Nano ZS. Chemical stability was assessed by determining the concentration of the active constituents, 6-gingerol and 6-shogaol, using a validated HPLC method. Formulations that maintained stable particle size distribution and retained chemical content over time were considered physically and chemically stable and were selected for further evaluation in subsequent studies.

2.10. Statistical analysis

Statistical analysis was performed using *t*-test and one-way analysis of variance (ANOVA) to identify significant differences among experimental groups. All results were expressed as mean ± standard deviation (SD). A p-value < 0.05 was considered statistically significant unless otherwise stated.

3. Results

3.1. Optimization of ginger extraction process

The results of ginger extraction at various extraction times are presented in Table 3. The crude extract obtained from dried ginger rhizomes appeared as a dark brown liquid. Among the tested durations (10, 20, and 30 min), the 10-min extraction yielded the lowest extract yield, whereas the 30-min extraction resulted in the highest yield ($p < 0.05$). Despite the higher yields at longer extraction times, the 6-gingerol content was significantly higher in the 10-min extract ($p < 0.05$), compared to those obtained at 20 and 30 min. In contrast, the 6-shogaol content did not differ significantly among the three extraction times. These findings indicate that although prolonged extraction enhances overall yield, due to increased cell wall disruption and improved solvent penetration, shorter extraction durations better preserve thermolabile constituents, such as 6-gingerol. Therefore, the 10-min extraction condition was considered the most suitable for obtaining high levels of bioactive compounds, particularly 6-gingerol, under the tested conditions.

3.2. Preliminary screening and selection of SNEDDS systems

3.2.1. Effects of excipients on particle size

A comparative analysis was performed to evaluate four distinct SNEDDS platforms, each comprising castor oil as the lipid phase and Cremophor RH40 as the primary surfactant. The systems differed in their co-surfactant type (Span 20 or Span 80) and co-solvent (PEG 400 or ethanol) combinations. The formulations were assessed using an I-optimal mixture design fitted to a quadratic model to determine the effect of each excipient and their interactions on nanoemulsion performance. The studied response variables included droplet size, PDI, and self-emulsification time.

Among these outcomes, only droplet size demonstrated statistically acceptable model fitting, as evidenced by high R^2 and adjusted R^2 values and acceptable lack-of-fit results. Therefore, the regression coefficients and interaction effects are discussed primarily with respect to droplet size, which reflects

Table 3. Extract yield and contents of major bioactive compounds in ginger extracts obtained at different extraction times (mean ± SD, n = 3)

Extraction time	Yield (%)	6-Gingerol (mg/g crude extract)	6-Shogaol (mg/g crude extract)
10 min	10.17 ± 0.71^{a}	68.43 ± 5.00^{a}	6.55 ± 0.22^{c}
20 min	13.01 ± 0.03^{b}	43.34 ± 28.91^{b}	6.82 ± 0.14^{c}
30 min	14.67 ± 1.41^{c}	44.30 ± 19.04^{b}	7.39 ± 0.08^{c}

Different superscript letters indicate statistically significant differences among means ($p < 0.05$, one-way ANOVA with Tukey's post hoc test).

the efficiency of spontaneous nanoemulsion formation and is a critical parameter for drug solubilization and absorption.

Figure 1 presents the prediction contour plots of droplet size across Systems 1-4 at a fixed co-solvent concentration of 5% w/w, while Table 4 summarizes the regression coefficients and model parameters. System 4, composed of castor oil, Cremophor RH 40, Span 80, and ethanol, demonstrated superior statistical performance, with R^2 = 0.9865, adjusted R^2 = 0.9712, and predicted R^2 = 0.9455, indicating excellent model fit and predictive reliability. In contrast, System 3 (Span 20 and ethanol) showed the weakest model fit, suggesting that the formulation may be less consistent in behavior or less amenable to modeling within the chosen experimental range.

Among the individual terms, the co-solvent (D) exhibited the strongest influence on droplet size across all systems, particularly in System 1 (PEG 400-based), where the coefficient for co-solvent presented the highest value. This finding suggests a pronounced droplet size-increasing effect, likely attributable to the higher hydrophilicity and viscosity of PEG 400, which could interfere with efficient emulsification. On the other hand, System 4, which used ethanol as the co-solvent, exhibited a more moderate effect of co-solvent, indicating that ethanol facilitated improved emulsification and smaller droplet formation.

Several interaction terms were also significant. In System 1, the interactions AD, BD, and CD showed large negative coefficients, indicating negative effects between oil and co-solvent, and between other formulation components, in reducing droplet size. Although similar negative interaction trends were observed across all systems, these effects were less pronounced in ethanol-based systems. Notably, the AB interaction term (oil × surfactant) in System 4 was statistically significant ($p < 0.05$), demonstrating that the balance between oil and surfactant significantly impacted droplet size reduction in this ethanol-based formulation.

The beneficial role of Span 80, a low hydrophilic–lipophilic balance (HLB) surfactant, in Systems 2 and 4 may be attributed to its enhanced compatibility with castor oil, contributing to more efficient interfacial tension reduction and smaller droplet sizes. Overall, System 4 emerged as the most promising formulation, based on both statistical modeling outcomes and practical formulation considerations. The combination of Span 80 and ethanol provided the most favorable droplet size profile and robust model reliability, supporting its selection as a suitable candidate for further development

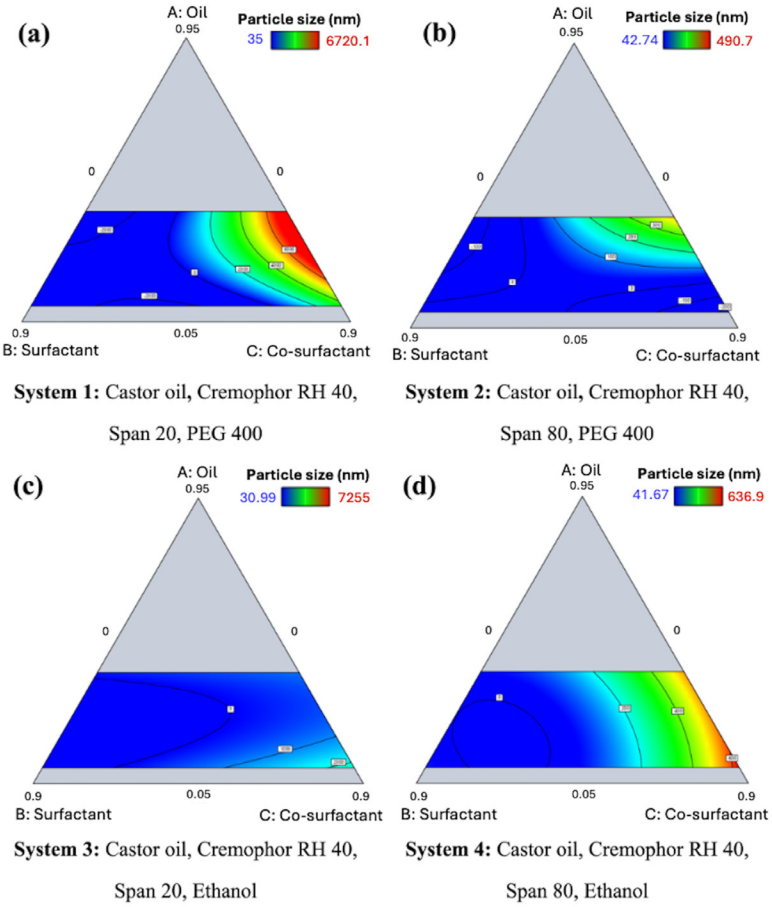

System 1: Castor oil, Cremophor RH 40, Span 20, PEG 400

System 2: Castor oil, Cremophor RH 40, Span 80, PEG 400

System 3: Castor oil, Cremophor RH 40, Span 20, Ethanol

System 4: Castor oil, Cremophor RH 40, Span 80, Ethanol

Figure 1. Prediction contour plots of droplet size (nm) after dispersing the SNEDDS system 1 (a), system 2 (b), system 3 (c), and system 4 (d) in 0.1 N hydrochloric acid. All systems were evaluated at a fixed co-solvent concentration of 5% w/w.

Table 4. Equation coefficients and model parameters for the fitted quadratic models for droplet size in each SNEDDS system

Parameters	System 1	System 2	System 3	System 4
A	-17755.29	1562.94	18600.97	1409.39
B	2595.31	315.65	1264.25	99.47
C	23.39	-333.42	1883.55	811.54
D	699700	62118.6	152200	11098.50
AB	21443.81	-2706.97	-29701.11	-2198.49*
AC	70696.81*	1263.12	-36392.36	-1495.01
AD	-821900*	-77500.6*	-171400	-15297.44
BC	-18728.71*	401.89	-359.86*	-1504.96*
BD	-790900*	-68930.5*	-187900	-11394.08
CD	-712600*	-66233.3*	-131900	-13495.91
R^2	0.984	0.952	0.548	0.986
R^2 adjusted	0.954	0.866	0.039	0.971
Predicted R^2	0.218	0.314	0.507	0.946

A, oil; B, surfactant; C, co-surfactant; D, co-solvent; the asterisks (*) signify coefficients relating to equation terms of significant effect on the response value.

and *in vivo* evaluation.

3.2.2. Effects of excipients on size distribution

The size distribution of the nanoemulsions, expressed as PDI, varied notably with the composition and relative proportions of excipients (Table 5). Formulations containing at least 35% w/w Cremophor RH40 and 20-35% w/w co-surfactant produced narrow size distributions (PDI = 0.12-0.20), as observed in Exp. 6-8 across Systems 2-4 and in Exp. 2 of all systems. In contrast, formulations with low surfactant content (≤ 10% w/w) and high co-surfactant levels (≥ 40% w/w), such as Exp. 3 and 10, exhibited high PDI values ranging from 0.84 to 1.00, indicating broad or multimodal particle size distributions. When comparing co-surfactants, Span 80 generally resulted in lower PDI values than Span 20, particularly in the presence of sufficient Cremophor RH40 (*e.g.*, System 2, Exp. 2 and 5-8). Ethanol-based systems (Systems 3 and 4) also achieved favorable PDI values (*e.g.*, System 4, Exp. 2: 0.17 and Exp. 18: 0.19).). However, increasing ethanol content combined with reduced Cremophor RH40 levels led to higher PDI values (*e.g.*, Exp. 3 and 10). In comparison, PEG 400–based systems (Systems 1 and 2) demonstrated a broader range of PDI values, ranging from 0.12 (System 2, Exp. 2) to 1.00 (System 1, Exp. 3, 10, and 17). Overall, formulations containing Span 80 and adequate levels of Cremophor RH40, in combination with either ethanol or moderate amounts of PEG 400, consistently produced the most uniform droplet size distributions (PDI ≤ 0.2).

3.2.3. Effects of excipients on self-emulsification time

The self-emulsification time of the four SNEDDS systems varied markedly depending on the type and proportion of excipients (Table 5). System 1, containing Span 20 and PEG 400, exhibited the fastest self-emulsification, with dispersion completed within approximately 1-3 min. In contrast, Systems 2-4 generally required longer emulsification times (> 10 min), except for formulations with higher surfactant concentrations, such as System 2 (Exp. 6-8; 9-10 min) and System 3 (Exp. 13: 6.5 ± 0.1 min). PEG 400-based formulations consistently achieved faster self-emulsification than ethanol-based systems. Ethanol-containing formulations (Systems 3-4) displayed delayed emulsification, with most samples requiring more than 10 min to disperse completely. Among co-surfactant types, formulations incorporating Span 20, which has a higher HLB, generally emulsified more rapidly than those containing Span 80, a lower HLB surfactant. However, the relationship between self-emulsification time and droplet characteristics was not linear, as shorter emulsification times did not always correspond to smaller droplet size or low PDI. Overall, PEG 400-based systems containing Span 20 and adequate Cremophor RH40 demonstrated the most efficient self-emulsification behavior among the formulations evaluated.

3.3. Evaluation of selected SNEDDS formulations

Although the quadratic models developed for each SNEDDS system demonstrated high R^2 and adjusted R^2 values, the predicted R^2 values for most systems were found to be substantially low. These values indicate limited predictive capability, rendering the models unreliable for extrapolating beyond the experimental design space. Given this limitation, it was necessary to adopt an alternative, criteria-based strategy to identify promising formulations for further development. Therefore, at least one formulation from each SNEDDS system was selected based on its ability to incorporate a relatively high proportion of oil (castor oil), which is a key component in enhancing the solubility of lipophilic bioactive constituents of ginger extract.

To guide this selection, theoretical optimal compositions were generated using the point prediction

Table 5. Polydispersity index (PDI) values of droplets and self-emulsification time obtained after dispersing each SNEDDS system in 0.1 N hydrochloric acid

Exp No.	Composition (% w/w)				PDI values				Self-emulsification time (min)			
	Oil	Surfactant	Co-surfactant	Co-solvent	System 1	System 2	System 3	System 4	System 1	System 2	System 3	System 4
1	40.0	60.0	0.0	0.0	0.69 ± 0.02	0.37 ± 0.09	0.52 ± 0.02	0.48 ± 0.04	2.3 ± 0.4	5.1 ± 0.1	>10	>10
2	40.0	26.7	24.9	8.4	0.28 ± 0.02	0.12 ± 0.07	0.21 ± 0.10	0.17 ± 0.13	2.5 ± 0.8	1.4 ± 0.5	>10	>10
3	40.0	9.7	40.3	10.0	1.00 ± 0.00	0.84 ± 0.03	1.00 ± 0.00	0.58 ± 0.03	1.4 ± 0.1	>10	>10	>10
4	37.3	0.0	61.2	1.5	NA	0.54 ± 0.31	0.52 ± 0.12	0.70 ± 0.22	NA	>10	>10	>10
5	32.8	44.9	12.2	10.0	0.38 ± 0.09	0.14 ± 0.02	0.23 ± 0.03	0.27 ± 0.04	1.2 ± 0.9	>10	>10	>10
6	23.8	39.2	31.9	5.2	0.28 ± 0.10	0.15 ± 0.04	0.13 ± 0.01	0.15 ± 0.08	1.5 ± 1.0	9.0 ± 0.2	9.4 ± 0.7	>10
7	23.8	39.2	31.9	5.2	0.13 ± 0.10	0.17 ± 0.13	0.12 ± 0.11	0.14 ± 0.05	1.8 ± 0.8	10.1 ± 0.4	9.2 ± 0.1	>10
8	23.8	39.2	31.9	5.2	0.20 ± 0.02	0.15 ± 0.05	0.12 ± 0.04	0.16 ± 0.04	1.5 ± 0.5	10.0 ± 0.2	9.1 ± 0.3	>10
9	22.6	0.0	67.4	10.0	NA	0.41 ± 0.03	0.43 ± 0.03	0.46 ± 0.13	NA	>10	>10	>10
10	22.1	17.3	50.6	10.0	1.00 ± 0.00	0.29 ± 0.21	1.00 ± 0.00	0.46 ± 0.30	1.4 ± 0.8	>10	>10	>10
11	20.8	69.2	0.0	10.0	0.32 ± 0.15	0.27 ± 0.02	0.26 ± 0.08	0.40 ± 0.02	1.7 ± 0.2	10.3 ± 0.1	>10	>10
12	15.0	35.6	49.4	0.0	0.56 ± 0.04	0.42 ± 0.20	0.46 ± 0.21	0.26 ± 0.02	3.4 ± 0.4	>10	>10	>10
13	15.0	35.6	49.4	0.0	0.56 ± 0.02	0.49 ± 0.05	0.39 ± 0.13	0.43 ± 0.03	2.1 ± 0.2	>10	6.5 ± 0.1	>10
14	11.7	85.0	0.0	3.3	0.41 ± 0.04	0.28 ± 0.13	0.19 ± 0.09	0.23 ± 0.04	1.3 ± 0.6	10.2 ± 0.2	>10	>10
15	10.2	0.0	85.0	4.8	NA	0.49 ± 0.03	0.66 ± 0.21	0.57 ± 0.16	NA	>10	>10	>10
16	5.6	63.0	21.4	10.0	0.50 ± 0.06	0.46 ± 0.02	0.40 ± 0.03	0.41 ± 0.01	1.7 ± 0.4	10.1 ± 0.4	>10	>10
17	5.0	16.2	68.8	10.0	1.00 ± 0.00	0.26 ± 0.07	0.58 ± 0.02	0.46 ± 0.05	1.2 ± 0.9	>10	>10	NA
18	5.0	44.0	41.0	10.0	0.60 ± 0.05	0.27 ± 0.15	0.42 ± 0.02	0.19 ± 0.04	6.3 ± 0.3	>10	>10	NA

NA = Not completely dispersed within 20 min.

Table 6. Composition and characteristics of selected SNEDDS formulations (mean ± SD, *n* = 3)

System	SNEDDS formulations	Composition (% w/w)						Parameter			
		Oil	Surfactant	Co-surfactant		Co-solvent		Nanoemulsion Appearance	Self-emulsification time (min)	Particle size (nm)	PDI
		Castor oil	Cremophor RH 40	Span 80	Span 20	PEG 400	Ethanol				
1	F1	31.0	36.0	-	27.5	5.5	-	Transparent	3.3 ± 0.6	54.5 ± 0.1	0.17 ± 0.00
	F2	18.0	36.0	-	40.5	5.5	-	Translucent	NA	69.9 ± 1.7	0.52 ± 0.02
2	F3	39.5	38.0	17.0	-	5.5	-	Transparent	5.3 ± 0.4	64.1 ± 0.5	0.16 ± 0.01
	F4	18.0	36.0	40.5	-	5.5	-	Translucent	9.7 ± 0.3	71.8 ± 1.2	0.20 ± 0.00
3	F5	31.8	35.5	-	27.5	-	5.2	Transparent	4.3 ± 0.7	42.5 ± 0.5	0.12 ± 0.00
	F6	18.0	36.0	-	40.5	-	5.5	Translucent	15.3 ± 1.2	63.8 ± 1.4	0.58 ± 0.04
4	F7	20.0	74.0	0.5	-	-	5.5	Transparent	2.3 ± 0.6	33.9 ± 0.2	0.17 ± 0.01
	F8	18.0	36.0	40.5	-	-	5.5	Translucent	5.3 ± 1.4	78.1 ± 0.5	0.20 ± 0.00

NA = Not completely dispersed within 20 min.

and desirability function tools in Design-Expert® software. In the desirability function approach, all component constraints were maintained within the predefined design space, while particle size was set as the primary response to be minimize. Eight formulations of blank SNEDDS (F1-F8) with various concentrations and components were identified, as summarized in Table 6. All eight blank SNEDDS formulations met the predefined criteria for acceptable self-emulsifying nanoemulsion performance: (1) particle size ≤ 200 nm, (2) PDI ≤ 0.3, and (3) self-emulsification time ≤ 10 min. Among these, F1, F3, F4, F5, and F7 exhibited rapid emulsification (2–10 min), clear to slightly opalescent appearance, and droplet sizes below 72 nm, indicating efficient dispersion and adequate interfacial stabilization. In contrast, F2, F6, and F8, although still within the acceptable limits, showed relatively longer emulsification times or higher PDI values, likely due to lower surfactant content or higher co-surfactant proportions, which may weaken interfacial film strength. The smallest droplet size was observed in F7 (33.9 ± 0.2 nm), containing Span 80 and ethanol. The combination of a low-HLB co-surfactant (Span 80) with a volatile, low-viscosity co-solvent (ethanol) likely promoted efficient interfacial packing and rapid droplet dispersion. In comparison, PEG 400-based systems (F1–F4) demonstrated slightly larger droplet sizes, which can be attributed to the higher viscosity and hydrophilicity of PEG 400, which can slow droplet disruption and diffusion during emulsification. Overall, these results support the selection of F1, F3, F4, F5, and F7 as the most suitable blank SNEDDS formulations for subsequent drug-loading studies.

3.4. Evaluation of G-SNEDDS formulations

G-SNEDDS formulations were developed based on the optimized blank SNEDDS systems (Table 7). Incorporation of ginger extract did not markedly alter the emulsification behavior, indicating sufficient solubilization of the lipophilic constituents of the extract within the selected excipient matrices. All formulations produced clear to slightly translucent nanoemulsions with self-emulsification times ranging from 2.7 to 9.9 min, droplet sizes between 51.5 and 124.1 nm, and PDI values ≤ 0.35. Among the tested formulations, G-F1, G-F3, G-F4, G-F5, and G-F7 exhibited overall favorable physicochemical performance.

The smallest droplet size and fastest self-emulsification were observed for G-F7 (System 4: Span 80 with ethanol), with a self-emulsification time of 2.7 ± 0.8 min, a particle size of 51.5 ± 1.8 nm, and a PDI of 0.22 ± 0.01. PEG 400-based formulations, such as G-F1 and G-F5, showed slightly larger droplet sizes (62-72 nm) but maintained low PDI values (< 0.2) and good visual clarity. In contrast, formulations containing higher proportion of co-surfactant, such as G-F4, exhibited larger droplet sizes and moderately increased PDI values

Table 7. Composition and characteristics of G-SNEDDS formulations (mean ± SD, *n* = 3)

System	G-SNEDDS formulations	Composition (% w/w)							Parameter			
		Ginger extract	Oil	Surfactant	Co-surfactant		Co-solvent		Nanoemulsion Appearance	Self-emulsification time (min)	Particle size (nm)	PDI
			Castor oil	Cremophor RH 40	Span 80	Span 20	PEG 400	Ethanol				
1	G-F1	33.3	20.7	24.0	-	18.3	3.7	-	Transparent	9.3 ± 0.6	62.2 ± 0.8	0.10 ± 0.01
2	G-F3	33.3	26.3	25.3	11.3	-	3.7	-	Translucent	7.3 ± 0.5	70.0 ± 1.2	0.14 ± 0.01
	G-F4	33.3	12.0	24.0	27.0	-	3.7	-	Translucent	9.9 ± 0.6	87.6 ± 2.8	0.26 ± 0.01
5	G-F5	33.3	21.2	23.7	-	18.3	-	3.5	Transparent	6.3 ± 0.1	71.7 ± 0.2	0.15 ± 0.02
6	G-F7	33.3	13.3	49.3	0.3	-	-	3.7	Transparent	2.7 ± 0.8	51.5 ± 1.8	0.22 ± 0.01

(up to 0.26), suggesting reduced interfacial stabilization at elevated co-surfactant levels. Overall, all five selected formulations, G-F1, G-F3, G-F4, G-F5, and G-F7, fulfilled the physicochemical criteria for acceptable self-emulsifying nanoemulsions, with droplet sizes < 100 nm and emulsification times < 10 min.

3.5. EE of 6-gingerol and 6-shogaol in G-SNEDDS formulations

The EE of 6-gingerol and 6-shogaol in the G-SNEDDS formulations was determined by ultrafiltration followed by HPLC quantification (Table 8). All formulations exhibited high encapsulation efficiencies for both bioactive compounds, with EE values exceeding 90% in nearly all cases. For 6-gingerol, EE values ranged from 91.75 % (G-F5) to 96.33 % (G-F3), while for 6-shogaol, EE values ranged from 92.94 % (G-F7) to 95.54 % (G-F4). Formulations G-F3 and G-F4 exhibited the highest mean EE values for 6-gingerol and 6-shogaol, respectively. No statistically significant differences ($p > 0.05$) were observed among formulations for either compound, indicating comparable encapsulation efficiencies across the tested systems. These results demonstrate that all optimized G-SNEDDS formulations are suitable for efficiently encapsulating ginger-derived bioactive compounds, thereby providing a robust foundation for subsequent stability and *in vitro* release studies.

Table 8. Entrapment efficiency of 6-gingerol and 6-shogaol in various G-SNEDDS formulations (mean ± SD, *n* = 3)

G-SNEDDS Formulation	Entrapment efficiency (%)	
	6-Gingerol	6-Shogaol
G-F1	95.04 ± 4.06	94.74 ± 3.89
G-F3	96.33 ± 8.69	92.95 ± 2.79
G-F4	95.54 ± 5.11	95.54 ± 4.14
G-F5	91.75 ± 1.04	94.26 ± 3.22
G-F7	91.99 ± 0.26	92.94 ± 3.34

3.6. Morphological characterization of G-SNEDDS

TEM was employed to evaluate the morphological features and nanoscale structure of G-SNEDDS formulations. Figure 2 presents representative TEM micrographs of five selected formulations: G-F1, G-F3, G-F4, G-F5, and G-F7. The TEM images confirmed the formation of spherical and well-dispersed nanoemulsion droplets in formulations G-F1, G-F3, G-F4, and G-F5. These droplets exhibited relatively uniform morphology, smooth surfaces, and minimal aggregation, which are characteristic features of a physically stable

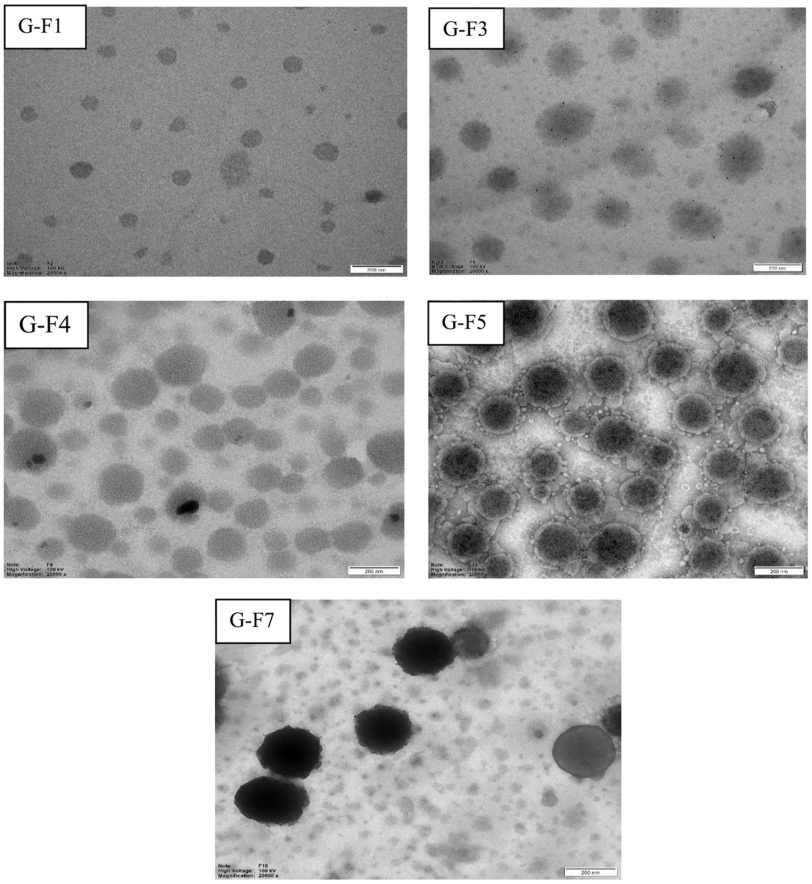

Figure 2. TEM images of G-SNEDDS formulations, including G-F1, G-F3, G-F4, G-F5, and G-F7. Scale bar: 200 nm.

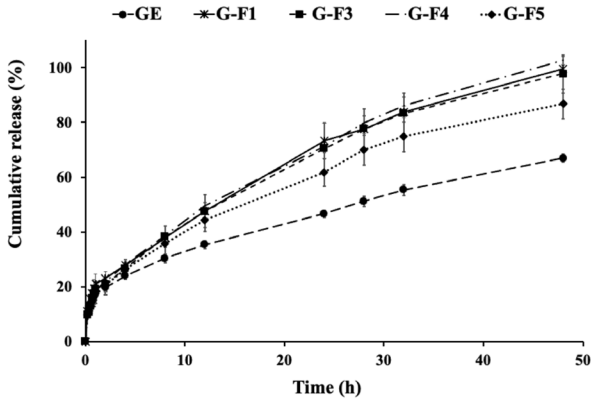

Figure 3. ***In vitro*** **cumulative release (%) of 6-gingerol from ginger extract (GE) and selected G-SNEDDS formulations (G-F1, G-F3, G-F4, and G-F5) over 48 h (mean ± SD, *n* = 3).**

nanoemulsion system. The observed nanoscale structures were generally consistent with the DLS results reported previously, in which these formulations demonstrated small droplet sizes (< 150 nm), low polydispersity indices (PDI < 0.3), and rapid self-emulsification behavior.

In contrast, G-F7 exhibited larger apparent particle sizes with evident aggregation in the TEM images, suggesting reduced interfacial stability of the emulsion system under the examined conditions. It is important to note that particle size values obtained by DLS, and morphological features observed by TEM do not necessarily correspond directly, as these techniques probe different physical states of the system. DLS measures the hydrodynamic diameter of droplets immediately after dispersion under high dilution conditions, whereas TEM visualizes droplets following sample preparation and drying, which may accentuate aggregation phenomena in formulations with limited interfacial stability, particularly those containing high proportions of volatile co-solvents such as ethanol.

Overall, the combined interpretation of TEM and DLS results provides a more comprehensive understanding of the physical behavior of the G-SNEDDS formulations, and further supports the suitability of G-F1, G-F3, G-F4, and G-F5 for continued development and drug delivery evaluation.

3.7. *In vitro* release study of G-SNEDDS

The *in vitro* release profiles of the pure ginger extract and selected G-SNEDDS formulations (G-F1, G-F3, G-F4, and G-F5) were investigated over a 48 h period in 0.1 N hydrochloric acid. As illustrated in Figure 3, all G-SNEDDS formulations exhibited significantly enhanced cumulative release of ginger extract compared to the unformulated control. After 48 h, the cumulative release of 6-gingerol from the G-SNEDDS formulations ranged from 88.54% to 102.52%, whereas the release from the pure ginger extract was markedly lower

Table 9. Physical stability studies of G-SNEDDS formulation

G-SNEDDS Formulation	Before heating-cooling cycle analysis				After heating-cooling cycle analysis			
	G-SNEDDS Appearance	Nanoemulsion Appearance	Particle Size (nm)	PDI	G-SNEDDS Appearance	Nanoemulsion Appearance	Particle Size (nm)	PDI
G-F1	Dark Brown, No phase separation	Transparent	61.5 ± 0.7	0.13 ± 0.01	Dark Brown, No phase separation	Transparent	61.5 ± 0.7	0.13 ± 0.01
G-F3	Dark Brown, No phase separation	Transparent	67.9 ± 0.5	0.09 ± 0.01	Dark Brown, No phase separation	Transparent and locculation	67.9 ± 0.5	0.09 ± 0.01
G-F4	Dark Brown, No phase separation	Transparent	87.1 ± 0.6	0.16 ± 0.02	Dark Brown, No phase separation	Translucent and locculation	87.1 ± 0.6	0.16 ± 0.02

*Significant difference compared to day 0 ($p < 0.05$).

Table 10. Droplet size of G-SNEDDS formulations (G-F1, G-F3, and G-F4) over a 90-day short-term storage period at 4°C, 30°C, and 45°C (mean ± SD, *n* = 3)

G-SNEDDS Formulation	Day 0	Day 30			Day 60			Day 90		
		4°C	30°C	45°C	4°C	30°C	45°C	4°C	30°C	45°C
G-F1	59.8 ± 1.6	60.2 ± 2.2	62.1 ± 1.7	64.2 ± 1.9	59.2 ± 2.0	63.9 ± 2.1	67.7 ± 2.0*	60.2 ± 2.2	65.3 ±1.7	72.2 ± 1.2*
G-F3	69.9 ± 2.2	70.5 ± 1.9	72.5 ± 2.2	73.2 ± 1.8	69.9 ± 1.9	73.5 ± 2.2	77.1 ± 1.1*	69.7 ± 1.4	76.3 ± 1.7*	81.8 ± 2.3*
G-F4	89.8 ± 1.6	90.0 ± 1.5	92.0 ± 1.3	94.5 ± 1.5*	89.9 ± 2.7	93.8 ± 1.8*	97.9 ± 2.1*	91.0 ± 1.2	95.7 ± 1.5*	102.4 ± 1.7*

*Significant difference compared to day 0 ($p < 0.05$).

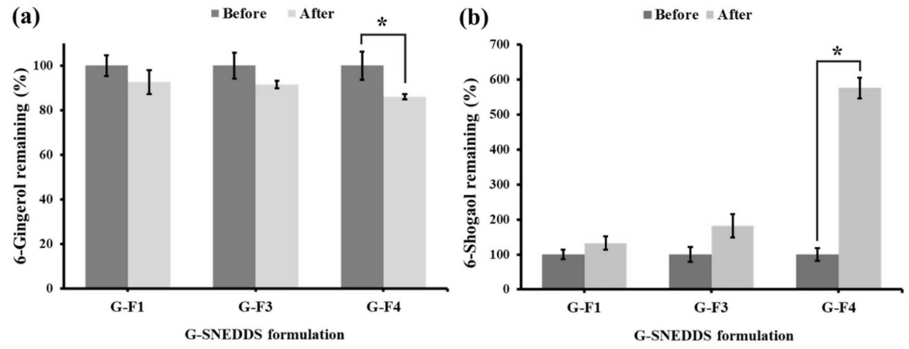

Figure 4. The percentage of 6-gingerol (a) and 6-shogaol (b) remaining in G-SNEDDS formulations (G-F1, G-F3, and G-F4) before and after the heating-cooling cycle. An asterisk (*) indicates a statistically significant difference compared to the values before the heating-cooling cycle ($p < 0.05$).

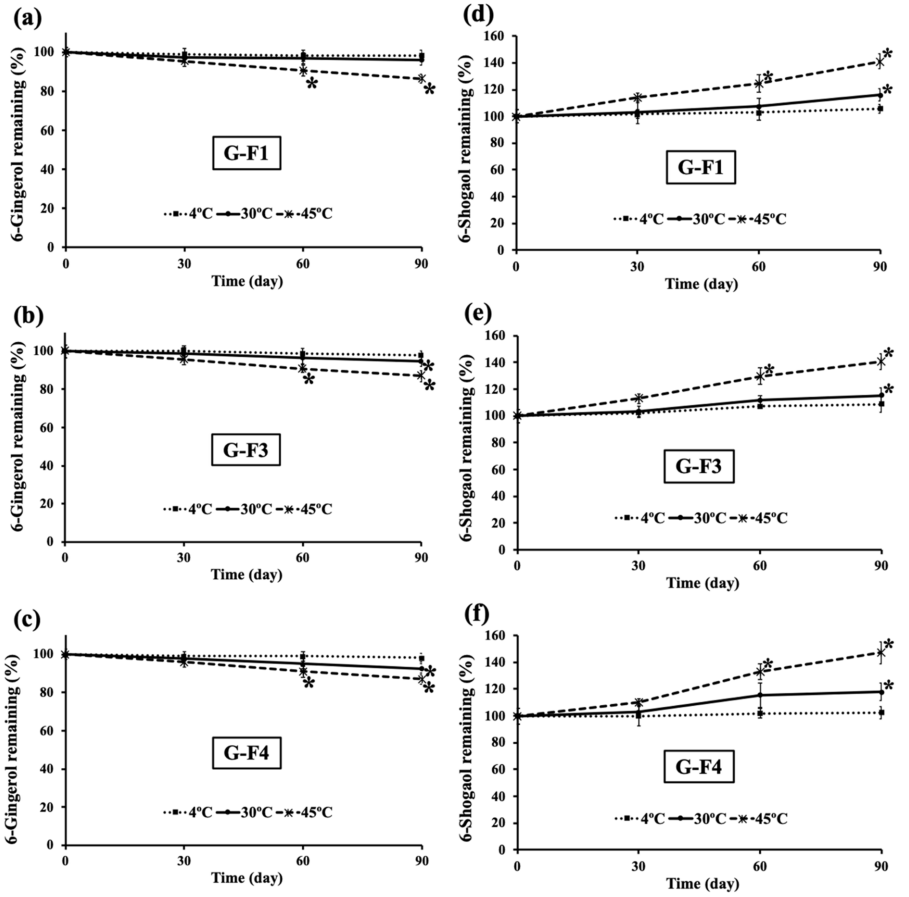

Figure 5. Stability profiles of 6-gingerol (a-c) and 6-shogaol (d-f) remaining (%) in G-SNEDDS formulations: G-F1, G-F3, and G-F4, stored at 4 °C, 30°C, and 45°C over 90 days. Data are presented as mean ± SD ($n = 3$). Asterisks (*) indicate statistically significant differences compared to Day 0 ($p < 0.05$).

at 66.95%. Among the formulations tested, G-F4 demonstrated the highest cumulative drug release (102.52%), followed by G-F1, G-F3, and G-F5. The enhanced release profile can be attributed to the spontaneous formation of fine nanoemulsions upon dilution, with droplet sizes < 200 nm, as previously confirmed by DLS and TEM analyses.

3.8. Stability study of G-SNEDDS

3.8.1. Heating-cooling cycle analysis

The physical stability of selected G-SNEDDS formulations (G-F1, G-F3, and G-F4) was evaluated under thermal stress using a heating-cooling cycle analysis. The results are presented in Table 9. All formulations initially presented as transparent nanoemulsions with dark brown coloration, with no visible phase separation, indicating successful self-

emulsification and homogeneity. After completion of the heating-cooling cycles, G-F1 retained its original appearance and demonstrated the most robust physical stability, with no statistically significant changes in particle size and PDI.

In contrast, G-F3 exhibited a slight increase in particle size (from 67.9 ± 0.5 nm to 70.5 ± 1.2 nm) and a minor increase in PDI (0.09 ± 0.01 to 0.10 ± 0.01), accompanied by the onset of flocculation, indicating moderate physical instability. The most physical instability was observed for G-F4, which showed marked increases in particle size (67.1 ± 0.6 nm to 97.7 ± 1.1 nm) and PDI (0.16 ± 0.02 to 0.33 ± 0.01), with clear flocculation and a visible change in appearance from transparent to translucent.

The chemical stability of G-F1, G-F3, and G-F4 under heating-cooling conditions was evaluated by quantifying the concentration of 6-gingerol and 6-shogaol before and after themal stress, as shown in Figure 4. Following thermal cycling, all formulations exhibited a reduction in 6-gingerol content, indicating thermal degradation of this compound. Conversely, the concentration of 6-shogaol increased significantly, particularly in G-F4. G-F4 exhibited the highest increase in 6-shogaol content, reaching 576.1 ± 28.9 % after heating-cooling treatment, corresponding to a > 4-fold increase ($p < 0.001$). In contrast, G-F1 and G-F3 showed only modest increases in 6-shogaol levels and smaller reductions in 6-gingerol content, indicating greater chemical stability compared with G-F4.

3.8.2. Short-term storage stability study

The stability of the G-SNEDDS formulations during short-term storage was assessed by monitoring changes in droplet size and the remaining percentages of 6-gingerol and 6-shogaol over 90-day period under different temperature conditions. The results presented in Table 10 demonstrate a significant temperature-dependent increase in droplet size for all formulations. At day 0, the initial droplet sizes for G-F1, G-F3, and G-F4 were 59.8 ± 1.6 nm, 69.9 ± 2.2 nm, and 89.8 ± 1.6 nm, respectively. Throughout the 90-day storage period, G-F1 remained relatively stable at 4°C and 30°C, with not statistically significant change observed ($p > 0.05$). However, at 45°C, G-F1 showed a significant increase in droplet size, reaching 72.2 ± 1.2 nm on day 90 ($p < 0.05$). Similarly, G-F3 and G-F4 exhibited significant increases in droplet size at 45°C, reaching 81.8 ± 2.3 nm and 102.4 ± 1.7 nm, respectively, indicating thermal-induced instability of the nanoemulsion droplets. Among the three formulations, G-F1 exhibited the highest overall physical stability in terms of maintaining its droplet size across all tested storage temperatures.

Figure 5 illustrates the degradation and transformation profiles of 6-gingerol and 6-shogaol during the storage period. A gradual decline in 6-gingerol content was observed in all formulations, particularly under elevated temperature conditions. At 45°C, 6-gingerol degradation was significantly accelerated, with remaining contents dropping to 86.5%, 81.8%, and 86.9% in G-F1, G-F3, and G-F4, respectively, on day 90 ($p < 0.05$). The reduction in 6-gingerol content is consistent with its known sensitivity to heat, light, and oxygen, leading to thermal degradation and dehydration reactions. In contrast, the content of 6-shogaol increased progressively with both storage time and temperature, suggesting an interconversion process in which 6-gingerol underwent dehydration to form 6-shogaol. This transformation was most pronounced in G-F4, which exhibited the highest remaining percentage of 6-shogaol (140.6%) at 45°C on day 90. G-F1 and G-F3 also showed elevated 6-shogaol levels at higher temperatures, although to a lesser extent. The consistent increase in 6-shogaol content at 45°C further supports the occurrence of the thermally induced conversion of 6-gingerol into its dehydrated analog during storage.

4. Discussion

The extraction time significantly affected both the extraction yield and phytochemical composition of the ginger extracts. As expected, prolonging the extraction time to 30 min increased the crude yield, likely due to enhanced solvent penetration and more extensive cell wall disruption, which facilitated solute diffusion (*19*). However, the 10-min extract exhibited the highest 6-gingerol content, suggesting that extended extraction durations may induce degradation of thermolabile constituents (*20*).

This observation aligns with previous reports indicating that 6-gingerol is sensitive to heat and prolonged extraction, undergoing dehydration and oxidation to 6-shogaol and other degradation products, particularly under elevated temperature or acidic conditions (*21*). The reduced 6-gingerol content observed in the 20- and 30-min extracts supports this degradation trend. In contrast, 6-shogaol levels remained relatively constant across the different extraction times, implying that the mild temperature employed in this study was insufficient to promote time-dependent conversion of 6-gingerol into 6-shogaol (*22*). Therefore, considering the balance between extraction yield and bioactive stability, a 10-min extraction time appears optimal for maximizing 6-gingerol retention.

Further investigation into the formulation phase revealed that the type and concentration of excipients critically governed droplet formation, size distribution, and emulsification efficiency in the SNEDDS. The co-solvent markedly influenced on system behavior, PEG 400 increased droplet size and heterogeneity, which can be attributed to its high viscosity and hydrogen-bonding potential that hinder interfacial mobility (*23*). In contrast, ethanol promoted the formation of smaller droplets and

faster emulsification by facilitating interfacial disruption and rapid solvent exchange. Nevertheless, excessive ethanol in combination with insufficient surfactant levels destabilized the interfacial film, resulting in broader size distributions (*24*).

The surfactant–co-surfactant ratio was also a critical determinant of nanoemulsion performance. Formulations containing sufficient Cremophor RH40 (≥ 35% w/w) and moderate co-surfactant levels (20-35% w/w) yielded small droplets with narrow PDI values, reflecting effective interfacial stabilization. Conversely, low surfactant concentrations or excessive co-surfactant content disrupted interfacial cohesion, resulting in multimodal droplet size distributions (*25*).

The type of co-surfactant also influenced self-emulsification behavior. Span 80, a low HLB surfactant, exhibited stronger affinity for the oil phase and promoted tighter interfacial packing than Span 20, thereby enhancing interfacial elasticity when combined with the high-HLB surfactant, Cremophor RH40 (*26*). In ethanol-based systems, this combination facilitated the formation of smaller and more uniform droplets. However, despite the favorable initial droplet size observed in systems containing Span 80 and ethanol (such as G-F7), these formulations exhibited physical instability over time, as evidenced by pronounced droplet aggregation. This phenomenon may be attributed to the high volatility of ethanol, which can rapidly diffuses into the continuous aqueous phase upon dilution, thereby reducing the effective surfactant concentration available to maintain the integrity of the interfacial film (*27*). Furthermore, although Span 80 enhances interfacial elasticity, its combination with high concentration of volatile co-solvents can lead to a transiently stable film that is susceptible to thinning and subsequent droplet coalescence during long-term storage or under environmental stress. In contrast, Span 20 promoted rapid but comparatively less stable emulsification, consistent with its higher hydrophilicity.

Overall, solvent polarity and surfactant composition jointly governed emulsification efficiency. PEG 400-based systems exhibited slower dispersion due to reduced interfacial mobility, whereas ethanol-based systems required higher surfactant levels to counteract transient interfacial destabilization during dilution (*28*). Among all tested systems, those incorporating Span 80 and Cremophor RH40 demonstrated the most favorable balance between interfacial flexibility and stability, consistent with previously reported findings (*29*). Incorporation of ginger extract did not adversely affect emulsification behavior, confirming its compatibility with the selected lipid excipients. Consequently, ethanol-based SNEDDS containing Span 80 and Cremophor RH40 achieved rapid self-emulsification, small droplet size, and narrow size distributions, features that collectively enhance solubility and the potential oral bioavailability of the ginger extract.

The consistently high entrapment efficiencies (> 90%) observed across all G-SNEDDS formulations confirm the strong lipophilic affinity of 6-gingerol and 6-shogaol. Their hydrophobic nature favors preferential partitioning into the oil and surfactant domains, resulting in efficient encapsulation within the lipid matrix rather than the aqueous phase. Comparable high loading efficiencies of 6-gingerol have been reported in solid lipid nanoparticles and liposomal systems, which further support the present findings (*30,31*).

The enhanced drug release profile of G-SNEDDS can be attributed to the spontaneous formation of fine oil-in-water nanoemulsions upon dilution, which substantially increases the interfacial surface area and facilitates rapid drug solubilization and diffusion (*32*). In addition, amphiphilic surfactants and co-surfactants enhance interfacial fluidity, thereby accelerating drug partitioning and diffusion across the oil-water interface. These mechanisms are consistent with the improved dissolution and absorption commonly reported for SNEDDS-based delivery systems (*23*).

The degradation pattern of 6-gingerol under thermal and storage stress further highlights the importance of formulation design and appropriate storage control. The transformation of 6-gingerol to 6-shogaol *via* intramolecular dehydration is well documented under thermal and oxidative conditions (*4,5*). Accordingly, the elevated levels of 6-shogaol observed in formulation G-F4 are indicative of thermally induced conversion of 6-gingerol, consistent with its established dehydration pathway under heat and oxidative stress. Among all systems evaluated, G-F1 exhibited the highest physicochemical and chemical stability, maintaining consistent droplet size, low PDI values, and minimal degradation during both accelerated and long-term storage. This enhanced stability can be attributed to an optimized surfactant-to-co-surfactant ratio, which promotes the formation of a cohesive interfacial film, thereby minimizing droplet coalescence and restricting molecular mobility under thermal stress.

Temperature exerted a strong influence on formulation stability: all formulations remained physically stable at 4°C and 30°C, whereas exposure to 45°C significantly accelerated the degradation of 6-gingerol and the formation of 6-shogaol. These results corroborate previous studies demonstrating that high-temperature storage of ginger oleoresin promotes dehydration of 6-gingerol (*33,34*). Collectively, the findings indicate that SNEDDS can effectively preserve 6-gingerol under short-term storage conditions by maintaining a stabilized lipidic microenvironment, although complete protection against heat-induced conversion cannot be achieved. Despite these advantages, the present study has certain limitations. The physicochemical performance of SNEDDS following dilution and exposure to simulated gastrointestinal conditions was not evaluated. *In vivo*, SNEDDS are

subjected to dynamic physiological processes, including dilution, enzymatic digestion, and bile salt interaction, which can markedly influence droplet integrity and drug solubilization (*35*). Therefore, future studies should investigate the stability and performance of the optimized formulations under simulated gastrointestinal digestion conditions to better predict their *in vivo* behavior. Among the formulations evaluated, G-F1 exhibited the most robust physicochemical integrity and chemical stability, thereby identifying it as the most promising candidate for long-term storage and further development.

5. Conclusions

In this study, a G-SNEDDS was successfully developed to overcome the poor water solubility and instability of ginger's bioactive constituents. UAE for 10 min was identified as the optimal extraction condition for maximizing 6-gingerol content while maintaining an acceptable extract yield. Using a DoE-guided optimization approach, an optimized SNEDDS formulation, comprising castor oil as the lipid phase, Cremophor RH40 as the surfactant, Span 20 or Span 80 as the co-surfactant, and a low proportion of PEG 400 as the co-solvent, achieved rapid self-emulsification, producing fine nanoemulsion droplets with a uniform size distribution. This formulation encapsulated more than 90% of the ginger bioactives and demonstrated compliance with essential performance criteria, including droplet size, PDI, and emulsification efficiency.

The optimized G-SNEDDS significantly enhanced the dissolution profile of 6-gingerol compared to the unformulated extract, indicating a strong potential for enhanced oral bioavailability. In addition, the system demonstrated good physical stability under ambient and refrigerated storage conditions, with minimal changes in particle size over a three-month period. A slight degradation of 6-gingerol to 6-shogaol was observed under accelerated high-temperature conditions, highlighting the importance of appropriate storage conditions. Overall, this work demonstrates that incorporation of ginger extract into a lipid-based nanoemulsion system is an effective strategy to enhance solubility and protect thermosensitive constituents. The SNEDDS approach developed herein shows considerable promise for improving the therapeutic efficacy of ginger and other poorly water-soluble phytochemicals, thereby supporting further *in vivo* evaluation for oral supplementation and drug delivery applications.

Acknowledgements

The authors are grateful to the Faculty of Pharmacy, Chiang Mai University for their support. The authors would like to thank and gratefully acknowledge Kanyanut Suksumran, Vasinpong Prembanyat, Praewa Makmee, Chayaporn Fongkham, and Goekpon Yoocharoen for their assistance in conducting the experiments for this research project.

Funding: This work was supported by a grant from CMU Junior Research Fellowship program, Chiang Mai University (Grant number: JRCMU2566R_014). Maung Maung Than expresses sincere gratitude for the Teaching Assistant and Research Assistant (TA/RA) scholarship provided by Chiang Mai University.

Conflict of Interest: The authors have no conflicts of interest to disclose.

References

1. Mashhadi NS, Ghiasvand R, Askari G, Hariri M, Darvishi L, Mofid MR. Anti-oxidative and anti-inflammatory effects of ginger in health and physical activity: Review of current evidence. Int J Prev Med. 2013; 4:36-42.
2. Ali BH, Blunden G, Tanira MO, Nemmar A. Some phytochemical, pharmacological and toxicological properties of ginger (*Zingiber Officinale Roscoe*): A review of recent research. Food Chem Toxicol. 2008; 46:409-420.
3. Ghasemzadeh A, Jaafar HZE, Rahmat A. Antioxidant activities, total phenolics and flavonoids content in two varieties of Malaysia young ginger (*Zingiber Officinale Roscoe*). Molecules. 2010; 15:4324-4333.
4. Semwal RB, Semwal DK, Combrinck S, Viljoen AM. Gingerols and shogaols: Important nutraceutical principles from ginger. Phytochemistry. 2015; 117:554-568.
5. Bhattarai S, Tran VH, Duke CC. The stability of gingerol and shogaol in aqueous solutions. J Pharm Sci. 2001; 90:1658-1664.
6. Pan MH, Hsieh MC, Kuo JM, Lai CS, Wu H, Sang S, Ho CT. 6-shogaol induces apoptosis in human colorectal carcinoma cells *via* ROS production, caspase activation, and GADD 153 expression. Mol Nutr Food Res. 2008; 52:527-537.
7. Ekor M. The growing use of herbal medicines: Issues relating to adverse reactions and challenges in monitoring safety. Front Pharmacol. 2014; 4:1-10.
8. Wei Q, Yang Q, Wang Q, Sun C, Zhu Y, Niu Y, Yu J, Xu X. Formulation, characterization, and pharmacokinetic studies of 6-gingerol-loaded nanostructured lipid carriers. AAPS Pharm Sci Tech. 2018; 19:3661-3669.
9. Abdelaziz MA, Alalawy AI, Sobhi M, Alatawi OM, Alaysuy O. Development and characterization of engineered gingerol loaded chitosan nanoparticles for targeting colon cancer, bacterial infection, and oxidative stress mitigation. Int J Biol Macromol. 2025; 321(Pt1):146093.
10. Akram A, Rasul A, Waqas MK, Irfan M, Khalid SH, Aamir MN, Murtaza G, Ur Rehman K, Iqbal M, Khan BA. Development, characterization and evaluation of *in-vitro* anti-inflammatory activity of ginger extract based micro emulsion. Pak J Pharm Sci. 2019; 32:1327-1332.
11. Xu Y, Wang Q, Feng Y, Firempong CK, Zhu Y, Omari-Siaw E, Zheng Y, Pu Z, Xu X, Yu J. Enhanced oral bioavailability of [6]-gingerol-smedds: Preparation, *in vitro* and *in vivo* evaluation. J Funct Foods. 2016; 27:703-710.
12. Wijayanti II, Budiharjo A, Pangastuti A, Prihapsara F, Artanti AN. Total phenolic content and antioxidant

activity of ginger extract and SNEDDS with eel fish bone oil (*Anguilla spp.*). Nusantara Biosci. 2018; 10:164-169.
13. Singh B, Bhatowa R, Tripathi C, Kapil R. Developing micro-/nanoparticulate drug delivery systems using "design of experiments." Int J Pharm Investig. 2011; 1:75-87.
14. Kheawfu K, Pikulkaew S, Rades T, Müllertz A, von Gersdorff Jørgensen L, Okonogi S. Design and optimization of self-nanoemulsifying drug delivery systems of clove oil for efficacy enhancement in fish anesthesia. J Drug Deliv Sci Technol. 2021; 61:102241.
15. Gonzalez-Gonzalez M, Yerena-Prieto BJ, Carrera C, Vázquez-Espinosa M, González-de-Peredo AV, García-Alvarado MÁ, Palma M, Rodríguez-Jimenes G del C, Barbero GF. Optimization of an ultrasound-assisted extraction method for the extraction of gingerols and shogaols from ginger (*Zingiber Officinale*). Agronomy. 2023; 13:2-16.
16. Thai Pharmacopoeia Committee Thai Herbal Pharmacopoeia 2021: Bureau of drug and narcotic, department of medical sciences, ministry of public health. Available online: *https://bdn.go.th/thp/home*. (accessed on 1 August 2025).
17. Bu H, He X, Zhang Z, Yin Q, Yu H, Li Y. A TPGS-incorporating nanoemulsion of paclitaxel circumvents drug resistance in breast cancer. Int J Pharm. 2014; 471:206-13.
18. Kheawfu K, Panraksa P, Jantrawut P. Formulation and characterization of nicotine microemulsion-loaded fast-dissolving films for smoking cessation. Molecules. 2022; 27:3166.
19. Azwanida NN. A review on the extraction methods use in medicinal plants, principle, strength and limitation. Med Aromat Plants. 2015; 4:1-6.
20. Zagórska J, Czernicka-Boś L, Kukula-Koch W, Szalak R, Koch W. Impact of thermal processing on the composition of secondary metabolites of ginger rhizome: A review. Foods. 2022; 11:1-23.
21. Jiang H, Sólyom AM, Timmermann BN, Gang DR. Characterization of gingerol-related compounds in ginger rhizome (*Zingiber Officinale Rosc*.) by high-performance liquid chromatography/electrospray ionization mass spectrometry. Rapid Commun Mass Spectrom. 2005; 19:2957-2964.
22. Jung MY, Lee MK, Park HJ, Oh EB, Shin JY, Park JS, Jung SY, Oh JH, Choi DS. Heat-induced conversion of gingerols to shogaols in ginger as affected by heat type (dry or moist heat), sample type (fresh or dried), temperature and time. Food Sci Biotechnol. 2017; 27:687-693.
23. Buya AB, Beloqui A, Memvanga PB, Préat V. Self-nanoemulsifying drug delivery systems: From the development to the current applications and challenges in oral drug delivery. Pharmaceutics. 2020; 12:1-55.
24. Porter CJH, Trevaskis NL, Charman WN. Lipids and lipid-based formulations: Optimizing the oral delivery of lipophilic drugs. Nat Rev Drug Discov. 2007; 6:231-248.
25. Lawrence MJ, Rees GD. Microemulsion-based media as novel drug delivery systems. Adv Drug Deliv Rev. 2000; 45:89-121.
26. Pouton CW, Porter CJH. Formulation of lipid-based delivery systems for oral administration: Materials, methods and strategies. Adv Drug Deliv Rev. 2008; 60:625-637.
27. Guzey D, McClements DJ. Formation, stability and properties of multilayer emulsions for application in the food industry. Adv Colloid Interface Sci. 2006; 128-130:227-248.
28. Chen YS, Chiu YH, Li YS, Lin EY, Hsieh DK, Lee CH, Huang MH, Chuang HM, Lin SZ, Harn HJ, Chiou TW. Integration of PEG 400 into a self-nanoemulsifying drug delivery system improves drug loading capacity and nasal mucosa permeability and prolongs the survival of rats with malignant brain tumors. Int J Nanomedicine. 2019; 14:3601-3613.
29. Zeng L, Xin X, Zhang Y. Development and characterization of promising cremophor EL-stabilized o/w nanoemulsions containing short-chain alcohols as a cosurfactant. RSC Adv. 2017; 7:19815-19827.
30. Bhalekar MR, Madgulkar A, Jagtap TV. Demonstration of lymphatic uptake of (6)-gingerol solid lipid nanoparticles. J Drug Del Ther. 2019; 9:461-469.
31. Thangavelu P, Sundaram V, Gunasekaran K, Mujyambere B, Raju S, Kannan A, Arasu A, Krishna K, Ramamoorthi J, Ramasamy S, Velusamy T, Samiappan S. Development of optimized novel liposome loaded with 6-gingerol and assessment of its therapeutic activity against NSCLC *in vitro* and *in vivo* experimental models. Chem Phys Lipids. 2022; 245:105206.
32. Salawi A. Self-emulsifying drug delivery systems: A novel approach to deliver drugs. Drug Deliv. 2022; 29:1811-1823.
33. Oriani VB, Alvim ID, Paulino BN, Procópio FR, Pastore GM, Hubinger MD. The influence of the storage temperature on the stability of lipid microparticles containing ginger oleoresin. Food Res Int. 2018; 109:472-480.
34. Bhattarai S, Tran VH, Duke CC. Stability of [6]-gingerol and [6]-shogaol in simulated gastric and intestinal fluids. J Pharm Biomed Anal. 2007; 45:648-653.
35. Buya AB, Beloqui A, Memvanga PB, Préat V. Self-nano-emulsifying drug-delivery systems: From the development to the current applications and challenges in oral drug delivery. Pharmaceutics. 2020; 12:1194.

Received November 14, 2025; Revised February 4, 2026; Accepted February 6, 2026.

**Address correspondence to:*
Kantaporn Kheawfu, Department of Pharmaceutical Sciences, Faculty of Pharmacy, Chiang Mai University, Chiang Mai, 50200, Thailand.
E-mail: kantaporn.kheawfu@cmu.ac.th

Released online in J-STAGE as advance publication February 13, 2026.

Original Article

DOI: 10.5582/ddt.2025.01120

Xuefu Zhuyu Capsule alleviates depression in post-stroke depression model rats *via* modulation of the gut microbiota–gut–brain axis

Bowen Jin[1], Yuqian Wang[1], Zhaowei Zhang[1], Xuejin Fan[1], Yanjun Zhang[1,2,3,*], Pengwei Zhuang[1,2,3,*]

[1] National Key Laboratory of Chinese Medicine Modernization, Haihe Laboratory of Modern Chinese Medicine, Tianjin University of Traditional Chinese Medicine, Tianjin, China;
[2] First Teaching Hospital of Tianjin University of Traditional Chinese Medicine, Tianjin, China;
[3] National Clinical Research Center for Chinese Medicine Acupuncture and Moxibustion, Tianjin, China.

SUMMARY: Xuefu Zhuyu Capsule (XFZY) demonstrated potential in alleviating post-stroke depression (PSD), a condition whose underlying mechanisms may involve the gut–brain axis. This study aimed to explore the therapeutic effects of XFZY on PSD and its possible modulation of the gut microbiota–gut–brain axis in a rat model. Wistar rats were randomly assigned to sham, PSD, three XFZY dose (0.216, 0.432, 0.864 g/kg), and fluoxetine (1.80 mg/kg) groups (n = 12 per group). The PSD model was established using transient middle cerebral artery occlusion (t-MCAO) combined with chronic unpredictable mild stress (CUMS), followed by 28 days of XFZY administration. In a separate experiment, gut microbiota was depleted *via* antibiotic cocktails, with rats divided into sham, PSD, XFZY medium Dose (XFM), pseudo-germ-free (PGF) and PGF + XFM (PGFX) groups. Behavioral tests indicated that XFZY ameliorated depressive-like behaviors, with the medium dose (0.432 g/kg) showing the most significant effect. Histological analysis using hematoxylin and eosin (H&E) and Nissl staining revealed that XFZY alleviated colonic and neuronal damage. Furthermore, 16S rRNA sequencing and gas chromatography revealed that XFZY modulated gut microbiota composition, increased species richness, and elevated levels of short-chain fatty acids such as acetic acid, propionic acid, and butyric acid. Enzyme-Linked Immunosorbent Assay (ELISA) results showed that XFZY reduced pro-inflammatory cytokines — interleukin-1β (IL-1β), interleukin-6 (IL-6), and tumor necrosis factor-α (TNF-α), while immunohistochemistry indicated enhanced intestinal barrier function and reduced neuroinflammation. Furthermore, after depletion of gut microbiota using antibiotic cocktails, these therapeutic effects of XFZY were abolished. In summary, XFZY may alleviate PSD by modulating the gut microbiota and regulating the gut–brain axis, offering a promising direction for future therapeutic research.

Keywords: Xuefu Zhuyu, post-stroke depression, gut-brain axis, intestinal flora, short-chain fatty acids, neuroinflammatory

1. Introduction

Post-stroke depression (PSD) is a mood disorder marked by symptoms such as low mood, decreased interest in activities, difficulty concentrating, feelings of worthlessness, thoughts of death or suicide, psychomotor changes, and fatigue following a stroke (*1*). As the population ages and the prevalence of cerebrovascular diseases rises, the incidence of post-stroke depression is also increasing (*2*). Research indicates that approximately 33% of stroke patients experience post-stroke depression (*3*), with a cumulative rate of 55% within five years of the stroke event (*4*). While the exact pathogenesis of PSD remains uncertain, numerous studies suggest that its occurrence and progression are influenced by a variety of factors, including biological, functional, social, and psychological elements (*5*). Among these factors, biological components are believed to play a significant role in the advancement of the condition. Research (*6,7*) indicates that PSD is linked to neuroinflammation, disruptions in the hypothalamic-pituitary axis, oxidative stress, abnormalities in brain-derived neurotrophic factor levels, decreased monoaminergic transmission, and genetic predisposition.

The intestinal flora plays a crucial role in the intestinal microenvironment, with research indicating the

significance of gut microbiota in central nervous system function (*8*). The bidirectional communication between the brain and gut can impact internal homeostasis, potentially resulting in the development of diseases, particularly those affecting the nervous system (*9*). The alteration of gut microbiota in the gastrointestinal tract and central nervous system, influenced by changes in the autonomic nervous system and immune system, can result in various consequences including alterations in fat storage and energy balance, dysfunction of the gastrointestinal barrier, low-grade systemic inflammation, stress response, increased anxiety and depression (*10*). These changes in physiological processes have been associated with the pathophysiology of depression (*11*). Numerous studies (*12*) in the literature have indicated a strong correlation between gut microbiota and cerebral ischemia, impacting stroke prognosis *via* mechanisms such as bacterial translocation and gut microbiota metabolites, and contributing to various pathological processes in the onset and progression of cerebral ischemia.

Currently, according to the monoamine neurotransmitter theory, antidepressants such as selective serotonin reuptake inhibitors (SSRIs) are considered the first-line treatment for PSD (*13*) . However, due to long term delay treatment and low response rate, they may not be the most optimal choice. Traditional Chinese medicine theory suggests that depression in PSD patients is caused by liver disorders leading to stagnation of qi and blood. Therefore, treatment should focus on promoting blood circulation to remove stasis and addressing qi imbalances as a priority (*14*).

The Xuefu Zhuyu decoction, originating from Yi Lin Gai Cuo (Corrections on the Errors in Medical Workst) by Wang Qingren during the Qing Dynasty, consists primarily of Angelicae Sinensis Radix, Rehmanniae Radix, Persicae Semen, Carthami Flos, Aurantii Fructus, Paeoniae Radix Rubra, Bupleuri Radix, Glycyrrhizae Radix et Rhizoma, Chuanxiong Rhizoma, Cyathulae Radix, among other ingredients (*15*). This prescription is renowned for its efficacy in promoting the circulation of qi and blood (*16*). Several clinical studies (*17,18*) have demonstrated the efficacy of XFZY decoction in alleviating depression-like symptoms in patients with PSD, as well as in restoring autonomic nerve function and enhancing overall quality of life. The combination of Xuefu Zhuyu capsule with flupentixol and melitracen tablets has also been shown to decrease the severity of depression in PSD patients. However, the precise mechanisms underlying the therapeutic effects of Xuefu Zhuyu treatment for PSD remain unclear.

This study utilized a model of cerebral ischemia-reperfusion (tMCAO) combined with chronic unpredictable stress (CUMS) to replicate the PSD animal model, in order to investigate the pharmacodynamic effects of Xuefu Zhuyu capsule on PSD model rats. Subsequently, 16SrDNA sequencing in conjunction with gas chromatography was employed to analyze the intestinal flora and short-chain fatty acids (SCFAs) in PSD rats treated with Xuefu Zhuyu capsule, facilitating the identification of differential intestinal microorganisms. Finally, utilizing the brain-gut axis as a framework, the study examined the neuroinflammation in the brains and the intestinal barrier function of rats in each experimental group. Furthermore, the potential mechanism by which Xuefu Zhuyu capsule may prevent and treat post-stroke depression in rat models by modulating intestinal flora was preliminarily investigated.

2. Materials and Methods

2.1. Animal grouping and drug administration

Male specific-pathogen-free Wistar rats (Vital River, Beijing, China), aged 8 weeks, were housed in a temperature-controlled room with a 12-hour light-dark cycle and *ad libitum* access to food and water at the Animal Center of Tianjin University of Traditional Chinese Medicine. All experimental procedures were conducted in compliance with the regulations set forth by the Animal Care and Utilization Committee of Tianjin University of Traditional Chinese Medicine (TCM-LAEC2021271).

Experiment 1: Rats were randomly assigned to six groups (n = 12 each): Sham, PSD, XFZY low-dose (XFL, 0.216 g/kg), medium-dose (XFM, 0.432 g/kg), high-dose (XFH, 0.864 g/kg), and fluoxetine (Flu, 1.80 mg/kg). Except for Sham, all groups underwent CUMS for 28 days. Behavioral tests were performed on day 28. XFZY was obtained from Tianjin Hong Ren Tang Pharmaceutical (Tianjin, China). Fluoxetine was obtained from Shanxi QianYuan Pharmaceutical (Shanxi, China).

Experiment 2: Rats were randomly assigned to five groups (n = 12 each): Sham, PSD, XFZY medium (XFM, 0.432 g/kg), pseudo-germ-free (PGF) and PGF + XFM (PGFX, 0.432 g/kg). Except for Sham, all groups underwent CUMS for 28 days. Behavioral tests were performed on day 28. Gut microbiota depletion was achieved by administering a nonabsorbable antibiotic cocktail in drinking water to rats in the PGF and PGFX groups from the onset of CUMS until its cessation (day 1 to day 28). The cocktail consisted of neomycin (5 mg/mL, Solarbio, Beijing, China, N8090), bacitracin (5 mg/mL, Yuanye Bio-Technology, Shanghai, China, S17005), and nystatin (1.25 μg/mL, Solarbio, P9210) — a regimen previously validated to effectively deplete gut microbiota without altering body weight or baseline locomotor activity (*19,20*).

XFZY was administered at low (0.216 g/kg), medium (0.432 g/kg), and high doses (0.864 g/kg) based on clinically equivalent dose calculations (*21*). The medium dose (0.432 g/kg) corresponds to the human

daily dosage (4.8 g/day for a 70 kg adult) adjusted *via* human-to-rat dose conversion formula: rat dose (g/kg) = human dose (g)/70 kg (standard human body weight) × 6.3 (conversion factor). The low and high doses were selected as 0.5× and 2× the clinical equivalent dose, respectively, to assess dose-response relationships. Fluoxetine (1.80 mg/kg), the positive control, was dosed equivalently to the human clinical regimen (20 mg/day) using the same formula (*22*) . All doses were administered orally once daily for 28 days.

2.2. PSD model establishment

PSD animal model was established by tMCAO and CUMS. Focal cerebral ischemia was induced by transient occlusion of the right middle cerebral artery (MCA) for 60 min (*23*). Through the neurological deficit score, rats with impaired neurological function were selected. Then chronic unpredictable mild stress (CUMS) was used to establish the depression model. Rats were subjected to a random allocation of two out of seven distinct stress modalities on a daily basis over a period of 28 days, including fasting, water deprivation, ice water swimming, horizontal shaking, wet cage confinement, oblique cage placement, and day/night reversal (*24*). Each stressor was administered only once every two days.

2.3. Neurological deficit score

Neurological deficit score was used to evaluate neurological status (*25*) . The scores are 0, no observable deficit; 1, forelimb flexion; 2, forelimb flexion and decreased resistance to lateral push; 3, forelimb flexion, decreased resistance to lateral push, and unilateral circling; 4, forelimb flexion and partial or complete lack of ambulation. The score from 1 to 3 included in subsequent analysis.

2.4. Sugar water preference test

The sucrose preference test (*26*) was utilized to evaluate the extent of anhedonia in rats. Prior to the commencement of the experiment, the rats underwent a training period to acclimate to consuming 1% sucrose solution. Following 21 hours fasting period, the experiment was initiated. During the experiment, the quantities of 1% sucrose solution and water were measured. Subsequently, after a one-hour period, the two bottles were weighed again, and the total fluid intake, sucrose consumption, and water consumption of the rats were documented.

2.5. Open field test

Open field testing (*27*) was conducted to assess exploratory behavior and locomotion. Rats were placed in the center (50 × 50 cm) of a 100 × 100 × 40 cm arena and allowed to acclimate for 60 s. Locomotor activity was then recorded for 5 min using a video tracking system (EthoVision XT, Noldus, Wageningen, Netherlands). Total distance traveled (horizontal movement) and number of rearing events (vertical movement) were quantified. Rats were habituated to the testing room for 1 h prior to testing.

2.6. Forced swimming test

The forced swimming test (*28*) was employed to evaluate the level of despair in rats by analyzing the duration of immobility during a 6 min swimming session and determining the presence of desperate behavioral states, typically indicated by the activity of the rat's hind limbs.

2.7. Histological analysis

After sacrifice and dissection, rat brains were fixed in 4% paraformaldehyde (Solarbio, P1110) for 24 h and dehydrated. Coronal brain sections (5 μm thick) were cut using a rotary microtome. For histological analysis, sections were deparaffinized in a 60°C oven for 1 h, cleared in xylene, and rehydrated through a graded ethanol series. Hematoxylin and eosin (H&E) staining (Solarbio, G1126) was performed as described (*29*). For Nissl staining, sections were incubated in 0.1% cresyl violet solution (Solarbio, G1430) at 60°C for 30 min (*30*). Alcian blue–Periodic acid–Schiff (AB-PAS) staining involved sequential incubation in Alcian blue (10 min) and Schiff's reagent (10 min) (Solarbio, G1285). All sections were dehydrated, cleared, and cover-slipped after staining. Images were acquired using a light microscope.

2.8. Immunohistochemical staining

Following deparaffinization and antigen retrieval using sodium citrate buffer (10 mM, pH 6.0, Solarbio, C1010) at 95°C for 10 min, endogenous peroxidase activity was blocked with 3% H_2O_2 (10 min, room temperature). Sections were incubated in 5% goat serum (Solarbio, SL038) for 1 h to block non-specific binding, then incubated overnight at 4°C with primary antibodies: donkey anti- ionized calcium-binding adapter molecule 1 (Iba1, 1:1,000, Novus Biologicals, Colorado, USA, NB100-1028), rabbit anti- mucin 2 (MUC2, 1:200, Bioss, Beijing, China, bs-60331R), rabbit anti-zonula occludens-1 (ZO-1, 1:200, Bioss, bs-34023R), and rabbit anti-Occludin (1:200, Bioss, bs-10011R). After washing with phosphate buffered saline (PBS), sections were incubated with horseradish peroxidase (HRP)-conjugated secondary antibody (30 min, room temperature, Beyotime Biotechnology, Shanghai, China, A0208, A0181), developed with 3,3'-diaminobenzidine (DAB, Solarbio, DA1010) chromogen (5 min), and counterstained with hematoxylin. Finally, sections were

dehydrated, cleared, and cover-slipped. Images were captured using a light microscope.

2.9. Enzyme-linked immunosorbent assay

The levels of interleukin-1β (IL-1β, Genime Biotechnology, Wuhan, China, JYM0419Ra), interleukin-6 (IL-6, Genime Biotechnology, JYM0646Ra), and tumor necrosis factor-α (TNF-α, Genime Biotechnology, JYM0635Ra) in serum were determined using enzyme-linked immunosorbent assay in accordance with the manufacturer's guidelines.

2.10. 16S rRNA sequencing analysis

Genomic DNA was extracted from rat fecal samples using the TGuide S96 Magnetic Soil/Stool DNA Kit (Tiangen Biochemical Technology, Beijing, China, DP812) according to the manufacturer's instructions. The bacterial 16S ribosomal RNA (rRNA) gene V3–V4 hypervariable region was amplified using an ABI GeneAmp 9902 thermal cycler (Applied Biosystems, USA) and specific primers. Polymerase chain reaction (PCR) products were purified with OMEGA DNA columns, confirmed by 1.8% agarose gel electrophoresis (120 V, 40 min), and the target bands excised and recovered. Sequencing was performed on the Illumina NovaSeq 6000 platform. Raw reads were merged using FLASH (v1.2.11), quality-filtered with Trimmomatic (v0.33), and chimeric sequences were removed with UCHIME (v8.1) to generate high-quality tags. Operational taxonomic units (OTUs) were clustered at 97% similarity using USEARCH (v10.0) with a minimum abundance threshold of 0.005% of total sequences. Taxonomic assignment was performed using the Ribosomal Database Project (RDP) Classifier (v2.2) with a confidence threshold of 0.8.

2.11. Gas chromatographic analysis

SCFAs were analyzed by gas chromatography (GC) (*31*). Fecal samples were weighed and homogenized in ultrapure water (1:5, w/v) by vortexing. An aliquot was further diluted 1:15 in a solution containing 1.33% HCl, 75% ethanol, 2-ethylbutyric acid (0.4821 mg/mL), and 2-ethylhexanoic acid (0.0283 mg/mL) as internal standards, vortexed, and sonicated for 2 min. After centrifugation at 17,950× *g* at 4°C for 10 min, the supernatant was collected for GC analysis. GC was performed on an Agilent 6890N gas chromatograph (Agilent, California, USA) equipped with a DB-FFAP column (30 m × 0.25 mm × 0.5 μm) using nitrogen as carrier gas. Injection volume was 3 μL with a split ratio of 3:1. The injector and detector (FID) temperatures were both set to 240°C.

2.12. Statistical analysis

Statistical analyses and graphical representations were conducted utilizing GraphPad Prism 8.0 software. Data sets adhering to a normal distribution were presented as mean ± standard deviation, with comparisons between two groups assessed using *t*-tests. Multiple-group comparisons were evaluated using one-way analysis of variance (ANOVA). Statistical significance was established at a threshold of $P < 0.05$.

3. Results

3.1. The XFZY treatment demonstrated efficacy in managing PSD rats

The PSD rats model was induced using tMCAO and CUMS methods. Following 28 days of drug treatment, behavioral assessments were conducted on the rats. Compared to the Sham group, the PSD group exhibited significantly lower scores in neurological function ($P < 0.05$), sucrose preference rate ($P < 0.05$), spontaneous activity in the open field test ($P < 0.05$), and longer immobility time ($P < 0.05$) in the forced swimming test. These findings indicate the presence of pronounced symptoms of post-stroke depression in the PSD rats. Compared with the PSD group, XFZY treatment significantly decreased the neurological score ($P < 0.05$, Figure 1B), increased the sucrose preference rate ($P < 0.05$, Figure 1C), enhanced spontaneous activity behavior ($P < 0.05$, Figures 1D and 1E), reduced immobility time ($P < 0.05$, Figure 1F), and ameliorated depression-like symptoms in PSD rats. Among the doses, the XFM group exhibited the most significant improvement ($P < 0.05$).

The presence of lesions in the hippocampus is commonly associated with the development of depression (*32*), with abnormalities in both the structure and function of the hippocampus observed in individuals with depression (*33*). In our study, the assessment of hippocampal damage in rats with PSD was conducted using H&E staining and Nissl staining techniques. The findings from Nissl staining revealed that PSD rats exhibited disrupted neuronal organization in the Cornu Ammonis 1 (CA1) regions (Fig. 1H), along with a decrease in the number of Nissl bodies ($P < 0.05$) (Figure 1G) compared to the Sham group. Furthermore, XFZY-treated groups significantly mitigated neuronal damage in the CA1 region and increased the number of Nissl bodies ($P < 0.05$). Among the doses, the XFM group (0.432 g/kg) demonstrated the most pronounced effect ($P < 0.05$).

3.2. The effectiveness of XFZY treatment was diminished as a result of the removal of intestinal flora

To determine whether the therapeutic effect of XFZY on PSD rats depends on gut microbiota, we depleted intestinal flora using antibiotic cocktails and evaluated

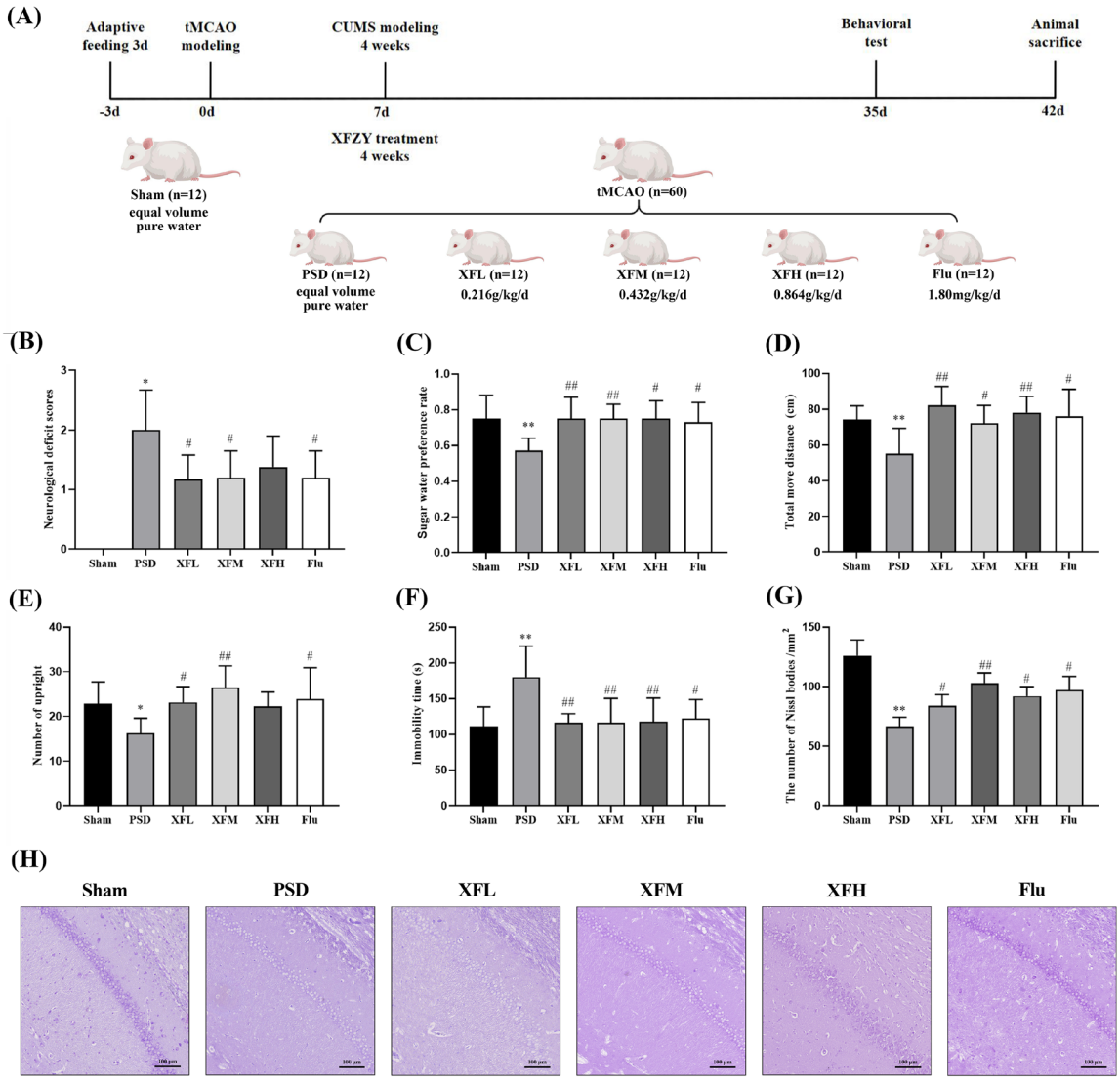

Figure 1. Pharmacodynamics of Xuefu Zhuyu capsule (XFZY) in post-stroke depression (PSD) rats. (**A**) Animals grouping and experimental timeline of the surgery, chronic unpredictable mild stress (CUMS) stimulation, drug treatment and behavioral test. (**B**) Neurological deficit score. (**C**) Sugar water preference rate. (**D**) The total moving distance in the open field test. (**E**) The number of vertical rearings in the open field test. (**F**) The immobility time of the forced swimming test (**G**) The number of Nissl bodies. (**H**) Nissl staining of hippocampus tissues. *$P < 0.05$ compared to Sham; **$P < 0.01$ compared to Sham; $^{\#}P < 0.05$ compared to PSD; $^{\#\#}P < 0.01$ compared to PSD.

behavioral and histological outcomes. Behavioral tests revealed that the PGFX group exhibited higher neurological scores ($P < 0.05$) (Figure 2B), a decreased sucrose preference rate ($P < 0.05$) (Figure 2C), reduced spontaneous activity in the open field test ($P < 0.05$) (Figures 2D and 2E), and longer immobility time ($P < 0.05$) (Figure 2F) in the forced swimming test when compared to the XFM group. The findings from Nissl staining analyses revealed a notable decrease in Nissl bodies ($P < 0.05$) (Figure 2G) in the CA1 region of the brain in the PGFX group compared to the XFM group (Figure 2H). These results suggest that the XFM group did not effectively ameliorate neurological deficits and depressive symptoms in PSD rats following intestinal flora depletion, indicating that the therapeutic efficacy of XFZY is potentially dependent on the presence of intestinal flora.

3.3. The effect of XFZY on the intestinal microbiota of rats with PSD

To investigate the impact of XFZY on the gut microbiota in PSD rats, 16S rDNA sequencing was performed. Alpha diversity analysis (Chao1, Observed species, Shannon) revealed reduced microbial richness and diversity in the PSD group compared to Sham ($P < 0.05$), which were restored in the XFM group (Figures 3A–3C). In contrast, PGF and PGFX groups showed significantly lower diversity, indicating severe dysbiosis unmitigated by XFZY. Beta diversity (PCoA, Figures 3E–3F) revealed distinct clustering, separating Sham, PSD, and XFM from PGF and PGFX groups, with clear

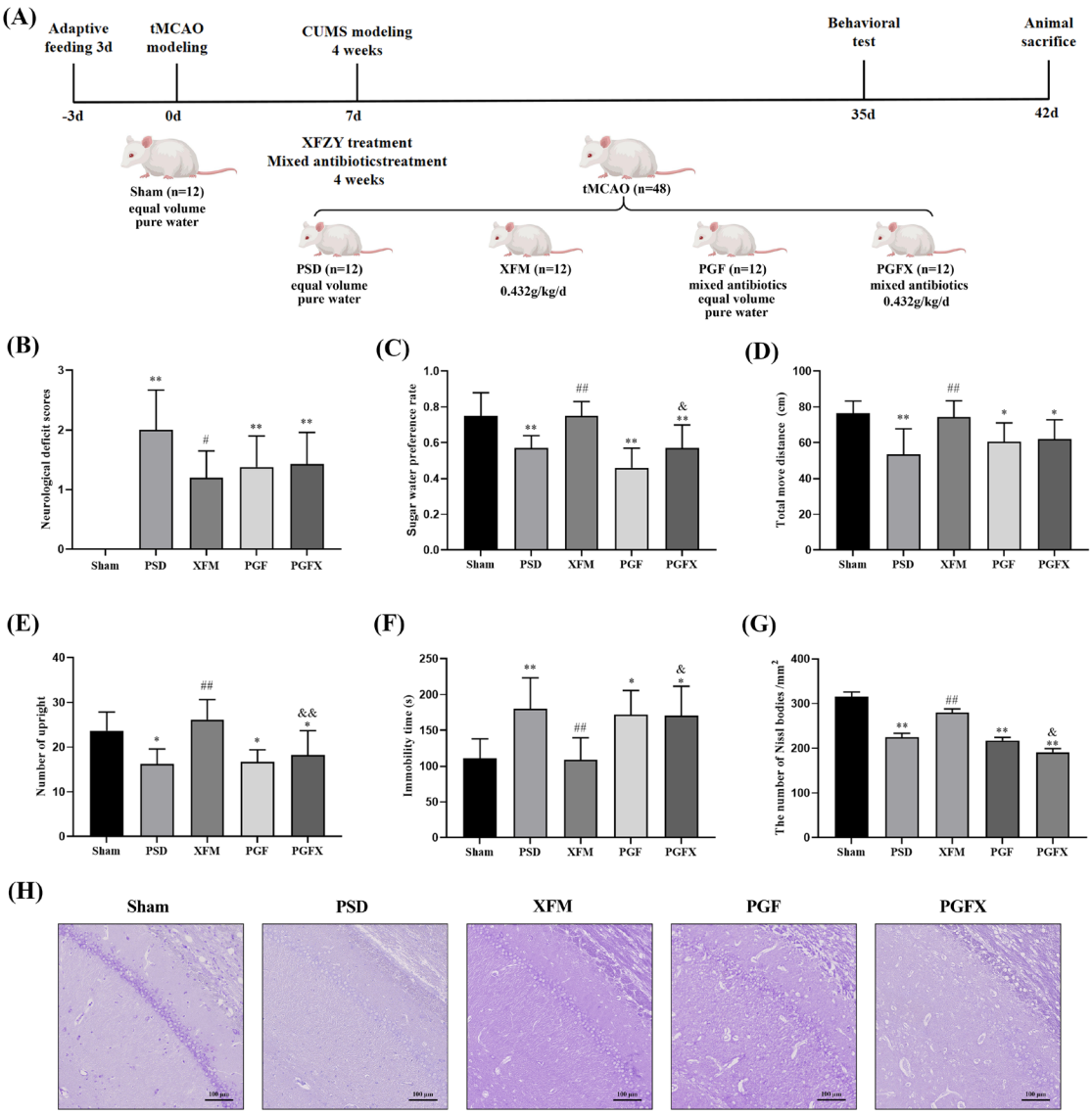

Figure 2. XFZY treatment's effectiveness decreased after removing intestinal flora. (**A**) Animals grouping and experimental timeline of the surgery, cums stimulation, drug treatment and behavioral test. (**B**) Neurological deficit score. (**C**) Sugar water preference rate. (**D**) The total moving distance in the open field test. (**E**) The number of vertical rearings in the open field test. (**F**) The immobility time of the forced swimming test (**G**) The number of Nissl bodies. (**H**) Nissl staining of hippocampus tissues. *$P < 0.05$ compared to Sham; **$P < 0.01$ compared to Sham; $^{\#}P < 0.05$ compared to PSD; $^{\#\#}P < 0.01$ compared to PSD; $^{\&}P < 0.05$ compared to XFM; $^{\&\&}P < 0.01$ compared to XFM.

differentiation among all five groups (PCoA1: 20.42%), indicating significant compositional differences.

At the phylum level, Firmicutes, Bacteroidetes, Proteobacteria, and Verrucomicrobia dominated the microbiota (Figure 4A). The PSD group showed decreased Firmicutes and increased Proteobacteria *vs.* Sham, which were reversed in the XFM group. The PGF and PGFX groups exhibited further reductions in Firmicutes and increases in Proteobacteria and Bacteroidetes. At the genus level, PSD was characterized by decreased beneficial genera (*e.g.*, *Lactobacillus*, *Ruminococcus*, *Clostridium*) and increased pathobionts (*e.g.*, *Escherichia-Shigella*, *Enterococcus*, *Klebsiella*), which were partially reversed in the XFM group. In contrast, PGF and PGFX groups showed enrichment of potential pathogens and loss of commensals.

Linear discriminant analysis effect size (LEfSe) analysis (Figures 4E–4F) identified *Romboutsia* and *Dorea* as discriminant taxa in PSD, while *Lactobacillus*, *Ruminococcus*, and *Clostridia*_UCG-014 were enriched in the XFM group. The PGF and PGFX groups were dominated by Enterobacteriaceae members (*e.g.*, *Escherichia*, *Klebsiella*), suggesting distinct microbial dysbiosis patterns.

3.4. The effect of XFZY on the short-chain fatty acids of rats with PSD

Short-chain fatty acids—including acetic, propionic, and butyric acid—are gut microbial metabolites implicated

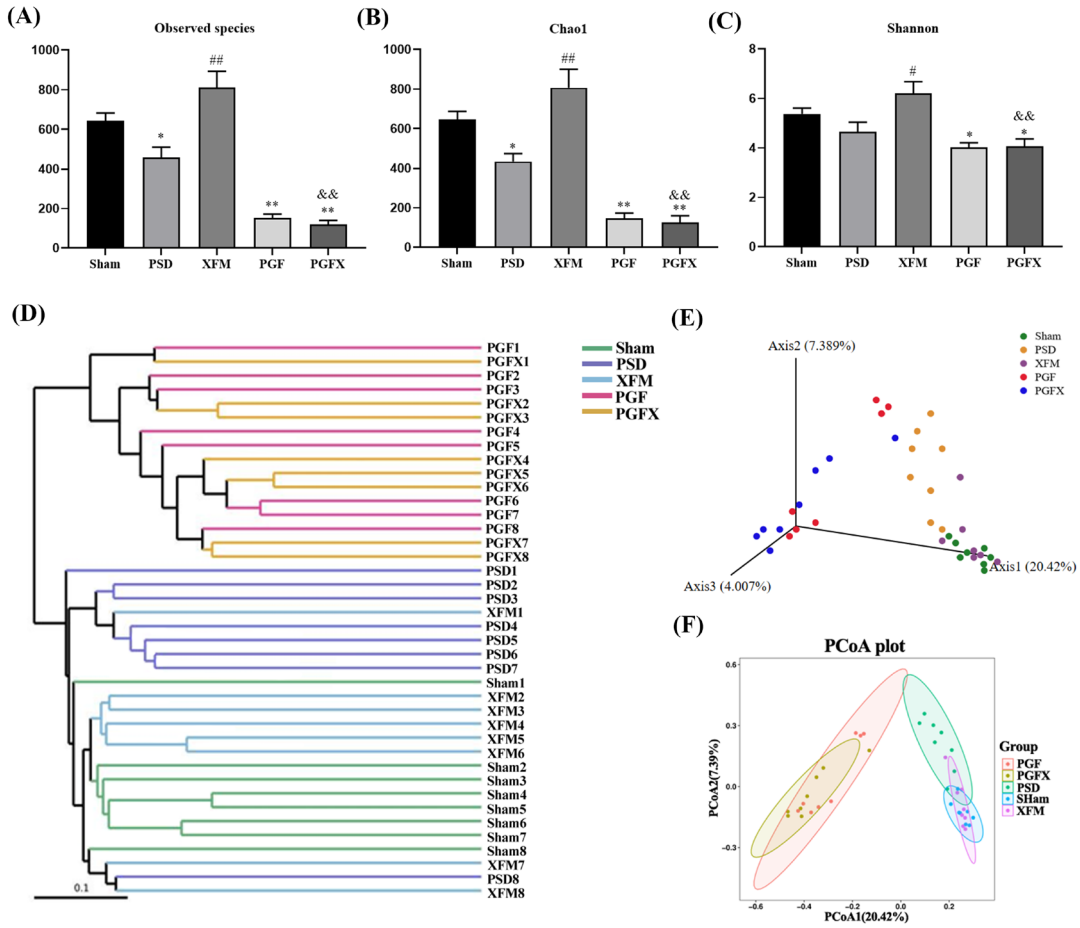

Figure 3. Analysis of the alpha diversity and beta diversity of intestinal flora. (**A**) Observed species. (**B**) Chao1 index. (**C**) Shannon index. (**D**) Unweighted Pair Group Method with Arithmetic Mean (UPGMA) hierarchical clustering plot. (**E**) PCoA plot in 3D. (**F**) Principal Coordinates Analysis (PCoA) plot in 3D. *$P < 0.05$ compared to Sham; **$P < 0.01$ compared to Sham; $^{\#}P < 0.05$ compared to PSD; $^{\#\#}P < 0.01$ compared to PSD; $^{\&\&}P < 0.01$ compared to XFM.

in the gut-brain axis, influencing emotional and cognitive functions (*34*). In this study, serum and fecal SCFAs were analyzed by gas chromatography. Both compartments showed similar trends: the PSD group exhibited significantly lower levels of all three major SCFAs compared to Sham group ($P < 0.05$), while the XFM group reversed these reductions (Figures 5A–5F). These results suggest that XFZY modulates SCFA production, particularly acetic and butyric acid, likely through remodeling of the gut microbiota.

3.5. XFZY demonstrates efficacy in improving the intestinal barrier function in rats with PSD

The gut microbiota influences intestinal barrier integrity, a factor implicated in neuropsychiatric disorders such as depression and anxiety (*35,36*). In this study, intestinal barrier function and inflammation were evaluated using H&E, AB-PAS, and immunohistochemical (IHC) staining. H&E staining revealed well-organized colonic glands in the sham group, whereas the PSD group exhibited inflammatory cell infiltration and structural damage to the epithelium and glands—pathology ameliorated in the XFM group. In contrast, PGF and PGFX groups showed more severe inflammation. AB-PAS staining showed reduced goblet cell numbers in the PSD group ($P < 0.05$), which were restored in the XFM group (Figures 6A and 6B). IHC analysis confirmed downregulation of mucosal and tight junction proteins—MUC2, ZO-1, and Occludin in PSD rats ($P < 0.05$; Figures 6A, 6C–6E), all of which were significantly upregulated following intervention with the XFM group ($P < 0.05$). These results indicate that PSD impairs intestinal barrier function, and XFZY exerts protective effects by reducing inflammation and restoring key barrier components.

3.6. XFZY demonstrates efficacy in suppressing neuroinflammation in rats with PSD

Microglia, central nervous system innate immune cells, contribute to depression *via* neuroinflammation (*37*). IHC analysis showed increased microglial activation in the PSD and PGF groups compared to Sham ($P < 0.05$), which was attenuated in the XFM group ($P < 0.05$; Figures 7A and 7B). Serum levels of pro-inflammatory

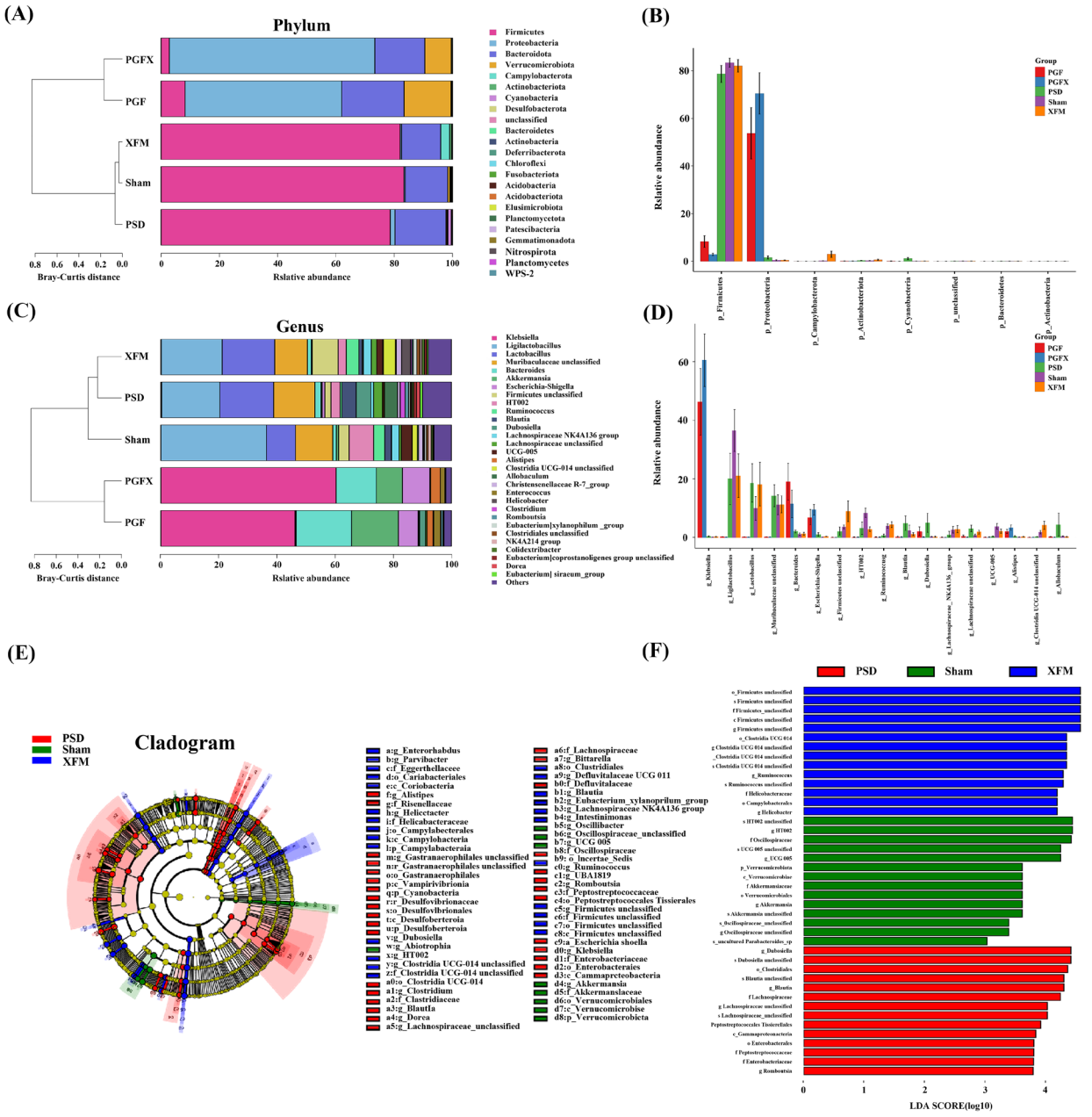

Figure 4. Analysis of relative abundance and LEfSE analysis of intestinal flora in various groups. (**A**) Cluster analysis at the gate level. (**B**) Analysis of differences at the gate level. (**C**) Cluster analysis at the genus level. (**D**) Analysis of differences at the genus level. (**E**) Cladogram from linear discriminant analysis effect size (LEfSe) analysis. (**F**) Linear discriminant analysis (LDA) scores from LEfSe analysis.

cytokines (TNF-α, IL-1β, IL-6) were significantly elevated in PSD rats ($P < 0.05$), and reduced in the XFM group ($P < 0.05$; Figures 7C–7E). No significant difference was observed between PGF and PGFX groups ($P > 0.05$). These findings indicate that systemic and central neuroinflammation is attenuated in the XFM group.

4. Discussion

Post-stroke depression is a prevalent complication of neuropsychiatric disorders following a stroke, with a reported prevalence rate of approximately 29% that has shown minimal variation over time (*38*). Research (*39*) indicates that the gut microbiota may play a significant role in the pathogenesis of neurological conditions *via* the brain-gut axis, highlighting its importance as a key factor in susceptibility to such disorders. There exists a relationship between stroke and dysbiosis of the intestinal flora, potentially impacting the prognosis of stroke through mechanisms including bacterial translocation, intestinal metabolites, and immune regulation (*40*). Additionally, the gut microbiota is implicated in the pathogenesis of depression, potentially exacerbating depressive symptoms through inflammatory responses, hypothalamic-pituitary-adrenal axis dysregulation

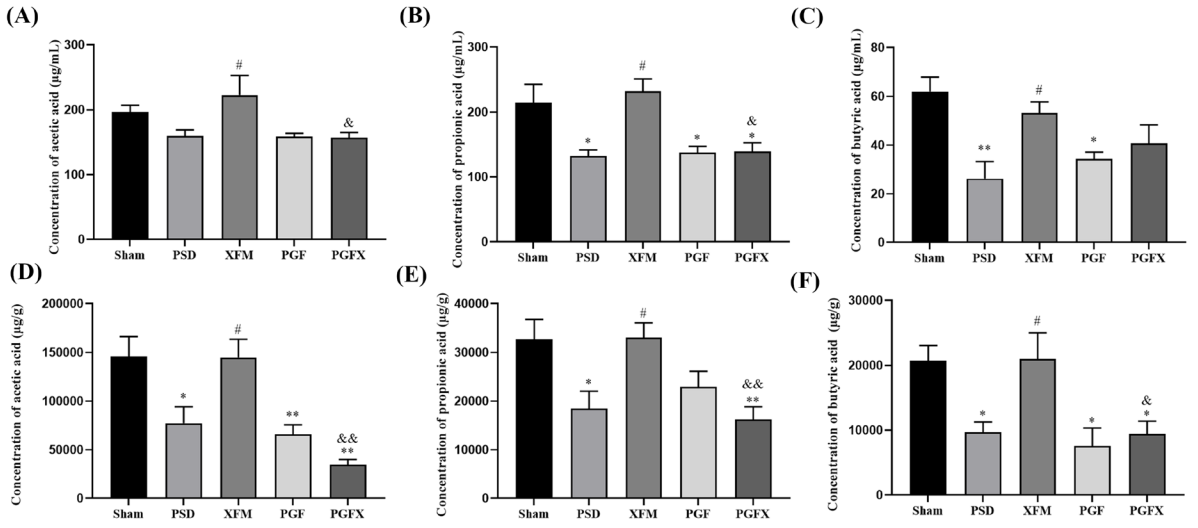

Figure 5. Short chain fatty acids in serum and feces. (**A**) Concentration of acetic acid in serum. (**B**) Concentration of propionic acid in serum. (**C**) Concentration of butyric acid in serum. (**D**) Concentration of acetic acid in feces. (**E**) Concentration of propionic acid in feces. (**F**) Concentration of butyric acid in feces. *$P < 0.05$ compared to Sham; **$P < 0.01$ compared to Sham; $^{\#}P < 0.05$ compared to PSD; $^{\&}P < 0.05$ compared to XFM; $^{\&\&}P < 0.01$ compared to XFM.

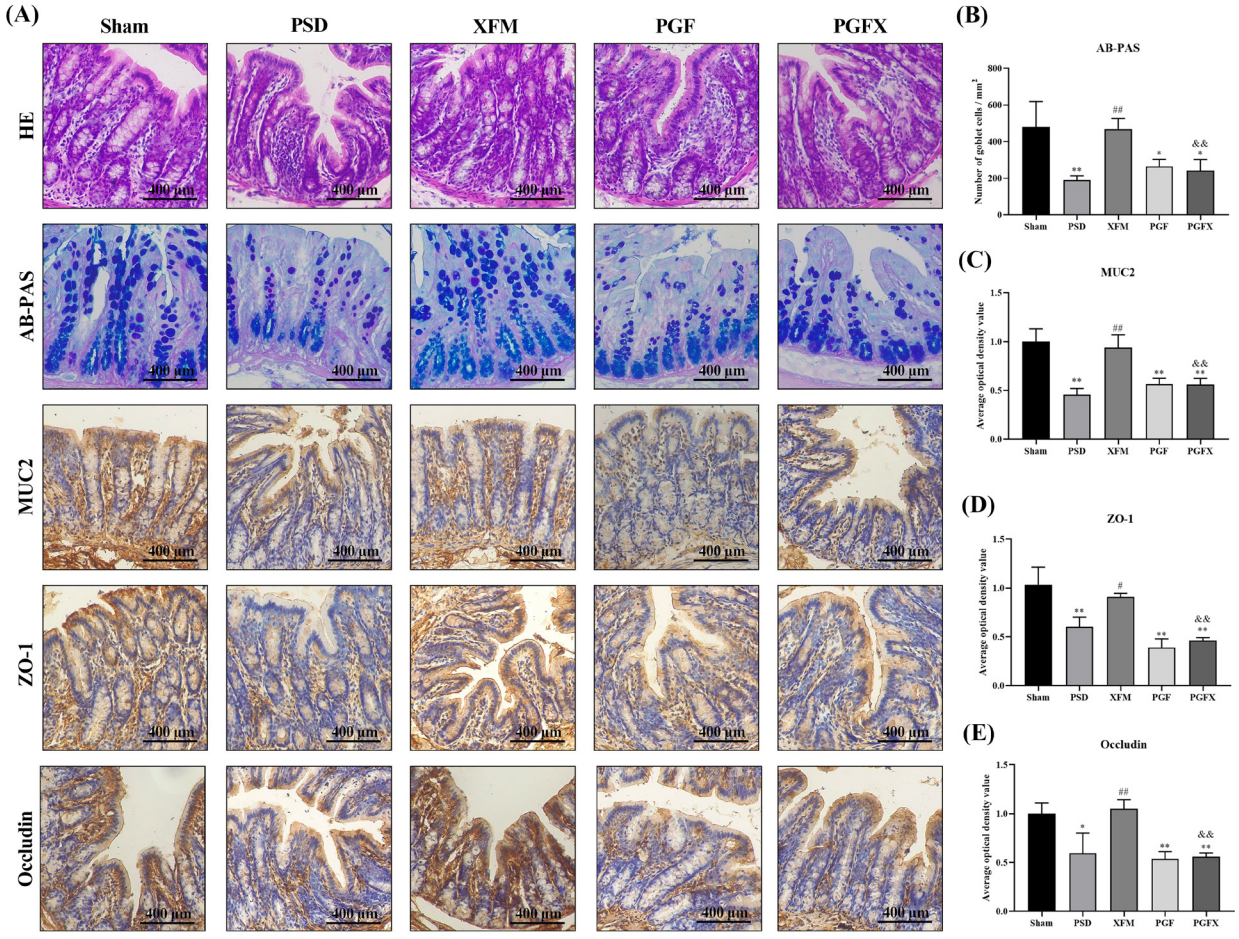

Figure 6. XFZY effectively enhances intestinal barrier function in rats with PSD. (**A**) Representative images of hematoxylin and eosin (H&E) staining, Alcian blue-periodic acid–Schiff (AB-PAS) staining, and immunohistochemistry (IHC) staining for mucin 2 (MUC2), zonula occludens-1 (ZO-1), and Occludin in the colon. (**B**) Goblet cell counts. (**C**) Average optical density value of MUC2. (**D**) Average optical density value of ZO-1. (**E**) Average optical density value of Occludin. *$P < 0.05$ compared to Sham; **$P < 0.01$ compared to Sham; $^{\#}P < 0.05$ compared to PSD; $^{\#\#}P < 0.01$ compared to PSD; $^{\&\&}P < 0.01$ compared to XFM.

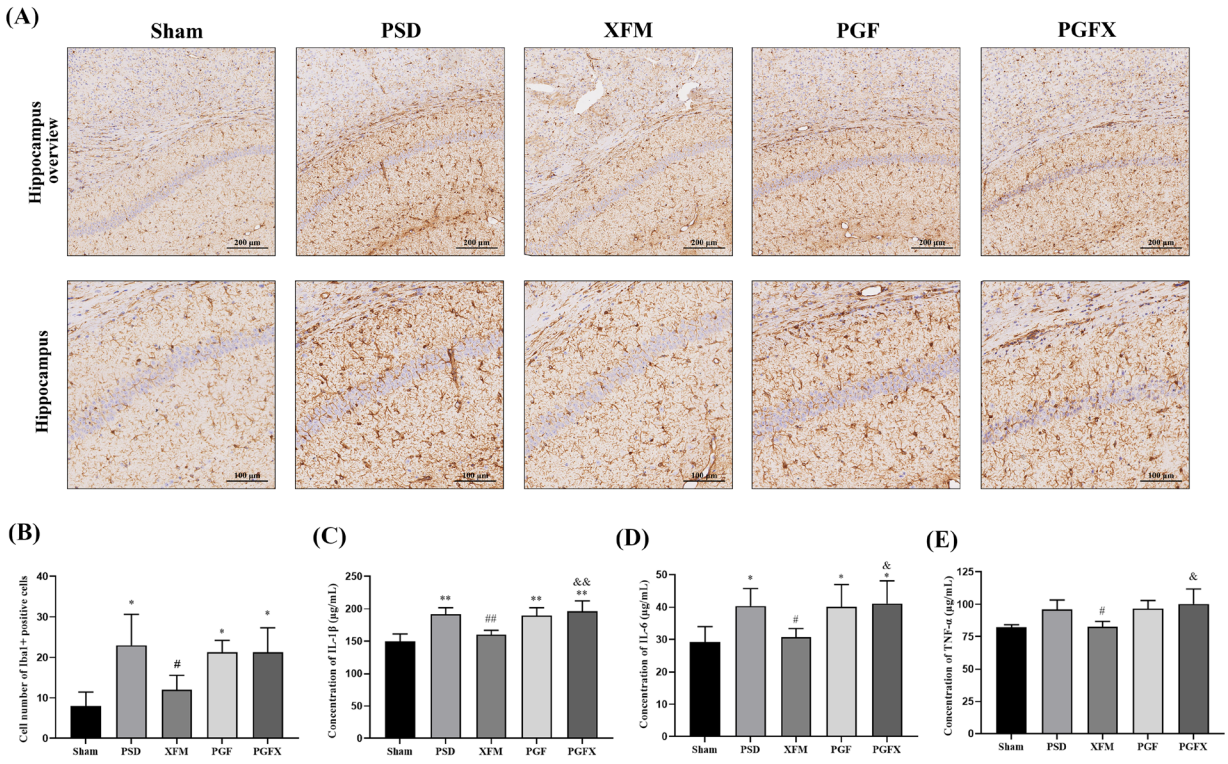

Figure 7. XFZY shows effectiveness in inhibiting neuroinflammation in rats with post-stroke depression. (**A**) IHC staining of ionized calcium-binding adapter molecule 1 (Iba1) in hippocampal. (**B**) Total number of Iba1-positive microglia. (**C**) Concentration of interleukin-1β (IL-1β) in serum. (**D**) Concentration of interleukin-6 (IL-6) in serum. (**E**) Concentration of tumor necrosis factor-α (TNF-α) in serum. $^{*}P < 0.05$ compared to Sham; $^{**}P < 0.01$ compared to Sham; $^{\#}P < 0.05$ compared to PSD; $^{\#\#}P < 0.01$ compared to PSD; $^{\&}P < 0.05$ compared to XFM; $^{\&\&}P < 0.01$ compared to XFM.

(*41,42*). Thus, the restoration of intestinal flora homeostasis is crucial for the prevention and treatment of PSD.

Existing pharmacological studies provide support for the microbiota-modulating potential of XFZY. The individual herbal components of XFZY have been reported to beneficially influence the gut microbiota. For instance, Bupleuri Radix polysaccharides can ameliorate colitis by modulating gut microbial composition (*43*). *Angelica sinensis* has been shown to reshape the gut microbiota and improve intestinal barrier function (*44*). *Rehmannia glutinosa* polysaccharides can promote the production of beneficial SCFAs by gut bacteria (*45*), while *Paeonia lactiflora* extracts alleviate intestinal inflammation partly through microbiota regulation (*46*). More directly, a study on the whole formula of XFZY demonstrated its ability to attenuate atherosclerosis in mice by reversing gut microbiota dysbiosis, highlighting the integral role of microbiota modulation in its therapeutic mechanism (*47*). These reports align with the core findings of the present study, wherein XFZY intervention significantly altered the gut microbial structure and increased SCFA levels in PSD rats.

Our findings indicate that XFZY has a significant impact on increasing Alpha diversity in rats with post-stroke depression. At the phylum level, there was a significant increase in the relative abundance of *Bacteroides* and Proteobacteria in the PSD group compared to the Sham group, while the abundance of Firmicutes and Campylobacterota decreased. Conversely, following intervention with XFZY, these microbiota exhibited a contrasting trend. This suggests that regulating intestinal flora to restore intestinal microecology may offer an effective treatment for PSD. The relative abundance of Proteobacteria and Ruminococcaceae shows a negative correlation with the increase in intestinal permeability (*48*). A decrease in the abundance of rumen bacteria in the gut may lead to intestinal inflammation and damage to the intestinal mucosal barrier, allowing harmful factors such as TNF-α to enter the bloodstream (*49*). Experimental findings indicate a reduction in *Ruminococcus* levels in the PSD, PGF, and PGFX groups, suggesting a potential increase in intestinal permeability and inflammatory factors. Most members of the *Desulfurococcus* genus are producers of lipopolysaccharides (LPS) (*50*). Research (*51*) has demonstrated that the peripheral administration of LPS can stimulate the immune system *via* Toll-like receptors, leading to the production of pro-inflammatory cytokines including IL-6, IL-1β, and TNF-α. Our study found that XFZY treatment reduced the presence of *Desulfovibrio* and *Vibrio* and mitigated the inflammatory reaction.

Short-chain fatty acids, the principal metabolites produced by gut microbiota, have been shown to

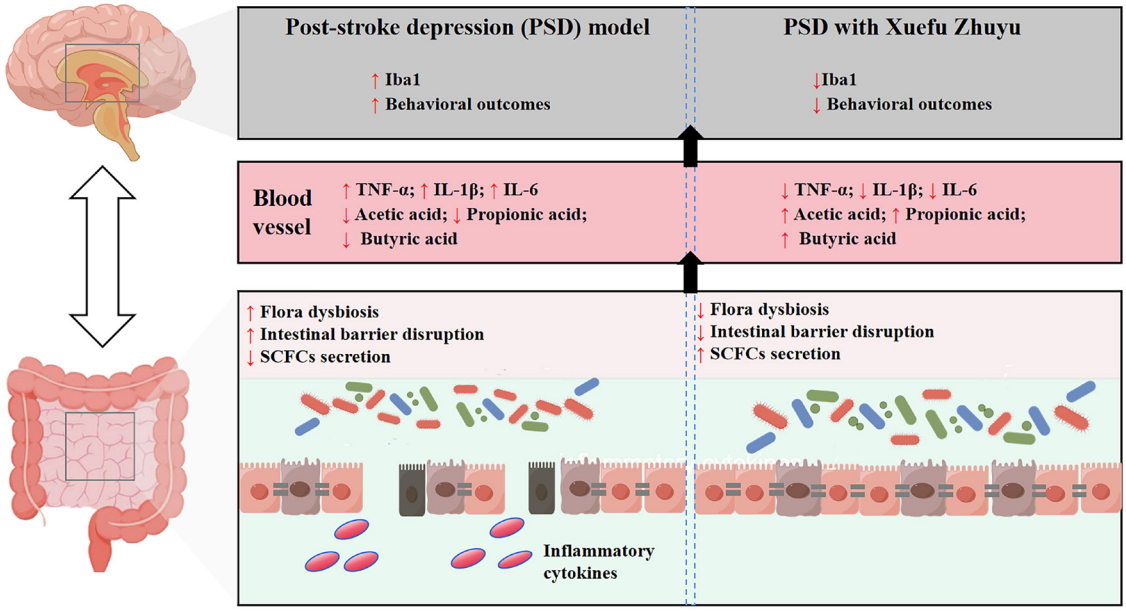

Figure 8. The diagram of the mechanism of XFZY anti-PSD. Brain injury after stroke induces gut dysbiosis and intestinal barrier damage, promoting systemic translocation of microbial metabolites (*e.g.*, short-chain fatty acids, SCFAs), which exacerbate neuroinflammation and hippocampal injury. XFZY restores gut homeostasis, reduces SCFA levels, and alleviates neuroinflammation and depressive-like behaviors.

have various beneficial effects on gut health (*52*). For instance, SCFAs can enhance intestinal barrier function and decrease inflammation. Butyrate, for instance, has been found to increase the expression of tight junction proteins, thereby reducing intestinal permeability (*53*). Additionally, SCFAs have been implicated in modulating immune responses and impacting the central nervous system (*54*). Increased levels of SCFAs have been associated with alleviation of depressive symptoms in animal experiment (*55*). Furthermore, studies (*56*) have indicated that individuals with major depression have reported consuming higher amounts of butyrate, acetate, and propionate. SCFAs can stimulate nerve pathways and induce behavioral changes through the activation of G protein-coupled receptors free fatty acid receptor 2 (FFAR2) and free fatty acid receptor 3 (FFAR3) (*57*). Additionally, research suggests (*58*) that germ-free mice treated with SCFAs show improvements in microglial function, indicating a potential role for SCFAs in reversing microglial deficiencies. Our experiments demonstrate that PSD rats exhibit dysbiosis in their gut microbiota, characterized by a reduction in the presence of SCFA-producing bacterial flora and a subsequent decrease in SCFA content. Following intervention with XFZY, there was an improvement in the abundance and composition of gut microbiota, leading to an increase in the relative abundance of SCFA-producing bacteria in the gut. Notably, our results revealed an inverted U-shaped dose-response relationship, where the high dose of XFZY (0.864 g/kg) showed inferior effects compared to the medium dose (0.432 g/kg). This can be attributed to excessive modulation of the gut microbiota and overproduction of SCFAs at the high dose, which may disrupt the homeostasis of the gut-brain axis. As supported by previous research, both microbial balance and SCFA levels require maintenance within an optimal physiological range for their beneficial effects; deviations beyond this range can impair therapeutic outcomes (*59,60*).

Of particular significance is that this study provides the first systematic evidence that XFZY ameliorates PSD by modulating the gut microbiota–gut–brain axis. To our knowledge, this is the first report demonstrating that XFZY alleviates depressive-like behaviors in a PSD model through restoration of gut microbial diversity and activation of the SCFAs pathway. These findings highlight the unique microbiota-modulating characteristics of XFZY and establish a novel link between this herbal formulation and PSD treatment.

Given the regulatory impacts of gut microbiota and SCFAs on the gut barrier and neuroinflammation, our study investigates the potential of XFZY in mitigating brain neuroinflammation and safeguarding the intestinal mucosal barrier. The findings of our study indicate that activated microglial cells in the PSD group exhibited an increase and a significant rise in the expression of proinflammatory cytokines in the serum. Following treatment with XFZY, there was a reduction in microglial activation and a significant decrease in the expression of inflammatory factors, suggesting a mitigation of neuroinflammation in PSD rats. However, the number of activated microglia and the expression of inflammatory factors increased in the PGF and PGFX groups, which further proved that XFZY can alleviate brain neuroinflammation in PSD rats by regulating intestinal flora.

The results of histological examination using HE staining revealed the presence of inflammatory infiltrates in the colon tissue of rats with PSD, while IHC demonstrated an increase in intestinal barrier permeability in these rats. Following treatment with XFZY, a significant reduction in colon tissue inflammation and improvement in intestinal barrier function were observed. These findings provide further evidence of the efficacy of XFZY in enhancing intestinal barrier function in PSD rats.

Hence, it is hypothesized that dysbiosis of gut microbiota disrupts intestinal barrier integrity, triggering activation of the peripheral immune system and subsequent synthesis and release of pro-inflammatory cytokines. This interaction between peripheral and central immunity may activate microglia in the brain, resulting in neuroinflammation and ultimately manifesting as symptoms depression. Under the intervention of XFZY, it can improve the intestinal barrier function and alleviate the inflammatory response by increasing the relative abundance of intestinal flora, thus reducing the depressive symptoms (Figure 8).

Despite the novel findings, several limitations of this study should be acknowledged. First, while our data indicate that gut microbiota modulation mediates the antidepressant effects of XFZY, causality has not been definitively proven through interventional approaches such as fecal microbiota transplantation. Second, the findings from this rodent model of PSD require validation in humans due to species-specific differences in physiology and microbiota. Third, the specific active component(s) within the XFZY formulation responsible for the observed effects remain unknown. Future studies should therefore employ FMT experiments, pursue clinical translation, and identify the key active constituents to fully elucidate the therapeutic mechanism.

XFZY alleviates depressive-like behaviors in PSD rats through modulation of the gut microbiota and restoration of intestinal barrier integrity, leading to reduced secretion of short-chain fatty acids, which in turn attenuates hippocampal neuronal damage and neuroinflammation.

Funding: This study was supported by the Science and Technology Project of Haihe Laboratory of Modern Chinese Medicine (22HHZYSS00015).

Conflict of Interest: The authors have no conflicts of interest to disclose.

References

1. Zhou H, Wei YJ, Xie GY. Research progress on post-stroke depression. Exp Neurol. 2024; 373:114660.
2. Chen J, Wu Y, Chen Z, Yi B, Zhang L, Yin C, Feng H. High incidence of stroke in COVID-19 patients. Aging (Albany NY). 2020; 12:22390-22398.
3. Hackett ML, Yapa C, Parag V, Anderson CS. Frequency of depression after stroke: a systematic review of observational studies. Stroke. 2005; 36:1330-1340.
4. Ayerbe L, Ayis S, Crichton S, Wolfe CD, Rudd AG. The natural history of depression up to 15 years after stroke: the South London Stroke Register. Stroke. 2013; 44:1105-1110.
5. De Ryck A, Brouns R, Geurden M, Elseviers M, De Deyn PP, Engelborghs S. Risk factors for poststroke depression: Identification of inconsistencies based on a systematic review. J Geriatr Psychiatry Neurol. 2014; 27:147-158.
6. Medeiros GC, Roy D, Kontos N, Beach SR. Post-stroke depression: A 2020 updated review. Gen Hosp Psychiatry. 2020; 66:70-80.
7. Paolucci S. Advances in antidepressants for treating post-stroke depression. Expert Opin Pharmacother. 2017; 18:1011-1017.
8. Dinan TG, Cryan JF. Regulation of the stress response by the gut microbiota: implications for psychoneuroendocrinology. Psychoneuroendocrinology. 2012; 37:1369-1378.
9. Elangovan A, Dahiya B, Kirola L, *et al.* Does gut brain axis has an impact on Parkinson's disease (PD)? Ageing Res Rev. 2024; 94:102171.
10. Abdellatif AM, Sarvetnick NE. Current understanding of the role of gut dysbiosis in type 1 diabetes. J Diabetes. 2019; 11:632-644.
11. Morais LH, Schreiber HLt, Mazmanian SK. The gut microbiota-brain axis in behaviour and brain disorders. Nat Rev Microbiol. 2021; 19:241-255.
12. Pu J, Liu Y, Zhang H, *et al*. An integrated meta-analysis of peripheral blood metabolites and biological functions in major depressive disorder. Mol Psychiatry. 2021; 26:4265-4276.
13. Mortensen JK, Andersen G. Pharmacological management of post-stroke depression: an update of the evidence and clinical guidance. Expert Opin Pharmacother. 2021; 22:1157-1166.
14. Zhu L, Han R, He L, Pan B, Zhong W, Li Y, Liu X. Innovative strategies for post-stroke depression: integrating traditional Chinese medicine with neurobiological insights, including the gut-brain axis. Front Pharmacol. 2025; 16:1539357.
15. Yuan J, Yan F, Li W, Yuan G. Network pharmacological analysis of Xuefu Zhuyu decoction in the treatment of atherosclerosis. Front Pharmacol. 2022; 13:1069704.
16. Wang X, Xing X, Huang P, Zhang Z, Zhou Z, Liang L, Yao R, Wu X, Yang L. A Chinese classical prescription Xuefu Zhuyu decoction in the treatment of coronary heart disease: An overview. Heliyon. 2024; 10:e28919.
17. Han H, Wu LM, Yang WM, Wang MX, Tang JJ, Wang H, Liu ZX, Liu RZ, Dong T, Zhang J, Yang B, Han MX. Characteristics of traditional Chinese medicine syndromes in post-stroke depression. Zhong Xi Yi Jie He Xue Bao. 2010; 8:427-431.
18. Lu LL, Shen XH, Chen JX. Xuefu zhuyu oral liquid intervened stress-stimulated depression model rats. Zhongguo Zhong Xi Yi Jie He Za Zhi. 2013; 33:638-640.
19. Bercik P, Denou E, Collins J, Jackson W, Lu J, Jury J, Deng Y, Blennerhassett P, Macri J, McCoy KD, Verdu EF, Collins SM. The intestinal microbiota affect central levels of brain-derived neurotropic factor and behavior in mice. Gastroenterology. 2011; 141:599-609, 609.e591-593.
20. O'Mahony SM, Felice VD, Nally K, Savignac HM, Claesson MJ, Scully P, Woznicki J, Hyland NP, Shanahan F, Quigley EM, Marchesi JR, O'Toole PW, Dinan TG,

Cryan JF. Disturbance of the gut microbiota in early-life selectively affects visceral pain in adulthood without impacting cognitive or anxiety-related behaviors in male rats. Neuroscience. 2014; 277:885-901.
21. Duan J, Lin J, Zhang N, Wang Q, Li N, Yao K. Effect of Xuefu Zhuyu Capsule on Myocardial Infarction: Network Pharmacology and Experimental Verification. Evid Based Complement Alternat Med. 2023; 2023:5652276.
22. Bai L, Zhang D, Cui TT, Li JF, Gao YY, Wang NY, Jia PL, Zhang HY, Sun ZR, Zou W, Wang L. Mechanisms Underlying the Antidepressant Effect of Acupuncture *via* the CaMK Signaling Pathway. Front Behav Neurosci. 2020; 14:563698.
23. Li J, Sha L, Xu Q. An early increase in glutamate is critical for the development of depression-like behavior in a chronic restraint stress (CRS) model. Brain Res Bull. 2020; 162:59-66.
24. Mourão AM, Vicente LCC, Abreu MNS, Vale Sant'Anna R, Vieira ELM, de Souza LC, de Miranda AS, Rachid MA, Teixeira AL. Plasma Levels of Brain-Derived Neurotrophic Factor are Associated with Prognosis in the Acute Phase of Ischemic Stroke. J Stroke Cerebrovasc Dis. 2019; 28:735-740.
25. Sicard KM, Fisher M. Animal models of focal brain ischemia. Exp Transl Stroke Med. 2009; 1:7.
26. Bogdanova OV, Kanekar S, D'Anci KE, Renshaw PF. Factors influencing behavior in the forced swim test. Physiol Behav. 2013; 118:227-239.
27. Hamon M, Blier P. Monoamine neurocircuitry in depression and strategies for new treatments. Prog Neuropsychopharmacol Biol Psychiatry. 2013; 45:54-63.
28. Davey CG, Yücel M, Allen NB. The emergence of depression in adolescence: development of the prefrontal cortex and the representation of reward. Neurosci Biobehav Rev. 2008; 32:1-19.
29. Bai F, Hu N, Yang R, Qu LY, Ma S, Huang J, Wang JH, Yang BF, Li CL. Tongmai granules improve rat hippocampal injury by regulating TLR4/MyD88/AP-1 signaling pathway. J Ethnopharmacol. 2022; 285:114874.
30. Wu Q, Chen J, Yue J, Ying X, Zhou Y, Chen X, Tu W, Lou X, Yang G, Zhou K, Jiang S. Electroacupuncture improves neuronal plasticity through the A2AR/cAMP/PKA signaling pathway in SNL rats. Neurochem Int. 2021; 145:104983.
31. Micalizzi G, Buzzanca C, Chiaia V, Mondello M, Cacciola F, Caccamo D, Mondello L. Measurement of short-chain fatty acids in human plasma by means of fast gas chromatography-mass spectrometry. J Chromatogr B Analyt Technol Biomed Life Sci. 2024; 1235:124044.
32. Liu W, Ge T, Leng Y, Pan Z, Fan J, Yang W, Cui R. The Role of Neural Plasticity in Depression: From Hippocampus to Prefrontal Cortex. Neural Plast. 2017; 2017:6871089.
33. Han S, Li XX, Wei S, Zhao D, Ding J, Xu Y, Yu C, Chen Z, Zhou DS, Yuan TF. Orbitofrontal cortex-hippocampus potentiation mediates relief for depression: A randomized double-blind trial and TMS-EEG study. Cell Rep Med. 2023; 4:101060.
34. Dalile B, Van Oudenhove L, Vervliet B, Verbeke K. The role of short-chain fatty acids in microbiota-gut-brain communication. Nat Rev Gastroenterol Hepatol. 2019; 16:461-478.
35. Aherne CM, Collins CB, Masterson JC, Tizzano M, Boyle TA, Westrich JA, Parnes JA, Furuta GT, Rivera-Nieves J, Eltzschig HK. Neuronal guidance molecule netrin-1 attenuates inflammatory cell trafficking during acute experimental colitis. Gut. 2012; 61:695-705.
36. Wang Y, Shi Y, Li W, Wang S, Zheng J, Xu G, Li G, Shen X, Yang J. Gut microbiota imbalance mediates intestinal barrier damage in high-altitude exposed mice. FEBS J. 2022; 289:4850-4868.
37. Li B, Yang W, Ge T, Wang Y, Cui R. Stress induced microglial activation contributes to depression. Pharmacol Res. 2022; 179:106145.
38. Lim GY, Tam WW, Lu Y, Ho CS, Zhang MW, Ho RC. Prevalence of Depression in the Community from 30 Countries between 1994 and 2014. Sci Rep. 2018; 8:2861.
39. Socała K, Doboszewska U, Szopa A, Serefko A, Włodarczyk M, Zielińska A, Poleszak E, Fichna J, Wlaź P. The role of microbiota-gut-brain axis in neuropsychiatric and neurological disorders. Pharmacol Res. 2021; 172:105840.
40. Hu W, Kong X, Wang H, Li Y, Luo Y. Ischemic stroke and intestinal flora: an insight into brain-gut axis. Eur J Med Res. 2022; 27:73.
41. Simpson CA, Diaz-Arteche C, Eliby D, Schwartz OS, Simmons JG, Cowan CSM. The gut microbiota in anxiety and depression - A systematic review. Clin Psychol Rev. 2021; 83:101943.
42. Ding W, Wang L, Li L, Li H, Wu J, Zhang J, Wang J. Pathogenesis of depression and the potential for traditional Chinese medicine treatment. Front Pharmacol. 2024; 15:1407869.
43. Li P, Wu M, Xiong W, Li J, An Y, Ren J, Xie Y, Xue H, Yan D, Li M, Zhong G. Saikosaponin-d ameliorates dextran sulfate sodium-induced colitis by suppressing NF-κB activation and modulating the gut microbiota in mice. Int Immunopharmacol. 2020; 81:106288.
44. Liu C, Wu Y, Wang Y, Yang F, Ren L, Wu H, Yu Y. Integrating 16 S rRNA gene sequencing and metabolomics analysis to reveal the mechanism of Angelica sinensis oil in alleviating ulcerative colitis in mice. J Pharm Biomed Anal. 2024; 249:116367.
45. Lv H, Jia H, Cai W, Cao R, Xue C, Dong N. Rehmannia glutinosa polysaccharides attenuates colitis *via* reshaping gut microbiota and short-chain fatty acid production. J Sci Food Agric. 2023; 103:3926-3938.
46. Yan BF, Chen X, Chen YF, Liu SJ, Xu CX, Chen L, Wang WB, Wen TT, Zheng X, Liu J. Aqueous extract of Paeoniae Radix Alba (Paeonia lactiflora Pall.) ameliorates DSS-induced colitis in mice by tunning the intestinal physical barrier, immune responses, and microbiota. J Ethnopharmacol. 2022; 294:115365.
47. Ji W, Jiang T, Sun Z, Teng F, Ma C, Huang S, Yan S. The Enhanced Pharmacological Effects of Modified Traditional Chinese Medicine in Attenuation of Atherosclerosis Is Driven by Modulation of Gut Microbiota. Front Pharmacol. 2020; 11:546589.
48. Leclercq S, Matamoros S, Cani PD, Neyrinck AM, Jamar F, Stärkel P, Windey K, Tremaroli V, Bäckhed F, Verbeke K, de Timary P, Delzenne NM. Intestinal permeability, gut-bacterial dysbiosis, and behavioral markers of alcohol-dependence severity. Proc Natl Acad Sci U S A. 2014; 111:E4485-4493.
49. Voltolini C, Battersby S, Etherington SL, Petraglia F, Norman JE, Jabbour HN. A novel antiinflammatory role for the short-chain fatty acids in human labor. Endocrinology. 2012; 153:395-403.
50. Huang G, Zheng Y, Zhang N, Huang G, Zhang W, Li Q, Ren X. *Desulfovibrio vulgaris* caused gut inflammation

and aggravated DSS-induced colitis in C57BL/6 mice model. Gut Pathog. 2024; 16:39.
51. O'Connor JC, Lawson MA, André C, Moreau M, Lestage J, Castanon N, Kelley KW, Dantzer R. Lipopolysaccharide-induced depressive-like behavior is mediated by indoleamine 2,3-dioxygenase activation in mice. Mol Psychiatry. 2009; 14:511-522.
52. Liu G, Tang J, Zhou J, Dong M. Short-chain fatty acids play a positive role in colorectal cancer. Discov Oncol. 2024; 15:425.
53. Mohamed Elfadil O, Mundi MS, Abdelmagid MG, Patel A, Patel N, Martindale R. Butyrate: More Than a Short Chain Fatty Acid. Curr Nutr Rep. 2023; 12:255-262.
54. Corrêa-Oliveira R, Fachi JL, Vieira A, Sato FT, Vinolo MA. Regulation of immune cell function by short-chain fatty acids. Clin Transl Immunology. 2016; 5:e73.
55. Kelly JR, Borre Y, C OB, *et al*. Transferring the blues: Depression-associated gut microbiota induces neurobehavioural changes in the rat. J Psychiatr Res. 2016; 82:109-118.
56. Schroeder FA, Lin CL, Crusio WE, Akbarian S. Antidepressant-like effects of the histone deacetylase inhibitor, sodium butyrate, in the mouse. Biol Psychiatry. 2007; 62:55-64.
57. Brown AJ, Goldsworthy SM, Barnes AA, *et al*. The Orphan G protein-coupled receptors GPR41 and GPR43 are activated by propionate and other short chain carboxylic acids. J Biol Chem. 2003; 278:11312-11319.
58. Erny D, Hrabě de Angelis AL, Jaitin D, *et al*. Host microbiota constantly control maturation and function of microglia in the CNS. Nat Neurosci. 2015; 18:965-977.
59. Huang Y, Wu J, Zhang H, *et al*. The gut microbiome modulates the transformation of microglial subtypes. Mol Psychiatry. 2023; 28:1611-1621.
60. Xu K, Wang G, Gong J, Yang X, Cheng Y, Li D, Sheng S, Zhang F. Akkermansia muciniphila protects against dopamine neurotoxicity by modulating butyrate to inhibit microglia-mediated neuroinflammation. Int Immunopharmacol. 2025; 152:114374.

Received November 13, 2026; Revised January 20, 2026; Accepted February 5, 2026.

**Address correspondence to:*
Yanjun Zhang, National Key Laboratory of Chinese Medicine Modernization, Haihe Laboratory of Modern Chinese Medicine, Tianjin University of Traditional Chinese Medicine, 88 Changling Road, Xiqing District, Tianjin, China.
E-mail: zyjsunye@163.com

Pengwei Zhuang, National Key Laboratory of Chinese Medicine Modernization, Haihe Laboratory of Modern Chinese Medicine, Tianjin University of Traditional Chinese Medicine, 88 Changling Road, Xiqing District, Tianjin, China.
E-mail: zhuangpengwei@163.com

Released online in J-STAGE as advance publication February 13, 2026.

Original Article

DOI: 10.5582/ddt.2025.01125

A blended learning program sustains pharmacists' oral health support competency for 15 months: A longitudinal study

Naoko Hayashi[1,2], Tomoyuki Goto[3,4], Yasuo Shiga[5,6], Mitsuhiro Okazaki[7,8], Atsuhiko Sano[9,10], Narumi Maida[1,2], Hiroki Iwata[1,2], Hikaru Matsui[11], Shingo Kondo[1,2], Noriko Kobayashi[1,2], Katsunori Yamaura[1,2,*]

[1] Keio University Community Pharmacy, Tokyo, Japan;
[2] Division of Social Pharmacy, Center for Social Pharmacy and Pharmaceutical Sciences, Faculty of Pharmacy, Keio University, Tokyo, Japan;
[3] FUREAI Dental Clinic, Tokyo, Japan;
[4] Shinjuku Shoku-Shien Kenkyukai (Shinjuku Food Support Study Group), Tokyo, Japan;
[5] i-Stat Co., Ltd., Tokyo, Japan;
[6] Business Breakthrough University, Tokyo, Japan;
[7] Telemedicine Development and Research Center, Graduate School of Medicine, Akita University, Akita, Japan;
[8] Smart Healthcare Association, Tokyo, Japan;
[9] Nippon Pharmacy Association, Tokyo, Japan;
[10] Tanabe Pharmacy Inc., Tokyo, Japan;
[11] Tsuruha Holdings Co., LTD., Hokkaido, Japan.

SUMMARY: The importance of oral health has gained increasing recognition in the recent years owing to its association with numerous systemic diseases such as diabetes and cardiovascular disease. Dental checkups are crucial for maintaining and promoting oral health; however, in Japan, a relatively low uptake of dental checkups remains a challenge. Community pharmacists are expected to play a vital role in supporting the health and well-being of local residents; however, they have been observed to be reluctant to provide support in the oral health domain. This study aimed to develop and evaluate a blended learning training program on oral health support aimed at educating pharmacists working in health support pharmacies. The training, which involved online learning and on-site training, covered topics such as the importance of oral health, methods of oral health assessment, and the mechanisms of eating and swallowing. The participants, including a total of 39 pharmacists from across the country, completed surveys before and after the training, as well as at 9 months and 15 months posttraining. The results demonstrated a significant improvement in the pharmacists' knowledge, explanatory abilities, and confidence in providing oral health support, and these effects were observed to persist for up to 15 months after the training had ended. In addition, the variety of oral health-related products in pharmacies increased. This blended learning program demonstrates the potential to redefine the role of pharmacists in promoting oral health and contribute to the improvement of oral health among local residents.

Keywords: oral health, pharmacist education, blended learning, health support, knowledge, explanatory abilities, confidence

1. Introduction

In recent years, the significance of oral health has been gaining increasing attention. Deteriorating oral health has been associated with multiple systemic diseases. Periodontal disease is known to be linked to diabetes (*1,2*), hypertension (*3*), heart disease (*4*), cerebrovascular disease (*5*), and even fetal development (*6,7*). Age-associated oral frailty more likely to affect older adults, individuals with underlying health conditions (*8*), and those taking multiple medications. Previously conducted research by us has also demonstrated a connection between drug-induced dysphagia due to polypharmacy (*9*), because of which the aspiration of oral bacteria leads to the development of aspiration pneumonia. Recognizing the association between oral frailty and systemic frailty (*10*), the government aims to introduce nationwide dental checkups. However, across Japan, the response of the population to dental checkup visits has been observed to be low (*11*).

On the other hand, pharmacists must possess in-depth knowledge to identify drug-induced oral side effects and

implement appropriate preventive measures. In addition to providing prescription medications, community pharmacists need to engage in maintaining and promoting the health of local residents as well. To clarify this role, the health support pharmacy has been established, which is defined by the Patient-Oriented Pharmacy Vision of 2015 (*12*) as a pharmacy that actively and concretely supports the health of local residents. In addition to the common expectations of accepting health consultations, selling Over-the-Counter (OTC) drugs, and encouraging medical consultations, this health support also includes disseminating information from pharmacies and pharmacists.

It is very likely that the awareness of local residents regarding oral health will change and lead to dental consultations if community pharmacists actively engage in and support oral health. Our research has shown that this aligns with the dentists' expectations as well (*13*). However, oral health content has not been included in the pharmacy education curriculum as yet, and community pharmacists have been observed to lack confidence in supporting oral health (*14*). A study in Australia also corroborated on the need to provide oral health training to pharmacists (*15*). Therefore, in this study, we developed a two-step program: first, we developed a training program for community pharmacists to provide oral health support to the public. Second, community pharmacists working at health support pharmacies who had attended the training program implemented an oral health event intervention trial, and we assessed the blended learning training program's utility through a survey evaluating the resulting improvements and sustainability in their knowledge, explanatory ability, confidence, awareness, and behavioral changes regarding oral health support.

2. Materials and Methods

2.1. Study subjects

The target group for this study was pharmacists who had completed health support pharmacy training and were currently working at health support pharmacies (target pharmacists), who were recruited nationwide and provided consent for participating in the study. Self-administered questionnaires were used for conducting this research. During the study period, the target pharmacists also participated as interveners in the "intervention study on oral health events by pharmacists" (Figure 1). The Research Ethics Committee of the Faculty of Pharmacy, Keio University approved this study (Approval No. 230620-4).

2.2. Blended learning training on oral health support by pharmacists

A total of seven videos, each about 10 min long, were filmed at a shooting studio by Dr. Gotō, a dentist. The themes of the videos were as follows: 1) the importance of oral health, 2) key points of oral observation, 3) basic knowledge of prosthetics, 4) abnormal findings in the oral cavity, 5) mechanisms of eating and swallowing, 6) observation techniques of the Revised Oral Assessment Guide (ROAG), and 7) practical use of ROAG. The Japan Society for Oral Care supervised the videos to ensure academic validity and expertise. The videos were uploaded on Box cloud storage (Box.comTM) and only the target pharmacists were provided access. To ensure that the participants had viewed and studied the training videos, immediately after watching the videos, the participants were required to submit three keywords that had been embedded randomly at different points during the viewing. The keywords had to be in proper order. If the submission order of the keywords did not match, it was mandatory for the pharmacist to rewatch the video. In addition, a confirmation test was conducted immediately after the video was viewed, and the module was considered completed only if the desired level of achievement was reached. Keywords and confirmation tests were conducted and submitted using Google Forms.

The target pharmacists were subsequently required to attend a one-day on-site training at the Keio University Faculty of Pharmacy campus, where university faculty, dentists, and pharmacists conducted lectures on the following topics: 1) "The relationship between oral health and systemic diseases" (30 min, university faculty), 2) "Methods of oral health support by pharmacists" (40 min, pharmacist), 3) "How to hold events and considerations

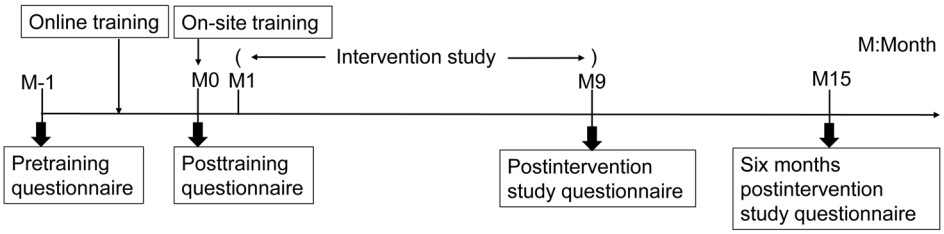

Figure 1. Study timeline and measurement schedule. This diagram illustrates the training phases and the timing of the questionnaire administration. Baseline measurement (M-1) was taken before the online and on-site training (M0). Follow-up questionnaires were administered 9 months (M9) and 15 months (M15) after M0.

for the hygiene environment" (30 min, university faculty), 4) "Practical training on oral observation and evaluation" (90 min, dentist).

2.3. Questionnaire survey

Following the online and the on-site training, an intervention study was conducted by the target pharmacists who agreed to participate. As demonstrated in Figure 1, the participants completed self-administered questionnaires four times throughout the study period: before the training (Month -1: M-1), after the online/on-site training (Month 0: M0), at the end of the intervention study (Month 9: M9), and six months after the intervention study (Month 15: M15). All self-administered questionnaires except for the one that had to be submitted immediately following the on-site training had to be requested and submitted *via* mail. Each participating target pharmacist had to complete self-administered questionnaires covering the following areas: 1) Attributes of the target pharmacists, 2) Effects of the training, 3) Knowledge, explanatory ability, and confidence regarding oral health support, 4) Availability of oral health-related products, and 5) Efforts related to the oral health field.

2.4. Statistical analysis

Friedman test was used for analyzing the changes in knowledge, explanatory ability, confidence, and awareness of pharmacists regarding oral health support. Repeated measures Analysis of Variance (ANOVA) was used for analyzing the availability of oral health-related products. To adjust for multiple comparisons, the Bonferroni method was used to make pairwise comparisons for significant differences. Comparison of the efforts taken related to the oral health field by pharmacists was done using the McNemar test. All significance levels were set at $\alpha = 0.05$ for two-sided tests. Missing values were excluded from each analysis. All statistical analyses were performed using the Statistical Package for the Social Sciences (SPSS) software, version 30 (International Business Machines (IBM) Corp., Armonk, NY, USA).

3. Results

3.1. Characteristics of the target pharmacists

Among a total of 39 participating target pharmacists, 25 pharmacists (response rate 64.1%) responded to the questionnaires up to M15. Their basic characteristics have been depicted in Table 1.

Majority of the participating target pharmacists were in their 30s. The gender distribution was almost equal. Majority of the participants had worked as pharmacists for a period of 10 to 15 years. Tochigi Prefecture was the workplace of most participants, followed by Tokyo and Kanagawa. Most worked in pharmacies located proximal to hospitals or clinics, and none worked in pharmacies located on hospital premises.

3.2. Evaluation of pharmacist training

We based the evaluation of the pharmacist training on the perceived growth of the target pharmacists immediately following the completion of both the online and on-site training. All pharmacists rated their knowledge, explanatory ability, and confidence regarding oral health support as "increased" or "somewhat increased."

3.3. Sustained effects on knowledge, explanatory ability, and confidence after pharmacist training

When responding to the M-1 point, four target pharmacists (16.7%) believed that they could provide "appropriate or somewhat appropriate knowledge" when consulted about oral troubles or oral care. This number significantly increased to 14 pharmacists (58.3%) when responding to M9 and 17 pharmacists (70.8%) when responding to M15 (Figure 2A). With regards to explanatory ability, two pharmacists (8.3%), thought they could "explain well or fairly well" at M-1. This number significantly increased to 13 pharmacists (54.2%) at M9 and M15 (Figure 2B). With regards to confidence in providing oral health support, two pharmacists (8.3%) responded "confident or somewhat confident" at M-1, and this number significantly increased to 10 pharmacists (41.7%) at M9 and 14 pharmacists (58.3%) at M15 (Figure 2C).

Table 1. Characteristics of the participants (*n* = 25)

	n (%)
Age	
30–39	21 (84.0)
40–49	1 (4.0)
50–59	2 (8.0)
60+	1 (4.0)
Sex	
Male	11 (44.0)
Female	14 (56.0)
Pharmacist career (years)	
5–9	9 (36.0)
10–14	11 (44.0)
15–19	1 (4.0)
20+	4 (16.0)
Work location (Prefecture)	
Tokyo	3 (12.0)
Tochigi	13 (52.0)
Kanagawa	3 (12.0)
Miyagi	4 (16.0)
Iwate	1 (4.0)
Saitama	1 (4.0)
Pharmacy setting	
Near a hospital/clinic	23 (92.0)
Community-based	2 (8.0)

3.4. Changes in the availability of oral health products

As demonstrated in Figure 3, the response to the point regarding the availability of oral health-related products, excluding OTC drugs, was 89 types at M-1, and the number increased to 107 types at M9 and 117 types at M15. Thus, a significant increase was observed at M15 compared to M-1 ($P = 0.014$).

3.5. Changes in efforts and awareness related to oral health

For comprehending the presence or absence of efforts related to the oral health field, we compared M-1 and M15, as the intervention study itself was considered an effort. At M-1, the number of pharmacists who were already engaged in efforts related to the oral health field was 8 (32.0%), which significantly increased to 20 pharmacists (80%) at M15 ($P < 0.01$) (Figure 4). Furthermore, when responding to the question of whether pharmacists should actively engage in oral health, at M-1, 19 pharmacists (79.2%) responded "agree or somewhat agree." This number increased to 23 pharmacists (95.8%) at M9, and 24 pharmacists at M15 (Figure 5). The remaining one pharmacist did not respond to the questionnaire at M15.

3.6. Changes in knowledge, explanatory ability, and confidence based on the attributes of target pharmacists

With regards to the comparisons regarding changes in knowledge, explanatory ability, and confidence based on gender and whether there were any efforts before the training, no differences were noted (data not shown). The bias was too large for other attributes and comparison was not possible.

4. Discussion

The training conducted in this study enabled all

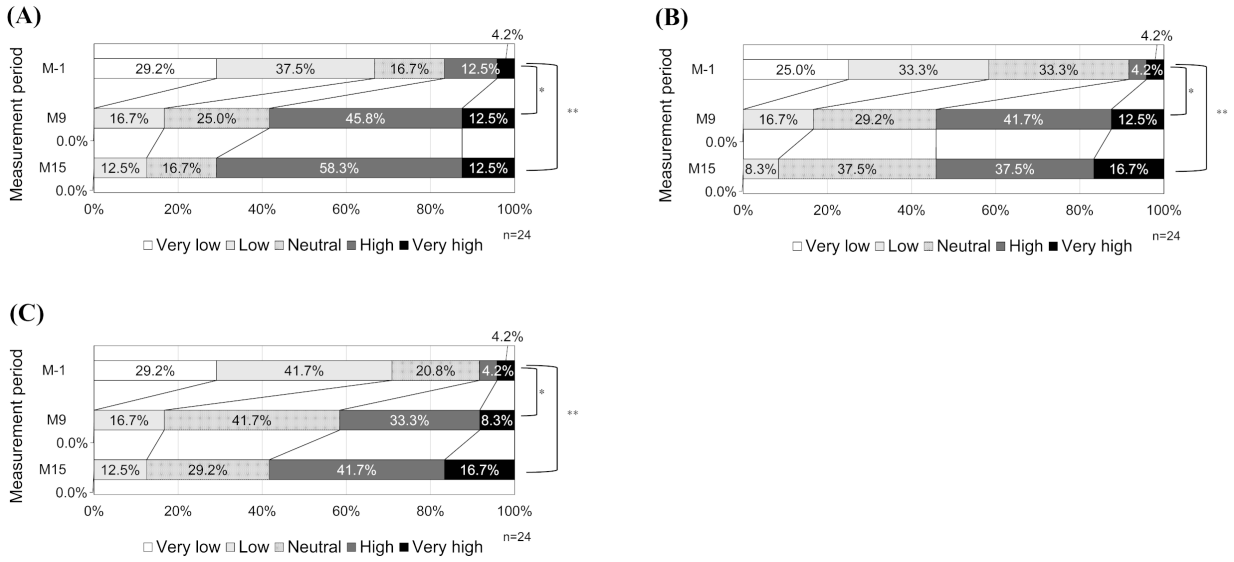

Figure 2. Training effectiveness: longitudinal changes in self-reported knowledge, explanation ability, and confidence rating. Data demonstrates the distribution of scores (5-point scale) at baseline (M-1), 9 months (M9), and 15 months (M15). All three items exhibit a significant overall difference across the time points (Friedman test, $P < 0.01$). Significance levels for multiple comparisons have been compared to M-1: (**A**) Knowledge Level: M9 ($P = 0.003$), M15 ($P < 0.001$); (**B**) Explanation Ability: M9 ($P = 0.001$), M15 ($P < 0.001$); (**C**) Confidence Rating: M9 ($P = 0.003$), M15 ($P < 0.001$). *$P < 0.05$; **$P < 0.001$.

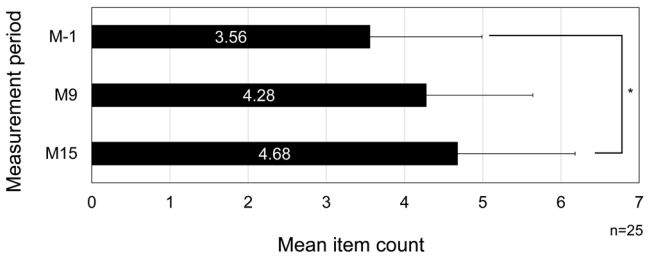

Figure 3. Changes in the total number of oral care items handled by pharmacists. Data have been presented as mean ± SE (Standard Error) and analyzed using repeated measures ANOVA. The overall effect of time (M-1, M9, M15) was statistically significant ($P = 0.003$). Post-hoc Bonferroni-corrected comparison demonstrated a significant increase between the baseline (M-1) and M15 ($P = 0.014$).

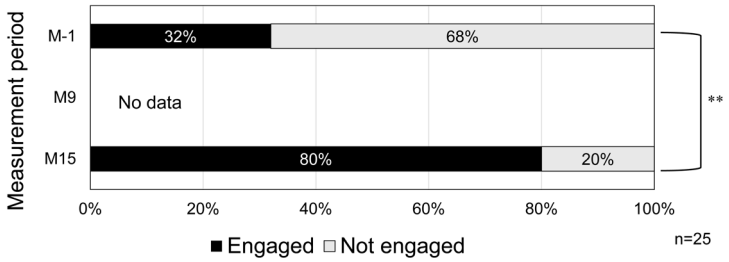

Figure 4. Pharmacists' engagement in oral health support before and after intervention. The figure depicts the percentage of pharmacists providing an affirmative response to personal efforts regarding oral health. Data represent M-1 and M15. M9 data was omitted as study participation itself constituted the effort during that period. The increase in engagement was highly significant (McNemar test, $P < 0.01$).

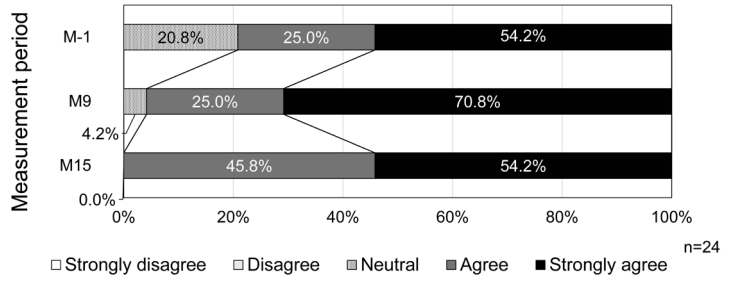

Figure 5. Pharmacists' attitudes toward proactive involvement in oral health. The figure displays the distribution of responses (5-point scale) to the question regarding proactive involvement in oral health at M-1, M9, and M15. No statistically significant difference was noted across the three time points (Friedman test, $P > 0.05$).

pharmacists to enhance their knowledge, explanatory abilities, and confidence with regards to oral health support, indicating that the challenges faced by the pharmacists in the field of oral health, as previously reported by us (*14*), can be resolved. Furthermore, the abilities acquired through this training were found to persist even 15 months after the training. Besides, an increase in the types of oral health-related products and the number of pharmacists involved in oral health support indicated enhanced health support capabilities with respect to the psychological aspects to respond to consultations from local residents and also through the provision of materials and services. To the best of our knowledge, this study is the first to quantitatively evaluate the utility of an oral health training program for community pharmacists, in terms of improved and sustained knowledge and behavior change among participants. Such training programs are likely to foster the oral care knowledge and skills of pharmacists working at health support pharmacies nationwide.

Similar to our previous study the percentage of pharmacists who believed that they had the knowledge, explanatory ability, and confidence in oral health support prior to participating in the training was around 10% (*14*). However, the items in which pharmacists exhibited progress immediately after completing the training, exhibited a significant growth almost 9 to 15 months after the training compared to the time period before that, which indicated that sustained use of the acquired knowledge promoted further retention. A previously conducted study by Man *et al*. (*16*), systematically investigated the current state of oral hygiene education interventions for pharmacists and pharmacy staff; however, the effects of the interventions, even though visible, were not quantitatively evaluated. The quantitative and longitudinal demonstration of the utility of the blended learning (online and on-site training sessions) in this study provides a basis for the broader application of similar training programs in the future. Additionally, this training is considered universally applicable to all pharmacists considering the absence of differences in changes in these items based on the presence or absence of pharmacists' daily oral health support efforts or the availability of oral health-related products in pharmacies.

The availability of oral health–related products continued to increase even 15 months after the training. More than 90% of the participating pharmacies were located near hospitals/clinics; therefore, unlike drug stores, only a few pharmacies stocked a wide range of dental hygiene materials. This increase in the stock of the oral health-related products indicates that the pharmacists not only comprehended the significance of oral hygiene during the training, but believed and realized its utility while supporting the oral health of local residents in the intervention study conducted after the training. This is evident from the increase in the proportion of the pharmacists practicing oral health support from 32% before the training to 80% at 15 months after the training, continuing some form of oral health support even after

the intervention study. This figure of 80% roughly matches the proportion of pharmacists who, before attending the training, had believed that pharmacists must provide oral health support. Remaining 20% of the pharmacists who were skeptical about getting involved in oral health support prior to attending the training also recognized the importance of oral health support 15 months later, indicating that even pharmacists who were not engaged in oral health support by the end of this study could eventually begin to do so in the future.

We have previously reported that providing oral health checks and information on oral self-care in pharmacies can benefit the oral health of local residents (*13*). Training pharmacists to have knowledge and skills in oral care and who consciously intervene with local residents during the course of their daily work can help in advancing oral health support for the local residents in the future.

This study does have some limitations. All participating pharmacists were those who had already completed health support pharmacy training and were proactively supporting the health of local residents, which was evident from their willingness to participate in the intervention study. The effects of this training might therefore be limited to pharmacists with an inherently high level of awareness and motivation. Additionally, as a part of this study, all participating pharmacists completed an intervention study after completing the training, following which, their subsequent status and sustainability were examined, making it impossible to separate the effects of the training from the effects of participating in the intervention study. Therefore, it is necessary to verify the usefulness and sustainability of the training with different cohorts of community pharmacists when we conduct training sessions in the future.

Furthermore, the reliance on self-reported questionnaires for primary outcome measures is an important consideration, as these measures are inherently susceptible to social desirability bias. Participating pharmacists may have subconsciously over-reported their improvements to align with the perceived objectives of the training. Although the study did not employ objective performance metrics such as proficiency tests, the previously discussed increases in both oral health-related products and the proportion of pharmacists practicing oral health support are considered to complement these subjective data. Future research should incorporate more objective metrics to further validate the impact of this blended learning program.

In conclusion, this study developed an oral health blended learning program for pharmacists at health support pharmacies, which can be instrumental in promoting oral health support in pharmacies throughout Japan. Such training programs can contribute to maintaining oral health among local residents, preventing oral frailty, and reducing mortality rates.

Acknowledgements

We sincerely thank Mr. Hamada, Researcher at the Department of Health Economics, The Institute for Health Economics and Policy, Association for Health Economics Research and Social Insurance and Welfare, Mr. Nomura of the Nippon Pharmacy Association (NPhA), Ms. Shiraishi, a dental hygienist, Ms. Kamei, Managing Director of the Japan Pharmaceutical Association, Mr. Matsui from Tsuruha Holdings Co., Ltd., and the Japan Dental Association for their professional insights and for supporting this study. We also express our sincere gratitude to the Japan Oral Care Society for overseeing the online training, which was crucial for this study. Additionally, we would like to thank all the pharmacists for their kind cooperation in our questionnaire survey.

Funding: This work was supported by the Ministry of Health, Labor, and Welfare (Program Grant Number JPMH23KC1004). This work was also partially supported by the Academic Development Fund (Keio University Academic Development Funds). The funding source had no role in the preparation of the data or manuscript.

Conflict of Interest: The authors have no conflicts of interest to disclose.

References

1. Stöhr J, Barbaresko J, Neuenschwander M, Schlesinger S. Bidirectional association between periodontal disease and diabetes mellitus: a systematic review and meta-analysis of cohort studies. Sci Rep. 2021; 11:13686.
2. Mirzaei A, Shahrestanaki E, Daneshzad E, Heshmati J, Djalalinia S, Asayesh H, Mahdavi-Gorabi A, Heshmat R, Qorbani M. Association of hyperglycaemia and periodontitis: an updated systematic review and meta-analysis. J Diabetes Metab Disord. 2021; 20:1327-1336.
3. Li Y, Yuan X, Zheng Q, Mo F, Zhu S, Shen T, Yang W, Chen Q. The association of periodontal disease and oral health with hypertension, NHANES 2009-2018. BMC Public Health. 2023; 23:1122.
4. Leng Y, Hu Q, Ling Q, Yao X, Liu M, Chen J, Yan Z, Dai Q. Periodontal disease is associated with the risk of cardiovascular disease independent of sex: A meta-analysis. Front Cardiovasc Med. 2023; 10:1114927.
5. Fagundes NCF, Almeida APCPSC, Vilhena KFB, Magno MB, Maia LC, Lima RR. Periodontitis as a risk factor for stroke: A systematic review and meta-analysis. Vasc Health Risk Manag. 2019; 15:519-532.
6. Corbella S, Taschieri S, Francetti L, De Siena F, Del Fabbro M. Periodontal disease as a risk factor for adverse pregnancy outcomes: a systematic review and meta-analysis of case-control studies. Odontology. 2012; 100:232-240.
7. Pozo E, Mesa F, Ikram MH, Puertas A, Torrecillas-Martínez L, Ortega-Oller I, Magán-Fernández A, Rodríguez-Martínez MD, Padial-Molina M, Sánchez-Fernández E, Galindo-Moreno P, O'Valle F. Preterm birth

and/or low birth weight are associated with periodontal disease and the increased placental immunohistochemical expression of inflammatory markers. Histol Histopathol. 2016; 31:231-237.
8. Huang P, Wu L, Zhang R, Chen S, Zhang Y, Chen Y. Systematic review and meta-analysis on the prevalence and risk factors of oral frailty among older adults. Front Med (Lausanne). 2025; 12:1512927.
9. Hayashi N, Yoshida M, Maida N, Kondo S, Ogawa M, Iwata H, Kobayashi N, Yamaura K. Use of Dysphagia-Inducing Drugs and Risk of Aspiration Pneumonia: A Cross-Sectional Analysis Using a Japanese Claims Database. Drugs Real World Outcomes. 2025; 12:607-614.
10. Tanaka T, Takahashi K, Hirano H, Kikutani T, Watanabe Y, Ohara Y, Furuya H, Tsuji T, Akishita M, Iijima K. Oral frailty as a risk factor for physical frailty and mortality in community-dwelling elderly. J Gerontol A Biol Sci Med Sci. 2018; 73:1661-1667.
11. Ministry of Health, Labor and Welfare. 2022 Survey of Dental Diseases. *https://www.mhlw.go.jp/content/10804000/001112405.pdf* (accessed October 18,2025).
12. Ministry of Health, Labor and Welfare. Vision for Pharmacies for Patients. *https://www.mhlw.go.jp/file/04-Houdouhappyou-11121000-Iyakushokuhinkyoku-Soumuka/vision_1.pdf* (accessed October 18, 2025).
13. Iwata H, Nakamura K, Kobayashi N, Fujimoto K, Hayashi N, Yamaura K. Most dentists approve of oral health check-ups for local residents at community pharmacies and desire collaboration with community pharmacists. Drug Discov Ther. 2022; 16:309-312.
14. Iwata H, Yoshida R, Hayashi N, Kobayashi N, Fujimoto K, Yamaura K. Community pharmacists' perceptions and needs regarding oral healthcare advice in Japan. Keio J Med. 2025; 74:205-213.
15. Taing MW, Ford PJ, Gartner CE, Freeman CR. Describing the role of Australian community pharmacists in oral healthcare. Int J Pharm Pract. 2016; 24:237-246.
16. Man H, George A, Rudman A, Taing M-W, Masoe A, Smith L, Sohn W, Christian B. Oral health educational interventions for pharmacists and pharmacy staff: A scoping review. Explor Res Clin Soc Pharm. 2025; 20:100658.

Received November 24, 2025; Revised January 11, 2026; Accepted January 31, 2026.

**Address correspondence to:*
Katsunori Yamaura, Division of Social Pharmacy, Center for Social Pharmacy and Pharmaceutical Sciences, Faculty of Pharmacy, Keio University, 1-5-30 Shibakoen, Minato-ku, Tokyo 105-8512, Japan.
E-mail: yamaura-kt@keio.jp

Released online in J-STAGE as advance publication February 12, 2026.

Original Article

DOI: 10.5582/ddt.2025.01133

Microneedle patch-enhanced palatal anesthesia with benzocaine: Efficacy and safety in a randomized double-blind crossover trial

Kensuke Kiriishi[1,*], Terumi Ayuse[1], Naomi Tanoue[2], Kaori Komeyama[1], Nobuaki Magata[1], Hanako Takahashi[2], Takashi Tominaga[3], Yuriko Hayashida[1], Hirotaka Imai[4], Takuro Sanuki[5], Takao Ayuse[3]

[1] Department of Special Care Dentistry, Nagasaki University Hospital, Nagasaki, Japan;
[2] Developmental and Nurturing Dentistry, Graduate School of Biomedical Sciences, Nagasaki University, Nagasaki, Japan;
[3] Clinical Research Center, Nagasaki University Hospital, Nagasaki, Japan;
[4] Imai Dental Clinic, Osaka, Japan;
[5] Department of Dental Anesthesiology, Nagasaki University Hospital, Nagasaki, Japan.

SUMMARY: Needle-insertion pain during dental local anesthesia remains one of the strongest triggers of dental anxiety. Conventional topical anesthetics show limited penetration through the thick palatal mucosa and often provide insufficient suppression of insertion pain. Microneedle (MN) patches have emerged as a minimally invasive drug-delivery platform capable of enhancing transmucosal permeability and topical anesthetic efficacy. This randomized, double-blind, crossover clinical trial evaluated the efficacy and safety of a benzocaine-loaded MN patch applied to the palatal mucosa prior to local anesthesia. Twenty adult patients requiring bilateral maxillary premolar scaling and root planing received MN or placebo patches in two study periods separated by a one-week washout. The primary outcome was the presence or absence of needle-insertion pain. Secondary outcomes included injection-phase pain assessed using a 100-mm visual analogue scale (VAS), numbness or discomfort at the application site, vital signs, and adverse events. Needle-insertion pain was reported in 2 of 20 cases (10%) under the MN patch condition, compared with 14 of 20 cases (70%) under the placebo patch condition, demonstrating a significantly lower incidence with the MN patch ($p = 0.00049$). In contrast, VAS scores for injection-phase pain did not differ significantly between conditions. No clinically relevant numbness, mucosal irritation, or MN-related adverse events were observed, and vital signs remained stable throughout both study periods. The benzocaine-loaded MN patch selectively attenuated superficial needle-insertion pain while maintaining an excellent safety profile. The absence of an effect on deeper injection-phase pain is likely attributable to the substantial thickness of the palatal mucosa. These findings support the clinical utility of MN-assisted transmucosal anesthesia as a novel drug-delivery modality in dentistry and provide a foundation for the development of minimally invasive analgesic systems.

Keywords: Microneedle patch, palatal anesthesia, randomized crossover trial, benzocaine, dental local anesthesia

1. Introduction

Dental treatment frequently evokes significant anxiety and fear among patients. Among the most consistently reported triggers are drilling noise and vibration and local anesthesia injections (*1-3*). Surveys of dental students and adult populations have demonstrated that local anesthesia injections represent one of the most anxiety-provoking dental procedures, regardless of sex. International studies similarly identify the drill and the injection needle as principal sources of dental fear, indicating that despite its clinical necessity, local anesthesia itself remains a psychological barrier for many patients (*1,2*).

Pain associated with dental local anesthesia is not a single entity but consists of at least two mechanistically distinct components: needle-insertion pain, arising from superficial mechanical stimulation at the moment of penetration, and injection-phase pain, primarily related to tissue distension, pressure, and chemical irritation during anesthetic deposition (*4,5*). However, most previous clinical studies have evaluated anesthetic pain as a single outcome, making it difficult to determine which component is affected by novel analgesic interventions.

The palatal mucosa represents one of the thickest and most pain-sensitive regions in the oral cavity, characterized by dense innervation, firm attachment to the periosteum, and limited tissue compliance (*6,7*).

For this reason, it has rarely been selected as a primary test site for minimally invasive anesthetic technologies. The present study intentionally targeted the palatal mucosa as a stringent and clinically relevant model and independently evaluated needle-insertion pain and injection-phase pain to allow a mechanistically precise assessment of microneedle (MN)-assisted transmucosal anesthesia.

2. Materials and Methods

2.1. Study design

This study was conducted as a randomized, double-blind, crossover clinical trial involving adult outpatients at Nagasaki University Hospital. Eligible participants were patients who required scaling and root planing (SRP) under local anesthesia in the bilateral maxillary premolar region. After obtaining written informed consent, participants were randomly assigned using a computer-generated allocation sequence (Research Electronic Data Capture [REDCap]) in a 1:1:1:1 ratio to one of four intervention sequences (MN→Placebo or Placebo→MN, with left-right variations). A crossover design was selected to minimize inter-individual variability in subjective pain outcomes. Allocation was concealed within REDCap and remained inaccessible to the operator until the start of each treatment session, thereby ensuring adequate allocation concealment.

2.2. Participants

Participants were eligible for inclusion if they met all of the following criteria: (1) Adults aged 18-85 years requiring bilateral maxillary premolar SRP under local anesthesia; (2) Presence of bilateral maxillary premolars; (3) Ability to provide written informed consent; (4) Regular outpatient attendance at Nagasaki University Hospital. Participants were excluded if any of the following applied: (1) Regular use of analgesic medications; (2) Known hypersensitivity to ester-type topical anesthetics; (3) History of or risk factors for methemoglobinemia; (4) Pregnancy or lactation; (5) Any condition deemed inappropriate for participation by the investigators. Written informed consent was obtained from all participants prior to enrollment.

2.3. Interventions

2.3.1. Washout and treatment schedule

Each participant attended two treatment sessions (Period I and Period II), separated by a washout interval of at least one week. This washout period was selected to minimize potential carryover effects related to microneedle-induced micro-perforation or residual benzocaine.

2.3.2. Randomized sequences

The four intervention sequences were as follows: (1) Period I: Left MN patch → Period II: Right placebo patch. (2) Period I: Right MN patch → Period II: Left placebo patch. (3) Period I: Left placebo patch → Period II: Right MN patch. (4) Period I: Right placebo patch → Period II: Left MN patch.

All procedures within each period-including patch application, local anesthesia, SRP, and outcome assessment-were performed by the same operator. To maintain double blinding, the anesthetist exited the treatment room during patch application, which was performed by the principal investigator. Only the investigator was aware of the allocation status.

2.3.3. MN patch

The MN patch used in this study was AnesPatch™ SS (CosMED Pharmaceutical), with the following specifications: (1) Needle length: 0.25-0.30 mm; (2) Number of microneedles: 350; (3) Patch size: 15.5 × 13 mm.

The microneedles generate micro-perforations approximately 150-200 μm in depth, confined to the epithelial layer and avoiding stimulation of deeper nociceptors. This structure enhances transmucosal permeability and may modulate superficial mechanical nociception.

A standardized amount of 0.1 g of 20% benzocaine gel was applied to the surface of the MN patch. The patch was placed on the palatal mucosa adjacent to the target premolar for 3 minutes.

Local anesthesia was administered using an Anesject II (NEI-201) syringe in Normal Mode (180 s/mL; approximately 1 MPa pressure). A fixed volume of 1.8 mL of 2% lidocaine containing 1:80,000 epinephrine was injected.

2.3.4. Placebo patch

The placebo patch was visually identical to the MN patch but lacked microneedles. The same amount of benzocaine gel (0.1 g) was applied to the patch surface. Application duration (3 minutes) and all subsequent anesthesia procedures were identical to those in the MN patch condition.

2.4. Outcome measures

The primary outcome is presence or absence of needle-insertion pain. Needle-insertion pain was assessed dichotomously (yes/no) at the moment of needle penetration. The secondary outcomes include: (1) Injection-phase pain, assessed using a 100-mm visual analogue scale (VAS) (0 mm = no pain; 100 mm = worst imaginable pain). Patients recorded VAS scores

while seated in the dental chair immediately after anesthetic delivery and before initiation of scaling or instrumentation. (2) Numbness or discomfort at the patch application site, assessed using VAS. (3) Vital signs, including heart rate, systolic and diastolic blood pressure, and oxygen saturation, monitored from baseline (T0) at 5-minute intervals. (4) Local reactions at the application site, including erythema, swelling, or ulceration. (5) Adverse events, recorded and classified according to severity.

2.5. Statistical analysis

Normality of VAS distributions was assessed using the Shapiro-Wilk test. Normally distributed data were analyzed using paired *t*-tests, whereas non-normally distributed data were analyzed using the Wilcoxon signed-rank test. The presence or absence of needle-insertion pain was compared between conditions using McNemar's test. Period and carryover effects were evaluated using a linear model that included treatment, period, and sequence (MN→Placebo or Placebo→MN). A threshold of $p > 0.10$ was considered indicative of no clinically relevant period or carryover effects. All statistical analyses were performed using SPSS version 28.0 (IBM Japan), with statistical significance set at $p < 0.05$.

2.6. Ethical considerations

This study was conducted in accordance with the Declaration of Helsinki and was approved by the Nagasaki University Hospital Clinical Research Ethics Committee (Approval No. CRB7180001). All participants provided written informed consent prior to participation. The trial was registered in the Japan Registry of Clinical Trials (jRCTs072240080), and this report adheres to the Consolidated Standards of Reporting Trials (CONSORT) 2010 guidelines.

3. Results

3.1. Participant characteristics

Twenty adult patients (10 males and 10 females) requiring bilateral maxillary premolar scaling and root planing were enrolled in this randomized, double-blind, crossover clinical trial. All participants completed both study periods without dropouts (Figure 1). Baseline demographic characteristics are summarized in Table 1. The mean age of the participants was 50.05 years (range: 26-74 years). The mean height was 163.21 cm (range: 147.00-180.00 cm), and the mean body weight was 60.28 kg (range: 42.35-82.00 kg). No statistically significant period effects or carryover effects were detected for any outcome measures (all $p > 0.10$). Detailed results of the period and carryover analyses are provided in Supplementary Table S1 (*https://www.ddtjournal.com/action/getSupplementalData.php?ID=286*).

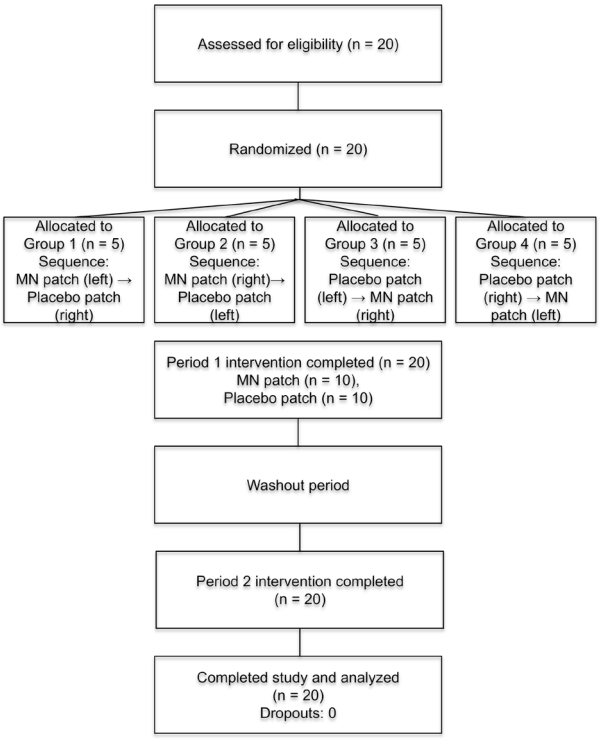

Figure 1. CONSORT flow diagram of the randomized crossover trial. Twenty participants were randomized into four groups ($n = 5$ per group) according to intervention sequence and application side (left or right). Each participant received both the microneedle (MN) patch and the placebo patch across two study periods separated by a washout interval. All participants completed both study periods and were included in the final analysis.

Table 1. Baseline characteristics of the study participants ($n = 20$: 10 males, 10 females; no dropouts)

Measures	Age (year)	Height (cm)	Body weight (kg)
Mean	50.05	163.21	60.28
Maximum	74.00	180.00	82.00
Minimum	26.00	147.00	42.35

Values are presented as mean (range). All participants completed both study periods of this randomized, double-blind, crossover trial without dropouts.

3.2. Needle-insertion pain

The proportion of participants reporting needle-insertion pain differed significantly between the two conditions. Needle-insertion pain was reported in 2 of 20 cases (10%) under the MN patch condition, whereas 14 of 20 cases (70%) reported pain under the placebo patch condition.

A 2 × 2 contingency table summarizing the presence or absence of needle-insertion pain is presented in Table 2. Figure 2 illustrates the marked reduction in the incidence of needle-insertion pain with the MN patch.

Paired comparison using McNemar's test demonstrated a statistically significant reduction in

	Placebo – Pain	Placebo – No pain
MN patch – Pain	2	0
MN patch – No pain	12	6

Figure 2. Comparison of needle-insertion pain between the microneedle (MN) patch and placebo patch conditions. Needle-insertion pain was reported in 2 of 20 cases (10%) under the MN patch condition and in 14 of 20 cases (70%) under the placebo patch condition. The 2 × 2 contingency table illustrates the presence or absence of needle-insertion pain, demonstrating a significantly lower incidence in the MN patch condition (McNemar test, $p = 0.00049$).

Table 2. 2×2 contingency table comparing the presence or absence of needle-insertion pain between the MN patch and placebo patch conditions

Patch Condition	Pain present	No pain	Total
MN patch	2	18	20
Placebo patch	14	6	20
Total	16	24	40

To assess potential carryover effects, VAS scores in the second period were compared between the two treatment sequences (MN→PL *vs*. PL→MN) using the Mann-Whitney *U* test. No significant differences were observed in any of the outcomes (all $p > 0.10$), indicating that no meaningful carryover effect was present.

needle-insertion pain under the MN patch condition compared with the placebo condition ($p = 0.00049$). These results indicate a clear and clinically meaningful attenuation of needle-insertion pain associated with MN patch application.

3.3. Injection-phase pain

Injection-phase pain was assessed immediately after anesthetic delivery using a 100-mm VAS and was evaluated independently by patients and by the operating dentist.

For patient-reported VAS scores, the mean ± standard deviation values were 28.8 ± 20.7 mm under the MN patch condition and 27.9 ± 27.7 mm under the placebo patch condition. Operator-rated VAS scores were 14.3 ± 18.5 mm for the MN patch condition and 19.0 ± 22.8 mm for the placebo condition.

Median values and interquartile ranges for both patient- and operator-rated VAS scores are summarized in Table 3. No statistically significant differences in injection-phase pain were observed between the MN patch and placebo patch conditions for either assessment, as illustrated in Figures 3A and 3B.

These findings indicate that the MN patch did not modify pain sensations associated with anesthetic deposition in deeper tissues, in contrast to its selective effect on superficial needle-insertion pain.

3.4. Numbness and local discomfort at the patch application site

VAS scores for numbness and discomfort at the patch application site were low in both conditions. Descriptive statistics for numbness induced by topical anesthesia and local discomfort are summarized in Table 4. No statistically significant differences were observed between the MN patch and placebo patch conditions, as illustrated in Figures 4A and 4B. No participants reported clinically meaningful numbness or discomfort attributable to patch application, indicating good local tolerability of the MN patch.

Table 3. Summary of dentist-rated and patient-reported VAS scores

Outcome	Patch Condition	Mean ± SD (mm)	Median (mm)	IQR(25-75%) (mm)
Dentist-rated VAS	MN	14.3 ± 18.5	7.5	0 - 28.0
	Placebo	19.0 ± 22.8	14.0	0 - 22.5
Patient-rated VAS	MN	28.8 ± 20.7	28.0	11.5 - 35.0
	Placebo	27.9 ± 27.7	18.0	7.0 - 42.0

Injection-phase pain was assessed immediately after anesthetic delivery using a 100-mm visual analogue scale (VAS; 0 = no pain, 100 = worst imaginable pain) and was evaluated independently by patients and by the operating dentist. Data are presented as mean ± standard deviation, median, and interquartile range (IQR).

Table 4. VAS scores for numbness induced by topical anesthesia and local discomfort at the patch application site

Outcome(VAS)	Patch Condition	Mean ± SD (mm)	Median (mm)	IQR(25-75%) (mm)
numbness induced by topical anesthesia	MN	20.0 ± 24.6	9.5	2 - 35.75
	Placebo	13.0 ± 18.7	9.5	0 - 12.25
Discomfort	MN	14.5 ± 23.5	6.0	0 - 13.5
	Placebo	7.9 ± 12.2	1.0	0 - 10.75

Values are presented as mean ± standard deviation, median, and interquartile range (IQR). VAS scores were assessed at the patch application site.

3.5. Physiological measures (vital signs)

Vital signs, including heart rate, systolic blood pressure, diastolic blood pressure, and oxygen saturation, remained stable throughout all procedures. No clinically relevant changes were observed over time, and no significant differences were detected between the MN patch and placebo patch conditions at any measurement point. These results confirm that MN patch application did not induce systemic physiological alterations during dental treatment.

3.6. Local reactions and adverse events

No adverse local reactions, such as erythema, swelling, or ulceration, were observed following application of either the MN patch or the placebo patch. Mild aphthous-like lesions were observed in a small number of cases

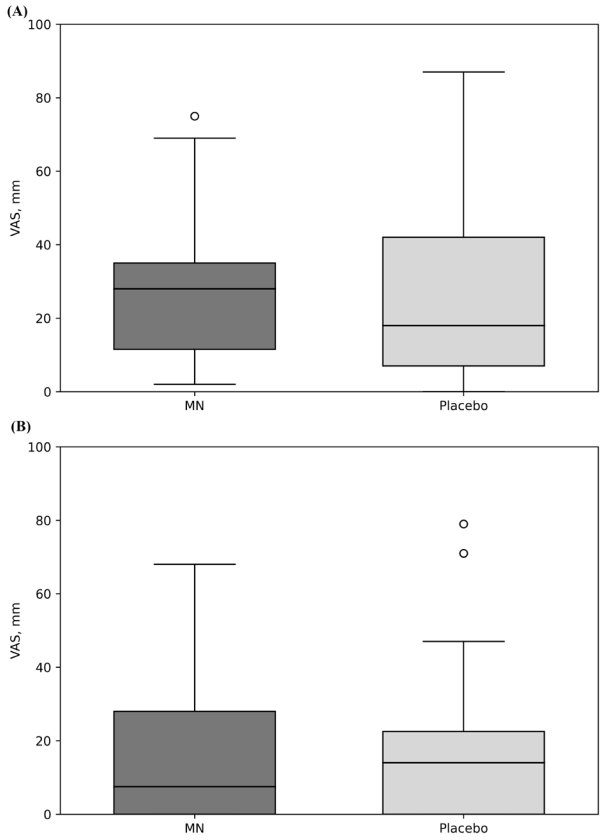

Figure 3. Injection-phase pain assessed using visual analogue scale (VAS) scores. (**A**) Patient-reported VAS scores during local anesthetic administration. (**B**) Dentist-rated VAS scores during local anesthetic administration. Box plots represent the median and interquartile range, with whiskers indicating the minimum and maximum values. Crosses indicate mean values. No statistically significant differences were observed between the MN patch and placebo patch conditions.

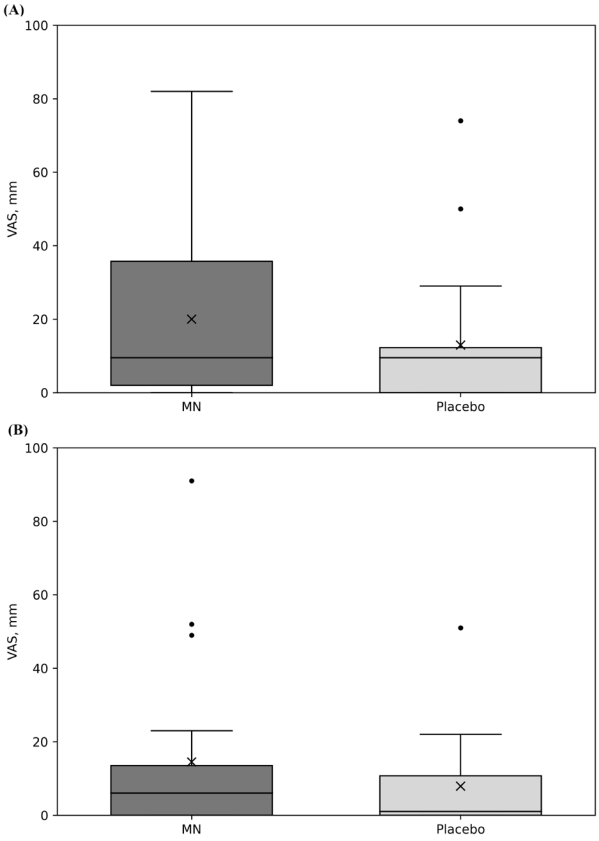

Figure 4. Patient-reported sensations associated with patch application. (**A**) VAS scores for surface numbness following patch application. (**B**) VAS scores for discomfort related to patch wearing. Box plots represent the median and interquartile range, with whiskers indicating the minimum and maximum values. Crosses indicate mean values.

after local anesthetic injection; however, all lesions were transient, clinically insignificant, and judged to be unrelated to MN patch use. No MN patch-related adverse events were identified.

4. Discussion

This randomized, double-blind, crossover clinical trial evaluated the clinical utility of a benzocaine-loaded MN patch applied to the palatal mucosa prior to dental local anesthesia. The principal finding of this study is that the MN patch significantly reduced needle-insertion pain, whereas injection-phase pain, assessed using VAS scores, did not differ between the MN and placebo conditions. Importantly, the MN patch demonstrated an excellent safety profile, with minimal local discomfort and no clinically relevant adverse events.

4.1. Selective attenuation of needle-insertion pain

The most clinically meaningful outcome of the present study was the marked reduction in needle-insertion pain observed with the MN patch. Needle-insertion pain represents the moment most strongly associated with dental anxiety and avoidance behavior. By significantly attenuating this superficial pain component, the MN patch directly targets the most fear-provoking phase of dental local anesthesia.

The selective nature of this effect is noteworthy. Needle-insertion pain arises primarily from mechanical stimulation of superficial nociceptors located within the epithelial and subepithelial layers of the oral mucosa. The MN patch generates controlled micro-perforations confined to these superficial layers, which may reduce mechanical resistance to needle penetration and modulate local nociceptive input. This mechanism is consistent with the observed reduction in insertion pain without concomitant changes in deeper pain sensations.

4.2. Lack of effect on injection-phase pain

In contrast to its effect on insertion pain, the MN patch did not significantly influence injection phase pain. Injection-phase pain is predominantly attributable to

tissue distension, pressure, and chemical irritation during anesthetic deposition and is mediated by deeper nociceptive structures, including the lamina propria and periosteal region.

The absence of an effect on injection-phase pain should not be interpreted as a limitation of the MN patch. Rather, it reflects a mechanistically expected outcome given the anatomical constraints of the palatal mucosa. The microneedles used in this study were designed to penetrate approximately 150-200 μm, remaining within the epithelial layer. In contrast, the palatal masticatory mucosa is substantially thicker, often exceeding 1.5 mm, particularly in posterior regions. As a result, MN-mediated micro-channels are unlikely to facilitate anesthetic diffusion to deeper nociceptive sites responsible for injection-phase pain.

4.3. Significance of palatal mucosa as a test site

A key strength of the present study lies in the intentional selection of the palatal mucosa as the application site. The palate represents one of the thickest and most pain-sensitive regions in the oral cavity, characterized by dense innervation, firm attachment to the periosteum, and limited tissue compliance. These anatomical features make effective pain control particularly challenging.

By demonstrating a significant reduction in needle-insertion pain even in this unfavorable environment, the present findings provide robust evidence for the superficial analgesic capability of the MN patch. This strengthens the external validity of the results and suggests that similar or greater benefits may be achievable in thinner and more compliant oral mucosal sites, such as the buccal attached gingiva.

4.4. Comparison with previous microneedle-based studies

Previous studies investigating MN-assisted oral anesthesia have reported heterogeneous results, largely due to differences in MN geometry, needle length, density, drug loading, and application site. For example, Daly *et al.* demonstrated reductions in injection-related pain using longer and denser MN arrays applied to thinner oral mucosa (*8*). Other experimental studies have reported enhanced transmucosal delivery of lidocaine using hydrogel-forming or high-density MN systems.

The present study differs from these investigations in several important respects (*9-15*). A relatively short MN length, limited needle density, and a small amount of benzocaine were employed, and the patch was applied to the palatal mucosa. Despite these conservative parameters, a significant reduction in needle-insertion pain was observed. This suggests that MN-induced modulation of superficial nociception may play a clinically relevant role independent of deep anesthetic diffusion.

4.5. Placebo patch effects and patient perception

The placebo patch used in this study was structurally identical to the MN patch except for the absence of microneedles. Both patches demonstrated good mucosal adhesion and prolonged benzocaine retention, which may have contributed to partial anesthetic effects in the placebo condition. In addition, psychological factors, including expectancy and procedural rituals associated with patch application, may have influenced pain perception.

These factors likely contributed to the lack of difference in injection-phase pain between conditions and highlight the importance of considering both pharmacological and contextual influences when evaluating pain outcomes in dental settings.

4.6. Clinical implications

From a clinical perspective, the MN patch offers a targeted and pragmatic approach to improving patient comfort during dental local anesthesia. By selectively reducing needle-insertion pain without introducing systemic effects or clinically relevant adverse events, the MN patch addresses a critical barrier to dental treatment acceptance.

This approach may be particularly beneficial for patients with dental anxiety or phobia, pediatric patients, individuals with special healthcare needs, and patients with heightened pain sensitivity. Importantly, the MN patch requires minimal additional chair time and does not interfere with standard anesthetic techniques.

4.7. Limitations and future directions

Several limitations should be acknowledged. This was a single-center study with a modest sample size, and the absence of a no-patch control group limits the ability to fully disentangle placebo and contextual effects associated with patch application. In addition, only palatal application was evaluated, and all procedures were performed by a single operator to minimize procedural variability, which may limit the generalizability of the findings.

First, the study population consisted exclusively of adult patients undergoing periodontal treatment that required palatal local anesthesia. Accordingly, caution is warranted when extrapolating these results to broader dental populations, such as pediatric patients, individuals with extreme dental anxiety or phobia, or patients with special healthcare needs. Although these populations may potentially benefit most from attenuation of needle-insertion pain, their pain perception, behavioral responses, and oral mucosal characteristics may differ from those of the present study cohort. Future investigations specifically designed for these populations are required to clarify the clinical applicability and

external validity of microneedle-assisted anesthesia across diverse dental settings.

Second, although no local or systemic infections were observed during the study period, the short-term impact of microneedle-induced micro-perforations on oral mucosal barrier function was not directly evaluated. The creation of transient micro-channels theoretically raises concerns regarding microbial translocation or increased susceptibility to local infection. This concern persists despite the fact that the microneedles were designed to remain within the epithelial layer and that all applications were conducted under routine clinical conditions. Future studies incorporating microbiological assessments, inflammatory markers, or biomarkers of mucosal barrier integrity would be valuable to more comprehensively address this theoretical safety consideration.

Finally, future research should explore further optimization of microneedle geometry, needle length, and drug loading, as well as evaluation at alternative oral mucosal sites with different anatomical and mechanical properties. The incorporation of objective pain-related or physiological measures, such as heart rate variability or pupillometry, may also strengthen mechanistic understanding and support broader clinical translation of this minimally invasive anesthetic approach.

5. Conclusion

This randomized, double-blind, crossover clinical trial demonstrated that a benzocaine-loaded MN patch significantly reduced needle-insertion pain during dental local anesthesia, while having no measurable effect on injection-phase pain. The MN patch was well tolerated, caused minimal local discomfort, and was not associated with clinically relevant adverse events or systemic physiological changes.

The selective attenuation of needle-insertion pain is likely attributable to the superficial action of MN-induced micro-perforations within the epithelial layer of the palatal mucosa, whereas deeper pain associated with anesthetic deposition remained unaffected due to anatomical constraints. These findings highlight the mechanistic specificity of MN-assisted transmucosal anesthesia.

While further studies in broader patient populations and with focused safety assessments are warranted, the MN patch represents a safe, simple, and clinically feasible adjunct for targeting the most anxiety-provoking component of dental local anesthesia. This approach may improve patient comfort and acceptance of dental treatment, particularly in patients with dental anxiety, heightened pain sensitivity, or special healthcare needs.

Funding: This randomized controlled trial was supported by CosMED Pharmaceutical Co., Ltd. This study was also partially supported by a research grant from Kyoto Research Park Corporation (Kyoto Sangyo 21), "Enterprise Forest/Industry-Academia Forest" Subsidy Program, Kyoto, Japan. The funders had no role in the study design; data collection, analysis, or interpretation; decision to publish; or preparation of the manuscript.

Conflict of Interest: Kensuke Kiriishi received research funding, in-kind support (microneedle patches), and lecture honoraria from CosMED Pharmaceutical Co., Ltd. The company had no role in the study design, data collection, analysis, interpretation of the data, or manuscript preparation. All other authors declare no conflicts of interest.

References

1. Milgrom P, Weinstein P, Getz T. Treating fearful dental patients: a patient management handbook. 2nd ed. Seattle, WA: University of Washington; 1995.
2. Meng X, Heft MW, Bradley MM, Lang PJ. Effect of fear on dental utilization behaviors and oral health outcomes. Community Dent Oral Epidemiol. 2007; 35:292-301.
3. Bologa E, Tărăboanță-Gamen AC, Tărăboanță I, Boișteanu O, Platon AL, Stelea ȘO, Simionescu AM A, Grădinariu AI, Jehac A, Bologa C, Stelea CG. Assessment of anxiety and local anesthesia experiences in dental students using the Modified Dental Anxiety Scale (MDAS). Dent J (Basel). 2025; 13:445.
4. Huskisson EC. Measurement of pain. Lancet. 1974; 2:1127-1131.
5. Price DD, McGrath PA, Rafii A, Buckingham B. The validation of visual analogue scales as ratio scale measures for chronic and experimental pain. Pain. 1983; 17:45-56.
6. Song JE, Um YJ, Kim CS, Choi SH, Cho KS, Kim CK, Chai JK, Jung UW. Thickness of posterior palatal masticatory mucosa: the use of computerized tomography. J Periodontol. 2008; 79:406-412.
7. Yaman D, Aksu S, Dişçi R, Demirel K. Thickness of palatal masticatory mucosa and its relationship with different parameters in Turkish subjects. Int J Med Sci. 2014; 11:1009-1014.
8. Daly SR, Claydon NCA, Newcombe RG, Seong J, Addy M, West NX. Randomised controlled trial of a microneedle patch with a topical anaesthetic for relieving the pain of dental injections. J Dent. 2021; 107:103617.
9. Maeliosa DR, McCrudden MTC, Courtenay AJ, Donnelly RF. Enhancement strategies for transdermal drug delivery systems: current trends and applications. Drug Deliv Transl Res. 2022; 12:758-791.
10. Donnelly RF, Singh TRR, Garland MJ, Migalska K, Majithiya R, McCrudden CM, Kole PL, Mahmood TM, McCarthy HO, Woolfson AD, Donnelly L. Hydrogel-forming microneedle arrays for enhanced transdermal drug delivery. Adv Funct Mater. 2012; 22:4879-4890.
11. Badran MM, Kuntsche J, Fahr A. Skin penetration enhancement by a microneedle device (Dermaroller®) *in vitro*: dependency on needle size and applied formulation. Eur J Pharm Sci. 2009; 36:511-523.
12. Prausnitz MR, Langer R. Transdermal drug delivery. Nat Biotechnol. 2008; 26:1261-1268.
13. Tuan-Mahmood TM, McCrudden MT, Torrisi BM, McAlister E, Garland MJ, Singh TRR, Donnelly RF. Microneedles for intradermal and transdermal drug delivery. Eur J Pharm Sci. 2013; 50:623-637.

14. Garland MJ, Migalska K, Mahmood TM, Singh TRR, Woolfson AD, Donnelly RF. Microneedle arrays as medical devices for enhanced transdermal drug delivery. Expert Rev Med Devices. 2011; 8:459-482.
15. Rzhevskiy AS, Singh TRR, Donnelly RF, Anissimov YG. Microneedles as the technique of drug delivery enhancement in diverse organs and tissues. J Control Release. 2018; 270:184-202.

Received December 19, 2025; Revised February 4, 2026; Accepted February 9, 2026.

**Address correspondence to:*
Kensuke Kiriishi, Department of Special Care Dentistry, Nagasaki University Hospital, 1-7-1 Sakamoto, Nagasaki 852-8501, Japan.
E-mail: kiriishi@nagasaki-u.ac.jp

Released online in J-STAGE as advance publication February 12, 2026.

Original Article

DOI: 10.5582/ddt.2025.01104

Three-dimensional imaging provides reliable size measurement of skin lesions associated with vascular anomalies: A comparison with two-dimensional photography

Kana Sakai[1], Kayo Kunimoto[1,*], Yuna Noda[1], Yutaka Inaba[1], Yuki Yamamoto[1], Shiho Yasue[2], Akifumi Nozawa[2], Daichi Hayashi[2], Saori Endo[2], Michio Ozeki[2], Masatoshi Jinnin[1]

[1] Department of Dermatology, Wakayama Medical University, Wakayama, Japan;
[2] Department of Pediatrics, Graduate School of Medicine, Gifu University, Gifu, Japan.

SUMMARY: Three-dimensional (3D) imaging techniques enable accurate quantitative size measurement, and have been used to evaluate treatment effects on skin lesions such as ulcers, burns, and skin laxity. This study aimed to establish and validate a 3D imaging–based method to evaluate the surface area, area, and volume of cutaneous lesions associated with vascular anomalies (VA). We compared measurements obtained from two-dimensional (2D) photographs traced by three dermatologists with those obtained from 3D images traced by three company operators, and assessed inter- and intra-rater reliability. The procedure in the present study involves tracing lesion contours using photographs of VA captured by a 3D camera, followed by 3D processing of the images to measure lesion area, surface area, and volume. All patients provided written informed consent, and the study protocol was approved by the institutional review boards. Both 2D and 3D methods demonstrated high inter- and intra-rater reliability; however, better reliability was observed in the measurements obtained by company operators using 3D imaging. The findings indicate that 3D surface imaging provides more consistent and objective evaluation of lesion size than 2D photography and support the potential application of this method in clinical practice and clinical trials for VA. Accurate quantitative measurement of lesion size as an endpoint may facilitate the development of new treatment options for patients with VA.

Keywords: vascular anomalies, three-dimensional, surface area, area, volume

1. Introduction

Vascular anomaly (VA) is a general term for diseases caused by abnormal formation of blood vessels and/or lymphatic vessels. According to the International Society for the Study of Vascular Anomalies (ISSVA) classification, diseases of VA are divided into two major groups: vascular tumors and vascular malformations (*1*). Vascular tumors are further classified into three categories: benign, locally invasive/borderline, and malignant, and each category includes multiple diseases (*e.g.* infantile hemangioma and tufted angioma [TA] of benign type) (*2*). On the other hand, vascular malformations are classified into "simple" "combined" "of major named vessels" and "associated with other anomalies". Simple vascular malformations are subclassified into venous malformation (VM), lymphatic malformation (LM), capillary malformation, and arteriovenous malformation.

VA occurs in tissues throughout the body, but are particularly common on the body surface and subcutaneous tissue, which manifest a variety of clinical presentations ranging from superficial macules to deep masses. Because these lesions are congenital or occur in childhood and afflict patients throughout their lives, there is a need to develop new treatments. Although there is no consensus measure for VA, a reduction of lesion volume ≥ 20% is commonly used as a definition of therapeutic response (*3-5*). Therefore, capturing the change in size (area or volume) is considered to be one of the most important indicators for evaluating drug efficacy in clinical trials for skin lesions associated with VA. However, in the case of skin lesions, different from visceral tumors, it is technically difficult to evaluate lesion volume accurately by CT, MRI or ultrasound, because these simple measurements include many normal areas due to the complex shape with irregularities.

Measurement techniques for surface area as well as area and volume using 3D images have been shown to be highly accurate and precise, and have been used

for the evaluation of treatment effects on skin lesions such as ulcers, burns and, laxity (*6-8*). Therefore, in this study, we aimed to establish a method to evaluate the size (surface area, area, and volume) of skin lesions of VA traced by multiple raters on 2D photographs or 3D images, *via* assessing the inter-rater and intra-rater reliability.

2. Materials and Methods

2.1. Ethical consideration

The present study was approved by the institutional review board of each participating institute (No. 4209). All patients voluntarily participated in this study and provided written informed consent. Legal representatives (*e.g.*, parent or guardian) provided consent on behalf of children (under 18 years of age at the time of obtaining consent).

2.2. Inclusion criteria

Patients who fulfill all of the following criteria were eligible for participation in the study: 1) Patients with skin lesions of VA in Wakayama Medical University Hospital and Gifu University Hospital; 2) Patients with at least one measurable target lesion of 2-420 cm^2 in area that can be assessed photographically using QuantifiCare LifeViz® Mini 3D camera (*6-8*) (QuantifiCare Inc., Cumming, GA); 3) Patients who agree to have their skin lesions photographed.

2.3. Exclusion criteria

Patients were excluded from participation in the study if they have any of the following: 1) Patients with significant bleeding in the target lesion or surrounding area; 2) Patients who were judged by the principal investigator or others to be unsuitable for enrollment in the study.

2.4. Study procedure

1) Two-dimensional (2D) photographs of the target lesions were obtained using QuantifiCare LifeViz® Mini 3D camera. Photographs for analysis should be as follows (Figure 1): i. The entire outline of the target lesion can be seen in a single photograph; ii. The target lesion is located on a flat area of the body; iii. The target lesion is photographed from the front; iv. The target lesion is not covered by hair; v. The photograph is not blurred, unclear, *etc.*; vi. A calibration sticker was applied near the target lesion.

2) The 2D photographs (Figure 2) were sent to Nobelpharma Co., Ltd. (Shinkawa, Tokyo, Japan) with clinical information (*e.g.* diagnosis, age, gender, and lesion site). In addition, a copy of each photograph with the target lesion marked was also provided (Figure 2b). Nobelpharma forwarded these image files to QuantifiCare Inc.

3a) Quantificare Inc. uploaded the 2D photographs (stereo images) on the online server (Dermapix Web Application version 1.8.10) for tracing the lesion

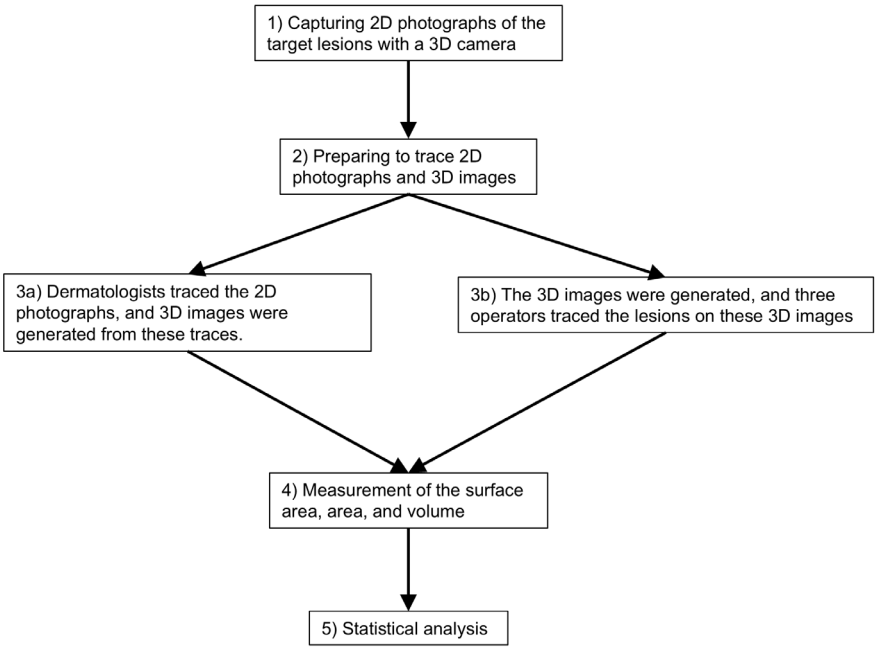

Figure 1. Scheme of study procedure. 1). Capture of 2D photographs of the target lesions using a 3D camera. 2). Preparation for tracing the 2D photographs and 3D images. 3a). Dermatologists traced the 2D photographs, and 3D images were generated from these traces. 3b). The 3D images were generated, and three operators traced the lesions on these 3D images. 4). Measurement of the surface area, area, and volume from the processed images. 5). Statistical analysis of the obtained measurements.

contours. Three dermatologists independent from the study each traced the lesion contours on 2D photographs of the online server (Figure 2c). To evaluate reproducibility, the trace was performed twice with a two-day interval. Quantificare Inc. created 3D images from the traced 2D photographs using QuantifiCare Suite (including DermaPix Software, Stitching, 3D reconstruction and 3D Analysis/3D Track, Version:3.16.4) (Figure 2d).

3b) Quantificare Inc. created 3D images from the untraced 2D photographs using QuantifiCare Suite (Figure 2e) and rendered the 3D image color-coded by depth. Three operators of Quantificare Inc., who were not involved in the study, also traced the lesion contours twice, by referring to color-coded 3D images (Figure 2f). This tracing was also projected onto the 2D photograph (Figure 2g).

4) Quantificare Inc. measured the surface area and volume on the traced 3D images, and measured the area from the traced 2D photographs. Area of 2D photographs was calculated using the scale provided by the calibration sticker. The 3D image was calibrated by combining the images of the calibration stickers to confirm the geometry of the 3D object. A fine grid was set up on the 3D constructed image, and the surface area of the lesion that completely covers the grid frame was calculated. Volume was also calculated based on the 3D images.

5) Nobelpharma Co., Ltd. performed statistical analysis as described below.

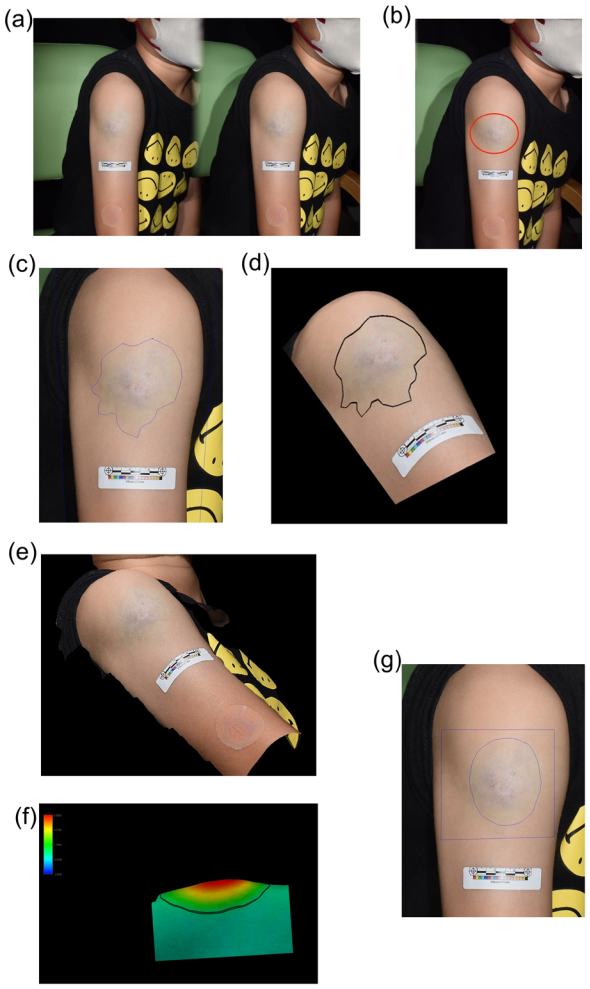

Figure 2. 3D processing of the images of patients with vascular anomalies. (a) An example of a 2D photograph (stereo image) of a patient with venous malformation (VM) of the right upper arm (case A1) obtained by the 3D camera. A calibration sticker was applied near the lesion. **(b)** An example of a 2D photograph in which the target lesion from Figure 2a was marked with a red circle by an investigator. **(c)** An example of the 2D photograph from Figure 2a traced by dermatologist rater 1. **(d)** An example of a 3D image reflecting the trace performed by dermatologist rater 1 as shown in Figure 2c. **(e)** An example of a 3D image processed using the 2D photograph from Figure 2a. **(f)** An example of 3D images color-coded by depth and traced by QuantifiCare operator 1. **(g)** An example of a 2D photograph reflecting the trace performed by QuantifiCare operator 4 as shown in Figure 2f.

2.5. Statistical analysis

1) The study analyses were performed as follows: i) Summary statistics (mean and geometric mean, standard deviation [SD] and geometric SD, and coefficient of variation [CV]%) for each parameter (surface area, area, and volume); ii) Intra-rater reliability (intra-class correlation coefficient [ICC]: intra-rater agreement); iii) Inter-rater reliability (ICC: inter-rater agreement); iv) Inter-rater reliability considering repeated assessments (ICC: inter-rater consistency).

Surface area was analysed as the primary endpoint using the following method. Area and volume were analysed in the same manner as exploratory endpoints.

Let Xijk denoted the k-th measurement of the surface area, traced by the j-th rater on the i-th lesion, where i = 1, 2, 3, ...n, j = 1, 2, 3, k = 1, 2. The repeated-measures model for reliability study with equal numbers in the subclass (*i.e.*, no missing data) was defined as

$$Xijk = \mu + \pi i + \gamma j + (\pi\gamma)ij + \varepsilon ijk$$

where μ was the overall population mean of measurements and πi and γj, are the subject and rater effects, respectively. The terms $(\pi\gamma)ij$ and εijk represented the inter-rater and intra-rater random errors. The components πi, and εijk were assumed to vary normally with means of zero and variances of σL^2 and σe^2, respectively; they were independent of each other and of all other components in the model. If the rater effects were random, then the components γj, and $(\pi\gamma)ij$ were assumed to vary normally with means of zero and variances of σR^2, and σLR^2, respectively; they were also independent of each other and of all other components.

2) Partial intra-rater reliability For each rater, intraclass correlation coefficients (ICC) (1, 1) was estimated based on a one-way ANOVA model. ($Xik = \mu + \pi i + \varepsilon ik$) as ICC (1, 1) = $\sigma L^2 / (\sigma L^2 + \sigma e^2)$, and the standard error (SE) was calculated as sqrt (σe^2). The 95%CI of ICC (1, 1) was also computed according to Shrout's method (*9*).

3) Partial inter-rater reliability For each measurement (*i.e.*, 1st or 2nd), ICC (2, 1) was estimated based on a two-way ANOVA model ($Xij = \mu + \pi i + \gamma j + \varepsilon ij$) as $ICC(2,1) = \sigma L^2/(\sigma L^2 + \sigma R^2 + \sigma e^2)$, and the SE was calculated as $SE = sqrt(\sigma R^2 + \sigma e^2)$.

The 95%CI of ICC (2, 1) was also computed according to Shrout's method (*9*).

4) Overall Inter-rater and intra-rater reliability with repeated measurements Based on the repeated two-way ANOVA model as described above, the inter-rater reliability coefficient (ρinter) and intra-rater reliability coefficient (ρintra) were estimated as $\rho inter = \sigma L^2 / (\sigma L^2 + \sigma R^2 + \sigma LR^2 + \sigma e^2)$, and $\rho intra = (\sigma L^2 + \sigma R^2 + \sigma LR^2) / (\sigma L^2 + \sigma R^2 + \sigma LR^2 + \sigma e^2)$ respectively. The standard error (SE) was calculated as $SEinter = sqrt(\sigma R^2 + \sigma LR^2 + \sigma e^2)$, and $SEintra = sqrt(\sigma e^2)$. The 95%CI of ρinter and ρintra was computed according to Shrout's method (*9*).

5) Interpretation of ICC The interpretation of ICC according to Fleiss was typically categorized as follows: < 0 = Less than chance agreement, 0.01-0.20 = Slight agreement; 0.21-0.40 = Fair agreement, 0.41-0.60 = Moderate agreement, 0.61-0.80 = Substantial agreement, and 0.81-0.99 = Almost perfect agreement (*10*).

All analyses were performed in SAS version 9.4.

3. Results

3.1. Participant demographics

In the present study, 16 lesions in 9 patients with VM (n = 5), LM (n = 3), or TA (n = 1) were included: The number of subjects, lesions measured, diagnosis, gender, and lesion site are summarized in Supplementary Table S1 (*https://www.ddtjournal.com/action/getSupplementalData.php?ID=287*). In 2 patients, photographs of multiple lesions (3 and 6) were obtained. The patients ranged in age from 2 to 40 years, with a mean ± SD of 12.4 ± 11.8 years.

3.2. Measurement of surface area, area, and volume in 2D photographs or 3D images traced by dermatologists and QuantifiCare operators

The measurement results for surface area, area, and volume obtained from 2D photographs and 3D images (traced by all raters independently) are shown in Supplementary Tables S2-S4 (*https://www.ddtjournal.com/action/getSupplementalData.php?ID=287*), respectively. Among patients A-I, A-E had VM, F-H had LM, and I had TA. Patient E with VM had 3 lesions (E1-3), while patient H with LM had 6 lesions (H1-6). When measuring case E1, the traced area was too small to evaluate in 2nd trace of dermatologist rater 2 and 2nd trace of operator rater 4, resulting in a measurement of '0.0' for the surface area and volume. Also, for example, case G1 showed considerable variation among dermatologist rater 1-3 (Figure 3a). Case I1 of dermatologist rater 1 also showed nearly 2-fold divergence between 1st and 2nd traces (Figure 3b). Furthermore, case B1 showed a 10-fold difference between dermatologists and operators (Figure 3c), with the operators detecting and tracing the raised portion of the lesion in the 3D image (Figure 3d).

A summary of the surface area, area and volume measurements by the dermatologists is shown in Table 1. The mean values of surface area for rater 2 were the lowest in both 1st (169.59 mm^2) and 2nd trace (222.86 mm^2), whereas those for rater 3 were the highest in both 1st (446.57 mm^2) and 2nd trace (466.23 mm^2). The mean area measurements also varied several fold among the raters, and the mean volume differed by nearly tenfold among them. However, median and geometric mean values of surface area were relatively similar among the three dermatologists. This discrepancy may be due to the influence of outliers or distortions in the data distribution.

By contrast, the surface area, area, and volume measurements by the QuantifiCare operators were generally consistent with each other (Table 1).

3.3. Analysis of ICC in the evaluation of surface area determined by dermatologists and operators

Partial intra-rater reliability of surface area measured by

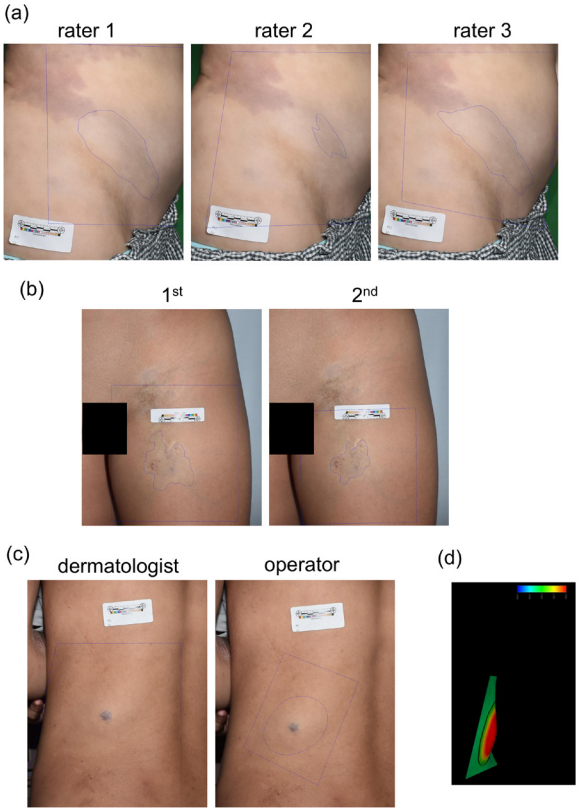

Figure 3. Examples of cases with variable tracing results. (a) Trace of 2D photographs for case G1 by dermatologist rater 1-3. **(b)** Trace of 2D photographs for case I1 by dermatologist rater 1 twice (1st and 2nd). **(c)** Trace of 2D photographs for case B1 by dermatologist rater 3 and QuantifiCare operator 6. **(d)** 3D images color-coded by depth and traced by QuantifiCare operator 6.

Table 1. Summary of measurements of surface area, area and volume evaluated by all raters

		dermatologists		
		Rater 1	Rater 2	Rater 3
Surface Area (mm^2)				
1st	Number of lesions	16	16	16
	Mean (SD)	398.02 (778.84)	169.59 (216.61)	446.57 (801.38)
	Median [Min, Max]	86.22 [17.2, 2810.7]	70.91 [14.4, 691.8]	68.82 [15.2, 2762.7]
	Geo-Mean (Geo-SD)	106.37 (4.82)	81.28 (3.56)	114.10 (5.35)
	CV%	195.7	127.7	179.5
2nd	Number of lesions	16	16	16
	Mean (SD)	339.82 (585.78)	222.86 (394.94)	466.23 (841.60)
	Median [Min, Max]	71.58 [11.3, 1718.3]	78.29 [0.0, 1582.7]	77.47 [15.0, 2966.6]
	Geo-Mean (Geo-SD)	93.17 (4.99)	98.85 (3.72)	121.34 (5.33)
	CV%	172.4	177.2	180.5
Area (mm^2)				
1st	Number of lesions	16	16	16
	Mean (SD)	357.49 (635.95)	161.11 (198.17)	415.87 (678.56)
	Median [Min, Max]	69.20 [19.1, 2041.0]	57.20 [19.0, 690.9]	80.70 [15.9, 2001.4]
	Geo-Mean (Geo-SD)	111.94 (4.40)	84.02 (3.22)	118.75 (5.08)
	CV%	177.9	123.0	163.2
2nd	Number of lesions	16	16	16
	Mean (SD)	324.92 (540.16)	194.44 (275.66)	429.03 (699.15)
	Median [Min, Max]	62.30 [15.8, 1581.0]	56.65 [18.7, 1016.7]	82.45 [15.3, 2160.6]
	Geo-Mean (Geo-SD)	99.05 (4.63)	89.25 (3.52)	126.30 (5.01)
	CV%	166.2	141.8	163.0
Volume (mm^3)				
1st	Number of lesions	16	16	16
	Mean (SD)	575.16 (1453.40)	65.76 (105.76)	578.58 (1406.47)
	Median [Min, Max]	11.87 [0.3, 4810.1]	11.11 [0.4, 363.2]	8.17 [0.4, 5224.2]
	Geo-Mean (Geo-SD)	17.25 (18.85)	11.16 (9.91)	21.40 (21.45)
	CV%	252.7	160.8	243.1
2nd	Number of lesions	16	16	16
	Mean (SD)	456.38 (1111.10)	79.98 (143.42)	531.33 (1165.03)
	Median [Min, Max]	10.06 [0.1, 4004.1]	14.10 [0.0, 468.3]	13.48 [0.2, 4142.7]
	Geo-Mean (Geo-SD)	14.62 (22.63)	15.74 (9.56)	24.54 (21.92)
	CV%	243.5	179.3	219.3
		QuantifiCare operators		
		Rater 4	Rater 5	Rater 6
Surface Area (mm^2)				
1st	Number of lesions	16	16	16
	Mean (SD)	530.57 (823.22)	572.91 (890.87)	536.50 (773.38)
	Median [Min, Max]	115.17 [15.6, 3008.7]	116.99 [20.5, 3133.1]	108.07 [16.9, 2365.3]
	Geo-Mean (Geo-SD)	144.92 (5.99)	164.56 (5.57)	148.07 (5.98)
	CV%	155.2	155.5	144.2
2nd	Number of lesions	16	16	16
	Mean (SD)	468.56 (781.52)	571.37 (872.27)	604.49 (910.73)
	Median [Min, Max]	88.87 [0.0, 2959.3]	114.88 [20.1, 3020.5]	82.28 [17.9, 2875.4]
	Geo-Mean (Geo-SD)	142.83 (5.80)	160.21 (5.73)	154.47 (6.15)
	CV%	166.8	152.7	150.7
Area (mm^2)				
1st	Number of lesions	16	16	16
	Mean (SD)	481.06 (710.90)	545.62 (796.77)	522.15 (725.48)
	Median [Min, Max]	103.75 [16.8, 2452.6]	122.70 [21.8, 2696.4]	98.40 [17.6, 2118.4]
	Geo-Mean (Geo-SD)	140.00 (5.68)	171.38 (5.27)	155.19 (5.67)
	CV%	147.8	146.0	138.9
2nd	Number of lesions	16	16	16
	Mean (SD)	424.87 (660.56)	549.37 (796.72)	575.14 (832.76)
	Median [Min, Max]	94.50 [15.2, 2346.1]	112.15 [21.9, 2633.2]	108.20 [18.1, 2478.5]
	Geo-Mean (Geo-SD)	122.44 (5.63)	169.14 (5.34)	159.81 (5.79)
	CV%	155.5	145.0	144.8

SD, standard deviation; Min, minimum; Max, maximum; Geo-Mean, geometric mean; Geo-SD, geometric standard deviation; CV, coefficient of variation.

Table 1. Summary of measurements of surface area, area and volume evaluated by all raters (continued)

		QuantifiCare operators		
		Rater 4	Rater 5	Rater 6
Volume (mm^3)				
1st	Number of lesions	16	16	16
	Mean (SD)	1008.51 (2028.10)	1199.63 (2366.48)	1135.07 (2099.54)
	Median [Min, Max]	30.28 [0.3, 7214.0]	37.45 [0.4, 7974.8]	31.22 [0.3, 6445.4]
	Geo-Mean (Geo-SD)	34.17 (31.40)	43.81 (26.70)	37.72 (29.97)
	CV%	201.1	197.3	185.0
2nd	Number of lesions	16	16	16
	Mean (SD)	825.75 (1815.78)	1239.12 (2454.64)	1374.67 (2593.08)
	Median [Min, Max]	20.78 [0.0, 6591.1]	33.59 [0.4, 8193.4]	15.99 [0.3, 7863.7]
	Geo-Mean (Geo-SD)	33.51 (29.59)	42.98 (28.27)	39.62 (31.34)
	CV%	219.9	198.1	188.6

SD, standard deviation; Min, minimum; Max, maximum; Geo-Mean, geometric mean; Geo-SD, geometric standard deviation; CV, coefficient of variation.

Table 2. Intra-rater and inter-rater reliability of surface area measurements by dermatologists

Partial Intra-rater reliability					
	Rater	Estimate of ICC (1, 1)	95% CI		SE
			Lower	Upper	
surface area (mm^2)	Rater 1	0.894	0.730	0.961	224.101
	Rater 2	0.702	0.344	0.884	173.625
	Rater 3	0.991	0.974	0.997	79.313
Partial Inter-rater reliability					
Parameter	Measurement	Estimate of ICC (2, 1)	95% CI		SE
			Lower	Upper	
surface area (mm^2)	1st	0.669	0.414	0.854	383.949
	2nd	0.804	0.609	0.920	284.484
Overall Inter-rater and Intra-rater reliability					
Parameter		Estimate	95% CI		SE
			Lower	Upper	
surface area (mm^2)	ρ_{inter}	0.746	0.578	1.000	330.137
	ρ_{intra}	0.933	0.822	1.000	169.958

ICC, intraclass correlation coefficients; CI, confidence interval; SE, standard error.

the dermatologists was 0.894 for rater 1, 0.702 for rater 2, and 0.991 for rater 3 (Table 2), while inter-rater reliability was 0.669 for the 1st trace and 0.804 for the 2nd trace (Table 2). In the analysis of overall inter-rater and intra-rater reliability with repeated measurements of surface area, the correlation coefficient between raters was quite high at 0.746 (interpretation: Substantial agreement), and the correlation coefficient within raters was very high at 0.933 (Almost perfect agreement) (Table 2).

On the other hand, partial intra-rater reliability of surface area measured by the QuantifiCare operators was 0.985 for rater 4, 0.995 for rater 5, and 0.961 for rater 6 (Table 3), while inter-rater reliability was 0.938 for the 1st trace and 0.954 for the 2nd trace (Table 3). In the analysis of overall inter-rater and intra-rater reliability with repeated measurements of surface area, the correlation coefficient between raters was quite high at 0.946 (Almost perfect agreement), and the correlation coefficient within raters was very high at 0.981 (Almost perfect agreement) (Table 3). Thus, all values obtained by the QuantifiCare operators were greater than those obtained by the dermatologists.

3.4. Analysis of ICC in the evaluation of area

Partial intra-rater reliability and inter-rater reliability of area evaluated by dermatologists were similar to those for surface area (Supplementary Table S5-S6, *https://www.ddtjournal.com/action/getSupplementalData.php?ID=287*). In the analysis of overall inter-rater and intra-rater reliability with repeated measurements of area, the correlation coefficient between raters was quite high

Table 3. Intra-rater and inter-rater reliability of surface area measurements by QuantifiCare operators

Partial Intra-rater reliability					
	Rater	Estimate of ICC (1, 1)	95% CI		SE
			Lower	Upper	
surface area (mm^2)	Rater 4	0.985	0.960	0.995	97.380
	Rater 5	0.995	0.987	0.998	60.444
	Rater 6	0.961	0.895	0.986	166.702
Partial Inter-rater reliability					
Parameter	Measurement	Estimate of ICC (2, 1)	95% CI		SE
			Lower	Upper	
surface area (mm^2)	1^{st}	0.938	0.865	0.976	205.830
	2^{nd}	0.954	0.896	0.982	184.411
Overall Inter-rater and Intra-rater reliability					
Parameter		Estimate	95% CI		SE
			Lower	Upper	
surface area (mm^2)	ρ_{inter}	0.946	0.902	1.000	195.200
	ρ_{intra}	0.981	0.954	1.000	116.799

ICC, intraclass correlation coefficients; CI, confidence interval; SE, standard error.

at 0.723 (Substantial agreement), and the correlation coefficient within raters was very high at 0.952 (Almost perfect agreement) (Supplementary Table S7, *https://www.ddtjournal.com/action/getSupplementalData.php?ID=287*).

Partial intra-rater reliability, inter-rater reliability, and overall inter-rater and intra-rater reliability with repeated measurements of area evaluated by QuantifiCare operators were also similar to those of surface area (Supplementary Table S8-S10, *https://www.ddtjournal.com/action/getSupplementalData.php?ID=287*), and all values obtained by the QuantifiCare operators were higher than those by dermatologists.

3.5. Analysis of ICC in the evaluation of volume

Similar to the evaluation of surface area and area, all values evaluated by QuantifiCare operators were greater than those by dermatologists (Supplementary Table S11-S16, *https://www.ddtjournal.com/action/getSupplementalData.php?ID=287*).

4. Discussion

We previously conducted a randomized phase II clinical trial of topical sirolimus therapy for cutaneous lesions of VM, LM, TA, and kaposiform hemangioendothelioma (*11*). The primary endpoint of the study was the overall improvement score in the target lesion (size and coloration) assessed according to photographs by the independent review committee at Week 12. However, there was no statistically significant difference in the mean improvement score in the 0.2% sirolimus gel group or the 0.4% group compared with the placebo group. Thus, we could not prove the efficacy of topical sirolimus for cutaneous VA in the protocol.

On the other hand, among secondary endpoints, the improvement in target lesion size at Week 12 as assessed by the independent review committee was significantly higher in the 0.4% sirolimus gel group than in the placebo group. Also, a mixed-effects model for repeated measures analysis showed a significant difference in the major diameter of lesion between the placebo and 0.4% groups at Week 16. We therefore hypothesized that the focus should be on size rather than coloration for the evaluation of efficacy against skin lesions of VA. Accordingly, the method of measuring the area of the target lesion was changed from calculating the area from the multiplication of major and minor diameters to tracing the contour of the lesion, which resulted in remarkable differences in some cases. As a result, the post-hoc analysis indicated that the percentage of patients with ≥ 20% reduction in the re-measured lesion area was significantly higher in the sirolimus groups at Week 8 and 12. Thus, the efficacy of sirolimus gel by the post-hoc analysis could be detected earlier than with the secondary endpoints (Week 12 and 16). However, this post-hoc re-measurement did not capture elevation of the lesions.

Based on these results of the clinical trial, we needed to find a better method to measure lesion size for the next phase III trial. The procedure in the present study involved tracing lesion contours on photographs of target diseases of the phase II clinical trial captured with a 3D camera, followed by 3D processing of the images to measure lesion area, surface area, and volume (*6-8*).

Comparisons were made between measurements based on 2D photographs traced by dermatologists and those based on 3D images traced by QuantifiCare operators. Both methods yielded high inter- and intra-rater reliability; however, the inter- and intra-rater reliability for measurements by the QuantifiCare operators was even higher.

One possible explanation is that tracing a 2D photograph relies only on planar information, whereas tracing a 3D image was based on three-dimensional information. This additional depth information makes it easier to discern a lesion's uneven surface and identify its true contour more accurately. The dermatologist raters gave feedback such as: "Several lesions have abruptly broken edges and others gradually become normal with a gradation. It is very difficult to determine the contour of such lesions with the naked eye." and "Some lesions have indistinct borders, resulting in variations between the 1st and 2nd tracings.".

Despite clinical needs, the specific problems of applying 3D imaging technology to measurement of VA included a variety of clinical presentations of lesions ranging from superficial macules to deep masses with unevenness, blurred boundaries, color similarity to surrounding tissues, and irregular/lobulated morphology. In the present study, we attempted to address these challenges by using a dedicated 3D camera system that generates color-coded depth maps, by standardizing patient positioning and camera distance, and by having operators trace the lesions on 3D images.

Given the higher inter- and intra-rater reliability of the 3D measurement method in this study, if a 3D-based quantitative endpoint such as surface area or volume had been adopted in the phase II trial, the drug efficacy might have been detected with greater sensitivity or at an earlier time point.

5. Limitations

This study has several limitations. First, in the case of E1, surface area and volume evaluated by two raters were "0.0" but area was "20.9" or "15.3". In the 3D measurement of surface area and volume, a dense mesh (or grid composed of several triangles) is applied to the reconstructed 3D surface. Then, the system calculates the surface area and volume based on how many triangles are fully covered by the lesion. However, there is a detectability limit when applying the mesh. The contours traced by the two raters did not cover a sufficient number of mesh triangles, resulting in those triangles being excluded and the measurement becoming 0.0. This discrepancy indicates that lesions must be above a certain size (to stay above the detection limit), when using 3D measurement in future practice through standardized operating procedures.

Second, there were cases where the surface area was smaller than the area (*e.g.* case A1 and H6). This was also due to the calculation method, and it is known that large variations can occur depending on (i) the photography angle, (ii) the flatness of the lesion and its surrounding area, and (iii) whether the calibration sticker is placed in exactly the same plane as the lesion. These imaging conditions should be carefully considered in future studies to achieve more accurate measurements.

Next, it is possible that the 3D method is more advantageous for prominently raised VM lesions, while offering less benefit for flat LM lesions. According to our subgroup analysis, no correlation was observed between the 3D measurement reliability and disease type, size, or unevenness of lesions (data not shown). However, caution is required in interpreting this subgroup analysis due to the limited sample size.

Lastly, the cost-effectiveness of this 3D measurement method also needs to be considered. From the viewpoint of clinical translation feasibility, in future clinical trials the contract research organization will provide the participating medical institutions with cameras, a subscription to the 3D visualization platform, and initial training for physicians and staff. According to the manufacturer, the initial cost includes a dedicated 3D camera system and a software license (with an annual software fee and warranty), which is higher than the cost of a standard digital camera. Nonetheless, the improved reproducibility and objectivity of lesion-size measurements may justify the upfront cost by enabling more efficient clinical trials and more reliable assessment of treatment response.

6. Conclusion

We compared size measurements of cutaneous VA lesions obtained from 2D photographs traced by three dermatologists with those obtained from 3D images traced by three company operators, and assessed inter- and intra-rater reliability. Both 2D and 3D methods demonstrated high inter- and intra-rater reliability; however, better reliability was observed in the measurements obtained by company operators using 3D imaging. The findings indicate that 3D surface imaging provides a more consistent and objective evaluation of lesion size than 2D photography, and support the potential application of this method in clinical practice and clinical trials for VA.

Acknowledgements

We would like to thank all investigators and secretaries of participating institutes of the present study. We acknowledge proofreading and editing by Benjamin Phillis at the Clinical Study Support Center at Wakayama Medical University, and the assistance in analyzing the data by QuantifiCare and Nobelpharma.

Funding: This study was funded by the research budget

of Wakayama Medical University. However, labor costs and subcontracting expenses related to statistical analysis and measurement were funded by Nobelpharma Co., Ltd.

Conflict of Interest: This study was funded by Nobelpharma. Masatoshi Jinnin received consultancy fee from Nobelpharma.

References

1. International Society for the Study of Vascular Anomalies. ISSVA classification of vascular anomalies[Internet]. 2025[cited 2025 May 28]. Available from: *https://www.issva.org/classification* (accessed May 28, 2025).
2. Kunimoto K, Yamamoto Y, Jinnin M. ISSVA Classification of Vascular Anomalies and Molecular Biology. Int J Mol Sci. 2022; 23:2358.
3. Ozeki M, Nozawa A, Yasue S, Endo S, Asada R, Hashimoto H, Fukao T. The impact of sirolimus therapy on lesion size, clinical symptoms, and quality of life of patients with lymphatic anomalies. Orphanet J Rare Dis. 2019; 14:141.
4. Ozeki M, Endo S, Yasue S *et al*. Sirolimus treatment for intractable lymphatic anomalies: an open-label, single-arm, multicenter, prospective trial. Front Med (Lausanne). 2024; 11:1335469.
5. Singh S, Bradford D, Li X *et al*. FDA Approval Summary: Alpelisib for PIK3CA-Related Overgrowth Spectrum. Clin Cancer Res. 2024; 30:23-28.
6. Chaby G, Lok C, Thirion JP, Lucien A, Senet P. Three-dimensional digital imaging is as accurate and reliable to measure leg ulcer area as transparent tracing with digital planimetry. J Vasc Surg Venous Lymphat Disord. 2017; 5:837-843.
7. Bharadia SK, Gabriel V. Comparison of Clinical Estimation and Stereophotogrammic Instrumented Imaging of Burn Scar Height and Volume. Eur Burn J. 2024; 5:38-48.
8. Bonan P, Verdelli A. Combined microwaves and fractional microablative CO2 laser treatment for postpartum abdominal laxity. J Cosmet Dermatol. 2021; 20:124-131.
9. Shrout PE, Fleiss JL. Intraclass correlations: uses in assessing rater reliability. Psychol Bull. 1979; 86:420-428.
10. Fleiss JL, Cohen J. The equivalence of weighted kappa and the intraclass correlation coefficient as measures of reliability. Educ Psychol Meas. 1973; 33:613-619.
11. Jinnin M, Shimokawa T, Kishi A *et al*. Topical sirolimus therapy for cutaneous vascular anomalies: A Randomized Phase II Clinical Trial. J Dermatol. 2025; 52:872-887.

Received September 27, 2025; Revised January 19, 2026; Accepted February 13, 2026.

**Address correspondence to:*
Kayo Kunimoto, Department of Dermatology, Wakayama Medical University, 811-1 Kimiidera, Wakayama 641-0012 Japan.
E-mail: k-jigen@wakayama-med.ac.jp

Released online in J-STAGE as advance publication February 20, 2026.

Brief Report

DOI: 10.5582/ddt.2025.01128

Analgesic effects of Goreisan in patients with glossodynia: A preliminary exploratory study

Takao Ayuse[1,*], Shuntaro Sato[1], Ichiro Okayasu[2], Mizuki Tachi-Yoshida[3], Jun Sato[4], Hironori Saisu[4], Yoko Yamazaki[5], Hiroko Imura[6]

[1] Nagasaki University Hospital, Clinical Research Center, Nagasaki, Japan;
[2] Department of Dental Anesthesiology, Osaka Dental University, Oosaka, Japan;
[3] Department of Dental Anesthesiology, Nagasaki University Hospital, Nagasaki, Japan;
[4] Department of Pain Medicine and Pain Relief Surgery•Pain Center, Aichi Medical University Hospital, Aichi, Japan;
[5] Department of Dental Anesthesiology, Graduate School of Medical and Dental Sciences, Institute of Science Tokyo, Tokyo, Japan;
[6] Orofacial Pain Clinic, Institute of Science Tokyo Hospital, Tokyo, Japan.

SUMMARY: Glossodynia-related pain refers to persistent, chronic pain occurring on the oral mucosal surface. Various medications are prescribed depending on symptom profiles and have demonstrated therapeutic benefits; however, these agents are often associated with adverse effects such as drowsiness or dizziness. Goreisan, a traditional Japanese Kampo medicine, has long been used empirically for glossodynia-related pain, particularly in patients reporting symptom fluctuation associated with weather changes. Nevertheless, high-quality clinical evidence supporting its efficacy remains limited. This multicenter, randomized, open-label preliminary exploratory study enrolled patients receiving treatment for glossodynia-related pain. Participants were assigned to receive either Goreisan (7.5 g/day for 12 weeks) in addition to standard therapy or standard therapy alone. Pain intensity was assessed using the visual analog scale (VAS) at baseline and at 4, 8, and 12 weeks. Salivary amylase activity was measured as an exploratory stress-related biomarker, and atmospheric pressure was recorded at each outpatient visit. Owing to insufficient enrollment, all analyses were descriptive and exploratory. Pain intensity improved from baseline in both groups. However, the proportion of patients achieving ≥ 20% improvement in VAS at week 12 was not higher in the Goreisan group than in the control group. Weak negative correlations between VAS scores and barometric pressure were observed in both groups ($r \approx -0.2$). No clinically relevant adverse events or hepatic dysfunction related to Goreisan were identified. This preliminary exploratory study did not confirm a clear analgesic efficacy of Goreisan for glossodynia. However, the findings provide descriptive data on pain trajectories, safety, and potential meteorological associations, supporting the need for future large-scale, double-blind, placebo-controlled trials.

Keywords: glossodynia, burning mouth syndrome, Kampo medicine, Goreisan, exploratory study

1. Introduction

"Glossodynia (tongue pain)," synonymous with burning mouth syndrome, refers to persistent, chronic pain occurring on the oral mucosal surface and is often accompanied by burning sensations in the oral cavity. According to the International Classification of Headache Disorders, 3rd edition, glossodynia is defined as a prickling sensation or unpleasant tingling that recurs daily for more than 2 h per day for over 3 months.

Because the etiology of glossodynia remains unclear, no curative treatment exists, and current management relies on symptomatic therapy. Various pharmacological agents—including pregabalin, antidepressants, anticonvulsants, duloxetine, amitriptyline, *N*-methyl-D-aspartate receptor antagonists, and tramadol—are prescribed depending on clinical presentation. Although these agents may alleviate pain, they are frequently associated with adverse effects such as drowsiness and dizziness, limiting long-term use.

Goreisan, a Kampo medicine, has been used empirically for pain management in glossodynia and other oral and maxillofacial pain conditions, particularly when symptoms are perceived to fluctuate with meteorological changes such as barometric pressure variations (*1-5*). The tongue and surrounding oral tissues are richly supplied with capillaries and lymphatic vessels, rendering them potentially sensitive to changes in fluid balance. Goreisan is thought to improve local tissue metabolism, alleviate congestion, and enhance lymphatic

flow, with relatively few central nervous system–related adverse effects.

However, according to current chronic pain treatment guidelines, the level of evidence supporting Kampo medicines for chronic pain remains low (2C–2D), and well-designed clinical studies are lacking. Therefore, this study was conducted as a preliminary exploratory randomized trial to descriptively evaluate the efficacy and safety of Goreisan in patients with glossodynia.

2. Methods / Design

2.1. Study design

This multicenter, randomized, open-label exploratory trial enrolled patients undergoing treatment for glossodynia-related pain. After providing written informed consent, participants were randomly assigned (1:1) to receive either Goreisan in addition to standard therapy or standard therapy alone. The study was registered in the Japan Registry of Clinical Trials (jRCTs071200017) and conducted in accordance with the Declaration of Helsinki and Good Clinical Practice in Japan. The research protocol was approved by The Clinical Research Review Board in Nagasaki University.

2.2. Participants

Participants were recruited and treated at Nagasaki University Hospital, Aichi Medical University Hospital, and Tokyo Medical and Dental University. Clinical research coordinators explained the study details to all participants, after which written informed consent was obtained. This study included patients undergoing treatment for glossodynia.

Inclusion criteria include: (1) Patients receiving treatment for chronic pain in the oral and maxillofacial region; (2) Adults aged ≥ 20 years at the time of informed consent; (3) No sex restrictions; (4) Outpatient only; (5) Patients who received sufficient explanation of the study, demonstrated understanding, and provided informed consent. Exclusion criteria include (1) Patients currently taking Kampo medicines containing kakkonto; (2) Patients with severe hypertension (systolic blood pressure ≥ 120 mmHg); (3) Patients with severe hepatic or renal dysfunction; (4) Patients with drug hypersensitivity; (5) Pregnant women, women who may be pregnant, and breastfeeding women; (6) Patients who participated in another clinical trial within the past 4 months; (7) Individuals deemed inappropriate for participation by the principal investigator.

2.3. Intervention

After consent, baseline assessments of pain intensity and salivary flow were performed. The intervention group received Goreisan at 7.5 g/day for 12 weeks in addition to ongoing standard therapy. Standard therapy consisted of Western pharmacological treatments selected by the treating physician, including antidepressants, anticonvulsants, and non-opioid analgesics, with stable dosing during the study period. The control group continued standard therapy alone without Kampo medicine.

Meteorological data, including temperature, humidity, and barometric pressure, were recorded during each outpatient visit. Patients also recorded self-assessed pain intensity at home.

2.4. Endpoints

The primary exploratory endpoint was defined as ≥ 20% improvement in VAS score from baseline to week 12. Secondary exploratory endpoints included changes in VAS score at weeks 4 and 8, salivary amylase activity, tongue findings, and safety outcomes.

2.5. Sample size

This study aimed to enroll 90 patients undergoing treatment for glossodynia. A preliminary study showed that 8 of 14 cases (57%) experienced ≥ 20% improvement in VAS scores after 2 weeks of Goreisan. Assuming a 10% improvement rate in the standard therapy group and a 40% expected improvement rate in the Goreisan group, with $\alpha = 0.05$, power = 0.9, and a 10% anticipated dropout rate, a target sample size of approximately 90 patients (41 per group) was required. Therefore, 45 patients were included in each group.

2.6. Randomization

Participants were registered and randomized using REDCap. Stratified block randomization was used to allocate participants in a 1:1 ratio to the Goreisan or control group.

2.7. Statistical analysis

The primary endpoint was defined as a ≥ 20% reduction in VAS score from baseline. This study aimed to statistically confirm whether the Goreisan group showed a higher response rate than the standard therapy group. However, due to insufficient enrollment, formal hypothesis testing was not feasible. Therefore, an estimation of endpoints and confidence intervals was performed instead. Baseline characteristics were expressed as medians and interquartile ranges for continuous variables and counts and percentages for categorical variables. Correlation between barometric pressure and VAS scores was also evaluated. All statistical analyses were performed using R version 4.4.0.

3. Results and Discussion

Twenty-six patients were enrolled, and 25 completed the study. Baseline characteristics, including pain severity and disease duration, were comparable between groups (Table 1). Pain location was predominantly the tongue in both groups (Goreisan: 12/13; Control: 10/13). Gingival or palatal pain was less frequently reported, and no marked imbalance in pain distribution between groups was observed at baseline. Initial pain severity evaluated by VAS score was identical in both group. Estimated disease duration with pain was identical in both group of several months.

Both groups demonstrated improvements in VAS scores over time. However, the proportion of patients achieving ≥ 20% improvement at week 12 was numerically higher in the standard therapy group than in the Goreisan group (Table 2). Figure 1 illustrates changes in VAS scores from baseline.

Salivary amylase levels showed variability during follow-up, with transient elevations observed in the control group at week 4 (Figure 1). Pearson's correlation analysis revealed weak negative correlations between VAS scores and barometric pressure in both groups (Goreisan group: $r = -0.19$; control group: $r = -0.22$).

No serious adverse events occurred. Liver function parameters remained within normal ranges throughout the study (Table 3).

This randomized, open-label exploratory study evaluated the efficacy and safety of Goreisan in patients receiving treatment for glossodynia. Although the originally planned sample size was not achieved, the present study provides preliminary descriptive information regarding pain trajectories, stress-related biomarkers, safety, and potential associations between pain perception and meteorological factors in this patient population.

3.1. Association between Goreisan and pain perception

Pain intensity, assessed using self-reported VAS scores, improved over time in both the Goreisan and control groups. However, contrary to the initial hypothesis, the proportion of patients achieving a ≥ 20% improvement in VAS at week 12 was not greater in the Goreisan group than in the standard therapy group. Given the exploratory nature of this study and the insufficient sample size, these findings should not be interpreted as evidence against the efficacy of Goreisan, nor do they support a definitive analgesic benefit.

Several factors may have contributed to the observed pattern. First, the open-label design may have introduced expectation bias. Patients allocated to the Goreisan group (standard therapy + Goreisan) may have anticipated a marked therapeutic effect, potentially influencing their subjective pain ratings. Conversely, patients in the control group may have experienced reassurance or therapeutic benefit from continued standard care and repeated clinical encounters, resulting in apparent pain improvement. Such bias is particularly relevant for subjective endpoints such as pain intensity and may partly explain the unexpectedly greater improvement observed in the control group.

From a mechanistic perspective, prior case reports and small observational studies have suggested that Goreisan may exert anti-inflammatory effects through modulation of aquaporin function and regulation of glymphatic flow, particularly in conditions associated with fluid imbalance or meteorological changes (*6*). However, the present study was not designed to test these mechanisms, and the current findings should be interpreted as hypothesis-generating rather than confirmatory.

Table 2. The proportion of patients who achieved ≥ 20% reduction in pain (VAS) from baseline at each time point

Group	Week	Event/Total	Proportion % (95%CI)
Goreisan	4	3/13	23.1 (8.2 to 50.3)
	8	4/13	30.8 (12.7 to 57.6)
	12	4/13	30.8 (12.7 to 57.6)
Standard treatment	4	6/12	50.0 (25.4 to 74.6)
	8	6/12	50.0 (25.4 to 74.6)
	12	6/12	50.0 (25.4 to 74.6)

Abbreviations: CI, confidence interval.

Table 1. Demographic data

Characteristic	Goreisan (n = 13)	Standard treatment (n = 12)
Female, n (%)	9 (69%)	11 (92%)
Age, median (IQR)	59 (39, 75)	66 (40, 78)
Height, median (IQR)	156.7 (150.0, 175.0)	155.0 (149.0, 170.0)
Weight, median (IQR)	56 (40, 78)	52 (39, 69)
Initial VAS score	4.0 (2,4, 5.7)	4.3 (2.5, 6.0)
Primary pain site (Tongue)	12	10
Primary pain site (Gingiva)	1	2
Primary pain site (Palate)	1	0

Abbreviations: IQR, interquartile range. The definition of primary pain site (Tongue) is as follows: Tongue refers to all areas including the tongue itself; Gingiva refers to areas including the gums; Palate refers to areas including the palate.

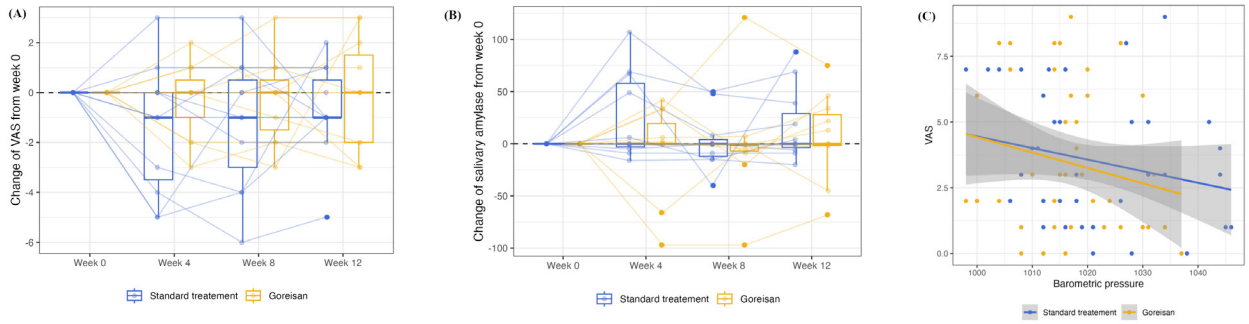

Figure 1. (A) The change in VAS from week zero. (B) The change in salivary amylase from week zero. There is slight increase in amylase level at week four in control group. (C) The correlation between VAS and barometric pressure.

Table 3. Evaluation of liver function at week 12

Characteristic	Goreisan (n = 13)	Standard treatment (n = 12)
AST	20.4 (4.9)	19.1 (5.3)
ALT	19.2 (8.0)	18.1 (7.9)
γ-GTP	46.1 (88.4)	32.2 (47.9)

AST: Alanine transaminase; ALT, Aspartate aminotransferase; γ-GTP, gamma-glutamyl transpeptidase.

3.2. Stress evaluation using salivary amylase

Patients with glossodynia frequently experience psychological stress related to chronic pain, anxiety, and frustration due to the absence of identifiable organic pathology. This study is, to our knowledge, the first to explore changes in salivary amylase activity during Goreisan treatment in patients with glossodynia.

Salivary amylase levels demonstrated variability during follow-up, with transient elevations observed in the control group at week 4. Salivary amylase is considered a surrogate marker of sympathetic nervous system activity and acute stress responses. The observed elevation in control group may reflect fluctuations in stress levels associated with changes in pain perception, adaptation to treatment, or comorbid psychological factors. However, because other stress-related biomarkers such as cortisol were not measured, and because salivary amylase is sensitive to multiple confounding factors, these findings must be interpreted cautiously. Further studies incorporating comprehensive psychophysiological assessments are warranted to clarify the relationship between glossodynia, stress, and treatment response.

3.3. Relationship between pain perception and barometric pressure

This study also explored the association between pain perception and barometric pressure changes. Weak negative correlations between VAS scores and barometric pressure were observed in both treatment groups, suggesting that pain perception may increase slightly as atmospheric pressure decreases. However, the magnitude of these correlations was small ($r \approx -0.2$), indicating limited explanatory power.

These findings should therefore be regarded as preliminary observations rather than evidence of a clinically meaningful relationship. Correlation does not imply causation, and numerous confounding factors—such as temperature, humidity, psychological state, and individual sensitivity to environmental changes—may influence pain perception. Nevertheless, the results are consistent with previous reports that certain chronic pain conditions, including trigeminal pain and meteorological headaches, may be influenced by barometric pressure fluctuations (*7,8*).

From the perspective of traditional East Asian medicine, meteorological factors have long been considered relevant to symptom fluctuation, and Goreisan has historically been prescribed for conditions thought to be associated with fluid imbalance. Although the present study does not establish a causal link between barometric pressure changes and glossodynia-related pain, it supports further investigation into whether specific subgroups of patients—such as those reporting weather-sensitive symptoms—may respond differently to treatment.

3.4. Limitations and future directions

The most fundamental limitation of this study is the insufficient sample size relative to the original study design, which precluded formal hypothesis testing and definitive conclusions regarding efficacy. The insufficient sample size is a fundamental flaw of this study, and the true efficacy of Goreisan cannot be confirmed or refuted based on these findings.

Additional limitations include the open-label design, heterogeneity of concomitant standard therapies, and reliance on subjective pain assessments. The use of an "open-label" design (non-blinded), where both patients and researchers are aware of the group allocation, introduces expectation bias and assessment bias. The anomalous finding of a higher VAS improvement rate in the control group strongly suggests the presence

of such bias in this study. Therefore, future studies should prioritize a double-blind, placebo-controlled design to minimize expectation and assessment bias. The development of a placebo formulation identical in appearance and taste to Goreisan appears feasible and should be considered a core design element for future clinical study. Larger sample sizes would also allow stratified analyses to explore whether specific patient subgroups, such as those with meteorologically sensitive symptoms, derive greater benefit from Goreisan.

4. Conclusion

In summary, this exploratory study did not confirm a clear analgesic advantage of Goreisan over standard therapy in patients with glossodynia. However, it provides valuable descriptive data on safety, pain trajectories, stress-related biomarkers, and potential meteorological associations. These findings underscore the need for well-designed, adequately powered randomized controlled trials to clarify the therapeutic role of Goreisan in glossodynia.

Acknowledgements

We thank our colleagues and staff at the Department of Dental Anesthesiology at Nagasaki University Hospital for their support.

Funding: None.

Conflict of Interest: The authors have no conflicts of interest to disclose.

References

1. Okayasu I, Tachi M, Suzue E, Ito N, Ozaki Y, Mishima G, Kurata S, Ayuse T. A Case Report of Burning Mouth Syndrome with Dry Mouth Managed by Kampo Medicine. Anesth Prog. 2023; 70:134-136.
2. Okamoto H. A valid approach in refractory Glossodynia; a singl-institute 5-year experience treating with Japanese traditional herbal (Kampo) medicine. Evid Based Complement Alternat Med. 2013; 2013:1-8.
3. Hijikata Y, Makiura N, Kano T, Higasa K, Shimizu M, Kawata K, Mine T. Kampo medicine, based on traditional medicine theory, in treating uncured glossodynia: efficacy in five clinical cases. Am J Chin Med. 2008; 36:835-847.
4. Bessho K, Okubo Y, Hori S, Murakami K, Iizuka T. Effectiveness of kampo medicine (sai-boku-to) in treatment of patients with glossodynia. Oral Surg Oral Med Oral Pathol Oral Radiol Endod. 1998; 86:682-686.
5. Kido H, Komasawa N, Fujiwara S, Minami T. Efficacy of Go-rei-san for Pain Management in Four Patients with Intractable Trigeminal Neuralgia. Masui. 2017; 66:184-186. (in Japanese)
6. Katsuki M, Kawamura S, Kashiwagi K, Koh A. Medication Overuse Headache Successfully Treated by Three Types of Japanese Herbal Kampo Medicine. Cureus. 2021; 13:e16800.
7. Sato J, Inagaki H, Kusui M, Yokosuka M, Ushida T. Lowering barometric pressure induces neuronal activation in the superior vestibular nucleus in mice. PLoS One. 2019; 14:e0211297.
8. Dixon WG, Beukenhorst AL, Yimer BB, *et al*. How the weather affects the pain of citizen scientists using a smartphone app. NPJ Digit Med. 2019; 2:105.

Received December 10, 2025; Revised January 26, 2026; Accepted February 11, 2026.

**Address correspondence to:*
Takao Ayuse, Nagasaki University Hospital, Clinical Research Center, Nagasaki, Japan, Nagasaki, Japan. Address: 1-7-1 Sakamoto Nagasaki, Japan.
E-mail: ayuse@nagasaki-u.ac.jp

Released online in J-STAGE as advance publication February 14, 2026.

Brief Report

DOI: 10.5582/ddt.2025.01115

Comparison of salivary Mucin 5B (MUC5B) secretion between heat-not-burn tobacco users and non-smokers

Yukihiro Mori[1], Mamoru Tanaka[2], Hana Kozai[2], Yuka Aoyama[3], Morihiro Ito[4,*]

[1] Department of Nursing, College of Life and Health Science, Chubu University, Aichi, Japan;
[2] Department of Food and Nutritional Sciences, College of Bioscience and Biotechnology, Chubu University, Aichi, Japan;
[3] Department of Clinical Engineering, College of Life and Health Sciences, Chubu University, Aichi, Japan;
[4] Graduate School of Life and Health Sciences, Chubu University, Aichi, Japan.

SUMMARY: The use of heat-not-burn (HNB) tobacco is rapidly increasing, particularly in Japan; however, its health effects, especially on innate immunity in the oral mucosa, remain unclear. This cross-sectional study aimed to compare the secretion levels of mucin 5B (MUC5B), a mucin that forms a protective barrier role on the oral mucosal surface, between HNB tobacco smokers and non-smokers. MUC5B levels in stored saliva samples from 208 males (147 in the non-smoking group, 32 in the HNB tobacco group, 15 in the paper cigarette group, and 14 in the dual-use group) were measured using enzyme-linked immunoassay (ELISA). The primary outcome was the MUC5B secretion rate (μg/min = MUC5B concentration × saliva secretion rate). Significant differences in MUC5B secretion rates were observed among the four groups, with multiple comparisons showing significantly lower rates in the HNB tobacco and dual-use groups than in the non-smoking group ($p = 0.042$ and $p < 0.001$, respectively). The observed decrease in salivary MUC5B secretion is a concern, as it may comprise oral hygiene and immune function. From a public health perspective, these findings provide a basis to discourage the use and combined use of HNB tobacco.

Keywords: saliva, innate immunity, heat-not-burn tobacco, mucin, mucin 5B

1. Introduction

Heat-not-burn (HNB) tobacco use has increased notably in Japan and is perceived as having less harmful than conventional paper cigarettes (*1*). Although HNB tobacco is reduces exposure to certain harmful components, concerns remain regarding exposure to chemical substances such as nicotine, cytotoxicity, and other adverse effects (*2*). Several studies have reported the link between HNB tobacco and oral immune components. For instance, a previous study reported that HNB tobacco users exhibit lower resting saliva secretion rates and significantly lower secretion rates of lactoferrin (Lac) and lysozyme (Lys) than non-smokers (*3*). Furthermore, significantly reduced salivary secretory immunoglobulin A (sIgA) levels have been observed in HNB tobacco users, especially females (*4*).

Saliva contains mucin, antimicrobial proteins (Lac and Lys), sIgA, and other protective factors. Furthermore, mucin 5B (MUC5B), the major gel-forming mucin, is secreted by the submandibular glands, sublingual glands, palatal, and minor salivary glands (*5*). As a highly glycosylated glycoprotein, MUC5B prevents pathogen adhesion, facilitates aggregation and detoxification, and contributes to mucosal barrier functions through lubrication and coating (*5,6*). Deficiency in MUC5B may compromise mucosal defense, increasing susceptibility to oral infections and inflammatory diseases (*5*).

We previously reported that the use of HNB tobacco reduces the secretion rates of Lac and Lys (*3*). However, few studies have quantitatively examined the association between HNB tobacco use and the secretion levels (especially secretion rate) of salivary MUC5B. Considering that HNB tobacco use reduces saliva secretion rates, as previously demonstrated (*3*), and that MUC5B contributes to the formation of oral salivary films (*7*), the hypothesis that the effective supply (secretion rate) of MUC5B may be relatively lower among HNB tobacco smokers warrants investigation.

This study aimed to quantitatively examine the association between HNB tobacco use and MUC5B secretion by comparing MUC5B secretion rates (as the primary endpoint) among four participant groups: a non-smoking, HNB tobacco, paper cigarette, and dual-use. While other mucins, including MUC1 (membrane-bound mucin) (*8*) and MUC7 (secretory and non-gel-forming mucin) (*9*), exist, this study focused on

MUC5B as the primary gel-forming mucin (*10*). To our knowledge, this study is the first to examine the association between MUC5B secretion rate in saliva and HNB tobacco use. This approach may provide novel insights into salivary innate immunity, with implications for preventive medicine and public health.

2. Materials and Methods

2.1. Study design and participants

This cross-sectional study included essential workers (firefighters, paramedics, and rescue workers) employed at five fire stations in Kasugai City, Aichi Prefecture, Japan. Participants were recruited *via* a research cooperation request form distributed through each manager of each station. Participants were selectively sampled because assessing immune factors in their saliva was considered critical, given their frontline contact with patients suspected of having infectious diseases. Saliva samples were collected in mid-June 2021.

A total of 219 individuals initially participated in this study; however, all seven female participants were non-smokers, so the analysis was limited to 212 males. Additionally, four samples with MUC5B concentrations outside the detection range were excluded, leaving 208 participants (147 in the non-smoking group, 32 in the HNB tobacco group, 15 in the paper cigarette group, and 14 in the dual-use group) in the final analysis. "Paper cigarettes" were defined as conventional combustible cigarettes. Dual users were those who used both HNB tobacco and paper cigarettes.

Smokers were defined as "individuals who had smoked continuously for at least six months" (*3*). None of the participants were e-cigarette users. Furthermore, as dental conditions could impact the results (*11,12*), individuals with periodontal disease were excluded in advance.

2.2. Ethics

All participants in this study were provided with a detailed explanation of the objectives, methods, sample collection procedures, and management of personal information in advance. Written informed consent was obtained from all participants. This study was conducted in accordance with the principles of the Declaration of Helsinki and was approved by the Ethical Review Committee of Chubu University (Approval No.: 20200081).

2.3. Saliva collection

Stimulated saliva was collected uniformly in a quiet room between 9:00 am and 12:00 pm using a previously established standardized protocol (*3*). The participants were specifically instructed (1) not to eat, drink, brush teeth, or smoke 60 min before and after saliva collection; (2) to thoroughly rinse their oral cavity with distilled water (gargle thrice) immediately before saliva collection; (3) to rest for 5 min in a sitting position and swallow once any saliva accumulated in the oral cavity; and then (4) to start a timer and chew a piece of odorless, tasteless, sterile cotton swab (Salimetrics Oral Swab™; Salimetrics, Carlsbad, CA, USA) once per second for 1 min. We ensured that the participants strictly adhered to this procedure. Newly secreted saliva was absorbed by the sterile cotton and collected in a storage tube (Swab Storage Tube™; Salimetrics). After collection, the storage tubes were centrifuged at 1,400× *g* for 5 min to separate saliva from the swab, and the volume of saliva obtained was recorded to calculate the saliva secretion rate (mL/min). The samples were promptly divided into small portions and stored at -30°C. The samples were thawed only once for measurement (*13*).

Saliva secretion rate (mL/min) was calculated by dividing the volume collected by the duration of the collection period.

2.4. Measurement of MUC5B concentration

MUC5B concentration (μg/mL) was determined using an enzyme-linked immunoassay (ELISA) with the Human MUC5B ELISA Kit (Novus Biologicals, Centennial, CO, USA; NBP2-76705), according to the manufacturer's instructions (*14*). Absorbance was measured at 450 and 630 nm using a microplate reader (BioTek Instruments, Winooski, VT, USA), and the concentration of MUC5B was calculated from the standard curve after wavelength correction.

2.5. Definition of the primary outcome

The primary outcome of this study was the rate of MUC5B secretion (μg/min), calculated by multiplying the MUC5B concentration (μg/mL) by the saliva secretion rate (mL/min). This parameter was employed to reflect the effective supply of the mucosal defense. MUC5B concentration was not measured in our previous study (*3*) and was newly quantified and analyzed as the primary outcome in this study.

2.6. Survey

The background information of the participants, including age group, sex, smoking habits, and history of chronic diseases, was collected using a questionnaire.

2.7 Statistical analysis

The variables are expressed as the median (interquartile range: IQR). The Kruskal–Wallis test was used to

compare each marker among the four groups, and multiple comparisons were corrected using the Bonferroni method. Statistical significance was set at a two-sided p-value < 0.05. Statistical analysis was performed using IBM SPSS Statistics, Version 27 (IBM, Armonk, NY, USA).

3. Results and Discussion

3.1. Participant characteristics

The participant characteristics are summarized in Table 1. Among them, seven (3.4%) participants had a history of hypertension, seven (3.4%) had a history of hyperlipidemia, one (0.5%) had a history of diabetes, and one (0.5%) had a history of rheumatoid arthritis (data not shown). Neither of these medical histories nor age was considered a major confounding factor for the study outcomes.

3.2. Saliva secretion rate

As shown in Figure 1, the median (IQR) saliva secretion rate was 1.4 (0.9–2.2) mL/min in the non-smoking group, 1.0 (0.7–1.5) mL/min in the HNB tobacco group, 1.1 (1.0–1.4) mL/min in the paper cigarette group, and 1.1 (0.7–1.5) in the dual-use group. A statistically significant difference was observed among the four groups (p = 0.02). Furthermore, multiple comparisons revealed a significantly lower saliva secretion rate in the HNB tobacco group compared with the non-smoking group (p = 0.04).

3.3. MUC5B concentration and secretion rate

Figure 2 shows the comparison of MUC5B concentrations among the four groups. The MUC5B concentration was 0.4 (0.2–0.7) μg/mL in the non-smoking group, 0.3 (0.2–0.6) μg/mL in the HNB tobacco group, 0.3 (0.2–0.9) μg/mL in the paper cigarette group, and 0.1 (0.1–0.3) μg/mL in the dual-use group, indicating a significant difference among the groups (p = 0.002). Multiple comparisons revealed a significantly lower MUC5B concentration in the dual-use group compared with the non-smoking group (p = 0.002).

Figure 3 shows the comparison of MUC5B secretion

Table 1. Participant characteristics

		%
Sex		
Male	208	100.0
Age group		
20–29	65	31.2
30–39	73	35.1
40–49	52	25.0
≥ 50	18	8.7
Smoking habit		
Non-smoker	147	70.7
HNB tobacco users	32	15.4
Cigarette smokers	15	7.2
Dual users (HNB + Cigarette)	14	6.7

HNB, Heat-not-burn.

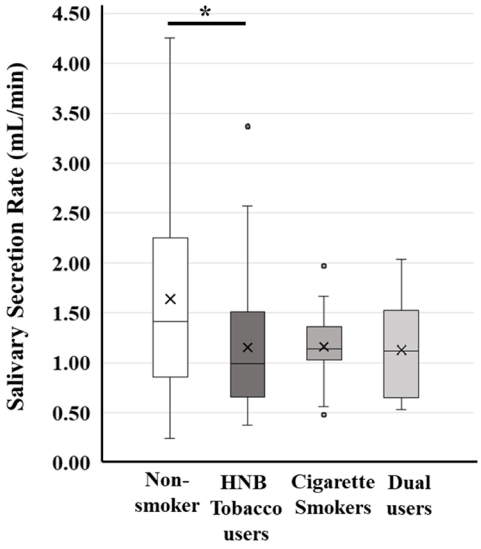

Figure 1. Comparison of saliva secretion rates. The Kruskal–Wallis test was applied, and Bonferroni's multiple comparison correction was performed. The boxes indicate the interquartile range, the line inside each box marks the median and the '×' denotes the mean. Whiskers represent the 10th to 90th percentiles, and values outside this range are shown as outliers. This result is based on analysis performed using a portion of samples employed in a previous study (Mori, Y, *et al*. 2022) (*3*). *, p < 0.05; HNB, Heat-not-burn; Dual users, HNB + Cigarette.

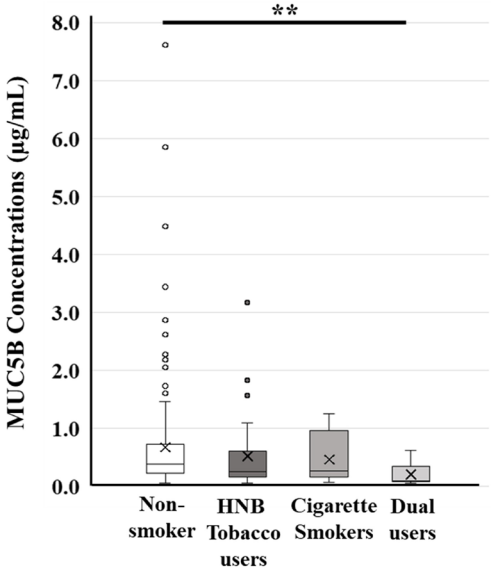

Figure 2. Comparison of MUC5B concentrations. The Kruskal–Wallis test was applied, and Bonferroni's multiple comparison correction was performed. The boxes indicate the interquartile range, the line inside each box marks the median and the '×' denotes the mean. Whiskers represent the 10th to 90th percentiles, and values outside this range are shown as outliers. **, p < 0.01; HNB, Heat-not-burn; Dual users, HNB + Cigarette.

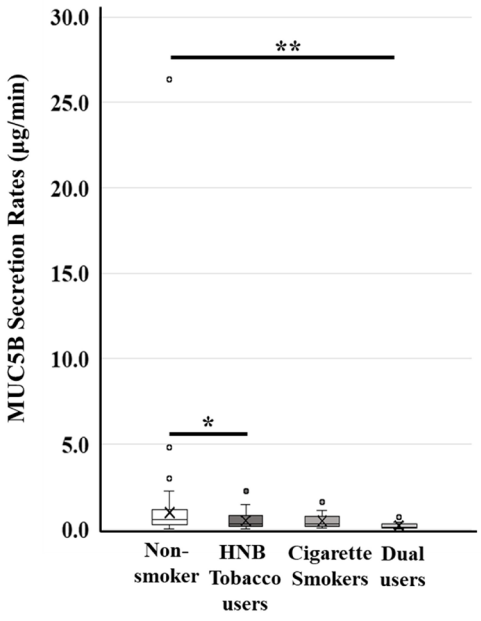

Figure 3. Comparison of MUC5B secretion rates. The Kruskal–Wallis test was applied, and Bonferroni's multiple comparison correction was performed. The boxes indicate the interquartile range, the line inside each box marks the median and the '×' denotes the mean. Whiskers represent the 10th to 90th percentiles, and values outside this range are shown as outliers. *, $p < 0.05$; **, $p < 0.01$; HNB, Heat-not-burn; Dual users, HNB + Cigarette.

rates among the four groups. The MUC5B secretion rate was 0.6 (0.3–1.1) μg/min in the non-smoking group, 0.3 (0.2–0.8) μg/min in the HNB tobacco group, 0.3 (0.2–0.7) μg/min in the paper cigarette group, and 0.1 (0.1–0.3) μg/min in the dual-use group. A significant difference in MUC5B secretion rates was observed between the four groups ($p < 0.001$), with multiple comparisons revealing a significantly lower MUC5B secretion rate in the HNB tobacco and dual-use groups than in the non-smoking group ($p = 0.04$ and $p < 0.001$, respectively). One sample exhibited an outlier MUC5B secretion rate (26.3 μg/min), although it was within the detection range. Nonetheless, the statistical conclusions remained unchanged when this sample was excluded.

As described above, this study revealed that, in an adult male population, MUC5B secretion rates were significantly lower in the HNB tobacco and dual-use groups than in the non-smoking group. This academically significant finding suggests that the use of HNB tobacco may be associated with the secretion dynamics of MUC5B, a key component of the innate immune system that is present in saliva.

HNB tobacco aerosols contains nicotine and other chemicals (*15*). Research on biomarkers in the oral cavity region has indicated that HNB tobacco use can alter inflammatory and immune indices in saliva (*16*). These exogenous stresses can alter the function of the salivary glands and regulation of MUC5B secretion by inducing chronic stress in the oral cavity and upper airway epithelium. However, the specific mechanisms through which HNB tobacco use is linked to MUC5B secretion have not yet been elucidated.

Salivary secretion is regulated by the autonomic nervous system (*17*). Nicotine-related autonomic nervous system changes associated with HNB tobacco smoking (*18*) may reduce salivary flow and contribute to decreased MUC5B secretion. Furthermore, reactive carbonyl compounds detected in HNB aerosols in previous studies, such as formaldehyde, acetaldehyde, and acrolein (*19,20*) have been shown in cell experiments to potentially promote increases in inflammation-related substances (*e.g.*, IL-8) (*21*). Furthermore, substances involved in inflammation (IL-6/IL-17 and IL-8) have been shown to potentially affect mucin secretion, including MUC5B, a major component of mucus (*22,23*). Therefore, a hypothetical pathway exists where HNB components alter the balance of inflammation-related substances, consequently affecting mucin production and secretion. However, since this study did not measure IL-6/IL-8 or similar substances in saliva, this mechanism could not be directly confirmed and requires future verification.

A particularly notable finding is that the dual-use group exhibited the most negative association with MUC5B secretion. This aligns with a previous study focusing on the cellular effects of dual exposure, which demonstrated that it adversely affects the function of airway epithelial cells *in vitro*, causing decreased cell viability, increased oxidative stress, and other functional abnormalities (*24*). A similar phenomenon may occur in the salivary glands; however, the association with decreased MUC5B secretion requires further investigation. Nevertheless, from a public health perspective, these findings provide a basis for strongly discouraging the combined use of HNB tobacco with paper cigarettes. Because mucins such as MUC5B suppress the growth of opportunistic pathogens (*5*), decreased salivary secretion of MUC5B, as observed in HNB tobacco users, raises major concerns regarding oral hygiene and immune function.

However, this study has several limitations. First, its cross-sectional nature limits causal inferences, and we could not completely exclude residual confounding factors (*e.g.*, water intake, exercise, oral cleaning, and stress). For instance, water loss has been suggested to affect salivary flow rate, potentially affecting the concentration and secretion rate of immune-related components in saliva (*25*). However, in the present study, it was difficult to determine the hydration status of the participants. Second, the sample size of this study depended on the availability of stored samples; consequently, the power was not designed in advance, and the sample size was relatively small. Additionally, approximately half the smokers were HNB tobacco users, which differs from the general usage trend in Japan (*1*). Therefore, further research is needed to examine whether the findings of this study can be

directly applied to the general population. Third, although the selection criterion of this study included "smokers who had smoked for a certain period of time," we were unable to obtain information regarding both the duration and quantity of smoking for the participants. This prevented us from performing a multivariate analysis that accounts for these factors as covariates. Moreover, it has been reported that the dual use of HNB tobacco and paper cigarettes "may have additive and synergistic disadvantages" (*24*); thus, prospective studies that accurately capture exposure indices (number of cigarettes, frequency of inhalation, and nicotine dependence) are needed. Fourth, the study population was biased toward males and firefighters; thus, the reproducibility of the findings needs to be verified in a population with more diverse age, sex, underlying diseases, medications, and other factors. Additionally, a link between circadian rhythm and saliva secretion has been reported (*26*); given that several participants in this study had irregular work schedules, their circadian rhythms may differ from those of the general population. Furthermore, the occupation of firefighters involves high levels of occupational stress during fire responses (*27*), as well as the risk of exposure to toxic gases in combustion products (*28,29*), alongside characteristic physical activity patterns (*30*). It cannot be denied that these factors may influence variations in salivary secretion volume and immune-related components in saliva. Therefore, the results of this study are preliminary and require validation in diverse populations.

A key strength of this study is that the rate of MUC5B secretion (μg/min), which was calculated using both MUC5B concentration and saliva secretion rate, was used as the primary outcome. This measure represents the effective functional supply of MUC5B to the oral mucosa and provides greater physiological relevance to mucosal barrier function than a simple concentration index. Furthermore, this method is highly practical and useful in clinical settings. Furthermore, from a public health perspective, demonstrating the quantitative association between HNB tobacco use and the innate immune system (MUC5B) in saliva is expected to encourage behavioural change and dispel the misconception that "HNB tobacco is safe because exposure levels are relatively low".

In conclusion, this study investigated the association between HNB tobacco use and salivary MUC5B secretion levels using a secretion index that integrated MUC5B concentration and saliva secretion rate. The MUC5B secretion rates were lower in the HNB tobacco and dual-use groups than those in the non-smoking group, suggesting an impairment of the innate immune barrier within the oral cavity. The novelty of this study lies in its focus on HNB tobacco and the direct comparison of MUC5B secretion levels. Our findings contribute valuable insights for assessing the risks associated with oral diseases and oral/upper respiratory tract infections among HNB tobacco users and aid in optimizing smoking cessation strategies. Therefore, this study contributes valuable knowledge for the fields of preventive medicine and public health.

Given the limitations of the cross-sectional analysis approach used in this study and the male-only study population, future studies should focus on establishing accurate exposure assessments and integrative associations with disease mechanisms and clinical outcomes.

Acknowledgements

We greatly appreciate all firefighters, paramedics, and rescue workers for their participation in this study.

Funding: This work was supported by the Smoking Research Foundation [No. 2022G039].

Conflict of Interest: The authors have no conflicts of interest to disclose.

References

1. Tabuchi T, Gallus S, Shinozaki T, Nakaya T, Kunugita N, Colwell B. Heat-not-burn tobacco product use in Japan: its prevalence, predictors and perceived symptoms from exposure to secondhand heat-not-burn tobacco aerosol. Tob Control. 2018; 27:e25-e33.
2. Dusautoir R, Zarcone G, Verriele M, Garcon G, Fronval I, Beauval N, Allorge D, Riffault V, Locoge N, Lo-Guidice JM, Anthérieu S. Comparison of the chemical composition of aerosols from heated tobacco products, electronic cigarettes and tobacco cigarettes and their toxic impacts on the human bronchial epithelial BEAS-2B cells. J Hazard Mater. 2021; 401:123417.
3. Mori Y, Tanaka M, Kozai H, Aoyama Y, Shigeno Y, Hotta K, Aoike M, Kawamura H, Tsurudome M, Ito M. Effects of Heat-Not-Burn Cigarette Smoking on the Secretion of Saliva and Its Innate Immune System Components. Healthcare (Basel). 2022; 11:132.
4. Pavlov N, Popova-Sotirova I, Musurlieva N, Raycheva R, Trifonov K, Atanasova M, Cholakova R. Influence of Ordinary Cigarettes and Their Substitute IQOS on Secretory Immunoglobulin A in Unstimulated Saliva. Dent J (Basel). 2025; 13:297.
5. Frenkel ES, Ribbeck K. Salivary mucins in host defense and disease prevention. J Oral Microbiol. 2015; 7:29759.
6. Alliende C, Kwon YJ, Brito M, Molina C, Aguilera S, Perez P, Leyton L, Quest AF, Mandel U, Veerman E, Espinosa M, Clausen H, Leyton C, Romo R, Gonzalez MJ. Reduced sulfation of muc5b is linked to xerostomia in patients with Sjogren syndrome. Ann Rheum Dis. 2008; 67:1480-1487.
7. Assy Z, Jager DHJ, Brand HS, Bikker FJ. Salivary film thickness and MUC5B levels at various intra-oral surfaces. Clin Oral Investig. 2023; 27:859-869.
8. Sengupta A, Valdramidou D, Huntley S, Hicks SJ, Carrington SD, Corfield AP. Distribution of MUC1 in the normal human oral cavity is localized to the ducts

of minor salivary glands. Arch Oral Biol. 2001; 46:529-538.
9. Bruno LS, Li X, Wang L, Soares RV, Siqueira CC, Oppenheim FG, Troxler RF, Offner GD. Two-hybrid analysis of human salivary mucin MUC7 interactions. Biochim Biophys Acta. 2005; 1746:65-72.
10. Amerongen AV, Veerman EC. Saliva--the defender of the oral cavity. Oral Dis. 2002; 8:12-22.
11. Glimvall P, Wickström C, Jansson H. Elevated levels of salivary lactoferrin, a marker for chronic periodontitis? J Periodontal Res. 2012; 47:655-660.
12. Cichońska D, Kusiak A, Kochańska B, Ochocińska J, Świetlik D. Influence of Electronic Cigarettes on Selected Antibacterial Properties of Saliva. Int J Environ Res Public Health. 2019; 16:4433.
13. Bhattarai KR, Kim HR, Chae HJ. Compliance with Saliva Collection Protocol in Healthy Volunteers: Strategies for Managing Risk and Errors. Int J Med Sci. 2018; 15:823-831.
14. Weng L, Liu W, Wang L, Wu Z, Liu D, Lin Y, Song S, Yu C, Chen Y, Chen J, Ge S. Serum MUC5AC protein levels are correlated with the development and severity of connective tissue disease-associated pulmonary interstitial lesions. Front Immunol. 2022; 13:987723.
15. Bekki K, Inaba Y, Uchiyama S, Kunugita N. Comparison of Chemicals in Mainstream Smoke in Heat-not-burn Tobacco and Combustion Cigarettes. J UOEH. 2017; 39:201-207.
16. Zieba S, Maciejczyk M, Antonowicz B, Porydzaj A, Szuta M, Lo Giudice G, Lo Giudice R, Krokosz S, Zalewska A. Comparison of smoking traditional, heat not burn and electronic cigarettes on salivary cytokine, chemokine and growth factor profile in healthy young adults-pilot study. Front Physiol. 2024; 15:1404944.
17. Proctor GB, Carpenter GH. Regulation of salivary gland function by autonomic nerves. Auton Neurosci. 2007; 133:3-18.
18. Goebel I, Mohr T, Axt PN, Watz H, Trinkmann F, Weckmann M, Dromann D, Franzen KF. Impact of Heated Tobacco Products, E-Cigarettes, and Combustible Cigarettes on Small Airways and Arterial Stiffness. Toxics. 2023; 11:758.
19. Mallock N, Boss L, Burk R, Danziger M, Welsch T, Hahn H, Trieu HL, Hahn J, Pieper E, Henkler-Stephani F, Hutzler C, Luch A. Levels of selected analytes in the emissions of "heat not burn" tobacco products that are relevant to assess human health risks. Arch Toxicol. 2018; 92:2145-2149.
20. Farsalinos KE, Yannovits N, Sarri T, Voudris V, Poulas K, Leischow SJ. Carbonyl emissions from a novel heated tobacco product (IQOS): comparison with an e-cigarette and a tobacco cigarette. Addiction. 2018; 113:2099-2106.
21. Moretto N, Bertolini S, Iadicicco C, Marchini G, Kaur M, Volpi G, Patacchini R, Singh D, Facchinetti F. Cigarette smoke and its component acrolein augment IL-8/CXCL8 mRNA stability *via* p38 MAPK/MK2 signaling in human pulmonary cells. Am J Physiol Lung Cell Mol Physiol. 2012; 303:L929-938.
22. Chen Y, Thai P, Zhao YH, Ho YS, DeSouza MM, Wu R. Stimulation of airway mucin gene expression by interleukin (IL)-17 through IL-6 paracrine/autocrine loop. J Biol Chem. 2003; 278:17036-17043.
23. Bautista MV, Chen Y, Ivanova VS, Rahimi MK, Watson AM, Rose MC. IL-8 regulates mucin gene expression at the posttranscriptional level in lung epithelial cells. J Immunol. 2009; 183:2159-2166.
24. Saha P, Jain S, Mukherjee I, Panda SR, Zeki AA, Naidu VGM, Sharma P. The effects of dual IQOS and cigarette smoke exposure on airway epithelial cells: implications for lung health and respiratory disease pathogenesis. ERJ Open Res. 2023; 9:00558-2022.
25. Walsh NP, Montague JC, Callow N, Rowlands AV. Saliva flow rate, total protein concentration and osmolality as potential markers of whole body hydration status during progressive acute dehydration in humans. Arch Oral Biol. 2004; 49:149-154.
26. Dawes C. Circadian rhythms in human salivary flow rate and composition. J Physiol. 1972; 220:529-545.
27. Alshahrani KM, Johnson J, Prudenzi A, O'Connor DB. The effectiveness of psychological interventions for reducing PTSD and psychological distress in first responders: A systematic review and meta-analysis. PLoS One. 2022; 17:e0272732.
28. Cuenca-Lozano MF, Ramirez-Garcia CO. Occupational Hazards in Firefighting: Systematic Literature Review. Saf Health Work. 2023; 14:1-9.
29. Alharbi BH, Pasha MJ, Al-Shamsi MAS. Firefighter exposures to organic and inorganic gas emissions in emergency residential and industrial fires. Sci Total Environ. 2021; 770:145332.
30. Bos J, Mol E, Visser B, Frings-Dresen M. The physical demands upon (Dutch) fire-fighters in relation to the maximum acceptable energetic workload. Ergonomics. 2004; 47:446-460.

Received October 30, 2025; Revised January 16, 2026; Accepted February 6, 2026.

**Address correspondence to:*
Morihiro Ito, Graduate School of Life and Health Sciences, Chubu University, 1200 Matsumoto-cho, Kasugai, Aichi 487-8501, Japan.
E-mail: m-ito@fsc.chubu.ac.jp

Released online in J-STAGE as advance publication February 12, 2026.

DD&T
Drug Discoveries & Therapeutics

Guide for Authors

1. Scope of Articles

Drug Discoveries & Therapeutics (Print ISSN 1881-7831, Online ISSN 1881-784X) welcomes contributions in all fields of pharmaceutical and therapeutic research such as medicinal chemistry, pharmacology, pharmaceutical analysis, pharmaceutics, pharmaceutical administration, and experimental and clinical studies of effects, mechanisms, or uses of various treatments. Studies in drug-related fields such as biology, biochemistry, physiology, microbiology, and immunology are also within the scope of this journal.

2. Submission Types

Original Articles should be well-documented, novel, and significant to the field as a whole. An Original Article should be arranged into the following sections: Title page, Abstract, Introduction, Materials and Methods, Results, Discussion, Acknowledgments, and References. Original articles should not exceed 5,000 words in length (excluding references) and should be limited to a maximum of 50 references. Articles may contain a maximum of 10 figures and/or tables. Supplementary Data are permitted but should be limited to information that is not essential to the general understanding of the research presented in the main text, such as unaltered blots and source data as well as other file types.

Brief Reports definitively documenting either experimental results or informative clinical observations will be considered for publication in this category. Brief Reports are not intended for publication of incomplete or preliminary findings. Brief Reports should not exceed 3,000 words in length (excluding references) and should be limited to a maximum of 4 figures and/or tables and 30 references. A Brief Report contains the same sections as an Original Article, but the Results and Discussion sections should be combined.

Reviews should present a full and up-to-date account of recent developments within an area of research. Normally, reviews should not exceed 8,000 words in length (excluding references) and should be limited to a maximum of 10 figures and/or tables and 100 references. Mini reviews are also accepted, which should not exceed 4,000 words in length (excluding references) and should be limited to a maximum of 5 figures and/or tables and 50 references.

Policy Forum articles discuss research and policy issues in areas related to life science such as public health, the medical care system, and social science and may address governmental issues at district, national, and international levels of discourse. Policy Forum articles should not exceed 3,000 words in length (excluding references) and should be limited to a maximum of 5 figures and/or tables and 30 references.

Case Reports should be detailed reports of the symptoms, signs, diagnosis, treatment, and follow-up of an individual patient. Case reports may contain a demographic profile of the patient but usually describe an unusual or novel occurrence. Unreported or unusual side effects or adverse interactions involving medications will also be considered. Case Reports should not exceed 3,000 words in length (excluding references).

Communications are short, timely pieces that spotlight new research findings or policy issues of interest to the field of global health and medical practice that are of immediate importance. Depending on their content, Communications will be published as "Comments" or "Correspondence". Communications should not exceed 1,500 words in length (excluding references) and should be limited to a maximum of 2 figures and/or tables and 20 references.

Editorials are short, invited opinion pieces that discuss an issue of immediate importance to the fields of global health, medical practice, and basic science oriented for clinical application. Editorials should not exceed 1,000 words in length (excluding references) and should be limited to a maximum of 10 references. Editorials may contain one figure or table.

News articles should report the latest events in health sciences and medical research from around the world. News should not exceed 500 words in length.

Letters should present considered opinions in response to articles published in *Drug Discoveries & Therapeutics* in the last 6 months or issues of general interest. Letters should not exceed 800 words in length and may contain a maximum of 10 references. Letters may contain one figure or table.

3. Editorial Policies

For publishing and ethical standards, *Drug Discoveries & Therapeutics* follows the Recommendations for the Conduct, Reporting, Editing, and Publication of Scholarly Work in Medical Journals issued by the International Committee of Medical Journal Editors (ICMJE, *https://icmje.org/recommendations*), and the Principles of Transparency and Best Practice in Scholarly Publishing jointly issued by the Committee on Publication Ethics (COPE, *https://publicationethics.org/resources/guidelines-new/principles-transparency-and-best-practice-scholarly-publishing*), the Directory of Open Access Journals (DOAJ, *https://doaj.org/apply/transparency*), the Open Access Scholarly Publishers Association (OASPA, *https://oaspa.org/principles-of-transparency-and-best-practice-in-scholarly-publishing-4*), and the World Association of Medical Editors (WAME, *https://wame.org/principles-of-transparency-and-best-practice-in-scholarly-publishing*).

Drug Discoveries & Therapeutics will perform an especially prompt review to encourage innovative work. All original research will be subjected to a rigorous standard of peer review and will be edited by experienced copy editors to the highest standards.

Ethical Approval of Studies and Informed Consent: For all manuscripts reporting data from studies involving human participants or animals, formal review and approval, or formal review and waiver, by an appropriate institutional review board or ethics committee is required and should be described in the Methods section. When your manuscript contains any case details, personal information and/or images of patients or other individuals, authors must obtain appropriate written consent, permission and release in order to comply with all applicable laws and regulations concerning privacy and/or security of personal information. The consent form needs to comply with the relevant legal requirements of your particular jurisdiction, and please do not send signed consent form to *Drug Discoveries & Therapeutics* to respect your patient's and any other individual's privacy. Please instead describe the information clearly in the Methods (patient consent) section of your manuscript while retaining copies of the signed forms in the event they should be needed. Authors should also state that the study conformed to the provisions of the Declaration of Helsinki (as revised in 2013, *https://wma.net/what-we-do/medical-ethics/declaration-of-helsinki*). When reporting experiments on animals, authors should indicate whether the institutional and national guide for the care and use of laboratory animals was followed.

Reporting Clinical Trials: The ICMJE (*https:// icmje.org/recommendations/browse/publishing-and-editorial-issues/clinical-trial-registration.html*) defines a clinical trial as any research project that prospectively assigns people or a group of people to an intervention, with or without concurrent comparison or control groups, to study the relationship between a health-related intervention and a health outcome. Registration of clinical trials in a public trial registry

at or before the time of first patient enrollment is a condition of consideration for publication in *Drug Discoveries & Therapeutics*, and the trial registration number will be published at the end of the Abstract. The registry must be independent of for-profit interest and publicly accessible. Reports of trials must conform to CONSORT 2010 guidelines (*https://consort-statement.org/consort-2010*). Articles reporting the results of randomized trials must include the CONSORT flow diagram showing the progress of patients throughout the trial.

Conflict of Interest: All authors are required to disclose any actual or potential conflict of interest including financial interests or relationships with other people or organizations that might raise questions of bias in the work reported. If no conflict of interest exists for each author, please state "There is no conflict of interest to disclose".

Submission Declaration: When a manuscript is considered for submission to *Drug Discoveries & Therapeutics*, the authors should confirm that 1) no part of this manuscript is currently under consideration for publication elsewhere; 2) this manuscript does not contain the same information in whole or in part as manuscripts that have been published, accepted, or are under review elsewhere, except in the form of an abstract, a letter to the editor, or part of a published lecture or academic thesis; 3) authorization for publication has been obtained from the authors' employer or institution; and 4) all contributing authors have agreed to submit this manuscript.

Initial Editorial Check: Immediately after submission, the journal's managing editor will perform an initial check of the manuscript. A suitable academic editor will be notified of the submission and invited to check the manuscript and recommend reviewers. Academic editors will check for plagiarism and duplicate publication at this stage. The journal has a formal recusal process in place to help manage potential conflicts of interest of editors. In the event that an editor has a conflict of interest with a submitted manuscript or with the authors, the manuscript, review, and editorial decisions are managed by another designated editor without a conflict of interest related to the manuscript.

Peer Review: *Drug Discoveries & Therapeutics* operates a single-anonymized review process, which means that reviewers know the names of the authors, but the authors do not know who reviewed their manuscript. All articles are evaluated objectively based on academic content. External peer review of research articles is performed by at least two reviewers, and sometimes the opinions of more reviewers are sought. Peer reviewers are selected based on their expertise and ability to provide quality, constructive, and fair reviews. For research manuscripts, the editors may, in addition, seek the opinion of a statistical reviewer. Every reviewer is expected to evaluate the manuscript in a timely, transparent, and ethical manner, following the COPE guidelines (*https://publicationethics.org/files/cope-ethical-guidelines-peer-reviewers-v2_0.pdf*). We ask authors for sufficient revisions (with a second round of peer review, when necessary) before a final decision is made. Consideration for publication is based on the article's originality, novelty, and scientific soundness, and the appropriateness of its analysis.

Suggested Reviewers: A list of up to 3 reviewers who are qualified to assess the scientific merit of the study is welcomed. Reviewer information including names, affiliations, addresses, and e-mail should be provided at the same time the manuscript is submitted online. Please do not suggest reviewers with known conflicts of interest, including participants or anyone with a stake in the proposed research; anyone from the same institution; former students, advisors, or research collaborators (within the last three years); or close personal contacts. Please note that the Editor-in-Chief may accept one or more of the proposed reviewers or may request a review by other qualified persons.

Language Editing: Manuscripts prepared by authors whose native language is not English should have their work proofread by a native English speaker before submission. If not, this might delay the publication of your manuscript in *Drug Discoveries & Therapeutics*.

The Editing Support Organization can provide English proofreading, Japanese-English translation, and Chinese-English translation services to authors who want to publish in *Drug Discoveries & Therapeutics* and need assistance before submitting a manuscript. Authors can visit this organization directly at *https://www.iacmhr.com/iac-eso/support.php?lang=en. IAC-ESO* was established to facilitate manuscript preparation by researchers whose native language is not English and to help edit works intended for international academic journals.

Copyright and Reuse: Before a manuscript is accepted for publication in *Drug Discoveries & Therapeutics*, authors will be asked to sign a transfer of copyright agreement, which recognizes the common interest that both the journal and author(s) have in the protection of copyright. We accept that some authors (*e.g.*, government employees in some countries) are unable to transfer copyright. A JOURNAL PUBLISHING AGREEMENT (JPA) form will be e-mailed to the authors by the Editorial Office and must be returned by the authors by mail, fax, or as a scan. Only forms with a hand-written signature from the corresponding author are accepted. This copyright will ensure the widest possible dissemination of information. Please note that the manuscript will not proceed to the next step in publication until the JPA Form is received. In addition, if excerpts from other copyrighted works are included, the author(s) must obtain written permission from the copyright owners and credit the source(s) in the article.

4. Cover Letter

The manuscript must be accompanied by a cover letter prepared by the corresponding author on behalf of all authors. The letter should indicate the basic findings of the work and their significance. The letter should also include a statement affirming that all authors concur with the submission and that the material submitted for publication has not been published previously or is not under consideration for publication elsewhere. The cover letter should be submitted in PDF format. For an example of Cover Letter, please visit: Download Centre (*https://www.ddtjournal.com/downcentre)*.

5. Submission Checklist

The Submission Checklist should be submitted when submitting a manuscript through the Online Submission System. Please visit Download Centre (*https://www.ddtjournal.com/downcentre)* and download the Submission Checklist file. We recommend that authors use this checklist when preparing your manuscript to check that all the necessary information is included in your article (if applicable), especially with regard to Ethics Statements.

6. Manuscript Preparation

Manuscripts are suggested to be prepared in accordance with the "Recommendations for the Conduct, Reporting, Editing, and Publication of Scholarly Work in Medical Journals", as presented at *http://www.ICMJE.org*.

Manuscripts should be written in clear, grammatically correct English and submitted as a Microsoft Word file in a single-column format. Manuscripts must be paginated and typed in 12-point Times New Roman font with 24-point line spacing. Please do not embed figures in the text. Abbreviations should be used as little as possible and should be explained at first mention unless the term is a well-known abbreviation (*e.g.* DNA). Single words should not be abbreviated.

Title page: The title page must include 1) the title of the paper (Please note the title should be short, informative, and contain the major key words); 2) full name(s) and affiliation(s) of the author(s), 3) abbreviated names of the author(s), 4) full name, mailing address, telephone/fax numbers, and e-mail address of the corresponding author; 5) author contribution statements to specify the individual contributions of all authors to this manuscript, and 6) conflicts of interest (if you have an actual or potential conflict of interest to disclose, it must be included as a footnote on the title page of the manuscript; if no conflict of interest

exists for each author, please state "There is no conflict of interest to disclose").

Abstract: The abstract should briefly state the purpose of the study, methods, main findings, and conclusions. For article types including Original Article, Brief Report, Review, Policy Forum, and Case Report, a one-paragraph abstract consisting of no more than 250 words must be included in the manuscript. For Communications, Editorials, News, or Letters, a brief summary of main content in 150 words or fewer should be included in the manuscript. For articles reporting clinical trials, the trial registration number should be stated at the end of the Abstract. Abbreviations must be kept to a minimum and non-standard abbreviations explained in brackets at first mention. References should be avoided in the abstract. Three to six key words or phrases that do not occur in the title should be included in the Abstract page.

Introduction: The introduction should provide sufficient background information to make the article intelligible to readers in other disciplines and sufficient context clarifying the significance of the experimental findings.

Materials/Patients and Methods: The description should be brief but with sufficient detail to enable others to reproduce the experiments. Procedures that have been published previously should not be described in detail but appropriate references should simply be cited. Only new and significant modifications of previously published procedures require complete description. Names of products and manufacturers with their locations (city and state/country) should be given and sources of animals and cell lines should always be indicated. All clinical investigations must have been conducted in accordance with the Declaration of Helsinki (as revised in 2013, *https://wma.net/what-we-do/medical-ethics/declaration-of-helsinki*). All human and animal studies must have been approved by the appropriate institutional review board(s) and a specific declaration of approval must be made within this section.

Results: The description of the experimental results should be succinct but in sufficient detail to allow the experiments to be analyzed and interpreted by an independent reader. If necessary, subheadings may be used for an orderly presentation. All Figures and Tables should be referred to in the text in order, including those in the Supplementary Data.

Discussion: The data should be interpreted concisely without repeating material already presented in the Results section. Speculation is permissible, but it must be well-founded, and discussion of the wider implications of the findings is encouraged. Conclusions derived from the study should be included in this section.

Acknowledgments: All funding sources (including grant identification) should be credited in the Acknowledgments section. Authors should also describe the role of the study sponsor(s), if any, in study design; in the collection, analysis, and interpretation of data; in the writing of the report; and in the decision to submit the paper for publication. If the funding source had no such involvement, the authors should so state.

In addition, people who contributed to the work but who do not meet the criteria for authors should be listed along with their contributions.

References: References should be numbered in the order in which they appear in the text. Citing of unpublished results, personal communications, conference abstracts, and theses in the reference list is not recommended but these sources may be mentioned in the text. In the reference list, cite the names of all authors when there are fifteen or fewer authors; if there are sixteen or more authors, list the first three followed by *et al*. Names of journals should be abbreviated in the style used in PubMed. Authors are responsible for the accuracy of the references. The EndNote Style of *Drug Discoveries & Therapeutics* could be downloaded at **EndNote** (*https://www.ddtjournal.com/examples/Drug_Discoveries_Therapeutics.ens*).

Examples are given below:

Example 1 (Sample journal reference):

Nakata M, Tang W. Japan-China Joint Medical Workshop on Drug Discoveries and Therapeutics 2008: The need of Asian pharmaceutical researchers' cooperation. Drug Discov Ther. 2008; 2:262-263.

Example 2 (Sample journal reference with more than 15 authors):

Darby S, Hill D, Auvinen A, *et al*. Radon in homes and risk of lung cancer: Collaborative analysis of individual data from 13 European case-control studies. BMJ. 2005; 330:223.

Example 3 (Sample book reference):

Shalev AY. Post-traumatic stress disorder: Diagnosis, history and life course. In: Post-traumatic Stress Disorder, Diagnosis, Management and Treatment (Nutt DJ, Davidson JR, Zohar J, eds.). Martin Dunitz, London, UK, 2000; pp. 1-15.

Example 4 (Sample web page reference):

World Health Organization. The World Health Report 2008 – primary health care: Now more than ever. *https://apps.who.int/iris/handle/10665/43949* (accessed September 23, 2022).

Tables: All tables should be prepared in Microsoft Word or Excel and should be arranged at the end of the manuscript after the References section. Please note that tables should not in image format. All tables should have a concise title and should be numbered consecutively with Arabic numerals. If necessary, additional information should be given below the table.

Figure Legend: The figure legend should be typed on a separate page of the main manuscript and should include a short title and explanation. The legend should be concise but comprehensive and should be understood without referring to the text. Symbols used in figures must be explained. Any individually labeled figure parts or panels (A, B, *etc*.) should be specifically described by part name within the legend.

Figure Preparation: All figures should be clear and cited in numerical order in the text. Figures must fit a one- or two-column format on the journal page: 8.3 cm (3.3 in.) wide for a single column, 17.3 cm (6.8 in.) wide for a double column; maximum height: 24.0 cm (9.5 in.). Please make sure that artwork files are in an acceptable format (TIFF or JPEG) at minimum resolution (600 dpi for illustrations, graphs, and annotated artwork, and 300 dpi for micrographs and photographs). Please provide all figures as separate files. Please note that low-resolution images are one of the leading causes of article resubmission and schedule delays.

Units and Symbols: Units and symbols conforming to the International System of Units (SI) should be used for physicochemical quantities. Solidus notation (*e.g*. mg/kg, mg/mL, mol/mm^2/min) should be used. Please refer to the SI Guide *www.bipm.org/en/si/* for standard units.

Supplemental data: Supplemental data might be useful for supporting and enhancing your scientific research and *Drug Discoveries & Therapeutics* accepts the submission of these materials which will be only published online alongside the electronic version of your article. Supplemental files (figures, tables, and other text materials) should be prepared according to the above guidelines, numbered in Arabic numerals (*e.g*., Figure S1, Figure S2, and Table S1, Table S2) and referred to in the text. All figures and tables should have titles and legends. All figure legends, tables and supplemental text materials should be placed at the end of the paper. Please note all of these supplemental data should be provided at the time of initial submission and note that the editors reserve the right to limit the size

and length of Supplemental Data.

7. Online Submission

Manuscripts should be submitted to *Drug Discoveries & Therapeutics* online at *https://www.ddtjournal.com/login*. Receipt of your manuscripts submitted online will be acknowledged by an e-mail from Editorial Office containing a reference number, which should be used in all future communications. If for any reason you are unable to submit a file online, please contact the Editorial Office by e-mail at *office@ddtjournal.com*

8. Accepted Manuscripts

Page Charge: Page charges will be levied on all manuscripts accepted for publication in *Drug Discoveries & Therapeutics* (Original Articles / Brief Reports / Reviews / Policy Forum / Communications: $140 per page for black white pages, $340 per page for color pages; News / Letters: a total cost of $600). Under exceptional circumstances, the author(s) may apply to the editorial office for a waiver of the publication charges by stating the reason in the Cover Letter when the manuscript online.

Misconduct: *Drug Discoveries & Therapeutics* takes seriously all allegations of potential misconduct and adhere to the ICMJE Guideline (*https://icmje.org/recommendations*) and COPE Guideline (*https://publicationethics.org/files/Code_of_conduct_for_journal_editors.pdf*). In cases of suspected research or publication misconduct, it may be necessary for the Editor or Publisher to contact and share submission details with third parties including authors' institutions and ethics committees. The corrections, retractions, or editorial expressions of concern will be performed in line with above guidelines.

(As of December 2022)

Drug Discoveries & Therapeutics
Editorial and Head Office
Pearl City Koishikawa 603,
2-4-5 Kasuga, Bunkyo-ku,
Tokyo 112-0003, Japan.
E-mail: office@ddtjournal.com